

ISSN 1854-6250

APEM
journal

Advances in Production Engineering & Management

Volume 16 | Number 2 | June 2021





University of Maribor

Published by CPE
apem-journal.org

Advances in Production Engineering & Management

Identification Statement

	ISSN 1854-6250 Abbreviated key title: Adv produc engineer manag Start year: 2006 ISSN 1855-6531 (on-line)
	Published quarterly by Chair of Production Engineering (CPE), University of Maribor Smetanova ulica 17, SI – 2000 Maribor, Slovenia, European Union (EU) Phone: 00386 2 2207522, Fax: 00386 2 2207990 Language of text: English APEM homepage: apem-journal.org University homepage: www.um.si

APEM Editorial

Editor-in-Chief

Miran Brezocnik

editor@apem-journal.org, info@apem-journal.org
University of Maribor, Faculty of Mechanical Engineering Smetanova ulica 17, SI – 2000 Maribor, Slovenia, EU

Desk Editor

Martina Meh

desk1@apem-journal.org

Janez Gotlih

desk2@apem-journal.org

Website Technical Editor

Lucija Brezocnik

desk3@apem-journal.org

Editorial Board Members

Eberhard Abele, Technical University of Darmstadt, Germany
Bojan Acko, University of Maribor, Slovenia
Joze Balic, University of Maribor, Slovenia
Agostino Bruzzone, University of Genoa, Italy
Borut Buchmeister, University of Maribor, Slovenia
Ludwig Cardon, Ghent University, Belgium
Nirupam Chakraborti, Indian Institute of Technology, Kharagpur, India
Edward Chlebus, Wroclaw University of Technology, Poland
Igor Drstvensek, University of Maribor, Slovenia
Illes Dudas, University of Miskolc, Hungary
Mirko Ficko, University of Maribor, Slovenia
Vlatka Hlupic, University of Westminster, UK
David Hui, University of New Orleans, USA
Pramod K. Jain, Indian Institute of Technology Roorkee, India
Isak Karabegović, University of Bihać, Bosnia and Herzegovina

Janez Kopac, University of Ljubljana, Slovenia
Qingliang Meng, Jiangsu University of Science and Technology, China
Lanndon A. Ocampo, Cebu Technological University, Philippines
Iztok Palcic, University of Maribor, Slovenia
Krsto Pandza, University of Leeds, UK
Andrej Polajnar, University of Maribor, Slovenia
Antonio Pouzada, University of Minho, Portugal
R. Venkata Rao, Sardar Vallabhbhai National Inst. of Technology, India
Rajiv Kumar Sharma, National Institute of Technology, India
Katica Simunovic, J. J. Strossmayer University of Osijek, Croatia
Daizhong Su, Nottingham Trent University, UK
Soemon Takakuwa, Nagoya University, Japan
Nikos Tsourveloudis, Technical University of Crete, Greece
Tomo Udiljak, University of Zagreb, Croatia
Ivica Veza, University of Split, Croatia



Subsidizer: The journal is subsidized by Slovenian Research Agency



Creative Commons Licence (CC): Content from published paper in the APEM journal may be used under the terms of the Creative Commons Attribution 4.0 International Licence (CC BY 4.0). Any further distribution of this work must maintain attribution to the author(s) and the title of the work, journal citation and DOI.

Statements and opinions expressed in the articles and communications are those of the individual contributors and not necessarily those of the editors or the publisher. No responsibility is accepted for the accuracy of information contained in the text, illustrations or advertisements. Chair of Production Engineering assumes no responsibility or liability for any damage or injury to persons or property arising from the use of any materials, instructions, methods or ideas contained herein.

Published by CPE, University of Maribor.

Advances in Production Engineering & Management is indexed and abstracted in the **WEB OF SCIENCE** (maintained by **Clarivate Analytics**): **Science Citation Index Expanded**, **Journal Citation Reports** – Science Edition, **Current Contents** – Engineering, Computing and Technology • **Scopus** (maintained by **Elsevier**) • **Inspec** • **EBSCO**: Academic Search Alumni Edition, Academic Search Complete, Academic Search Elite, Academic Search Premier, Engineering Source, Sales & Marketing Source, TOC Premier • **ProQuest**: CSA Engineering Research Database – Cambridge Scientific Abstracts, Materials Business File, Materials Research Database, Mechanical & Transportation Engineering Abstracts, ProQuest SciTech Collection • **TEMA (DOMA)** • The journal is listed in **Ulrich's** Periodicals Directory and **Cabell's** Directory



University of Maribor
Chair of Production Engineering (CPE)

Advances in Production Engineering & Management

Volume 16 | Number 2 | June 2021 | pp 141–264

Contents

Scope and topics	144
Hybrid ANFIS-Rao algorithm for surface roughness modelling and optimization in electrical discharge machining	145
Agarwal, N.; Shrivastava, N.; Pradhan, M.K.	
A multi-objective optimal decision model for a green closed-loop supply chain under uncertainty: A real industrial case study	161
Fang, I.W.; Lin, W.-T.	
Improved Genetic Algorithm (VNS-GA) using polar coordinate classification for workload balanced multiple Traveling Salesman Problem (mTSP)	173
Wang, Y.D.; Lu, X.C.; Shen, J.R.	
Change impact analysis of complex product using an improved three-parameter interval grey relation model	185
Yang, W.M.; Li, C.D.; Chen, Y.H.; Yu, Y.Y.	
Bone drilling with internal gas cooling: Experimental and statistical investigation of the effect of cooling with CO₂ on reduction of temperature rise due to drill bit wear	199
Shakouri, E.; Haghighi Hassanalideh, H.; Fotuhi, S.	
Joint distribution models in fast-moving consumer goods wholesale enterprise: Comparative analysis and a case study	212
Wang, L.; Chen, X.Y.; Zhang, H.	
Designing a warehouse internal layout using a parabolic aisles based method	223
Zhang, Z.Y.; Liang, Y.; Hou, Y.P.; Wang, Q.	
Optimization of disassembly line balancing using an improved multi-objective Genetic Algorithm	240
Wang, Y.J.; Wang, N.D.; Cheng, S.M.; Zhang, X.C.; Liu, H.Y.; Shi, J.L.; Ma, Q.Y.; Zhou, M.J.	
Modelling and optimization of sulfur addition during 70MnVS4 steelmaking: An industrial case study	253
Kovačič, M.; Lešer, B.; Brezocnik, M.	
Calendar of events	262
Notes for contributors	263

Journal homepage: apem-journal.org

ISSN 1854-6250 (print)

ISSN 1855-6531 (on-line)

Published by CPE, University of Maribor.

Scope and topics

Advances in Production Engineering & Management (APEM journal) is an interdisciplinary refereed international academic journal published quarterly by the *Chair of Production Engineering* at the *University of Maribor*. The main goal of the *APEM journal* is to present original, high quality, theoretical and application-oriented research developments in all areas of production engineering and production management to a broad audience of academics and practitioners. In order to bridge the gap between theory and practice, applications based on advanced theory and case studies are particularly welcome. For theoretical papers, their originality and research contributions are the main factors in the evaluation process. General approaches, formalisms, algorithms or techniques should be illustrated with significant applications that demonstrate their applicability to real-world problems. Although the *APEM journal* main goal is to publish original research papers, review articles and professional papers are occasionally published.

Fields of interest include, but are not limited to:

Additive Manufacturing Processes	Machine Learning in Production
Advanced Production Technologies	Machine-to-Machine Economy
Artificial Intelligence in Production	Machine Tools
Assembly Systems	Machining Systems
Automation	Manufacturing Systems
Big Data in Production	Materials Science, Multidisciplinary
Block Chain in Manufacturing	Mechanical Engineering
Computer-Integrated Manufacturing	Mechatronics
Cutting and Forming Processes	Metrology in Production
Decision Support Systems	Modelling and Simulation
Deep Learning in Manufacturing	Numerical Techniques
Discrete Systems and Methodology	Operations Research
e-Manufacturing	Operations Planning, Scheduling and Control
Evolutionary Computation in Production	Optimisation Techniques
Fuzzy Systems	Project Management
Human Factor Engineering, Ergonomics	Quality Management
Industrial Engineering	Risk and Uncertainty
Industrial Processes	Self-Organizing Systems
Industrial Robotics	Smart Manufacturing
Intelligent Manufacturing Systems	Statistical Methods
Joining Processes	Supply Chain Management
Knowledge Management	Virtual Reality in Production
Logistics in Production	

Hybrid ANFIS-Rao algorithm for surface roughness modelling and optimization in electrical discharge machining

Agarwal, N.^{a,*}, Shrivastava, N.^a, Pradhan, M.K.^b

^aDepartment of Mechanical Engineering, UIT, Rajiv Gandhi Proudyogiki Vishwavidyalaya, Bhopal, India

^bDepartment of Mechanical Engineering, Maulana Azad National Institute of Technology, Bhopal, India

ABSTRACT

Advanced modeling and optimization techniques are imperative today to deal with complex machining processes like electric discharge machining (EDM). In the present research, Titanium alloy has been machined by considering different electrical input parameters to evaluate one of the important surface integrity (SI) parameter that is surface roughness *Ra*. Firstly, the response surface methodology (RSM) has been adopted for experimental design and for generating training data set. The artificial neural network (ANN) model has been developed and optimized for *Ra* with the same training data set. Finally, an adaptive neuro-fuzzy inference system (ANFIS) model has been developed for *Ra*. Optimization of the developed ANFIS model has been done by applying the latest optimization techniques Rao algorithm and the Jaya algorithm. Different statistical parameters such as the mean square error (MSE), the mean absolute error (MAE), the root mean square error (RMSE), the mean bias error (MBE) and the mean absolute percentage error (MAPE) elucidate that the ANFIS model is better than the ANN model. Both the optimization algorithms results in considerable improvement in the SI of the machined surface. Comparing the Rao algorithm and Jaya algorithm for optimization, it has been found that the Rao algorithm performs better than the Jaya algorithm.

ARTICLE INFO

Keywords:

Electrical-discharge machining (EDM);
Titanium alloy;
Surface roughness;
Modelling;
Optimization;
Artificial neural networks (ANN);
Adaptive neuro fuzzy inference system (ANFIS);
Rao algorithm;
Jaya algorithm

*Corresponding author:

neeraj.bhopal@gmail.com
(Agarwal, N.)

Article history:

Received 27 October 2021

Revised 14 March 2021

Accepted 15 May 2021



Content from this work may be used under the terms of the Creative Commons Attribution 4.0 International Licence (CC BY 4.0). Any further distribution of this work must maintain attribution to the author(s) and the title of the work, journal citation and DOI.

1. Introduction

Electrical discharge machining (EDM) is used to machine materials that are difficult to machine [1-2]. In EDM, sparking takes place between the workpiece and tool electrode in the machining zone and due to sparking the removal of material takes place by melting and evaporation [3-4]. Shrivastava *et al.* reviewed the EDM-based hybrid machining process to enhance the different machining performance [5]. Titanium alloy possesses excellent mechanical properties, but it has poor machinability towards conventional machining [6]. Qudeiri *et al.* did an extensive review on EDM of the Titanium alloy and provided valuable research directions [7]. Kumar *et al.* presented an extensive review of the EDM machining of Titanium alloy and discussed important qualitative and quantitative aspects [8]. To control the EDM process, a wide range of control parameters are available. Control parameters and their range significantly affect the quality re-

sponse and hence the appropriate selection of control parameters is necessary to improve the process efficiency [9]. The most important consistency indicator of the machining method is surface roughness. The reliability, wear, and corrosion resistance and the substance are enhanced by good surface integrity [10-11]. After review of the literature, four important control parameters, peak-current (X_1), pulse-on-time (X_2), duty-factor (X_3), and voltage (X_4) selected for the research [12-13].

Response surface methodology (RSM) offers a minimum number of experiments required and inherits enormous information [14-15]. It is also used as an optimization tool for the process. RSM uses a sequence for the design of experiments (DOE) to gather information and establish a relation between input and output with a second-degree polynomial regression model [16-17].

A model depicts the relation between control parameters with one or more quality responses [18]. RSM is the most popular tool for the development of the regression model and as an optimization tool, but the regression model is not suitable for noisy data. This leads to an inefficient model with higher prediction errors [19]. Artificial intelligence is widely adopted in manufacturing industries nowadays. The ANN is a popular modeling technique [20]. Researchers concluded that the ANN model has higher performance as compared to the regression model [21-22]. The ANFIS model combines both the fuzzy set and the ANN model. The ANFIS is gaining popularity as a modeling tool [23]. Buragohain *et al.* used a full factorial design to train the ANFIS model [24]. The ANFIS model is trained by gradient descent or least square estimation. Now a day, heuristic optimization algorithms like the Genetic Algorithm (GA), and many other tools are widely used to train the model to minimize error. It is found that a heuristic-based algorithm produces better results [25-26]. The ANN model and the ANFIS model have a better prediction efficiency as compared to the regression model [27]. The ANFIS and the ANN model have approximately similar accuracy [28]. Generally, large experimental data is used as training data. To minimize the training data requirement, RSM is adopted as an experimental design, and for generating the training data set.

Model of any process generally used for prediction purposes. Researchers are interested to find an optimum solution of the process output, to effectively utilize the resource [29]. A predictable model is used in optimization where one or more response is optimized with an optimization technique. Classical optimization is not able to solve complex problems [30]. To overcome the limitation of classical optimization, metaheuristic or advanced optimization is used. Particle swarm optimization (PSO), GA, ACO, is the most popular metaheuristic optimization algorithm [31]. Klancnik *et al.* proposed a new gravitational search algorithm for optimization [32]. Jaya algorithm is a new advanced optimization tool. In this, algorithm-specific parameters are not required. The solution moves towards the best solution iteratively [33-34]. Rao *et al.* proposed MO Jaya algorithm for multi-response optimization [35]. Singh *et al.* applied MO Jaya algorithm for simultaneous optimization of three responses [36]. Al-Refaie *et al.* used pentagonal fuzzy regression modeling to optimize multiple process measures [37]. Payal *et al.* did the parametric optimization investigation for EDM of Inconel 825 with seven controllable parameters [38]. Daneshmand *et al.* investigate the effect of input parameters on surface roughness during EDM of CK45 steel [39]. Rao optimization is a newly proposed, simple, and powerful optimization tool for technique engineering optimization. Rao optimization is a metaphor-less algorithm [40]. RSM is a widely used optimization tool, but for noisy data, it is not appropriate. Rao reviewed an advanced optimization technique used in modern machining processes [41]. Recently, most researchers used RSM as a modeling and optimization tool. The ANN model is also optimized by advanced optimization by researchers with a better result. In the literature review, advanced optimization is limited to train the ANFIS model only [42]. Singh *et al.* used an integrated GA-ANFIS model where GA is adopted for the training of the ANFIS network [43]. There is no work reported on the ANFIS model optimization using advanced optimization for surface roughness or EDM machining. This is a major research gap.

After an exhaustive literature survey, the authors concluded that there is no work reported in the EDM machining process where the ANFIS model is optimized for quality measures by an advanced optimization technique. So, in this work, the ANFIS trained model is optimized for one of the major quality response i.e. surface roughness (Ra). The ANFIS offers an accurate, predicta-

ble model for complex machining processes like EDM. This ANFIS model is optimized by the Rao algorithm and Jaya Algorithm for better optimum results. The Rao algorithm is suitable to optimize the ANFIS model under 50 iterations. The ANN model for the EDM process is also developed and optimized using Rao optimization. ANFIS model offers better prediction results as compared to the ANN model.

2. Experimental setup

For the study, a plate of titanium alloy 685 was chosen. As an electrode, a copper tool with a diameter of 10 mm is picked. Minitab 18 software is used to implement the RSM design of experiments. Four important control parameters, peak current (X_1), pulse on time (X_2), duty factor (X_3), and voltage (X_4) are selected as a control parameter, surface roughness (Ra) is selected as process outcome. The thirty machining operation is performed as per DOE. Table 1 depicts parameters for process control and their level. Table 2 displays the experimental observation. Surface roughness is measured with profilometer "TESA-rugosurf 10-G" having 0.001 μm accuracy.

Table 1 Process control parameters and their level

Parameters	X_1 (A)	X_2 (μs)	X_3 (%)	X_4 (V)
Level 1	4.0	50.0	25.0	40.0
Level 2	6.0	100.0	37.5	70.0
Level 3	8.0	150.0	50.0	100.0

Table 2 Experimental observations

No.	X_1 (A)	X_2 (μs)	X_3 (%)	X_4 (V)	Ra (μm)
1	8	150	50	40	5.134
2	8	50	25	40	3.152
3	4	50	25	40	2.952
4	8	50	50	40	5.294
5	6	100	37.5	70	3.784
6	6	100	37.5	70	3.815
7	6	100	37.5	70	3.746
8	4	50	50	40	3.267
9	4	150	50	40	4.202
10	4	150	25	100	3.954
11	4	150	25	40	4.468
12	4	50	50	100	4.138
13	4	50	25	100	3.274
14	8	50	50	100	6.637
15	6	100	37.5	70	3.812
16	8	150	50	100	5.260
17	8	150	25	100	4.480
18	8	150	25	40	3.993
19	4	150	50	100	3.880
20	8	50	25	100	4.267
21	6	50	37.5	70	3.581
22	6	100	37.5	40	3.716
23	6	100	37.5	100	4.092
24	6	100	50	70	4.334
25	6	100	25	70	3.543
26	6	100	37.5	70	3.727
27	6	150	37.5	70	3.632
28	8	100	37.5	70	4.129
29	6	100	37.5	70	3.872
30	4	100	37.5	70	3.506

3. Modeling

Model is the relation between control parameters and process outcomes. Nowadays the intelligent model is popular for modeling complex processes. An artificial neural network (ANN) is an interconnected network of neurons. The adaptive neuro-fuzzy inference system (ANFIS) model combines a fuzzy set into ANN, thus it inherits the advantages of fuzzy systems and the ANN.

3.1 The ANFIS model

The ANFIS model is developed to predict the surface roughness (*Ra*). Fig. 1 depicts the ANFIS architecture.

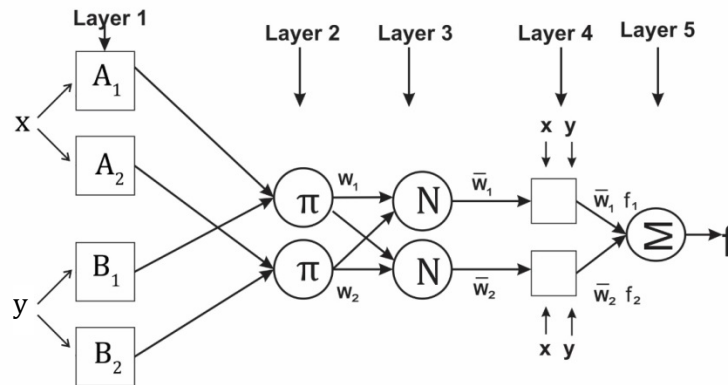


Fig. 1 The adaptive network-based fuzzy interface system architecture

There are two inputs in the model: *x, y*, and one output. Both fuzzy logic and ANN are merged into the ANFIS scheme. Sugeno fuzzy model first-order, there are two If-then laws used as

Rule 1: If *x* is *A*₁ and *y* is *B*₁, then $f_1 = l_1x + m_1y + n_1$

Rule 2: If *x* is *A*₂ and *y* is *B*₂, then $f_2 = l_2x + m_2y + n_2$

The (*l_z, m_z, and n_z*) is a set of parameters related to the process.

Layer 1 is known as the fuzzified layer and it calculates the membership function (MF) value of the premise parameter. Every node is squarely in this layer. ‘Trimf’ and ‘trmpmf’ are popular MFs for the experimental data.

$$O_{1,i} = \mu A_i(x) \text{ for } i = 1,2 \text{ or}$$

$$O_{1,i} = \mu B_i(y) \text{ for } i = 3,4$$

$$\mu A_i(x) = \frac{1}{1 + \left| \frac{x - c_i}{a_i} \right|^{2b_i}} \tag{1}$$

The (*a_i, b_i, and c_i*) is a set of parameters.

Layer 2 is considered as a layer of law. The second layer reflects the shooting force of the rules. Every node is a circle in this layer and labeled as Π. T-norms operator (like min, product, fuzzy AND) rule applies in this layer. The response of the second layer is given in Eq. 2.

$$O_{2,i} = w_i = \mu A_i(x) * \mu B_i(y) \text{ for } i = 1, 2 \tag{2}$$

Layer 3 is known as normalizing firing strength. Every node is a circle in this layer and labeled as *N*. The *i*-th node calculates the ratio of the *i*-th rule’s firing strength to the sum of all rules firing strengths. It is also known as normalized firing strength as follows.

$$O_{3,i} = \bar{w}_i = \frac{w_i}{w_1 + w_2} \text{ where } i = 1,2 \tag{3}$$

Layer 4: Every node *i* is an adaptive node with a function as follows

$$O_{4,i} = \bar{w}_i f_i = \bar{w}_i (l_i x + m_i y + n_i) \tag{4}$$

Where *i* = 1, 2 and *w_i* is a normalized firing strength from layer 3 and (*l_i, m_i, n_i*) is the set of parameters for this particular node. This layer computes the contribution of each *i*-th rules towards the total output

Layer 5 is known as overall output. This is labeled as Σ. By adding up all incoming signals, determines the total performance.

Overall output is given below

$$O_{5,1} = \sum \bar{w}_i f_i = \frac{\sum w_i f_i}{\sum w_i} \text{ where } i = 1, 2. \tag{5}$$

Matlab 2015a is used to form the ANFIS model. There are several MFs and MF type is available for training for the ANFIS model. Table 3 shows the ANFIS training parameters. These parameters are decided after trial and error to minimize the error. Fig. 2 shows The ANFIS model for this study. Fig. 3 depicts the error curve for the ANFIS model training. All input is connected to 'inputmf'. There is a rule layer between 'inputmf' and 'outputmf'. All output signals from 'outputmf' is summed at the junction to produce output. For X_1 and X_3 , Fig. 4 displays the surface plot. The surface plot for X_1 and X_4 is depicted in Fig. 5. The surface plot for X_3 and X_4 is shown in Fig. 6.

Table 3 ANFIS training parameters selected

ANFIS parameter	Selected parameter
Membership function (MFs)	trimf (Triangular membership function)
Numbers of Mfs	2 2 2 2
Numbers of epochs	1000
Output MF function	Linear
Training function	Hybrid

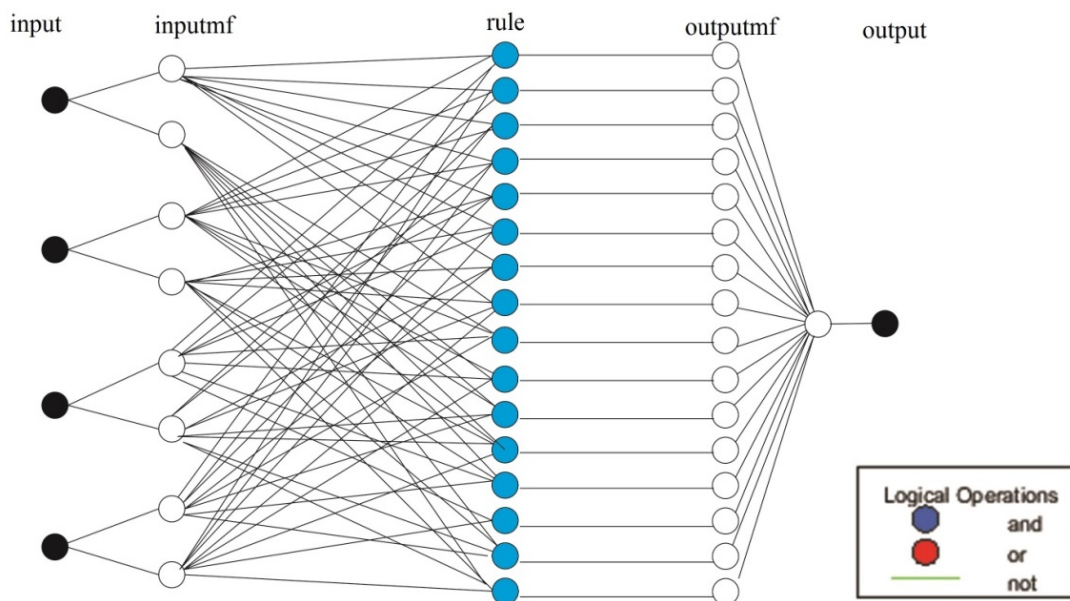


Fig. 2 The ANFIS architecture with four inputs and one output

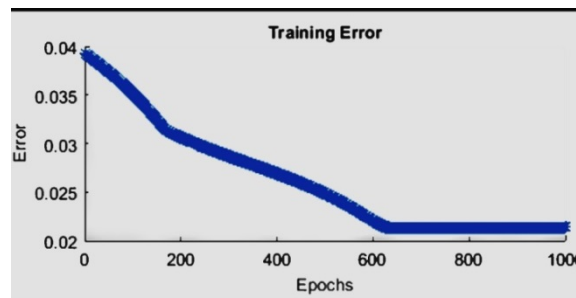


Fig. 3 Error curve for the training of the ANFIS model

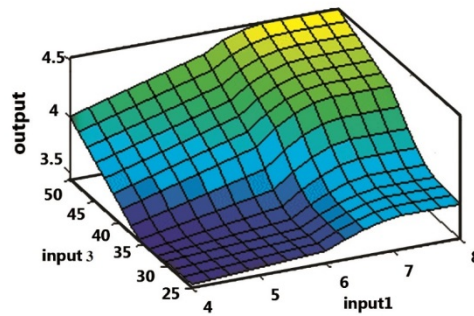


Fig. 4 The surface plot for surface roughness where output is Ra , input1 is X_1 , input3 is X_3 (hold values $X_2 = 100 \mu s$ and $X_4 = 70 V$)

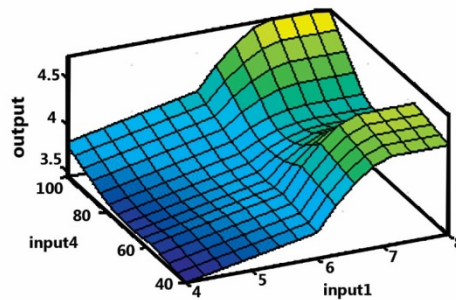


Fig. 5 Surface plot for surface roughness where output is Ra , input1 is X_1 , input4 is X_4 (hold values $X_2 = 100 \mu s$ and $X_3 = 37.5 \%$)

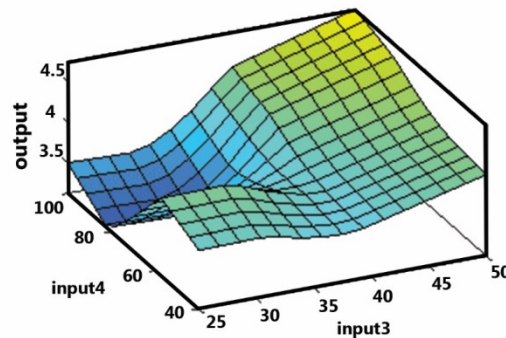


Fig. 6 Surface plot for surface roughness where output is Ra , input3 is X_3 , input4 is X_4 (hold values of X_2 is $100 \mu s$ and $X_1 = 6A$)

3.2 The ANN Model

Several interconnected neurons form an ANN network. There are an input layer, an output layer and a hidden layer exist in an ANN network. The input layer and output layer are connected by few hidden layers. The cumulative number of neurons in the input layer equals to the number of input. There are four input parameters, hence input layer has four neurons. The output layer's number of neurons is equal to the model's output. There is one output, hence output layer has a single neuron. After experimenting with various combinations, it is found that a single hidden layer with the five neurons generates a better predictive model. The activation function 'logsig' is used between the input layer and hidden layer. The 'purelin' transfer function is used for the output layer.

The activation function 'purelin' is used with the output layer. To train the network, the back-propagation algorithm is adopted. It is based on gradient descent. It updates the weight of the layer to minimize the mean square error (MSE). The network is trained using the experimental data from Table 2. Fig. 7 shows the ANN architecture.

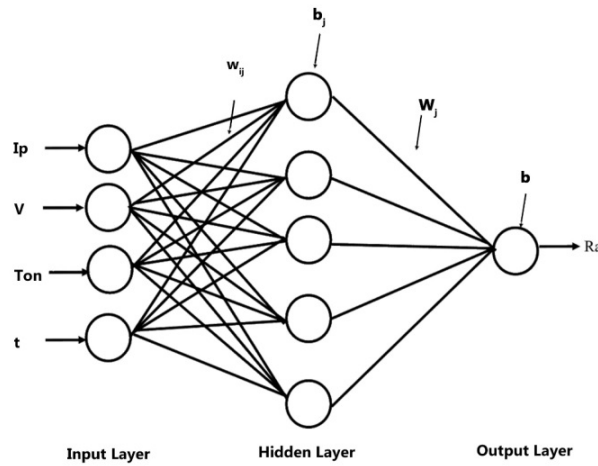


Fig. 7 The ANN architecture

Input layer: There are four inputs in the model, hence four neurons present in this layer.

Hidden Layer: Every neuron of the hidden layer receives input from all neurons of the input layer. It is multiplied by weight w_{ij} with addition to bias b_j . The net input received by each neuron as the following Eq. 6.

$$net_j = \sum_0^j w_{ij}x_i + b_j \quad (6)$$

Where j is a number of neurons in the hidden layer, x_i is input quantity, w_{ij} is weight of i -th input to j -th neuron, b_j is bias of j -th neuron.

The output from the input layer's neurons is fed into the activation function 'logsig' which converts the input signal into the output of the given neuron. The net summation of the j -th neuron is fed into activation function 'logsig' and the output of j -th neuron is given in the following Eq. 7.

$$out_j = f(net_j) = \frac{1}{1 + e^{(-net_j)}} \quad (7)$$

Output layer: There is 1 neuron in this layer. The output from each of the hidden layer's neurons is now multiplied by the individual weight. The signal from all neurons goes to the summation junction with an addition of the bias, then fed into activation function 'purelin' to generate the final output (Ra). The output is represented in the following Eq. 8, where b is the bias for the output.

$$output = \sum_0^j w_j out_j + b \quad (8)$$

3.3 The evaluation criteria

There is a statistical tool used to calculate the error and efficiency of the model. MSE measures the average of the square of the errors, MAE is the average of the absolute errors, RMSE is the square root of MSE, MBE is the average value of errors, MAPE is the mean absolute percentage error, whereas NSE is the efficiency of the model.

$$MSE = \frac{\sum_{i=1}^n (E_i - P_i)^2}{n} \quad (9)$$

$$RMSE = \sqrt{\frac{\sum_{i=1}^n (E_i - P_i)^2}{n}} \quad (10)$$

$$MAE = \frac{\sum_{i=1}^n |E_i - P_i|}{n} \quad (11)$$

$$MBE = \frac{\sum_{i=1}^n (E_i - P_i)}{n} \tag{12}$$

$$MAPE = \frac{\sum_{i=1}^n \left| \frac{(E_i - P_i)}{E_i} \right|}{n} \tag{13}$$

$$NSE = 1 - \frac{\sum_{i=1}^n (E_i - P_i)^2}{\sum_{i=1}^n (E_i - \bar{E})^2} \tag{14}$$

Where E_i is observed value, P_i is predicted value from the model, n is total number of experiments, \bar{E} is mean of the observed value.

4. Optimization

4.1 Rao optimization for the ANFIS model

The ANFIS model is made with Matlab software. A Matlab program is written to optimize the ANFIS model. The flow chart is given in Fig. 8. The objective is to minimize the surface roughness (Ra).

Step 1: All variables are randomly generated within the upper bound and lower bound as an initial solution Constraints are $4 \leq X_1 \leq 8$, $50 \leq X_2 \leq 150$, $25 \leq X_3 \leq 50$, $40 \leq X_4 \leq 100$. Initial solutions are simulated in the ANFIS model and corresponding Ra is recorded in Table 4.

Table 4 Initial solution for Rao optimization.

Candidate	X_1 (A)	X_2 (μ s)	X_3 (%)	X_4 (V)	Ra (μ m)	Status
1	7.6672	95.14	42.6479	80.5815	4.3819	
2	5.6282	106.4608	32.7404	42.4912	3.7440	
3	7.6384	100.0375	49.1606	94.5473	4.8520	worst
4	7.4458	144.7569	46.2096	73.229	4.6217	
5	4.9393	51.6323	27.4826	90.5408	3.0694	best

Step 2: New value of the variable is calculated as follows the formula, Eq. 15.

$$X'_{j,k,i} = X_{j,k,i} + r_{1,j,i}(X_{j,best,i} - X_{j,worst,i}) \tag{15}$$

There are a number of iterations required to solve this optimization problem. If i is current iteration, j represents for j -th variable, k represents for candidate number. Where $X'_{j,k,i}$ is new value of variable, $X_{j,k,i}$ is old value of variable, $r_{1,j,i}$ is random number of variable j , $X_{j,best,i}$ is best value j -th variable k -th candidate at i -th iteration, $X_{j,worst,i}$ is worst value j -th variable k -th candidate at i -th iteration. Candidate 5 is chosen as the best candidate since it has the lowest Ra value and all variables are marked as best variable as X_{1_best} is 4.9393, X_{2_best} is 51.6323, X_{3_best} is 27.4826, X_{4_best} is 90.5408. Candidate 3 has highest value of objective function Ra , hence it selected as worst candidate and corresponding variables are marked as worst candidate as X_{1_worst} is 7.6384, X_{2_worst} is 100.0375, X_{3_worst} is 49.1606, X_{4_worst} is 94.5473. There are four random number $r_1 = 0.3135$, $r_2 = 0.5200$, $r_3 = 0.1954$, $r_4 = 0.0131$ for X_1 , X_2 , X_3 , and X_4 respectively. The new calculated value of variables are shown in Table 5.

The new value of the variable for candidate 1 is:

$$X_1 \text{ for candidate 1: } 7.6672 + 0.3135(4.9393 - 7.6384) = 6.8211,$$

$$X_2 \text{ for candidate 1: } 95.14 + 0.5200(51.6323 - 100.0375) = 69.9679,$$

$$X_3 \text{ for candidate 1: } 42.6479 + 0.1954(27.4826 - 49.1606) = 38.413,$$

$$X_4 \text{ for candidate 1: } 80.5815 + 0.0131(90.5408 - 94.5473) = 80.5289.$$

Similarly, candidates 2, 3, 4, and 5 are calculated. All candidates to the ANFIS model simulated for Ra value and the corresponding Ra value is recorded in Table 5.

Table 5 New value of variables for Rao optimization

Candidate	X_1 (A)	X_2 (μ s)	X_3 (%)	X_4 (V)	Ra (μ m)
1	6.8211	69.9679	38.413	80.5289	4.8138
2	4.7821	81.2887	28.5056	42.4386	4.0047
3	6.7922	74.8654	44.9257	94.4947	5.6586
4	6.5996	119.5847	41.9748	73.1764	3.8493
5	4.0931	50	25	90.4882	3.0212

Step 3: There is a comparison between Tables 4 and 5 for a better value of Ra . Since candidate 1 of Table 4 has a lower Ra value as compare to Table 5, hence candidate 1 is selected from Table 4 and placed as nominee 1 in Table 6. Similarly, members 2, 3 are selected from Table 4 and inserted into Table 6 as candidates 2 and 3. Similarly, candidate 4 and candidate 5 have better objective values in Table 5 hence candidate 4 and candidate 5 are selected from table 5 and inserted into Table 6 as candidate 4 and candidate 5 respectively. Table 6 shows a modified variable value for the Rao algorithm.

Step 4: Repeat 100 iteration and report the optimum solution. Table 7 shows the iteration-wise best results.

Table 6 The modified variable value for the Rao algorithm

Candidate	X_1 (A)	X_2 (μ s)	X_3 (%)	X_4 (V)	Ra (μ m)	Status
1	7.6672	95.14	42.6479	80.5815	4.3819	From Table 4
2	5.6282	106.4608	32.7404	42.4912	3.7440	From Table 4
3	7.6384	100.0375	49.1606	94.5473	4.8520	From Table 4
4	6.5996	119.5847	41.9748	73.1764	3.8493	From Table 5
5	4.0931	50	25	90.4882	3.0212	From Table 5

Table 7 The best result selected from each iteration for Rao optimization

Iteration No.	X_1 (A)	X_2 (μ s)	X_3 (%)	X_4 (V)	Ra (μ m)
1	4.9393	51.6323	27.4826	90.5408	3.0694
2	4.0931	50	25	90.4882	3.0212
3	4	50	25	88.6559	2.9679
4	4	50	25	87.0529	2.9246
5	4	50	25	87.0529	2.9246
6	4	50	25	76.1071	2.9158
7	4	50	25	85.2707	2.8766
8	4	50	25	80.0359	2.8181
9	4	50	25	80.9771	2.7949
10	4	50	25	80.9771	2.7949
11	4	50.5715	25	81.5514	2.7859
12	4	50	25	81.5721	2.7804
24	4.0097	50.0018	25.0032	81.6323	2.7793
27	4.0008	50.0008	25	81.6348	2.7789
30	4	50	25	81.6445	2.7787

4.2 Jaya algorithm for the ANFIS model optimization

With the Jaya algorithm, a Matlab program is written to optimize the ANFIS model. In Fig. 8, the flow diagram of the process is given.

$$X'_{j,k,i} = X_{j,k,i} + r_{1,j,i} * (X_{j,best,i} - |X_{j,k,i}|) - r_{2,j,i} * (X_{j,worst,i} - |X_{j,k,i}|) \tag{16}$$

Where If i is current iteration, j represents for j -th variable, k represents for candidate number. Where $X'_{j,k,i}$ is new value of variable, $X_{j,k,i}$ is old value of variable, $r_{1,j,i}$, and $r_{2,j,i}$ are random numbers for j -th variable, $X_{j,best,i}$ is best value j -th variable k -th candidate at i -th iteration, $X_{j,worst,i}$ is worst value j -th variable k -th candidate at i -th iteration.

Step 1: Inside the upper and the lower boundaries, all variables are created randomly as an initial solution. Constraints are $4 \leq X_1 \leq 8$, $50 \leq X_2 \leq 150$, $25 \leq X_3 \leq 50$, $40 \leq X_4 \leq 100$. A set of variables (candidate) are communicated to the ANFIS model and a corresponding response (Ra) of the ANFIS model is recorded in Table 8. Since if surface roughness is lower, the criteria will be

better, hence candidate 1 is marked as the best candidate (marked best variable as $X_{1_best} = 7.1251$, $X_{2_best} = 109.6631$, $X_{3_best} = 29.36$, $X_{4_best} = 44.8277$) while candidate 2 is marked as the worst candidate because it has the highest value of Ra (hence marked worst variables are as $X_{1_worst} = 7.315$, $X_{2_worst} = 96.5559$, $X_{3_worst} = 44.8495$, and $X_{4_worst} = 52.0834$).

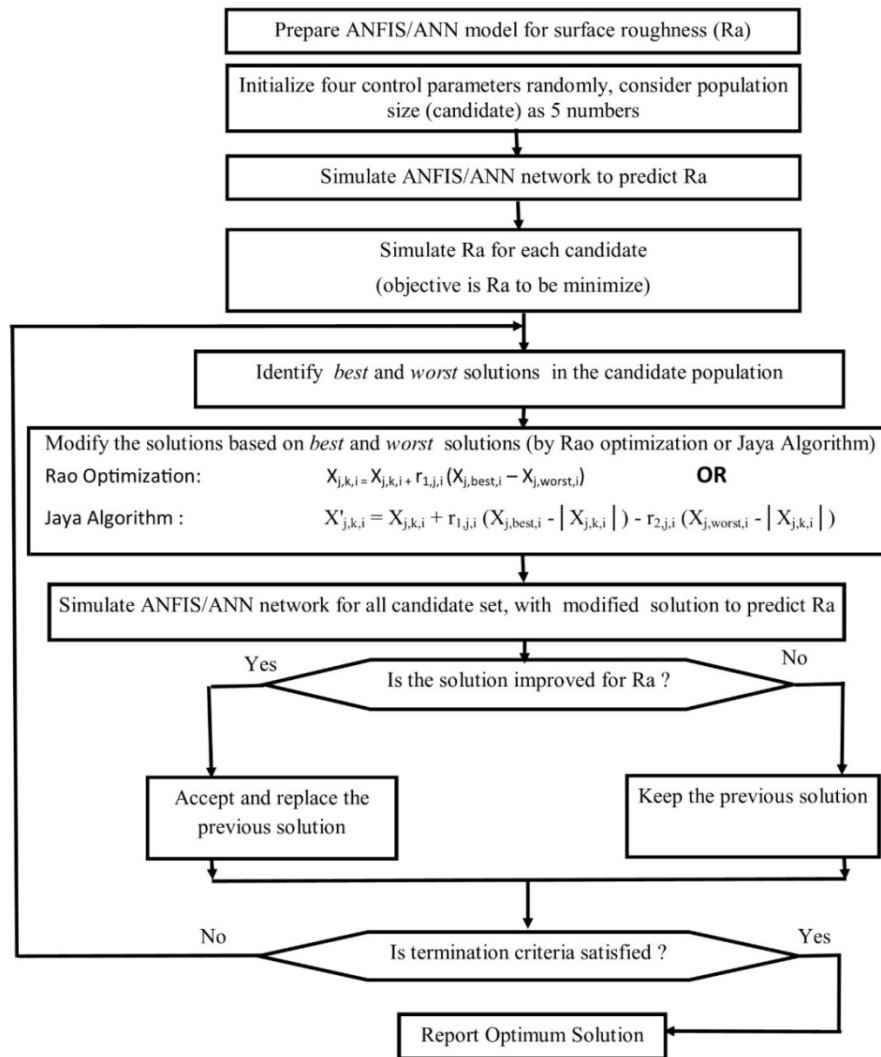


Fig. 8 Flow diagram of the ANFIS/ANN model optimization

Table 8 The initial solution for Jaya algorithm

Candidate	X_1 (A)	X_2 (μ s)	X_3 (%)	X_4 (V)	Ra (μ m)	Status
1	7.1251	109.6631	29.3623	44.8277	3.5789	best
2	7.315	96.5559	44.8495	52.0834	5.0244	worst
3	4.6139	96.2368	41.8183	55.3064	3.6694	
4	4.2459	140.9336	47.9749	77.332	3.5931	
5	6.3595	65.9438	39.0437	62.5608	4.4153	

Step 2: Eq. 16 is used to calculate the value of new variables. Consider the random number $r_1 = 0.3590$, $r_2 = 0.0287$ for X_1 , $r_3 = 0.7674$, and $r_4 = 0.2374$ for X_2 , $r_5 = 0.6659$ $r_6 = 0.7485$ for X_3 , $r_7 = 0.7284$ $r_8 = 0.8143$ for X_4 .

X_1 for candidate 1:

$$7.1251 + 0.3590(7.1251 - |7.1251|) - 0.0287(7.315 - |7.1251|) = 7.1197$$

X_2 for candidate 1:

$$109.6631 + 0.7674(109.6631 - |109.6631|) - 0.2374(96.5559 - |109.6631|) = 112.7745$$

X_3 for candidate 1:

$$29.3623 + 0.6659(29.3623 - |9.3623|) - 0.7485(44.8495 - |29.3623|) = 17.7701$$

(= 25 lower bound)

X_4 for candidate 1:

$$44.8277 + 0.7284(44.8277 - |44.8277|) - 0.8143(52.0834 - |44.8277|) = 38.9193$$

(= 40 lower bound)

These new variables are communicated to the ANFIS model and corresponding Ra records in Table 9, similar calculation is done for candidates 2, 3, 4 and 5 and recorded in the table.

Step 3: The Ra of Tables 8 and 9 are compared for better value and select the candidate with better Ra and insert into Table 10.

Step 4: The first iteration is over, now repeat a similar procedure for a few iterations. A total of 67 iterations are required to achieve the solution.

Table 9 New value of variables for Jaya algorithm

Candidate	X_1 (A)	X_2 (μ s)	X_3 (%)	X_4 (V)	Ra (μ m)
1	7.1197	112.7745	25*	40*	3.4345
2	7.2469	106.614	34.5364	46.7981	3.9293
3	5.4379	106.464	31.2549	50.2978	3.8770
4	5.1915	127.472	37.9199	74.2143	3.3248
5	6.607	92.226	28.2512	58.175	4.2568

* Means adjusted to lower/upper bound

Table 10 The updated value of the variable for the Jaya algorithm

Candidate	X_1 (A)	X_2 (μ s)	X_3 (%)	X_4 (V)	Ra (μ m)	Status
1	7.1197	112.7745	25	40	3.4345	From Table 9
2	7.2469	106.614	34.5364	46.7981	3.9293	From Table 9
3	4.6139	96.2368	41.8183	55.3064	3.6694	From Table 8
4	5.1915	127.472	37.9199	74.2143	3.3248	From Table 9
5	6.607	92.226	28.2512	58.175	4.2568	From Table 9

Table 11 Best result selected from each iteration for Rao optimization

Iteration No.	X_1 (A)	X_2 (μ s)	X_3 (%)	X_4 (V)	Ra (μ m)
1	7.12	109.6631	29.3623	44.8277	3.5789
2	5.1915	127.472	37.9199	74.2143	3.3248
3	5.1915	127.472	37.9199	74.2143	3.3248
4	4.4527	136.1197	36.8609	81.7775	3.2419
5	4.4868	121.3322	35.2794	77.0596	3.1456
40	4	120.5003	36.1024	74.6033	3.0936
55	4	92.1362	29.0386	84.1491	3.0655
59	4	94.2808	28.7777	81.9607	3.0152
62	4	62.3788	27.9143	81.973	2.8921
63	4	54.0164	27.605	82.1781	2.8256
64	4	52.8637	27.5728	81.6957	2.8026
65	4	50.4888	27.5587	81.5481	2.7831
66	4.0061	50	27.0561	81.5907	2.7784
67	4.007	50	26.6052	81.6279	2.7779
68	4.0041	50	26.6336	81.6432	2.7774

4.3 Optimization of the ANN model

A predictable ANN model of Ra is developed. The Jaya algorithm is used to optimize this model.

Step 1: Population size 5 is considered. Table 12 shows the initial solution. Random numbers within the selected range serve as initial variables. The ANN model is simulated for this input set and corresponding responses of Ra are recorded. The flow chart is shown in Fig. 8. Since surface roughness is better for smaller values, hence candidate 3 is marked as the best candidate while candidate 2 is marked as the worst candidate.

Table 12 Initial solution and corresponding predicted *Ra* value

Candidate	X_1 (A)	X_2 (μ s)	X_3 (%)	X_4 (V)	Predicted <i>Ra</i> (μ m)	Status
1	7.2589	140.5792	28.1747	94.8026	4.5768	
2	6.5294	145.7507	48.9292	65.3057	5.1702	worst
3	4.3902	146.4889	37.1344	94.9441	3.7971	best
4	5.114	65.7613	45.007	87.5324	4.061	
5	6.1875	147.0593	28.5472	97.5695	4.603	

Eq. 15 is used to calculate the new value of parameters. These new values of parameters are used to simulate *Ra* from the ANN model and corresponding *Ra* values are recorded in Table 13. Matlab 2015 software is used for the calculation.

Step 2: Two random numbers $r_1= 0.82$ and $r_2= 0.86$ are considered for calculation. Variables corresponding to the best candidate 3 are marked as the best variables, hence Marked $X_{1_best} = 4.3902$, $X_{2_best} = 146.4889$, $X_{3_best} = 37.1344$, and $X_{4_best} = 94.9441$. Corresponding to candidate 2, all variable have been marked as worst variables as $X_{1_worst} = 6.5294$, $X_{2_worst} = 145.7507$, $X_{3_worst} = 48.9292$ and $X_{4_worst} = 65.3057$. The calculation for the new value of the variables is as per the Eq. 15 as follows.

X_1 for candidate 1:

$$7.2589 + 0.82(4.3902 - |7.2589|) - 0.86(6.5294 - |7.2589|) = 5.533936$$

X_2 for candidate 1:

$$140.5792 + 0.82(146.4889 - |140.5792|) - 0.86(145.7507 - |140.5792|) = 140.977664$$

X_3 for candidate 1:

$$28.1747 + 0.82(37.1344 - |28.1747|) - 0.86(48.9292 - |28.1747|) = 17.672784$$

(=25 as lower limit)

X_4 for candidate 1:

$$94.8026 + 0.82(94.9441 - |94.8026|) - 0.86(65.3057 - |94.8026|) = 120.285964$$

(=100 upper limit)

A similar calculation was done for X_1 , X_2 , and X_3 , X_4 for candidates 2, 3 4, and 5.

Step 3: Tables 12 and 13 are compared, select the candidate with better *Ra*, and insert into Table 13.

Step 4: This process continues for some iterations. A total of 17 iterations of the Jaya algorithm is used to achieve an optimum solution. Table 15 shows the iteration-wise best result.

Table 13 New value of the variable with predicted *Ra*

Candidate	X_1 (A)	X_2 (μ s)	X_3 (%)	X_4 (V)	Predicted <i>Ra</i> (μ m)
1	5.5339	140.9776	25*	100*	4.9376
2	4.7752	146.3560	39.2574	89.6091	3.7629
3	4*	147.1237	26.9908	100*	3.9144
4	4*	63.1670	35.1783	100*	3.6689
5	4.4196	147.7169	25*	100*	4.1232

*Adjusted to lower or upper limit.

Table 14 Updated value of the variable with corresponding *Ra* value

Candidate	X_1 (A)	X_2 (μ s)	X_3 (%)	X_4 (V)	Predicted <i>Ra</i> (μ m)	Status
1	7.2589	140.5792	28.1747	94.8026	4.5768	From Table 12
2	4.7752	146.3560	39.2574	89.6091	3.7629	From Table 13
3	4.3902	146.4889	37.1344	94.9441	3.7971	From Table 12
4	4	63.1670	35.1783	100	3.6689	From Table 13
5	4.4196	147.7169	25*	100*	4.1232	From Table 13

Table 15 Iteration-wise best result.

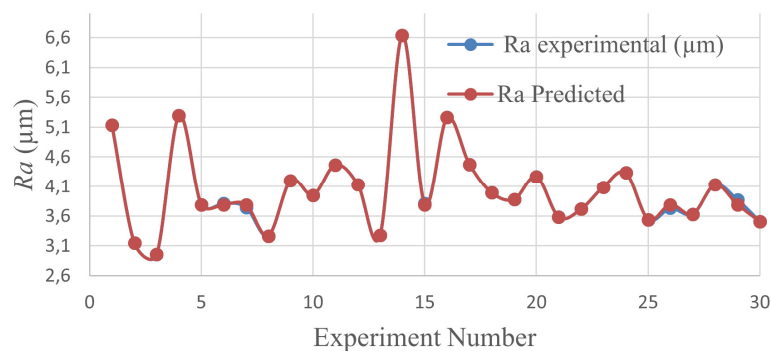
Iteration No.	X_1 (A)	X_2 (μ s)	X_3 (%)	X_4 (V)	Ra
1	4.3902	146.4889	37.1344	94.9441	3.7971
2	4	63.1670	35.1783	100	3.6689
3	4	74.8268	40.9319	94.8336	3.4462
4	4	76.4593	39.5315	95.6589	3.3627
5	4.4139	78.2127	39.6985	58.0534	3.2436
6	4	50	36.3944	66.47	3.1736
7	4.0315	52.6894	30.3658	56.4976	2.9378
8	4	53.1526	30.5158	56.4976	2.9972
9	4	50	31.795	40	2.8705
17	4	50	28.5	52.1	2.8427
100	4	50	28.5	52.1	2.8427

5. Result and discussion

The ANFIS model has a very low MSE 4.5×10^{-4} and the regression coefficient is 'R' = 0.9995. Fig. 9 compares the experimental values of quality characteristics Ra with the ANFIS model predicted values. This indicates a good prediction model. A confirmatory experiment is performed with an optimum set of input variables. The result of confirmatory experiments is given in Table 16. Since the limitation of the EDM machine setting, the value of X_4 is selected as 81 instead of 81.6445. Therefore, the experimental value is rather similar to the expected value, validating the ANFIS model.

The ANN model is developed for quality measure (Ra) and the mean square error of Ra is calculated as 0.0122 and the regression coefficient is 'R' = 0.98862 which is closer to 1. Fig. 10 shows the comparison between experimental versus the ANN model predicted data for Ra . The ANN model is optimized using the Jaya algorithm. The result of confirmatory experiments is given in Table 16.

Comparison between the ANN and ANFIS model: Regression coefficient R and Nash Sutcliffe Efficiency coefficient are higher for the ANFIS model. The error MSE, RMSE, MAE, and MBE are lower for the ANFIS model. Therefore the ANFIS model has better prediction accuracy. Table 17 shows the comparison between the ANN model and the ANFIS model.

**Fig. 9** Comparison result of experimental vs. the ANFIS model predicted data for Ra **Table 16** Confirmatory experiments result

Response	Model	Process variables				Predicted	Experimental	Error (%)
		X_1 (A)	X_2 (μ s)	X_3 (%)	X_4 (V)			
Surface roughness (Ra)	ANFIS	4	50	25	81*	2.790 μ m	2.861 μ m	2.48
Surface roughness (Ra)	ANN	4	50	28*	52*	2.843 μ m	2.945 μ m	3.59

*Adjusted to the nearest available setting of the EDM machine

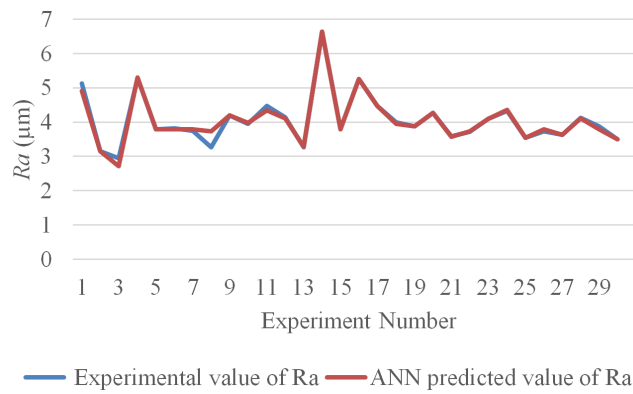


Fig. 10 Comparison results of experimental vs. the ANN model predicted data for Ra

Table 17 Comparison between the ANN and ANFIS model

Property	Measurement	ANFIS	ANN
Model error	MSE	4.5×10^{-4}	0.012205
	RMSE	0.021394	0.110474
	MAE	0.00807701	0.050963
	MBE	4.5169×10^{-5}	0.009038
	MAPE	0.212868 %	1.388436 %
Model efficiency	Nash Sutcliffe efficiency coefficient (NSE)	0.999149	0.97732
	Regression coefficient	0.9995	0.9886

6. Conclusion

Successful machining of Titanium alloy has been done in the present research by using EDM process and performance comparison of Rao Optimization Algorithm and Jaya Algorithm has been done for one of the important surface integrity parameters. Followings are the important findings of the present research work:

- The Rao optimization algorithm demonstrates better performances than the Jaya algorithm as 68 iterations were required by the Jaya algorithm for optimization of the ANFIS model, whereas Rao optimization required only 30 iterations for the same.
- Both the algorithms successfully optimized the ANFIS model and predicted the identical set of input control factors. The input control factors predicted are; peak current $X_1 = 4$ A, pulse-on time $X_2 = 50$ µs, duty factor $X_3 = 25$ %, and voltage $X_4 = 81.6445$ V.
- The ANFIS model is found more accurate prediction model for the machining response as compared to the ANN model for this study. Hence, it can be inferred that the ANFIS model is better than the ANN model under the present machining environment.
- ANN model and the ANFIS model are successfully optimized using the Jaya algorithm and the Rao algorithm.

References

- [1] Jain, V.K. (2009). *Advanced machining processes*, Allied publishers, Mumbai, India.
- [2] Klink, A. (2019). Electric discharge machining, In: Chatti, S., Laperrrière, L., Reinhart, G., Tolio, T. (eds.), *CIRP Encyclopedia of Production Engineering*, Springer, Berlin, Germany, doi: 10.1007/978-3-662-53120-4_6478.
- [3] Abbas, N.M., Solomon, D.G., Bahari, M.F. (2007). A review on current research trends in electrical discharge machining (EDM), *International Journal of Machine Tools and Manufacture*, Vol. 47, No. 7-8, 1214-1228, doi: 10.1016/j.ijmactools.2006.08.026.
- [4] Ho, K.H., Newman, S.T. (2003). State of the art electrical discharge machining (EDM), *International Journal of Machine Tools and Manufacture*, Vol. 43, No. 13, 1287-1300, doi: 10.1016/S0890-6955(03)00162-7.
- [5] Shrivastava, P.K., Dubey, A.K. (2014). Electrical discharge machining-based hybrid machining processes: A review, *Proceedings of the Institution of Mechanical Engineers, Part B: Journal of Engineering Manufacture*, Vol. 228, No. 6, 799-825, doi: 10.1177/0954405413508939.

- [6] Arrazola, P.-J., Garay, A., Iriarte, L.-M., Armendia, M., Marya, S., Le Maître, F. (2009). Machinability of titanium alloys (Ti6Al4V and Ti555.3), *Journal of Materials Processing Technology*, Vol. 209, No. 5, 2223-2230, doi: [10.1016/j.jmatprotec.2008.06.020](https://doi.org/10.1016/j.jmatprotec.2008.06.020).
- [7] Abu Qudeiri, J.E., Mourad, A.-H.I., Ziout, A., Abidi, M.H., Elkaseer, A. (2018). Electric discharge machining of titanium and its alloys: Review, *The International Journal of Advanced Manufacturing Technology*, Vol. 96, 1319-1339, doi: [10.1007/s00170-018-1574-0](https://doi.org/10.1007/s00170-018-1574-0).
- [8] Kumar, S., Singh, R., Batish, A., Singh, T.P. (2012). Electric discharge machining of titanium and its alloys: A review, *International Journal of Machining and Machinability of Materials*, Vol. 11, No. 1, 84-111, doi: [10.1504/IJMMM.2012.044922](https://doi.org/10.1504/IJMMM.2012.044922).
- [9] Muthuramalingam, T., Mohan, B. (2015). A review on influence of electrical process parameters in EDM process, *Archives of Civil and Mechanical Engineering*, Vol. 15, No. 1, 87-94, doi: [10.1016/j.acme.2014.02.009](https://doi.org/10.1016/j.acme.2014.02.009).
- [10] Krishna Mohana Rao, G., Rangajanardhaa, G., Hanumantha Rao, D., Sreenivasa Rao, M. (2009). Development of hybrid model and optimization of surface roughness in electric discharge machining using artificial neural networks and genetic algorithm, *Journal of Materials Processing Technology*, Vol. 209, No. 3, 1512-1520, doi: [10.1016/j.jmatprotec.2008.04.003](https://doi.org/10.1016/j.jmatprotec.2008.04.003).
- [11] Keskin, Y., Halkacı, H.S., Kizil, M. (2006). An experimental study for determination of the effects of machining parameters on surface roughness in electrical discharge machining (EDM), *The International Journal of Advanced Manufacturing Technology*, Vol. 28, 1118-1121, doi: [10.1007/s00170-004-2478-8](https://doi.org/10.1007/s00170-004-2478-8).
- [12] Salonitis, K., Stournaras, A., Stavropoulos, P., Chryssolouris, G. (2009). Thermal modeling of the material removal rate and surface roughness for die-sinking EDM, *The International Journal of Advanced Manufacturing Technology*, Vol. 40, 316-323, doi: [10.1007/s00170-007-1327-y](https://doi.org/10.1007/s00170-007-1327-y).
- [13] Kumar, A., Kumar, V., Kumar, J. (2013). Investigation of machining parameters and surface integrity in wire electric discharge machining of pure titanium, *Proceedings of the Institution of Mechanical Engineers, Part B: Journal of Engineering Manufacture*, Vol. 227, No. 7, 972-992, doi: [10.1177/0954405413479791](https://doi.org/10.1177/0954405413479791).
- [14] Myers, R.H., Montgomery, D.C., Anderson-Cook, C.M. (2016). *Response surface methodology: Process and product optimization using designed experiments*, 4th Edition, John Wiley & Sons, New Jersey, USA.
- [15] Makadia, A.J., Nanavati, J.I. (2013). Optimisation of machining parameters for turning operations based on response surface methodology, *Measurement*, Vol. 46, No. 4, 1521-1529, doi: [10.1016/j.measurement.2012.11.026](https://doi.org/10.1016/j.measurement.2012.11.026).
- [16] Behera, S.K., Meena, H., Chakraborty, S., Meikap, B.C. (2018). Application of response surface methodology (RSM) for optimization of leaching parameters for ash reduction from low-grade coal, *International Journal of Mining Science and Technology*, Vol. 28, No. 4, 621-629, doi: [10.1016/j.ijmst.2018.04.014](https://doi.org/10.1016/j.ijmst.2018.04.014).
- [17] Shandilya, P., Jain, P.K., Jain, N.K. (2012). Parametric optimization during wire electrical discharge machining using response surface methodology, *Procedia Engineering*, Vol. 38, 2371-2377, doi: [10.1016/j.proeng.2012.06.283](https://doi.org/10.1016/j.proeng.2012.06.283).
- [18] Bhowmik, S., Jagadish, Gupta, K. (2019). *Modeling and optimization of advanced manufacturing processes*, Springer International Publishing, Cham, Switzerland, doi: [10.1007/978-3-030-00036-3](https://doi.org/10.1007/978-3-030-00036-3).
- [19] Baş, D., Boyacı, İ.H. (2007). Modeling and optimization I: Usability of response surface methodology, *Journal of Food Engineering*, Vol. 78, No. 3, 836-845, doi: [10.1016/j.jfoodeng.2005.11.024](https://doi.org/10.1016/j.jfoodeng.2005.11.024).
- [20] Casalino, G., Facchini, F., Mortello, M., Mummolo, G. (2016). ANN modelling to optimize manufacturing processes: The case of laser welding, *IFAC-PapersOnLine*, Vol. 49, No. 12, 378-383, doi: [10.1016/j.ifacol.2016.07.634](https://doi.org/10.1016/j.ifacol.2016.07.634).
- [21] Paliwal, M., Kumar, U.A. (2009). Neural networks and statistical techniques: A review of applications, *Expert Systems with Applications*, Vol. 36, No. 1, 2-17, doi: [10.1016/j.eswa.2007.10.005](https://doi.org/10.1016/j.eswa.2007.10.005).
- [22] Ranganathan, S., Senthilvelan, T., Sriram, G. (2010). Evaluation of machining parameters of hot turning of stainless steel (Type 316) by applying ANN and RSM, *Materials and Manufacturing Processes*, Vol. 25, No. 10, 1131-1141, doi: [10.1080/10426914.2010.489790](https://doi.org/10.1080/10426914.2010.489790).
- [23] Çaydaş, U., Haşçalık, A., Ekici, S. (2009). An adaptive neuro-fuzzy inference system (ANFIS) model for wire-EDM, *Expert Systems with Applications*, Vol. 36, No. 3, Part 2, 6135-6139, doi: [10.1016/j.eswa.2008.07.019](https://doi.org/10.1016/j.eswa.2008.07.019).
- [24] Buragohain, M. (2009). *Adaptive network based fuzzy inference system (ANFIS) as a tool for system identification with special emphasis on training data minimization*, Doctoral dissertation, Indian Institute of Technology Guwahati, Assam, India, from <http://gvan.iitg.ernet.in/handle/123456789/256>, accessed October 27, 2020.
- [25] Karaboga, D., Kaya, E. (2016). An adaptive and hybrid artificial bee colony algorithm (aABC) for ANFIS training, *Applied Soft Computing*, Vol. 49, 423-436, doi: [10.1016/j.asoc.2016.07.039](https://doi.org/10.1016/j.asoc.2016.07.039).
- [26] Karaboga, D., Kaya, E. (2019). Adaptive network based fuzzy inference system (ANFIS) training approaches: A comprehensive survey, *Artificial Intelligence Review*, Vol. 52, 2263-2293, doi: [10.1007/s10462-017-9610-2](https://doi.org/10.1007/s10462-017-9610-2).
- [27] Chandrasekaran, M., Muralidhar, M., Krishna, C.M., Dixit, U.S. (2010). Application of soft computing techniques in machining performance prediction and optimization: A literature review, *The International Journal of Advanced Manufacturing Technology*, Vol. 46, 445-464, doi: [10.1007/s00170-009-2104-x](https://doi.org/10.1007/s00170-009-2104-x).
- [28] Yilmaz, I., Kaynar, O. (2011). Multiple regression, ANN (RBF, MLP) and ANFIS models for prediction of swell potential of clayey soils, *Expert Systems with Applications*, Vol. 38, No. 5, 5958-5966, doi: [10.1016/j.eswa.2010.11.027](https://doi.org/10.1016/j.eswa.2010.11.027).
- [29] Mukherjee, I., Ray, P.K. (2006). A review of optimization techniques in metal cutting processes, *Computers & Industrial Engineering*, Vol. 50, No. 1-2, 15-34, doi: [10.1016/j.cie.2005.10.001](https://doi.org/10.1016/j.cie.2005.10.001).
- [30] Yang, X.S. (2013). 1 - Optimization and metaheuristic algorithms in engineering, *Metaheuristics in Water, Geotechnical and Transport Engineering*, 1-23. doi: [10.1016/B978-0-12-398296-4.00001-5](https://doi.org/10.1016/B978-0-12-398296-4.00001-5).
- [31] Beheshti, Z., Shamsuddin, S.M.H. (2013). A review of population-based meta-heuristic algorithm, *International Journal of Advances in Soft Computing and Its Applications*, Vol. 5, No. 1, 1-35.

- [32] Klancnik, S., Hrelja, M., Balic, J., Brezocnik, M. (2016). Multi-objective optimization of the turning process using a Gravitational Search Algorithm (GSA) and NSGA-II approach, *Advances in Production Engineering & Management*, Vol. 11, No. 4, 366-376, [doi: 10.14743/apem2016.4.234](https://doi.org/10.14743/apem2016.4.234).
- [33] Rao, R.V. (2016). Jaya: A simple and new optimization algorithm for solving constrained and unconstrained optimization problems, *International Journal of Industrial Engineering Computations*, Vol. 7, 19-34, [doi: 10.5267/ijieec.2015.8.004](https://doi.org/10.5267/ijieec.2015.8.004).
- [34] Agarwal, N., Shrivastava, N., Pradhan, M.K. (2020). Optimization of relative wear ratio during EDM of titanium alloy using advanced techniques, *SN Applied Sciences*, Vol. 2, Article No. 99, [doi: 10.1007/s42452-019-1877-2](https://doi.org/10.1007/s42452-019-1877-2).
- [35] Rao, R.V., Rai, D.P., Ramkumar, J., Balic, J. (2016). A new multi-objective Jaya algorithm for optimization of modern machining processes, *Advances in Production Engineering & Management*, Vol. 11, No. 4, 271-286, [doi: 10.14743/apem2016.4.226](https://doi.org/10.14743/apem2016.4.226).
- [36] Singh, M., Ramkumar, J., Rao, R.V., Balic, J. (2019). Experimental investigation and multi-objective optimization of micro-wire electrical discharge machining of a titanium alloy using Jaya algorithm, *Advances in Production Engineering & Management*, Vol. 14, No. 2, 251-263, [doi: 10.14743/apem2019.2.326](https://doi.org/10.14743/apem2019.2.326).
- [37] Al-Refaie, A., Lepkova, N., Abbasi, G., Bani Domi, G. (2020). Optimization of process performance by multiple pentagon fuzzy responses: Case studies of wire-electrical discharge machining and sputtering process, *Advances in Production Engineering & Management*, Vol. 15, No. 3, 307-317, [doi: 10.14743/apem2020.3.367](https://doi.org/10.14743/apem2020.3.367).
- [38] Payal, H., Bharti, P.S., Maheshwari, S., Agarwal, D. (2020). Machining characteristics and parametric optimisation of Inconel 825 during electric discharge machining, *Tehnički Vjesnik – Technical Gazette*, Vol. 27, No. 3, 761-772, [doi: 10.17559/TV-20190214135509](https://doi.org/10.17559/TV-20190214135509).
- [39] Daneshmand, S., Neyestanak, A.A.L., Monfared, V. (2016). Modelling and investigating the effect of input parameters on surface roughness in electrical discharge machining of CK45, *Tehnički Vjesnik – Technical Gazette*, Vol. 23, No. 3, 725-730, [doi: 10.17559/TV-20141024224809](https://doi.org/10.17559/TV-20141024224809).
- [40] Rao, R.V. (2020). Rao algorithms: Three metaphor-less simple algorithms for solving optimization problems, *International Journal of Industrial Engineering Computations*, Vol. 11, 107-130, [doi: 10.5267/ijieec.2019.6.002](https://doi.org/10.5267/ijieec.2019.6.002).
- [41] Rao, R.V., Kalyankar, V.D. (2014). Optimization of modern machining processes using advanced optimization techniques: A review, *The International Journal of Advanced Manufacturing Technology*, Vol. 73, 1159-1188, [doi: 10.1007/s00170-014-5894-4](https://doi.org/10.1007/s00170-014-5894-4).
- [42] Liu, P., Leng, W., Fang, W. (2013). Training ANFIS model with an improved quantum-behaved particle swarm optimization algorithm, *Mathematical Problems in Engineering*, Vol. 2013, Article ID 595639, [doi: 10.1155/2013/595639](https://doi.org/10.1155/2013/595639).
- [43] Singh, N.K., Singh, Y., Kumar, S., Upadhyay, R. (2020). Integration of GA and neuro-fuzzy approaches for the predictive analysis of gas-assisted EDM responses, *SN Applied Sciences*, Vol. 2, Article No. 137, [doi: 10.1007/s42452-019-1533-x](https://doi.org/10.1007/s42452-019-1533-x).

A multi-objective optimal decision model for a green closed-loop supply chain under uncertainty: A real industrial case study

Fang, I.W.^a, Lin, W.-T.^b

^aNational ChengChi University, Department of Management Information Systems, Taipei, Taiwan (R.O.C)

^bNational ChengChi University, Department of Management Information Systems, Taipei, Taiwan (R.O.C)

ABSTRACT

Green closed-loop supply chain management is an important topic for business operations today because of increasing resource scarcity and environmental issues. Companies not only have to meet environmental regulations, but also must ensure high quality supply chain operation as a means to secure competitive advantages and increase profits. This study proposes a multi-objective mixed integer programming model for an integrated green closed-loop supply chain network designed to maximize profit, amicable production level (environmentally friendly materials and clean technology usage), and quality level. A scenario-based robust optimization method is used to deal with uncertain parameters such as the demand of new products, the return rates of returned products and the sale prices of remanufactured products. The proposed model is applied to a real industry case example of a manufacturing company to illustrate the applicability of the proposed model. The result shows a robust optimal resource allocation solution that considers multiple scenarios. This study can be a reference for closed-loop supply chain related academic research and also can be used to guide the development of a green closed-loop supply chain model for better decision making.

ARTICLE INFO

Keywords:

Green closed-loop supply chain;
Sustainability;
Modelling;
Robust optimization;
Mixed integer programming model;
Supply chain management;
Uncertainty;
LP-metric method

*Corresponding author:

102356508@nccu.edu.tw
(Fang, I.W.)

Article history:

Received 5 June 2021
Revised 23 June 2021
Accepted 24 June 2021



Content from this work may be used under the terms of the Creative Commons Attribution 4.0 International Licence (CC BY 4.0). Any further distribution of this work must maintain attribution to the author(s) and the title of the work, journal citation and DOI.

1. Introduction

Due to increasing awareness of environmental issues, governments' legislation, and natural resource limitation, related research on the closed-loop supply chain which integrate the forward and reverse supply chain are increasingly growing [1-5]. According to Govindan *et al.* [6], the research gaps of closed-loop supply chain include the discussion of green/ sustainable issues, the utilization of robust optimization method, the consideration of uncertain factors such as return rate, and multi-objective functions with environmental indicators.

The economic and environmental factors are mostly considered in the multiple objective functions [7-16], while other evaluation indicators of supply chain performance are seldom included. Promoting better quality of the supply chain operations is the method to sustain the long-term competition for earning the market share [17]. This study proposes a multi-objective

mixed-integer programming model of the closed-loop supply chain network to maximize profit, amicable production level, and quality level.

In order to describe real industry environments, uncertain parameters are considered in the mathematical model. With sensitivity analysis, the demand of new products, the return rates of returned products and the sale prices for remanufactured products which are highly sensitive to the objective functions are selected. A scenario-based robust optimization method is utilized for solving the uncertain problem. After the uncertainty problem is solved, the multi-objective problem is solved by LP-metric method. A real industry case example of a manufacturing company is applied to illustrate the applicability of the proposed model. The goal of this study is to develop the multi-objective mathematical model for supporting better decision making in the green closed-loop supply chain network management. Besides, the impact of the economic, environmental, and quality factors to the green closed-loop supply chain model is discussed in this study.

This paper advances current research into closed-loop supply chain models in two ways. First, the amicable production level and quality level are considered in the objective functions for analysing simultaneously the impacts of three objective functions in different parameter settings. Second, sensitivity analysis is used to determine the multiple uncertain parameters for fully consideration of the important factors in this model. The rest of this paper is organized as follows. Section 2 reviews related literature. Section 3 is devoted to the proposed multi-objective mixed-integer linear programming model. Section 4 shows an illustrative case example, and section 5 discusses conclusions.

2. Literature review

The objectives of closed-loop supply chain models include carbon emissions, costs, profits, environmental influence/ cost, environmentally friendly materials, and clean technology etc. Zhao *et al.* [8] proposed a multi-objective optimization model for minimizing the inherent risk occurred by hazardous materials, associated carbon emission, and economic cost. Three scenarios are discussed in this study for analyzing the green impact in the supply chain management. Talaei *et al.* [9] proposed a bi-objective mixed-integer linear programming model for minimizing the total network costs and the rate of carbon dioxide emission. The effects of uncertainties of the variable costs and demand rate are considered in the closed-loop supply chain network design. In order to improve economic and environmental performance in an environmental closed-loop supply chain for enterprises' competitiveness, Ma *et al.* [10] proposed a robust multi-objective mixed integer nonlinear programming model to minimize two conflicting objectives simultaneously, the economic cost and the environmental influence. Also, the uncertain cost parameters and demand fluctuations are considered in the supply chain network design. To illustrate the relationships between supply chain management policies and natural environmental impacts, Altmann and Bogaschewsky [11] proposed a robust multi-objective closed-loop supply chain design model which minimizes expected total costs as well as carbon dioxide equivalents. Customer demand and used-product return rate are considered to be the uncertain parameters. For considering the environmental factors in the closed-loop supply chain facility-location model, Amin and Zhang [12] proposed a mixed-integer linear programming model to minimize the total costs and to maximize the environmentally friendly materials and clean technology usage. The impact of uncertain demand and return is investigated on the network configuration. Pourjavad and Mayorga [16] developed a fuzzy multi-objective mixed integer linear programming model to minimize costs and environmental impacts and maximize social impacts. Three fuzzy parameters such as return rates of products from customer centers, the capacity of all facilities, and product demand are considered. The related literatures are summarized in Table 1.

Some performance indicators such as quality in the traditional supply chain model are less frequently included in the green closed-loop supply chain model for comparing the impacts of performance indicators simultaneously (shown as Table 1). Quality is an important concern in response to the performance in supply chain operations [5,14, 17-20]. Liu *et al.* [13] proposed a bi-objective mathematical programming model considering uncertain demand in a green closed

loop supply chain network. Two objectives are minimizing the total costs including production cost, operation cost, transportation cost, and construction cost, while maximizing the satisfaction of customers which includes shipping time, product quality, and recovery quantity. Liu *et al.* [13] only considers the recovery quantity as the environmental indicator that can't effectively and suitably reveal the impact of green manufacturing to the whole supply chain performance, and only treat demand as the uncertain parameter. For fulfilling the research gap, this study considers the economic, amicable production level, and quality simultaneously for optimizing the green closed-loop supply chain model which is referenced by Fang and Lin [5]. For in-depth analysis, this study utilizes the sensitivity analysis to determine the uncertain parameters such as the demand of new products, the return rates of returned products, and the sale prices of re-manufactured products which are highly sensitive to the three objective functions. Besides, the comparison between the infeasibility weight and model robustness is made to provide more helpful information for decision making.

For solving stochastic problems in closed-loop supply chain, Govindan *et al.* [6] suggested that two-stage stochastic method or robust optimization method can be considerable solutions in the future directions of the related researches. Compared with stochastic programming method, the robust optimization method has the advantage of implementing without the known probability distributions of uncertain parameters. Besides, the robust optimization is easier than stochastic programming method for finding the optimal solution [24].

In terms of the suggestions mentioned above, the multi-objective stochastic problem of this study is solved by robust optimization method and LP-metrics method referenced by Altmann and Bogaschewsky [11], Ma *et al.* [10] and Fang and Lin [5] to find the final optimal solution. Sensitivity analysis is utilized to determine the selected uncertain parameters and the AHP method is used to determine the weights of three objective functions for being combined into a single objective function.

Table 1 Summary of related literature

Papers	Uncertain parameters		Objective function indicators			Solutions/Methods
	Single	Multiple	Environmental	Economic	Quality	
Amin and Zhang (2013)	*		*	*		Multi-objective approach Stochastic programming
Ramezani <i>et al.</i> (2013)		*		*	*	Pareto-optimal solutions
Altmann and Bogaschewsky (2014)		*	*	*		Robust optimization
Das and Rao Posinasetti (2015)			*	*		Bi-objective Pareto optimal solutions, Goal programming
Saffar <i>et al.</i> (2015)		*	*	*		Jimenez approach
Ma <i>et al.</i> (2016)		*	*	*		Robust optimization
Talaei <i>et al.</i> (2016)		*	*	*		Robust fuzzy optimization
Mohammed <i>et al.</i> (2017)		*		*		Robust optimization
Zhao <i>et al.</i> (2017)			*	*		Big data analytic approach, Scenario analysis
Liu <i>et al.</i> (2018)	*		*	*	*	Approximation, ϵ -constraint method, MOSA, NSGA-II
Pourjavad and Mayorga (2018)		*	*	*		NSGA-II, NPGA
Karimi <i>et al.</i> (2019)	*			*		NSGA-II, NPGA
Valizadeh <i>et al.</i> (2020)	*			*		Bertsimas and Sim stable optimization approach
This study		*	*	*	*	Multi-objective approach, Robust optimization

3. Model formulation

3.1 Problem definition

Referenced by Fang and Lin [5], the green closed-loop supply chain network model in this study (depicted as Fig. 1) includes manufacturing centers, customers, collection centers, and customers of the other market. The new products are manufactured by manufacturing centers and sent to customers. The returned products are purchased from customers and sent to collection centers. After the returned products are dismantled by the collection centers, some reused materials are sent back to the manufacturing centers for new products, and some reused materials are manufactured by the collection centers for remanufactured products. The remanufactured products are sent from collection centers to customers of the other market.

The goal of this study is to maximize total profit, amicable production level, and quality of products with three uncertain parameters. The assumptions of this research are referenced by Fang and Lin [5].

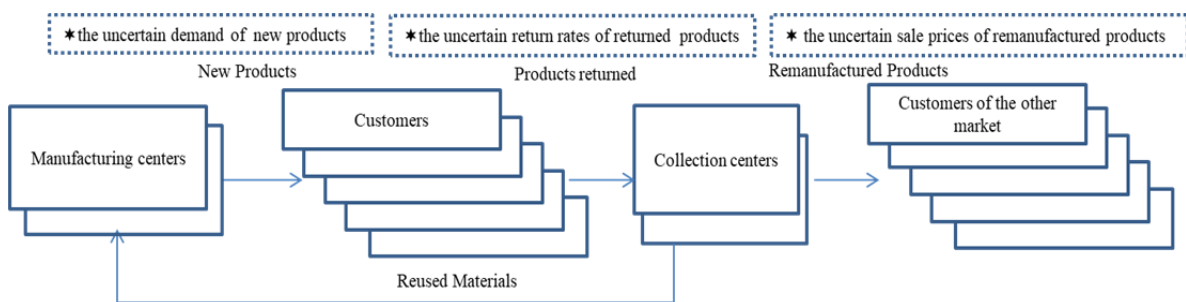


Fig. 1 Green closed-loop supply chain network model in this study

3.2 Model description

The sets, indices, parameters, decision variables, and scenario variables for the model formulation are shown in Table 2.

Objective functions:

$$Max F1 = Revenue - Purchase Cost - Processing Cost - Transportation Cost \tag{1}$$

$$Revenue = \sum_{p=1}^P \sum_{m=1}^M \sum_{c=1}^C QM_{pmc} \times P_{pc} + \sum_{r \in re} \sum_{e=1}^E \sum_{l=1}^L \sum_{t=1}^T QE_{relt} \times P_{et} \tag{2}$$

$$Purchase Cost = \sum_{c=1}^C \sum_{p=1}^P \sum_{l=1}^L CC_{cp} \times QL_{plc} \tag{3}$$

$$Processing Cost = \sum_{m=1}^M FC \times IM_m + \sum_{p=1}^P \sum_{c=1}^C \sum_{m=1}^M PC_{mp} \times QM_{pmc} + \sum_{l=1}^L FC \times IL_l + \sum_{r \in re} \sum_{e=1}^E \sum_{t=1}^T \sum_{l=1}^L RC_{le} \times QE_{relt} \tag{4}$$

$$Transportation Cost = \sum_{p=1}^P \sum_{m=1}^M \sum_{c=1}^C TC_{pmc} \times QM_{pmc} + \sum_{p=1}^P \sum_{r \in rm} \sum_{l=1}^L \sum_{m=1}^M TC_{prlm} \times QR_{rlmp} + \sum_{r \in re} \sum_{e=1}^E \sum_{l=1}^L \sum_{t=1}^T TC_{elt} \times QE_{relt} \tag{5}$$

$$Max F2 = W_{em} \times (\sum_{p=1}^P \sum_{m=1}^M \sum_{c=1}^C EM_{pm} \times QM_{pmc} + \sum_{r \in re} \sum_{e=1}^E \sum_{l=1}^L \sum_{t=1}^T EM_{le} \times QE_{relt}) + W_{ct} \times (\sum_{p=1}^P \sum_{m=1}^M \sum_{c=1}^C CTM \times QM_{pmc} + \sum_{p=1}^P \sum_{m=1}^M \sum_{c=1}^C CTS \times QM_{pmc} + \sum_{r \in re} \sum_{e=1}^E \sum_{l=1}^L \sum_{t=1}^T CTM \times QE_{relt} + \sum_{e=1}^E \sum_{l=1}^L \sum_{t=1}^T CTS \times QE_{relt} + \sum_{p=1}^P \sum_{r=1}^R \sum_{l=1}^L \sum_{m=1}^M CTS \times QR_{rlmp}) \tag{6}$$

$$Min F3 = \sum_{m=1}^M \sum_{p=1}^P \sum_{c=1}^C DR_{pm} \times W_p \times QM_{mpc} + \sum_{r \in re} \sum_{e=1}^E \sum_{l=1}^L \sum_{t=1}^T DR_{le} \times W_e \times QE_{relt} \tag{7}$$

Table 2 The descriptions of variables and parameters

Sets & indices			
C	index of fixed locations of customers, $c = 1, 2, \dots, C$	E	index of remanufactured products, $e = 1, 2, \dots, E$
F	index of objective functions, $f = 1, 2, \dots, F$	I	index of scenarios, $i = 1, 2, \dots, I$
L	index of potential locations of collection centers, $l = 1, 2, \dots, L$	M	index of potential locations of manufacturing centers, $m = 1, 2, \dots, M$
R	index of reused materials, $R = RM \cup RE$, RM is for manufacturing centers, RE is for customers of the other markets	T	index of fixed locations of customers of the other market, $t = 1, 2, \dots, T$
P	index of new products, $p = 1, 2, \dots, P$		
Parameters			
PC_{pm}	unit production cost of product p from manufacturing center m	RC_{le}	unit remanufacturing cost of remanufactured product e from collection center l
CC_{cp}	purchasing cost of product p from customer c	FC	fixed cost for opening manufacturing center and collection center
DE_{et}	demand of customer t of the other market for remanufactured product e	CM_{lp}	capacity of collection center l for product p
DP_{cp}	demand of customer c for product p	RA_p	the return rate of product p
CP_{pm}	capacity of manufacturing center m for product p	CE_{le}	capacity of collection center l for remanufactured product e
P_{et}	unit sale price of remanufactured product e for customer t of the other market	P_{pc}	unit sale price of product p for customer c
DR_{le}	defect rate of remanufactured product e from collection center l	DR_{mp}	defect rate of product p from manufacturing center m
RM_{rp}	the rate of reused material r ($r \in rm$) dismantled from returned product p	RE_{rp}	the rate of reused material r ($r \in re$) dismantled from returned product p
W_p	weight factor for importance of product p	W_f	weight factor of objective function f
W_e	weight factor for importance of remanufactured product e	W_{em}	weight factor of using environmentally friendly materials
W_{ct}	weight factor of using clean technology	EM_{pm}	the rate of using environmentally friendly materials by manufacturing center m for product p
EM_{le}	the rate of using environmentally friendly materials by collection center l for remanufactured product e	CTM	the rate of using clean technology for producing product p and remanufactured product e
CTS	the rate of using clean technology for shipping product p and remanufactured product e between facilities	TC_{pmc}	unit distribution cost for product p shipped from manufacturing center m to customer c
TC_{prtm}	unit distribution cost for reused material r ($r \in rm$) of product p shipped from collection center l to manufacturing center m	TC_{elt}	unit distribution cost for remanufactured product e shipped from collection center l to customer t of the other market
Decision variables			
QM_{pmc}	quantity of product p produced from manufacturing center m to customer c	QL_{plc}	quantity of product p returned from customer c to collection center l
QR_{rlmp}	quantity of reused material r ($r \in rm$) for product p from collection center l to manufacturing center m	QE_{relt}	quantity of reused material r ($r \in re$) for producing remanufactured product e from collection center l to customer t of the other market
IM_m	1 if manufacturing center m is opened, otherwise 0	IL_l	1 if collection center l is opened, otherwise 0
Scenario variables			
QU_{pc}	unfulfilled quantity of product p for customer c	QU_{et}	unfulfilled quantity of remanufactured product e for customer t of the other market
SP_i	the occurrence probability of scenario i	ω	the infeasibility weight
λ	the weight of risk	θ_{1i}	the linearization variable of the first objective function under scenario i
θ_{2i}	the linearization variable of the second objective function under scenario i	θ_{3i}	the linearization variable of the third objective function under scenario i

The first objective function $F1$ is to maximize the total profit which is computed by subtracting purchase cost, processing cost, and transportation cost from total revenue. The total revenue includes the sale revenue of new products and remanufactured products. The purchase cost includes purchasing cost of returned products from customers. The processing cost includes fixed cost of manufacturing centers, production cost of new products, fixed cost of collection centers, and production cost of remanufactured products. The transportation cost is for shipping products or materials between facilities in the closed-loop supply chain network. The second objec-

tive function $F2$ is to maximize the amicable production level which means the level of using environmental parameters such as environmentally friendly materials or clean technology in the supply chain operations. The third objective function $F3$ is to maximize the quality level by minimizing the defect rate of new products and remanufactured products.

Constraints:

$$\sum_{m=1}^M QM_{pmc} \geq DP_{cp} \quad \forall c, p \quad (8)$$

$$\sum_{r=1}^R \sum_{l=1}^L QE_{relt} \geq DE_{et} \quad \forall t, e \quad (9)$$

$$\sum_{c=1}^C QM_{pmc} \leq IM_m \times CP_{pm} \quad \forall p, m \quad (10)$$

$$\sum_{c=1}^C QL_{plc} \leq IL_l \times CM_{lp} \quad \forall l, p \quad (11)$$

$$\sum_{r \in r2} \sum_{t=1}^T QE_{relt} \leq IL_l \times CE_{le} \quad \forall l, e \quad (12)$$

$$\sum_{l=1}^L QL_{plc} = DP_{pc} \times RA_p \quad \forall p, c \quad (13)$$

$$\sum_{m=1}^M QR_{rlmp} = \sum_{c=1}^C QL_{plc} \times RM_{rp} \quad \forall p, l, r \in rm \quad (14)$$

$$\sum_{e=1}^E \sum_{t=1}^T QE_{relt} = \sum_{c=1}^C QL_{plc} \times RE_{rp} \quad \forall p, l, r \in re \quad (15)$$

$$QN_{nspm}, QM_{pmc}, QL_{plc}, QR_{rlmp}, QE_{relt}, QU_{pc}, QU_{et}, \theta_{1i}, \theta_{2i}, \theta_{3i} \geq 0 \quad \forall r, s, p, c, m, l, n, t, e \quad (16)$$

$$IM_m, IL_l \in \{0,1\} \quad \forall m, l \quad (17)$$

Eq. 8 ensures that the sum of the produced quantity of each product for each customer can meet customer demand. Eq. 9 ensures that the sum of the produced quantity of each remanufactured product for each customer of the other market can meet the customer demand of the other market. Eq. 10 states that the sum of each product produced for customers by each manufacturing center does not exceed the capacity of this manufacturing center. Eq. 11 presents that the sum of each returned product collected by each collection center does not exceed the capacity of this collection center. Eq. 12 presents that the sum of each remanufactured product produced by each collection center does not exceed the capacity of this collection center. Eq. 13 ensures the returned quantity of each product from customers to collection centers. Eq. 14 ensures the quantity of each reused material which is dismantled from each returned product in each collection center supplied to manufacturing centers for manufacturing products. Eq. 15 ensures the quantity of each reused material which is dismantled from each returned product in each collection center used for producing remanufactured products. Eq. 16 preserves the non-negativity restriction on the decision variables, and Eq. 17 imposes the binary restriction on the decision variables.

3.3 The transformation to a robust optimization model

The proposed multi-objective mixed integer programming model can be transformed to a robust optimization model by the approach proposed by Mulvey *et al.* [25] and a more suitable formulation for the first term of the objective function introduced by Yu and Li [26]. The three objective functions and additional constraints of the proposed model can be expressed as follows [5]:

$$Max\ ob1 = \sum_{i=1}^I SP_i F1_i - \lambda \sum_{i=1}^I SP_i [(F1_i - \sum_{i'=1}^I SP_{i'} F1_{i'}) + 2\theta_{1i}] - \omega \sum_{i=1}^I SP_i (QU_{pc} + QU_{et}) \quad (18)$$

$$Max\ ob2 = \sum_{i=1}^I SP_i F2_i - \lambda \sum_{i=1}^I SP_i [(F2_i - \sum_{i'=1}^I SP_{i'} F2_{i'}) + 2\theta_{2i}] - \omega \sum_{i=1}^I SP_i (QU_{pc} + QU_{et}) \quad (19)$$

$$Min\ ob3 = \sum_{i=1}^I SP_i F3_i + \lambda \sum_{i=1}^I SP_i [(F3_i - \sum_{i'=1}^I SP_{i'} F3_{i'}) + 2\theta_{3i}] + \omega \sum_{i=1}^I SP_i (QU_{pc} + QU_{et}) \quad (20)$$

s.t.

$$F1_i - \sum_{i=1}^I SP_i F1_i + \theta_{1i} \geq 0 \quad \forall i \in \Omega \quad (21)$$

$$F2_i - \sum_{i=1}^I SP_i F2_i + \theta_{2i} \geq 0 \quad \forall i \in \Omega \quad (22)$$

$$F3_i - \sum_{i=1}^I SP_i F3_i + \theta_{3i} \geq 0 \quad \forall i \in \Omega \quad (23)$$

$$\sum_{m=1}^M QM_{pmc} + QU_{pc} \geq DP_{cp} \quad \forall c, p \quad (24)$$

$$\sum_{r=1}^R \sum_{l=1}^L QE_{relt} + QU_{et} \geq DE_{et} \quad \forall t, e \quad (25)$$

$$\sum_{l=1}^L QL_{plc} = (DP_{cp} - QU_{pc}) \times RA_p \quad \forall p, c \quad (26)$$

Where $F1_i$ denotes the first objective function in the proposed model as Eq. 1, $F2_i$ denotes the second objective function as Eq. 6, and $F3_i$ denotes the third objective function as Eq. 7. Eqs. 21-23 can be interpreted that if the Fx_i is greater than $\sum_{i=1}^I SP_i Fx_i + \theta_{xi}$, then θ_{xi} is equal to 0. If the $\sum_{i=1}^I SP_i Fx_i + \theta_{xi}$ is greater than Fx_i , then $Fx_i - \sum_{i=1}^I SP_i Fx_i = \theta_{xi}$. Eqs. 10-12 and Eqs.14-17 in section 3.2 are still considered in the robust optimization model.

3.4 The transformation to single objective function model

The LP-metrics method is utilized for solving the multi-objective problem in this study referenced by Fang and Lin [5]. Firstly, each objective function of the proposed multi-objective model is solved separately and the objective value $ob1^*$, $ob2^*$ and $ob3^*$ is gained respectively. Then, the objective function can be formulated as Eq. 27. W_1 , W_2 , and W_3 , the weights of the three components in the Eq. 27, are determined by the AHP method and $W_1+W_2+W_3=1$.

$$Min \ W_1 \times \frac{(ob1-ob1^*)}{ob1^*} + W_2 \times \frac{(ob2-ob2^*)}{ob2^*} - W_3 \times \frac{(ob3-ob3^*)}{ob3^*} \quad (27)$$

4. Results and discussion: A case study

4.1 Example description

A real case example of a manufacturing company referenced by Fang and Lin [5] is provided to illustrate the applicability of the proposed green closed-loop supply chain model. According to the supply chain operations of this company, the closed-loop supply chain network includes two products, two manufacturing centers, five customers, two collection centers, two kinds of reused materials (the first one is for new products, the second one is for remanufactured products), two remanufactured products, and five customers of the other market. The two new products can be manufactured by the two manufacturing centers and sent to the five customers. The returned products can be purchased and sent to collection centers for recycling use. The returned products can be dismantled into several kinds of reusable materials in collection centers. The returned product 1 can be dismantled into two kinds of reused materials, namely, $R11$ and $R12$. $R11$ will be sent back to the manufacturing centers for new product 1, $R12$ will be input material for remanufactured product 1. The returned product 2 can be dismantled into three kinds of reused materials, namely, $R21$, $R22$, and $R23$. $R21$ and $R22$ will be sent back to the manufacturing centers for new product 2, and $R23$ will be input material for remanufactured product 2. The two remanufactured products can be produced by the two collection centers and sent to the five customers of the other markets.

4.2 Parameters setting

In order to consider the confidentiality of the company data, the real company data is modified in different scenarios. The parameter data is shown in Table 3-8. The AHP method is used for assigning the weights of the three objective functions and the weights of the environmentally friendly materials and clean technology usage. The weight of $ob1$, $ob2$ and $ob3$ is 0.36, 0.36, and 0.28. The weight of the environmentally friendly materials and clean technology usage is 0.5 and 0.5. The weight factor for importance of new product 1 and 2 is 0.3 and 0.2, the same as remanufactured product 1 and 2 is. The return rate of new products is 0.9. The defect rate of new products and remanufactured products is 0.1. The fixed cost is 30. For the sake of computation convenience, the rates of using environmentally friendly materials and clean technology will be transformed to the corresponding scores as follows: the rate which is less than or equal to 25 % is set to be 25, the rate which is 26-50 % is set to be 50, the rate which is 51-75 % is set to be 75, and the rate which is greater than 75 % is set to be 100.

Table 3 New products and customer data

Parameters	New products	Customers				
		1	2	3	4	5
Unit selling price (P_{pc})	1/2	80/55	85/60	90/65	95/70	100/75
Purchase cost (CC_{cpr})	1/2	90/80	90/80	90/80	90/80	90/80

Table 4 Remanufactured products and customers of the other market data

Parameters	Remanufactured products	Customers of the other market				
		1	2	3	4	5
Demand amount (DE_{et})	1/2	55/154	55/110	110/55	66/55	110/154

Table 5 Manufacturing centers and new products data

Parameters	Manufacturing centers	New product 1	New product 2
Production cost (PC_{mp})	1/2	80/85	40/35
Capacity limitation (CP_{pm})	1/2	800/600	1000/800

Table 6 Collection centers and remanufactured products data

Parameters	Collection centers	Remanufactured product 1	Remanufactured product 2
Production cost (RC_{ie})	1/2	80/60	45/35
Capacity limitation (CE_{ie})	1/2	500/500	300/300

Table 7 The rates of reused materials dismantled from the returned products

Returned products	The rates of reused materials (RM_{rp})			The rates of reused materials (RE_{rp})	
	R11	R21	R22	R12	R23
1	0.5	-	-	0.5	-
2	-	0.55	0.05	-	0.4

Table 8 Other parameters data

Parameters	Values	Parameters	Values
The rate of clean technology use (CT_{mp}, CT_{ie})	0.1	Distribution cost (TC_{pmc})	2
The rate of clean technology use (CT_{prim})	0.2	Distribution cost (TC_{prtm})	30
The rate of clean technology use (CT_{elt})	0.1	Distribution cost (TC_{elt})	20
The rate of clean technology use (CT_{pmc})	0.1/m1,0.2/m2	The rate of environmentally friendly material use (EM_{ie})	1
The rate of environmentally friendly material use (EM_{pm})	0.2/p1,0.9/p2		
Capacity limitation(CM_{ip})	600/p1,700/p2		

4.3 Scenarios setting

Sensitivity analysis is used for determining which uncertain parameters are highly sensitive to the three objective functions in this study. Referencing the result of sensitivity analysis, the parameters including the demand of new products, the return rates of returned products, and the sale prices of remanufactured products are taken into account for expressing uncertain situations in the real business environment. In this study, each uncertain parameter has 2 scenarios (high and low), so the combination of three uncertain parameters provides eight scenarios. The probability of each scenario is assumed to be the same. The high and low product return rates are 0.9 and 0.7 for new product 1 and 0.9 and 0.8 for new product 2. The setting of the new product demand and the sale prices of remanufactured products are shown in Table 9.

Table 9 The setting of the new product demand and the sale prices of remanufactured products

New products demand		Customers				
		1	2	3	4	5
1	High/Low	220/180	220/180	220/180	220/180	220/180
2	High/Low	344/296	344/296	384/336	124/76	124/76
The sale prices of remanufactured products		Customers of the other market				
		1	2	3	4	5
1	High/Low	1400/1000	1400/1000	1500/1100	1500/1100	1600/1200
2	High/Low	680/280	700/300	700/300	700/300	720/320

4.4 Computing results

To solve the proposed model using the test case data, the Lingo 12.0 software was employed. λ is set to be 1 and ω is set to be 90. The computing results are shown in Table 10-13. Using the robust optimization approach to solve the uncertain problems, multiple scenarios are considered and the infeasibility in the control constraints can be allowed by means of penalties. Through the solution solving procedures, we have the following findings:

- From the sensitivity analysis, the demand of new products, the return rates of returned products, and the sale prices of remanufactured products was highly sensitive to the three objective functions of the proposed model. It can be inferred that the three parameters are relatively important elements to the total performance of this proposed model. The company manager should pay more attention to evaluating the impacts of the three parameters to keep good performance of the green closed-loop supply chain.
- Using the AHP method, the weight of the economic objective is the same with the weight of the environmental objective. Also, the weights of the economic and environmental objectives are higher than the weight of the quality objective. It can be inferred that the environmental issues have gotten much attention in the closed-loop supply chain operations, and are treated as important as the company's profit.

Table 10 The allocation of new products

New products	Manufacturing centers	Customers				
		1	2	3	4	5
1	1/2	57.5/122.5	43.6/136.4	108.1/71.9	61.7/118.3	529.1/150.9
2	1/2	243.6/52.4	127.3/168.7	0/336	0/76	629.1/166.9

Table 11 The allocation of returned products

Returned products	Collection centers	Customers				
		1	2	3	4	5
1	1/2	0/126	15.5/110.5	0/126	0/126	14.5/111.5
2	1/2	0/236.8	17.4/219.4	95/173.8	25.9/34.9	25.6/35.2

Table 12 The allocation of reused materials offered to manufacturing centers

New products	Reused materials	Manufacturing centers		Collection centers			
		Manufacturing centers	Collection centers		Manufacturing centers	Collection centers	
			1	1		2	2
1	R11		0	0		15	300
2	R21/R22		0/0	0/0		90.2/8.2	385/35

Table 13 The allocation of remanufactured products

Remanufactured products	Collection centers	Customers of the other market				
		1	2	3	4	5
1	1/2	0/0	0/29	0/110	15/51	0/110
2	1/2	0/0	18.7/91.3	20.9/19.7	20.9/20.1	5/149

4.5 Trade-off between the infeasibility weight and model robustness

The infeasibility weight ω is applied as the model infeasibility under the scenarios of having the unfulfilled demand. Fig. 2 shows the comparison between the infeasibility weight and the unfulfilled demand of remanufactured products. We can find that when the value of ω increases to 90, we get the lowest unfulfilled demand of remanufactured products. Therefore, the best value for ω in the test case is 90.

We can find the relations between objective functions and infeasibility weights shown as Fig. 3. As the infeasibility weight increases, the value of objective function 1 and 2 decreases but the value of objective function 3 increases. The decreased percentage of objective function 1 and 2 are 25 % and 30 % respectively, and the increased percentage of objective function 3 is 199 %. It is shown that the value of objective function 3 is influenced most appreciably by the change of the infeasibility weight, while the value of objective function 1 and 2 is influenced a little by the

change of the infeasibility weight. From this analysis, the decision maker may consider the differences between the three objective functions generated by the infeasibility weight to find a suitable decision for the green closed-loop supply chain management.

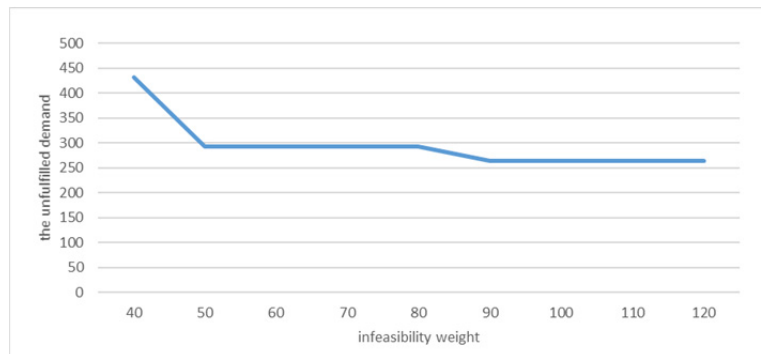


Fig. 2 Comparison between the infeasibility weight and model robustness

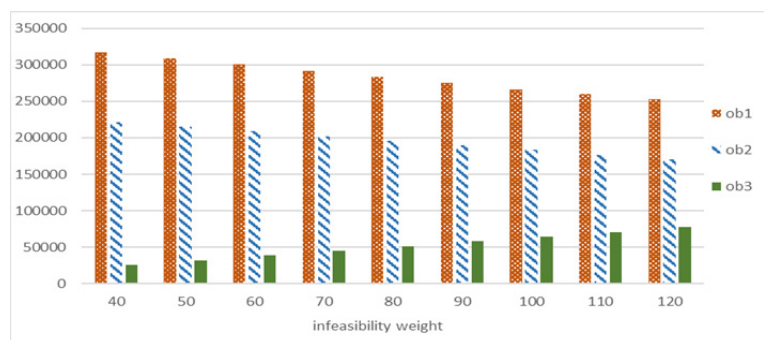


Fig. 3 Value of objective functions in different infeasibility weights

5. Conclusion

Given resource limitation and environmental issues, companies not only have to strive to stay competitive to make more profit, but also have to consider the effective recycling utilization for environmental protection and social legislations. In order to have the holistic view to discuss the optimization of the supply chain, the closed-loop supply chain network model is adopted in this study. Referenced by Fang and Lin [5], this study proposes a multi-objective model for a green closed-loop supply chain network to maximize profit, amicable production level, and quality level. The uncertain parameters such as the demand of new products, the return rates of returned products, and the sale prices of remanufactured products are selected by sensitivity analysis. The multi-objective stochastic problem of this study is solved by robust optimization method and LP-metrics method. A real case example is provided for demonstrating the applicability of this proposed model. Through the computation result, we can find a robust optimal resource allocation solution for the proposed multi-objective mixed integer programming model.

There are several important managerial insights for managers. First, in order to gain competitive advantages and sustainable development, considering the multiple objectives in the closed-loop supply chain help managers obtain more completed and precise information to make better decision. Second, uncertain factors will affect the performance of the closed-loop supply chain operations. Utilizing sensitivity analysis to determine the critical uncertain parameters in this proposed model help managers pay more attention to evaluating the impacts of the uncertain parameters to keep good performance of the green closed-loop supply chain. Third, economic factors and environmental factors have the same importance for optimizing green closed-loop supply chain operations in this study. It is found that green manufacturing should be noticed more seriously for supply chain management.

In future research, regarding environmental issues, other environmental metrics, such as Oršič *et al.* [27] mentioned, can be considered in the environmental objective function. The im-

pacts of green closed-loop supply chain performance by the environmental factors can be further evaluated and discussed. This proposed model can also be applied to another industry to compare the impacts of the three objectives to the green closed-loop supply chain operations in different industries. For solving large scale and stochastic models, many algorithms such as generalized outer approximation, generalized cross decomposition, generalized benders decomposition, genetic algorithm, simulated annealing, etc. can be good references for further research of this study.

Acknowledgement

The authors are grateful to the Ministry of Science and Technology, ROC, for the partial financial support of this work under the grant MOST 105-2410-H-004-111.

References

- [1] Shi, J., Zhang, G., Sha, J. (2011). Optimal production planning for a multi-product closed loop system with uncertain demand and return, *Computers & Operations Research*, Vol. 38, No. 3, 641-650, doi: [10.1016/j.cor.2010.08.008](https://doi.org/10.1016/j.cor.2010.08.008).
- [2] Jabbarzadeh, A., Haughton, M., Khosrojerdi, A. (2018). Closed-loop supply chain network design under disruption risks: A robust approach with real world application, *Computers & Industrial Engineering*, Vol. 116, 178-191, doi: [10.1016/j.cie.2017.12.025](https://doi.org/10.1016/j.cie.2017.12.025).
- [3] Tseng, M., Lim, M., Wong, W.P. (2015). Sustainable supply chain management: A closed-loop network hierarchical approach, *Industrial Management & Data Systems*, Vol. 115, No. 3, 436-461, doi: [10.1108/IMDS-10-2014-0319](https://doi.org/10.1108/IMDS-10-2014-0319).
- [4] Gu, X., Ieromonachou, P., Zhou, L., Tseng, M.-L. (2018). Optimising quantity of manufacturing and remanufacturing in an electric vehicle battery closed-loop supply chain, *Industrial Management & Data Systems*, Vol. 118, No. 1, 283-302, doi: [10.1108/IMDS-04-2017-0132](https://doi.org/10.1108/IMDS-04-2017-0132).
- [5] Fang, I.-W., Lin, W.-T. (2019). A robust optimization model for a green closed-loop supply chain network design, In: *2019 IEEE 6th International Conference on Industrial Engineering and Applications (ICIEA)*, Waseda University, Tokyo, Japan, 723-727, doi: [10.1109/IEA.2019.8714928](https://doi.org/10.1109/IEA.2019.8714928).
- [6] Govindan, K., Soleimani, H., Kannan, D. (2015). Reverse logistics and closed-loop supply chain: A comprehensive review to explore the future, *European Journal of Operational Research*, Vol. 240, No. 3, 603-626, doi: [10.1016/j.ejor.2014.07.012](https://doi.org/10.1016/j.ejor.2014.07.012).
- [7] Žic, J., Žic, S. (2020). Multi-criteria decision making in supply chain management based on inventory levels, environmental impact and costs, *Advances in Production Engineering & Management*, Vol. 15, No. 2, 151-163, doi: [10.14743/apem2020.2.355](https://doi.org/10.14743/apem2020.2.355).
- [8] Zhao, R., Liu, Y., Zhang, N., Huang, T. (2017). An optimization model for green supply chain management by using a big data analytic approach, *Journal of Cleaner Production*, Vol. 142, Part 2, 1085-1097, doi: [10.1016/j.jclepro.2016.03.006](https://doi.org/10.1016/j.jclepro.2016.03.006).
- [9] Talaei, M., Moghaddam, B.F., Pishvae, M.S., Bozorgi-Amiri, A., Gholamnejad, S. (2016). A robust fuzzy optimization model for carbon-efficient closed-loop supply chain network design problem: A numerical illustration in electronics industry, *Journal of Cleaner Production*, Vol. 113, 662-673, doi: [10.1016/j.jclepro.2015.10.074](https://doi.org/10.1016/j.jclepro.2015.10.074).
- [10] Ma, R., Yao, L., Jin, M., Ren, P., Lv, Z. (2016). Robust environmental closed-loop supply chain design under uncertainty, *Chaos, Solitons & Fractals*, Vol. 89, 195-202, doi: [10.1016/j.chaos.2015.10.028](https://doi.org/10.1016/j.chaos.2015.10.028).
- [11] Altmann, M., Bogaschewsky, R. (2014). An environmentally conscious robust closed-loop supply chain design, *Journal of Business Economics*, Vol. 84, 613-637, doi: [10.1007/s11573-014-0726-4](https://doi.org/10.1007/s11573-014-0726-4).
- [12] Amin, S.H., Zhang, G. (2013). A multi-objective facility location model for closed-loop supply chain network under uncertain demand and return, *Applied Mathematical Modelling*, Vol. 37, No. 6, 4165-4176, doi: [10.1016/j.apm.2012.09.039](https://doi.org/10.1016/j.apm.2012.09.039).
- [13] Liu, M., Liu, R., Zhu, Z., Chu, C., Man, X. (2018). A bi-objective green closed loop supply chain design problem with uncertain demand, *Sustainability*, Vol. 10, No. 4, 967-988, doi: [10.3390/su10040967](https://doi.org/10.3390/su10040967).
- [14] Das, K., Posinasetti, N.R. (2015). Addressing environmental concerns in closed loop supply chain design and planning, *International Journal of Production Economics*, Vol. 163, 34-47, doi: [10.1016/j.ijpe.2015.02.012](https://doi.org/10.1016/j.ijpe.2015.02.012).
- [15] Saffar, M.M., Shakouri, H.G., Razmi, J. (2015). A new multi objective optimization model for designing a green supply chain network under uncertainty, *International Journal of Industrial Engineering Computations*, Vol. 6, 15-32, doi: [10.5267/ijie.2014.10.001](https://doi.org/10.5267/ijie.2014.10.001).
- [16] Pourjavad, E., Mayorga, R.V. (2018). Optimization of a sustainable closed loop supply chain network design under uncertainty using multi-objective evolutionary algorithms, *Advances in Production Engineering & Management*, Vol. 13, No. 2, 216-228, doi: [10.14743/apem2018.2.286](https://doi.org/10.14743/apem2018.2.286).
- [17] Franca, R.B., Jones, E.C., Richards, C.N., Carlson, J.P. (2010). Multi-objective stochastic supply chain modeling to evaluate tradeoffs between profit and quality, *International Journal of Production Economics*, Vol. 127, No. 2, 292-299, doi: [10.1016/j.ijpe.2009.09.005](https://doi.org/10.1016/j.ijpe.2009.09.005).

- [18] Ramezani, M., Bashiri, M., Tavakkoli-Moghaddam, R. (2013). A new multi-objective stochastic model for a forward/reverse logistic network design with responsiveness and quality level, *Applied Mathematical Modelling*, Vol. 37, No. 1-2, 328-344, doi: [10.1016/j.apm.2012.02.032](https://doi.org/10.1016/j.apm.2012.02.032).
- [19] Gharaei, A., Karimi, M., Hoseini Shekarabi, S.A. (2019). An integrated multi-product, multi-buyer supply chain under penalty, green, and quality control polices and a vendor managed inventory with consignment stock agreement: The outer approximation with equality relaxation and augmented penalty algorithm, *Applied Mathematical Modelling*, Vol. 69, 223-254, doi: [10.1016/j.apm.2018.11.035](https://doi.org/10.1016/j.apm.2018.11.035).
- [20] Jafari Ashlaghi, M. (2014). A new approach to green supplier selection based on fuzzy multi-criteria decision making method and linear physical programming, *Tehnički Vjesnik – Technical Gazette*, Vol. 21, No. 3, 591-597.
- [21] Mohammed, F., Selim, S.Z., Hassan, A., Syed, M.N. (2017). Multi-period planning of closed-loop supply chain with carbon policies under uncertainty, *Transportation Research Part D: Transport and Environment*, Vol. 51, 146-172, doi: [10.1016/j.trd.2016.10.033](https://doi.org/10.1016/j.trd.2016.10.033).
- [22] Karimi, B., Niknamfar, A.H., Gavyar, B.H., Barzegar, M., Mohtashami, A. (2019). Multi-objective multi-facility green manufacturing closed-loop supply chain under uncertain environment, *Assembly Automation*, Vol. 39, No. 1, 58-76, doi: [10.1108/AA-09-2018-0138](https://doi.org/10.1108/AA-09-2018-0138).
- [23] Valizadeh, J., Sadeh, E., Sabegh, Z.A., Hafezalkotob, A. (2020). Robust optimization model for sustainable supply chain for production and distribution of polyethylene pipe, *Journal of Modelling in Management*, Vol. 15 No. 4, 1613-1653, doi: [10.1108/JM2-06-2019-0139](https://doi.org/10.1108/JM2-06-2019-0139).
- [24] Alem, D.J., Morabito, R. (2012). Production planning in furniture settings via robust optimization, *Computers & Operations Research*, Vol. 39, No. 2, 139-150, doi: [10.1016/j.cor.2011.02.022](https://doi.org/10.1016/j.cor.2011.02.022).
- [25] Mulvey, J.M., Vanderbei, R.J., Zenios, S.A. (1995). Robust optimization of large-scale systems, *Operations Research*, Vol. 43, No. 2, 264-281, doi: [10.1287/opre.43.2.264](https://doi.org/10.1287/opre.43.2.264).
- [26] Yu, C.-S., Li, H.-L. (2000). A robust optimization model for stochastic logistic problems, *International Journal of Production Economics*, Vol. 64, No. 1-3, 385-397, doi: [10.1016/S0925-5273\(99\)00074-2](https://doi.org/10.1016/S0925-5273(99)00074-2).
- [27] Oršič, J., Rosi, B., Jereb, B. (2019). Measuring sustainable performance among logistic service providers in supply chains, *Tehnički Vjesnik – Technical Gazette*, Vol. 26, No. 5, 1478-1485, doi: [10.17559/TV-20180607112607](https://doi.org/10.17559/TV-20180607112607).

Improved Genetic Algorithm (VNS-GA) using polar coordinate classification for workload balanced multiple Traveling Salesman Problem (mTSP)

Wang, Y.D.^a, Lu, X.C.^{b,*}, Shen, J.R.^c

^aBeijing Jiaotong University, Shangyuan Village, Haidian District, Beijing, P.R. China

^bBeijing Jiaotong University, Shangyuan Village, Haidian District, Beijing, P.R. China

^cBeijing Capital Agribusiness & Food Group Co., Ltd., Xicheng District, Beijing, P.R. China

ABSTRACT

The multiple traveling salesman problem (mTSP) is an extension of the traveling salesman problem (TSP), which has wider applications in real life than the traveling salesman problem such as transportation and delivery, task allocation, etc. In this paper, an improved genetic algorithm (VNS-GA) that uses polar coordinate classification to generate the initial solutions is proposed. It integrates the variable neighbourhood algorithm to solve the multiple objective optimization of the mTSP with workload balance. Aiming to workload balance, the first design of this paper is about generating initial solutions based on the polar coordinate classification. Then a distance comparison insertion operator is designed as a neighbourhood action for allocating paths in a targeted manner. Finally, the neighbourhood descent process in the variable neighbourhood algorithm is fused into the genetic algorithm for the expansion of search space. The improved algorithm is tested on the TSPLIB standard data set and compared with other genetic algorithms. The results show that the improved genetic algorithm can increase computational efficiency and obtain a better solution for workload balance and this algorithm has wide applications in real life such as multiple robots task allocation, school bus routing problem and other optimization problems.

ARTICLE INFO

Keywords:

Multiple traveling salesman problem (mTSP);
Workload balance;
Variable neighbourhood search algorithm (VNS);
Genetic algorithm (GA);
Polar coordinates;
Classification

*Corresponding author:

xclu@bjtu.edu.cn
(Lu, X.C.)

Article history:

Received 4 June 2021
Revised 15 June 2021
Accepted 17 June 2021



Content from this work may be used under the terms of the Creative Commons Attribution 4.0 International License (CC BY 4.0). Any further distribution of this work must maintain attribution to the author(s) and the title of the work, journal citation and DOI.

1. Introduction

Multiple Traveling Salesmen Problem (mTSP) is an extension of the classic Traveling Salesman Problem (TSP)[1]. The mTSP with workload balance is different from the basic TSP. In some scenarios, the balanced distribution of workload is an important consideration. For example, school bus routing problem, route arrangement problem, postman distribution problem, express delivery area division, etc., can all be abstracted as mTSP with balanced workload. Omar *et al.* [2] proposed that mTSP can be used to solve vehicles, robots, and UAVs routing problems. In single-objective optimization of mTSP, the total cost is the most commonly used optimization objective. It causes the problem of an unbalanced distribution of distance among traveling salesmen, which is directly reflected in the path as the distance traveled by one traveler is longer than other travelers. This situation is hoped to be improved in some industries in reality because the

unbalanced workload distribution results in operational difficulties. Moreover, avoiding crossing paths with one another is the most significant problem in practical work. For instance, in school bus routing problem, if a certain route is too long during planning school bus route, it may cause the first arrival point to arrive too early, which will affect students' study and other performance. In postmen routing problem, avoiding crossing paths can improve the efficiency of work. Therefore, our main focus is on the mTSP with workload balance. To solve this problem, we build a multiple objective optimization model and propose an improved genetic algorithm that aims to minimize the total cost and balancing the workload in this paper.

2. Literature review

Research on TSP and mTSP is of long historical making. The original solution to this type of problem mainly used accurate algorithms. Ali *et al.* [3] used the branch and bound method to solve the symmetrical mTSP with 59 cities. Gavish *et al.* [4] described that limiting the lower bound of the branch improved the branch-and-bound method, which can solve the mTSP with 10 traveling salesmen and 100 cities. However, as the scale of the problem expands, the scale of the solution space also increases exponentially, making it difficult to use accurate algorithms. Therefore, heuristic algorithms have become the choice of more and more researchers.

Russell [5] was the first one to apply the heuristic algorithm to solve the mTSP, which transformed mTSP into TSP and then solved it with the Lin-Kernighan algorithm. It also obtained a more accurate approximate solution. For solving the mTSP with the shortest total distance and the shortest sub-path, Carter *et al.* [6] designed a two-stage chromosome coding scheme and designed a genetic operator to improve the solution speed. Singh *et al.* [7] used the invading weed algorithm to obtain a comparative optimal solution. Zhou and Li [8] used a mutation operator combined with a 2-opt search operator to improve the genetic algorithm, avoiding the premature phenomenon of genetic algorithm, and used simulation methods to verify the effectiveness of the algorithm. Xu *et al.* [9] also combined the 2-opt operator with a genetic algorithm to solve the mTSP. Hu *et al.* [10] proposed an improved genetic algorithm that integrates the reproduction mechanism of the weed algorithm and the locally optimized mutation operator to solve the mTSP with balanced workload. Guo [11] used a genetic algorithm to analyze and verify the design of chromosome coding scheme for the genetic algorithm to solve mTSP. Lu *et al.* [12] adopted a two-stage algorithm to solve mTSP while avoiding the path-crossing problem between traveling salesmen. Bostanci *et al.* [13] used the integer linear programming method to solve the problem of finding the shortest route on networks with GIS. This study provided a new method to solve the optimization problems, however, only TSP was solved by this method, problems more complicated such as mTSP are difficult to find the optimal solution.

Recently, with the rise of various heuristic algorithms and machine learning, in addition to genetic algorithms, ant colony optimization algorithm (ACO) [14], artificial bee colony algorithm (ABC)[15], tabu search algorithm (TS)[16] and other heuristic algorithms have also been tried to solve mTSP. Song [17] used the simulated annealing algorithm (SA) to solve the problem of three traveling salesmen in 400 cities, but the algorithm took a long time. Hu [18] constructed an architecture composed of a shared graph neural network and a distributed strategy network to generate an approximate optimal solution for mTSP and used reinforcement learning to train the model, and this method shows good results in large-scale examples. Justus [19] abstracted the problems in the path of staff guiding tourists during the Mecca pilgrimage as multiple objective mTSP with time window and proposed an interactive method for providing a solution. Aiming the mTSP under different goals, Liu *et al.* [20] proposed the ForestTraversal algorithm and the Retrace algorithm to solve the maximum-minimum mTSP and the mTSP that minimizes travel costs, respectively.

Genetic algorithm (GA) is a heuristic algorithm that is often used when solving mTSP. This method mainly focuses on coding design [5] and how to avoid genetic algorithms prematurely falling into local optimality. The variable neighbourhood search algorithm (VNS) has the ability to expand the search range by systematically changing the neighbourhood structure. It guarantees the local search capability while ensuring solutions for having good diversity [21]. There-

fore, this paper designs a genetic algorithm based on polar coordinates to quickly generate high-quality initial solutions, and combines VNS to retain the characteristics of neighbourhood diversity, designs different neighbourhood actions to improve the algorithm's search ability to solve mTSP with workload balance.

3. Mathematical model and problem solving

This paper proposes an improved genetic algorithm, which is improved by fusing the variable neighbourhood algorithm (Variable neighbourhood search genetic algorithm), and VNS-GA is referred too, as an abbreviation in the text.

3.1 Problem description and mathematical model

The mTSP studied in this paper can be described as given n cities, m traveling salesmen and the distance matrix between nodes $D_{ij} = (d_{ij})_{n \times n}$, travelers start from the same node (source node), visit a certain number of nodes and then return to the source node. All nodes are required to be accessed, and the rest of the nodes except the source node can only be accessed once. The aim is to find a Hamiltonian circuit that makes total distance shortest and workload balance. Assuming the problem is symmetrical mTSP, that is, $d_{ij} = d_{ji}$, the multiple objective optimization model can be described as follows:

$$\text{Min} \sum_{i=0}^n \sum_{j=0}^n d_{ij} x_{ijk} \quad (k = 1, 2, \dots, m) \tag{1}$$

$$\text{Min} J = \max(d_{ij} \times x_{ijk}) - \min(d_{ij} \times x_{ijk}), i, j \in A, k \in T \tag{2}$$

$$\sum_{i=0}^n x_{ijk} = y_{kj} \quad \forall j = 0, 1, \dots, n; k = 1, 2, \dots, m \tag{3}$$

$$\sum_{j=0}^n x_{ijk} = y_{ki} \quad \forall i = 0, 1, \dots, n; k = 1, 2, \dots, m \tag{4}$$

$$\sum_{k=1}^m y_{ki} = \begin{cases} 1, & i = 1, 2, \dots, n \\ m, & i = 0 \end{cases} \tag{5}$$

$$X = (x_{ijk}) \in S \tag{6}$$

$$S = \{x_{ijk} \mid \sum_{i \in Q} \sum_{j \notin Q} x_{ijk} \geq 1, Q \subset \{0, 1, 2, \dots, n\}, \forall k = 1, 2, \dots, m\} \tag{7}$$

$$x_{ijk} = \begin{cases} 1 & \text{traveler } k \text{ went through arc } ij \\ 0 & \text{otherwise} \end{cases} \tag{8}$$

$$y_{ki} = \begin{cases} 1 & \text{traveler } k \text{ visited node } i \\ 0 & \text{otherwise} \end{cases} \tag{9}$$

Where $V = \{0, 1, 2, \dots, n\}$ is the node set, n is the number of nodes; $T = \{1, 2, \dots, m\}$ is the travelers set, m is the traveling salesman number; $A = \{(i, j, k) \mid i, j = 0, 1, 2, \dots, n, i \neq j, \forall k = 1, 2, \dots, m\}$ is the arc set, which represents the set of routes that the travelers may pass; $D = \{d_{ij} \mid i, j \in A\}$ is the distance matrix, representing the distance from node i to node j .

Eqs. 1 and 2 are the objectives of these functions. Eq. 1 minimizes the total path distance; Eq. 2 minimizes the difference between the longest path and the shortest path in m paths. Eq. 3 means that for any downstream node, only one upstream node is allowed for its connection, and Eq. 4 means that in each upstream node, only one downstream node is allowed to be connected; Eq. 5 means that except for the source node, all other nodes are only visited once, and all travelers start from the source node. In Eq. 6, S is the branch elimination constraint, and Eq. 7 is an expression of S [22], which means that for any node in the travelers' paths, any of its subsets must be connected to the other subsets in the solution.

3.2 Fitness function

In multiple objective optimization problems, the goals often conflict with each other. The most common method is the generation method (including weighting method, constraint method, etc.), interactive method, and hybrid method to solve multiple objectives. The weighting method assigns different weights to multiple goals which can convert the multiple objective optimization problem into a single-objective optimization problem and makes the simple and easy implementation of the problem. Therefore, the weighting method is used in this paper to transform the two objectives optimization problem into a single-objective optimization problem.

$$\text{Min } Z = w_1 \times Z_1 + w_2 \times J \quad (10)$$

Where $z_1 = \sum_{i=0}^n \sum_{j=0}^n d_{ij} x_{ijk}$, $k = 1, 2, \dots, m$. w_1 , w_2 are the weight coefficients, which belong to hyperparameters and the values of coefficients vary with the data set. It can be determined by expert evaluation method or comparison method, etc.

Therefore, the fitness function in the genetic algorithm is:

$$F = 1/Z \quad (11)$$

It can be seen from Eq. 11 that the greater the fitness, the stronger the individual adaptability, and the better the represented feasible solution.

3.3 Chromosome coding

In the genetic algorithm, the design of the chromosome encoding needs to reflect the genetic characteristics of the individual and should be easy to operate. To express the path more effectively, a one-piece decimal coding scheme is adopted in this paper. A chromosome should include at least one node except the source node, as shown below: Take ten nodes and three travelers as an example, use 0, 1, 2, 3, 4, 5, 6, 7, 8, 9 as it respectively represents ten nodes, of which 0 is the starting node of the three travelers. Then the path of a traveler can be expressed as: 0-1-2-3-4-5-6-7-8-9.

To represent multiple travelers, virtual nodes 10 and 11 are inserted to represent the starting node of the route, which is also the source node. Then, the new chromosome can be formed as: 0-1-2-3-4-5-10-6-7-11-8-9.

Taking virtual nodes 10 and 11 as the path dividing nodes, then the three paths can be expressed as: (1) 0-1-2-3-4-5-0, (2) 0-6-7-0, (3) 0-8-9-0.

3.4 Polar coordinate classification method initialize population

The quality of the initial population plays an important role in the intelligent group optimization algorithm. For mTSP with a single starting node and closed cycle, it is a common optimization method to firstly use the clustering method to optimize grouping, and then use a heuristic algorithm to optimize the order within the group. In 2019, Min *et al.* [23] proposed a method using MRISA (multi-restart-iteration sweeping) and tabu search to solve vehicle routing problem. This two-stage algorithm also can be described as clustering by distance in polar coordinates and optimization by tabu search. Then in the same year, they improved this algorithm by adding an adjust operation named put in & put out. This improved algorithm has three stages: cluster the customer points, use put in & put out operations to adjust the load demand and use tabu search to solve the TSP [24]. Traditional clustering algorithms such as K-means clustering or fuzzy C-means clustering and other clustering methods based on centroids (although they can quickly cluster the set of nodes that need to be visited) can't well represent the starting point as the origin where each traveler's sub-path is distributed around the same starting point. Therefore, a classification method based on polar coordinates is proposed in this paper.

The specific operation process of the polar coordinate classification algorithm to generate the initial population is as follows. First, establish a polar coordinate system with the starting node as the origin and map node-set (n nodes) into the polar coordinate system then sort each node by the angle in the polar coordinate system. Then calculate the two nodes with the furthest angular distances and select one of them to connect with the origin to establish a new polar coor-

dinate system axis. After that use the new axis as the starting position to rotate clockwise, and use the traveler number (m travelers) to equally divide the number of nodes that the travelers need to visit. The nodes in the area swept during the rotation are the node-set to be visited by a traveler, and m initial paths (that is, every traveler roughly needs to visit n/m nodes) constitute an initial feasible solution. Finally, using chromosome fragment flipping as neighborhood shaking to generate enough chromosomes as the initial population. The process of the polar coordinate classification algorithm is as shown in Algorithm1:

Algorithm1: Polar Coordinate initialize population

Input: The number of population p , the number of salesmen n , cartesian coordinates of the cities (x_i, y_i) and the number of cities m
 Output: Initialized population
 $k = 1$
 (θ_i, d_i) : change cartesian coordinates (x_i, y_i) to polar coordinates and sort the cities by the angle θ_i
 $max(\theta, d)$: calculate the maximum angle difference among the cities and build new polar coordinate by joining the origin city and one of maximum angle difference cities
 s_0 : generate a solution by spinning clockwise and each salesman visits n/m cities
 repeat
 s : neighborhood shaking s_0
 $k = k + 1$
 until
 $k > p$
 end

3.5 Neighbourhood actions in VNS

Cross-recombination and mutation operators are often used in genetic algorithm to generate new populations. To enable the algorithm in finding a more efficient combination that makes the travelers' workload roughly balanced, the distance comparison insertion operator cooperates with cross-recombination (neighbourhood action 2) and mutation operator (neighbourhood action 3) is designed in this paper to produce the next generation more efficiently.

Neighbourhood action 1: Distance comparison operator to find a better solution for making the workload balance faster. The neighbourhood action adopted in this paper is to randomly select a node from the sub-path with the longest distance and insert it into the sub-path with the shortest distance. As shown in Fig. 1: Assume that path 0-1-2-3-4-5-0 has the longest distance among all sub-paths, and 0-6-7-0 is the path with the shortest distance among all sub-paths; In the domain action, randomly select a node in the longest path (select node 3) and insert it into the shortest path to form a new chromosome. If the fitness of the new chromosome increases after inserting the selected node, the new chromosome will then be retained. Otherwise, the paternal chromosome will be retained and this inferior solution will be recorded to prevent duplication.

If the fitness of the new chromosome increases after inserting the selected node, suggests that the new offspring chromosomes generated after the neighbourhood action are: 0-1-2-4-5-10-6-3-7-11-8-9.

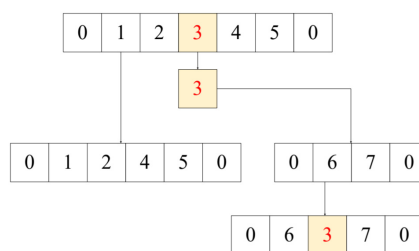


Fig. 1 Schematic of gene insertion in neighbourhood action 1

To avoid repeated calculations, only the difference between the distance of the sequence is calculated each time in the calculation process. Assuming that the selected node is the node at the i -th position in the n -th path, and the insertion position is the node at the j -th position in the m -th path, then actual distance to be calculated is $d = d_n - (d_{i-1,i} + d_{i,i+1}) + d_{i-1,i+1} - (d_m + d_{j-1,j} + d_{j,j+1} - d_{j-1,j+1})$. Where d_n, d_m are the path length before path n and m to perform the neighbourhood action, $i - 1$ and $i + 1$ are the previous and next nodes of i in path n , the same as $j - 1$, and $j + 1$ is the previous and next nodes of j in path m , respectively. $d \geq 0$ means that the fitness is not increased after performing the neighbourhood action, otherwise, it also means that the fitness is increased, and the current solution is better than the parent solution.

Neighbourhood action 2: local crossover operator. Neighbourhood action 1 can make the offspring develop in the direction of workload balance, but it is easy to fall into the local optimum. Therefore, an improved crossover operator to avoid the offspring from falling into the local optimum is proposed in this paper.

To avoid repeated fragments or missing fragments in the offspring that are generated after the crossover and for quickly completing the crossover, we first randomly select a sample gene fragment from the parent 2 and inserts it into the offspring at the original position. Then traverses parent 1 to find the genes that are different from the sample gene fragment and inserted them into the offspring in sequence, the genes that are the same as the sample gene fragment is skipped. The crossover process is shown in Fig. 2.

Neighbourhood action 3: mutation operator. Judging from the characteristics of the traveling salesman problem, there should be no cross edges in the route of the optimal solution. Based on this feature, as shown in Fig. 3 (a is before mutation, b is after mutation), the destruction & reconstruction method is used to mutate individuals to reduce crossover between paths. Suppose the path set is $S = \{s_1, s_2, \dots, s_i, \dots, s_k, \dots, s_n\}$, then sort the distance matrix by distance to get sorted node pairs and randomly selecting a node p in a path s_i and interchange it with the nearest neighbour node m in the nearest neighbour route s_k to reduce the intersection between paths. If the fitness increases, update the current solution; otherwise, it will not update and record the node pair to node pair distance matrix for avoiding repeated exchanges.

G1	0	6	3	8	10	4	5	11	7	9	1	2
G2	0	1	2	3	4	10	5	6	7	11	8	9
New	0	3	8	11	4	10	5	6	7	9	1	2

Fig. 2 Cross process diagram

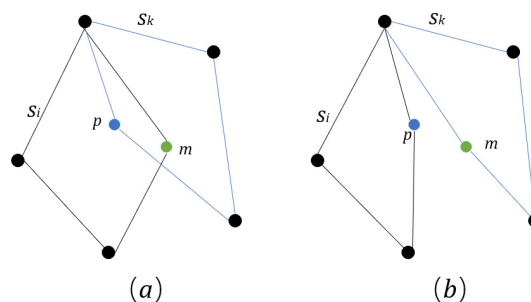


Fig. 3 Mutation operator diagram

3.6 Generate offspring

We introduced the idea of searching the neighbourhood structure alternately in VNS to expand the search space of GA, along with the elite retention strategy which is used for retaining the dominant individuals to improve the convergence speed.

The specific process of generating the next population is firstly for calculating the fitness of each chromosome in the current population and record the optimal individual. Then, use the rou-

lette to select separate chromosomes and search in the neighbourhood structure $N_k (k = 1, 2, \dots, n)$ to find a better solution. The better solution will be added to the progeny population and k will be set to 1. If any better solution cannot be found, skip to the next neighbourhood, and repeat the process of selection and neighbourhood descent until the size of the population reaches maximum. At this time, individuals with greater fitness can be selected more in the selection process and the individual's neighbourhood space can also be fully searched. The pseudo-code of the generating next population algorithm is shown in Algorithm2:

Algorithm2: Variable neighbourhood descent to generate next generation

Input: origin population S_0

Output: new population S

s_0 : optimal solution of origin population

$k = 1$

add s_0 to S

$S_n = 1$

repeat

s : roulette a solution from S_0

 repeat

s' : find best neighbour s'

 if $f(s') > f(s)$ then

 add s' to S

$k = 1$

 else

$k = k + 1$

 until

$k = k_{max}$

until

$S_n = S_{max}$

end

3.7 Algorithm flow

The VNS-GA algorithm process is as below:

- 1) Use polar coordinate classification algorithm to generate initial population S_0 ; defines n neighbourhoods and denoted as $N_k (k = 1, 2, \dots, n)$.
- 2) Verify the feasibility of the initial population, and use neighbourhood shaking to eliminate infeasible solutions.
- 3) Calculate the fitness of individuals in the population, and select the current optimal solution s .
- 4) The variable neighbourhood descent process: search optimal solutions in neighbourhood structure N_k , if it finds better solution s' than s , then let $s = s'$.
- 5) If no better solution can be found in the neighbourhood structure N_k , then let $k + 1$ and go to step 4.
- 6) Add the current optimal solution to the next-generation population;
- 7) Repeat steps 4-6 until the number of individuals in the population reaches the maximum value.
- 8) Repeat step 7 until the maximum number of iterations is reached, then output the current optimal solution.

4. Results and discussion

To verify the performance of VNS-GA, first, we quoted the data of the Chinese Traveling Salesman Problem (CTSP) in literature [25]. Use Python code to test it on a computer with the operating system Windows10, I5-8250, 8G RAM. The algorithm runs ten times independently on each case set. For the sake of fairness, the same genetic algorithm parameters as in literature [25] are

used, and the population size is set to 50, the heredity is 1000 generations, the crossover probability is 0.8, and the mutation probability is 0.15. Because the results obtained using SA in literature [25] are wrong. According to the detailed path diagram obtained by the simulated annealing algorithm in the literature, the results are revised as shown in Table 1.

In the comparison of the three algorithms, the traditional genetic algorithm performs the worst among the three algorithms because of the problem easy falling into the local optimal solution. After using the variable neighbourhood algorithm to improve the genetic algorithm, the effect is promoted. Compared with the detailed path diagram given in [25] (Fig. 4), it can be stated that the improved genetic algorithm is consistent with the nodes set assigned by the simulated annealing algorithm in the literature. But the improved genetic algorithm has better performance than the genetic algorithm on a single path, so, the total obtained path is shorter.

In addition, this paper selects three data sets: eil51, kroA100, and kroB150 in TSPLIB to test the performance of the algorithm. The performance of the algorithm under the conditions of 3, 5, 10, and 20 travelers is tested against the scale of three data sets, and the parameter settings used in each data set are shown in Table 2 through experiments.

We compared the measured data set results with the test results of other algorithms (data from literature [14] and [26]). The results are shown in Table 3, where n is the number of nodes and m is the number of travelers. GA1C is single chromosome coding genetic algorithm, GA2C is the two-chromosome coding genetic algorithm, GA2PC is two-segment chromosome coding genetic algorithm, GGA-SS is steady-state grouping genetic algorithm, TCX is improved two-segment chromosome coding genetic algorithm, and RGA is belt Genetic algorithm with reproduction mechanism, RLGA is a genetic algorithm that integrates the reproduction mechanism of the weed algorithm and local optimization, IWO is the invasive weed algorithm, and VNS-GA is the improved genetic algorithm proposed in this paper.

Table 1 Comparison results between VNS-GA and other algorithms (CTSP data set)

Algorithm	Total distance(km)		Sub-path distance(km)		Variance
GA	20225		6106		643261
			6477		
			7643		
SA	Origin data	Modified data	Origin data	Modified data	Modified variance
	17731	17404	5527	5527	1116314
			5616	4909	
VNS-GA	17153		6968		1361290
			4658		
			5527		

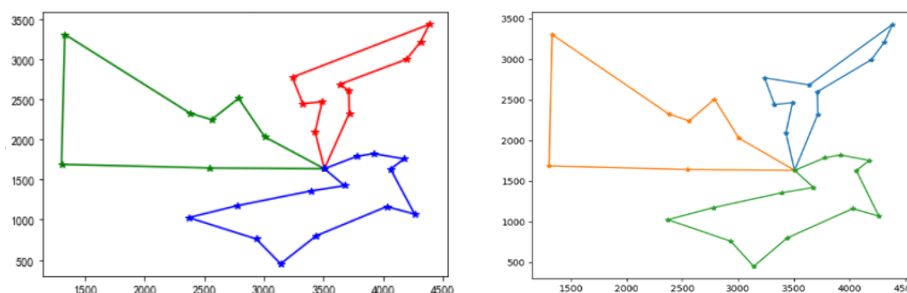


Fig. 4 The specific solution path of VNS-GA and SA

Table 2 Parameter setting of different examples

Standard data set	Number of travelers	Population size	Cross rate	Mutation rate
eil51	3, 5, 10	60	0.8	0.2
kroA100	3, 5, 10, 20	80	0.8	0.2
kroB150	3, 5, 10, 20	80	0.8	0.2

Table 3 Comparison of the longest path (VNS-GA with other genetic algorithms)

Data	<i>n</i>	<i>m</i>	GA1C	GA2C	GA2PC	GGA-SS	TCX	RGA	RLGA	IWO	VNS-GA	<i>D</i> (%)
51	51	3	234	275	203	161	203	174	167	160	165	-3.13
	51	5	173	220	164	119	154	125	118	118	121	-2.54
	51	10	140	165	123	112	113	122	112	112	112	0.00
100	100	3	14722	16229	13556	8542	12726	10231	10115	8509	8613	-1.22
	100	5	11193	11606	10589	6852	10086	7895	7812	6767	6445	4.76
	100	10	9960	10200	9463	6370	7064	6234	6225	6358	5764	7.41
	100	20	9235	9470	8388	6359	6402	6233	6211	6358	5395	13.14
150	150	3	19875	21067	19687	13268	18019	14886	14629	13168	10878	17.39
	150	5	15229	15450	14748	8660	12619	8998	8927	8479	7711	9.06
	150	10	12154	12382	11158	5875	8054	5723	5613	5594	5937	-6.13
	150	20	10206	10338	10044	5252	5673	5372	5251	5246	5750	-9.61

The data given in Table 3 are the values of the longest sub-path. Under the three data sets and different traveler numbers circumstances, the results of VNS-GA are far superior to the GA1C, GA2C, and GA2PC algorithms. The comparison with the GGA-SS algorithm shows that only in the case of 3 travelers in the kroA100 data set, the results are slightly worse and the remaining results are better than the results of GGA-SS. When compared with the TCX algorithm, the results are slightly worse only in the case of 20 travelers in the kroB150 data set, and the other results are better than the TCX algorithm. In the case of the kroB150 data set of 10 and 20 travelers, the results are slightly worse than RGA and RLGA algorithms. We use *D* to visually demonstrate the improvement or lack of results where $D = (\text{best_result_among_other_genetic_algorithms} - \text{VNS-GA_result}) / \text{best_result_among_other_genetic_algorithms} \times 100\%$. Thus, $D > 0$ means the result is improved and is the best result among all genetic algorithms while $D < 0$ means the result is worse than the best result. To visualize how the performance of the algorithm changes with the number of travelers increase, we introduce the parameter E_i . E_i is the average of different numbers of travelers (*i* is the number of travelers and $i = 3, 5, 10, 20$). As can be seen from Fig. 5, with the increase of travelers' number, the performance of the algorithm decrease, but in general, the performance of the algorithm is improved compared with other genetic algorithms.

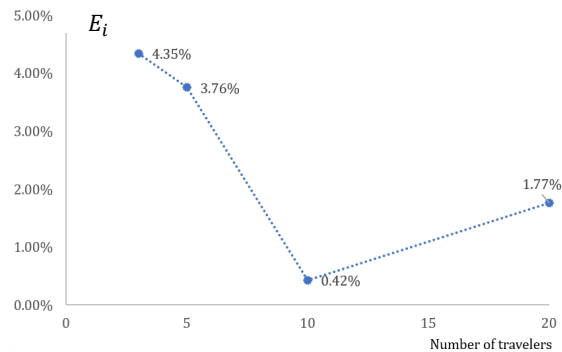


Fig. 5 VNS-GA performance variation with the number of travelers

Table 4 Comparison of total path (VNS-GA with other genetic algorithms)

Data	<i>n</i>	<i>m</i>	GA1C	GA2C	GA2PC	GGA-SS	TCX	IWO	VNS-GA
51	51	3	529	570	543	449	492	448	495
	51	5	564	627	586	479	519	478	552
	51	10	801	879	723	584	670	583	1100
100	100	3	27036	30972	26653	22051	26130	21941	25524
	100	5	29753	44062	30408	23678	28612	23319	31222
	100	10	36890	65116	31227	28488	30988	27072	49606
	100	20	62471	95568	54700	40892	44686	38357	101235
150	150	3	46111	48108	47418	38434	44674	38055	31960
	150	5	49443	51101	49947	39962	47811	38881	35754
	150	10	59341	64893	54958	44274	51326	42462	55505
	150	20	94291	100037	73934	56412	62400	53612	106917

The data in Table 4 are the values of the total path. The balance degree needs to be compared with the longest sub-path value and the total path value. Although on some data sets, the value of the longest path in the solution obtained by the VNS-GA algorithm is slightly higher than other algorithms, literature [14] is not multiple objective optimization and the objective of RGA and RLGA algorithms in the literature [26] is to make the longest sub-path the shortest, neither provide the total path length and the balance degree. Therefore, we propose the balance ratio (R) to measure the workload balance. The calculation formula is $(\text{longest sub-path length} - \text{shortest sub-path length}) / \text{average length of each sub-path} \times 100\%$, given the total path length of each standard data set in the case of different traveler numbers and the calculation results of balance degree are shown in Table 5.

It can be seen from Tables 3 to 5 that in comparison with other algorithms, the VNS-GA can ensure that the value of the total path is within an acceptable range while ensuring that the value of the longest sub-path is shortest. Thus, it can be seen as VNS-GA can find solutions with better balance and shorter total path length.

Fig. 6 is a detailed path diagram of the optimal solution of the VNS-GA algorithm after running on each data set. It can be intuitively seen from the figure that the number of nodes contained in each path is roughly equivalent, and the travel distance required for each traveling salesman is roughly the same.

In the case of different numbers of travelers, the VNS-GA has achieved good results when experimenting on several standard data sets. It indicates that the VNS can better solve the situation where GA is easy to fall into local optimality. VNS has a deeper search of the solution space, and the insertion operator designed in the neighbourhood action can optimize the workload balance problem so that the solution can be developed in the direction of equilibrium and the total path is shorter.

Table 5 Balance of VNS-GA on standard data set

Data	n	m	Total path	Longest path	R
51	51	3	495	165	0 %
	51	5	552	121	29.04 %
	51	10	1100	112	4.5 %
100	100	3	25524	8613	2.60 %
	100	5	31222	6445	9.40 %
	100	10	49606	5764	22.48 %
	100	20	101235	5395	26.90 %
150	150	3	31960	10878	4.76 %
	150	5	35754	7711	17.98 %
	150	10	55505	5937	11.03 %
	150	20	102650	5754	14.50 %

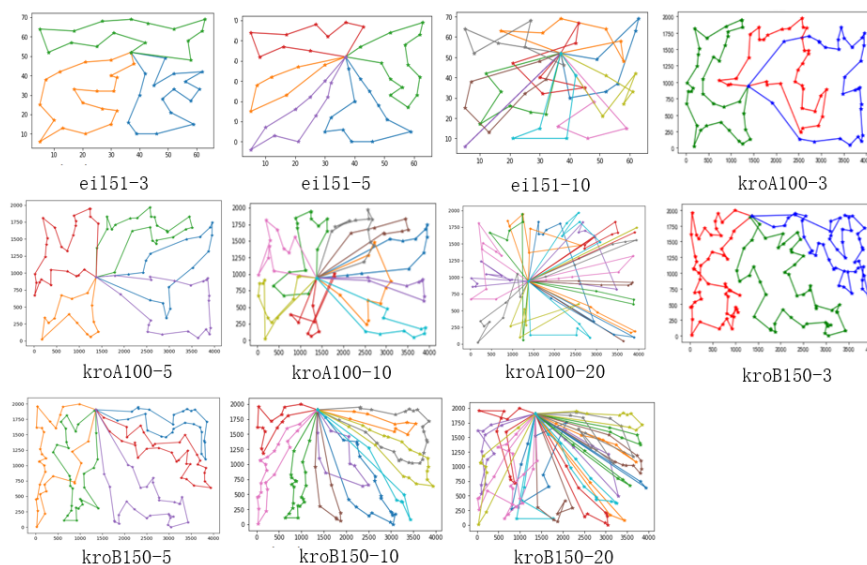


Fig. 6 Path diagram of VNS-GA on standard data set

5. Conclusion

In current times, the research on TSP has been relatively mature, but the mTSP of workload balance involves more constraints and the problem is more complicated. Thus, there are relatively few studies. This paper proposes an improved genetic algorithm (VNS-GA) to solve mTSP with workload balance. Aiming at the goal of workload balance in the mTSP, firstly, the polar coordinate classification algorithm is designed to reduce the intersection between paths and quickly obtain better initial solutions. Then, a distance comparison insertion operator is designed, which specifically takes out the node in the longest path and inserts it into the shortest path to achieve the goal of workload balance faster and to improve the efficiency of the algorithm. To avoid the genetic algorithm falling into the local optimal solution prematurely, the variable neighbourhood descent process is introduced to generate offspring, and different neighbourhood actions are used to search alternately the neighbourhood solution space adequately. Finally, the algorithm is tested on the standard data set of TSPLIB. The experimental results showed that the improved genetic algorithm (VNS-GA) is very competitive. VNS-GA is superior to other improved genetic algorithms on small and medium-sized example sets especially when the number of travelers is small.

At the same time, there are still a lot of crossed paths in the detailed path graph, which indicates that the algorithm still has room for improvement. In the future, other neighbourhood actions with better performance can be introduced to increase the space for the search of the algorithm and to improve the search efficiency. Secondly, how to find a better solution when the number of travelers is large remains to be studied further. In addition, the performance of the algorithm on very large data sets still needs further study.

Acknowledgement

We thank the Editor and two anonymous referees for their many helpful comments on an earlier version of our paper. This work was supported in part by the National Natural Science Foundation of China under grant numbers 72171016; and Beijing Social Science Foundation under grant numbers 20JCC005; and the Beijing Logistics Informatics Research Base.

References

- [1] Bektas, T. (2006). The multiple traveling salesman problem: An overview of formulations and solution procedures, *Omega*, Vol. 34, No. 3, 209-219, doi: [10.1016/j.omega.2004.10.004](https://doi.org/10.1016/j.omega.2004.10.004).
- [2] Bostanci, B., Karaağaç, A. (2019). Investigating the shortest survey route in a GNSS traverse network, *Tehnički Vjesnik - Technical Gazette*, Vol. 26, No. 2, 355-362, doi: [10.17559/TV-20170924174221](https://doi.org/10.17559/TV-20170924174221).
- [3] Iqbal Ali, A., Kennington, J.L. (1986). The asymmetric M-traveling salesmen problem: A duality based branch-and-bound algorithm, *Discrete Applied Mathematics*, Vol. 13, No. 2-3, 259-276, doi: [10.1016/0166-218X\(86\)90087-9](https://doi.org/10.1016/0166-218X(86)90087-9).
- [4] Gavish, B., Srikanth, K. (1986). An optimal solution method for large-scale multiple traveling salesman problems, *Operations Research*, Vol. 34, No. 5, 698-717, doi: [10.1287/opre.34.5.698](https://doi.org/10.1287/opre.34.5.698).
- [5] Yu, Q.S., Lin, D.M., Wang, D. (2012). An overview of multiple traveling salesman problem, *Value Engineering*, Vol. 31, No. 2, 166-168, doi: [10.14018/j.cnki.cn13-1085/n.2012.02.143](https://doi.org/10.14018/j.cnki.cn13-1085/n.2012.02.143).
- [6] Carter, A.E., Ragsdale, C.T. (2006). A new approach to solving the multiple traveling salesperson problem using genetic algorithms, *European Journal of Operational Research*, Vol. 175, No. 1, 246-257, doi: [10.1016/j.ejor.2005.04.027](https://doi.org/10.1016/j.ejor.2005.04.027).
- [7] Singh, A., Baghel, A.S. (2009). A new grouping genetic algorithm approach to the multiple traveling salesperson problem, *Soft Computing*, Vol. 13, 95-101, doi: [10.1007/s00500-008-0312-1](https://doi.org/10.1007/s00500-008-0312-1).
- [8] Zhou, W., Li, Y. (2010). An improved genetic algorithm for multiple traveling salesman problem, In: *Proceedings of 2nd International Asia Conference on Informatics in Control, Automation and Robotics (CAR 2010)*, Wuhan, China, 493-495, doi: [10.1109/CAR.2010.5456787](https://doi.org/10.1109/CAR.2010.5456787).
- [9] Koh, S.P., bin Aris, I., Ho, C.K., Bashi, S.M. (2006). Design and performance optimization of a multi-TSP (Traveling Salesman Problem) algorithm, *Artificial Intelligence and Machine Learning AIML*, Vol. 6, No. 3, 29-33.
- [10] Hu, S.J., Lu, H.Y., Huang, Y., Xu, K.B. (2019). Improved genetic algorithm for solving multiple traveling salesman problem with balanced workload, *Computer Engineering and Applications*, Vol. 55, No. 17, 150-155.
- [11] Guo, S. (2019). *Solutions space analysis of MTSP and application in VRP optimization*, Beijing University of Posts and Telecommunications, Beijing, China, from <https://kns.cnki.net/KCMS/detail/detail.aspx?dbname=CMFD201902&filename=1019113259.nh>, accessed April 11, 2021.

- [12] Lu, Z., Zhang, K., He, J., Niu, Y. (2016), Applying K-means clustering and genetic algorithm for Solving MTSP, In: Gong, M., Pan, L., Song, T., Zhang, G. (eds.), *Bio-inspired Computing – Theories and Applications*, Springer Singapore, 278-284, doi: [10.1007/978-981-10-3614-9_34](https://doi.org/10.1007/978-981-10-3614-9_34).
- [13] Cheikhrouhou, O., Khoufi, I. (2021). A comprehensive survey on the multiple travelling salesman problem: Applications, approaches and taxonom, *Computer Science Review*, Vol. 40, doi: [/10.1016/j.cosrev.2021.100369](https://doi.org/10.1016/j.cosrev.2021.100369).
- [14] Pan, J., Wang, D. (2006). An ant colony optimization algorithm for multiple travelling salesman problem, In: *Proceedings of the First International Conference on Innovative Computing, Information and Control - Volume I (ICICIC'06)*, Beijing, China, 210-213, doi: [10.1109/icicic.2006.40](https://doi.org/10.1109/icicic.2006.40).
- [15] Venkatesh, P., Singh, A. (2015). Two metaheuristic approaches for the multiple traveling salesperson problem, *Applied Soft Computing*, Vol. 26, 74-89, doi: [10.1016/j.asoc.2014.09.029](https://doi.org/10.1016/j.asoc.2014.09.029).
- [16] Ryan, J.L., Bailey, T.G., Moore, J.T., Carlton, W.B. (1998), Reactive tabu search in unmanned aerial reconnaissance simulations, In: *Proceedings of the 30th 1998 Winter Simulation Conference. Proceedings (Cat. No.98CH36274)*, Washington, USA, Vol. 1, 873-879, doi: [10.1109/wsc.1998.745084](https://doi.org/10.1109/wsc.1998.745084).
- [17] Song, C.H., Lee, K., Lee, W.D. (2003). Extended simulated annealing for augmented TSP and multi-salesmen TSP, In: *Proceedings of the International Joint Conference on Neural Networks 2003*, Oregon, USA, Vol. 3, 2340-2343, doi: [10.1109/IJCNN.2003.1223777](https://doi.org/10.1109/IJCNN.2003.1223777).
- [18] Hu, Y., Yao, Y., Lee, W.S. (2020). A reinforcement learning approach for optimizing multiple traveling salesman problems over graphs, *Knowledge-Based Systems*, Vol. 204, Article No. 106244, doi: [10.1016/j.knosys.2020.106244](https://doi.org/10.1016/j.knosys.2020.106244).
- [19] Bonz, J. (2021). Application of a multi-objective multi traveling salesperson problem with time windows, *Public Transport*, Vol. 13, 35-57, doi: [10.1007/s12469-020-00258-6](https://doi.org/10.1007/s12469-020-00258-6).
- [20] Liu, H., Zhang, H., Xu, Y. (2021). The m-Steiner traveling salesman problem with online edge blockages, *Journal of Combinatorial Optimization*, Vol. 41, 844-860, doi: [10.1007/s10878-021-00720-6](https://doi.org/10.1007/s10878-021-00720-6).
- [21] Dong, H.Y., Huang, M., Wang, X.W., Zheng, B.L. (2009). Review of variable neighborhood search algorithm, *Control Engineering of China*, Vol. 16, No. 2, 1-5.
- [22] Li, J., Guo, Y.H. (2001). *Theory and method of optimal scheduling of logistics distribution vehicles*, China Fortune Press, Beijing, China.
- [23] Min, J.N., Jin, C., Lu, L.J. (2019). Split-delivery vehicle routing problems based on a multi-restart improved sweep approach, *International Journal of Simulation Modelling*, Vol. 18, No. 4, 708-719, doi: [10.2507/IJSIMM18\(4\)CO19](https://doi.org/10.2507/IJSIMM18(4)CO19).
- [24] Min, J.N., Jin, C., Lu, L.J. (2019). Maximum-minimum distance clustering method for split-delivery vehicle-routing problem: Case studies and performance comparisons, *Advances in Production Engineering & Management*, Vol. 14, No. 1, 125-135, doi: [10.14743/apem2019.1.316](https://doi.org/10.14743/apem2019.1.316).
- [25] Xiong, C., Wu, H.P., Li, B. (2010). Improved genetic algorithm for solving MTSP, In: *Proceedings of the 4th China Intelligent Computing Conference*, Beijing, China, 143-149.
- [26] Hu, S.J. (2019). *Research on multiple traveling salesman problem based on improved genetic algorithm*, Master Thesis, Jiangnan University, Jiangnan, China.

Change impact analysis of complex product using an improved three-parameter interval grey relation model

Yang, W.M.^a, Li, C.D.^{a,*}, Chen, Y.H.^b, Yu, Y.Y.^{a,*}

^aSchool of Management Jinan University, Guangzhou, P.R. China

^bInternational Business School, Jinan University, Zhuhai, P.R. China

ABSTRACT

Change impact evaluation of complex product plays an important role in controlling change cost and improving change efficiency of engineering change enterprises. In order to improve the accuracy of engineering change impact evaluation, this paper introduces three-parameter interval grey number to evaluate complex products according to the data characteristics. The linear combination of BWM and Gini coefficient method is used to improve the three-parameter interval grey number correlation model. It is applied to the impact evaluation of complex product engineering change. This paper firstly constructs a multi-stage complex network for complex product engineering change. Then the engineering change impact evaluation index system is determined. Finally, a case analysis was carried out with the permanent magnet synchronous centrifugal compressor in a large permanent magnet synchronous centrifugal unit to verify the effectiveness of the proposed method.

ARTICLE INFO

Keywords:

Manufacturing;
Engineering;
Complex product;
Change impact analysis;
Three-parameter interval grey number;
Grey relational model;
BWM method (best-worst model);
Gini weighting method

*Corresponding author:

licd@jnu.edu.cn
(Li, C.D.)
3035905183@qq.com
(Yu, Y.Y.)

Article history:

Received 10 April 2021
Revised 23 May 2021
Accepted 5 June 2021



Content from this work may be used under the terms of the Creative Commons Attribution 4.0 International Licence (CC BY 4.0). Any further distribution of this work must maintain attribution to the author(s) and the title of the work, journal citation and DOI.

1. Introduction

There are increasingly fierce competition among complex product manufacturing enterprises in the rapidly changing market environment. In order to improve competitiveness and meet the changing needs of customers for engineering change, companies inevitably face more and more complex engineering changes. When engineering changes occur, many structures of complex products will be affected. The management of engineering change is roughly divided into four stages: engineering change application, engineering change process impact analysis and evaluation, engineering change decision and approval, and engineering change implementation. In these four stages, the analysis of the engineering change impact can not only be used to determine the necessity of change implementation, but also provide guidance for the formulation of change decision and strategies [1-4]. It is of great significance to control the cost of change and

improve the efficiency of change, especially to consider the multi-stage impact when evaluating the impact of engineering change.

Many studies have done some research on the production of complex products [5-9]. However, due to the complexity of parts, the complexity of disciplines and the heterogeneity of knowledge, as well as the difficulty of data acquisition, there is great opacity in the process of change impact evaluation. Therefore, this article improved three-parameter interval grey relational and applied to the evaluation of the impact of engineering changes.

Many scholars have studied the impact evaluation of engineering change. It mainly includes the evaluation of change impact scope and the change impact degree. Based on the weighted network theory, (Cheng and Chu, 2012) proposed three variable indexes (degree variable, reachable variable and interval variable) [9]. The degree variability is used to calculate the impact of direct change by Ahmad *et al.* (2013) studied a cross domain approach to decompose design and identify possible change propagation links, supplemented by an interactive tool to functions, components and detailed design process [10]. Chen *et al.* (2015) proposed an assess the impact of changes. This method considered the information domain of requirements, object-oriented method, and described its components and related requirements by attributes and links, so as to model the integrated content of products and perform CIA tasks in variant product design [11]. Maazoun *et al.* (2016) proposed an automatic method to analyze the evolution of feature change model, tracked their impact on SPL design, and provided a set of suggestions to ensure the consistency of the two models [12]. Gong *et al.* (2021) analyzed the problems existing in modern product packaging and its impact on the ecological environment, and summarized the design methods of modern green packaging [13]. Zheng *et al.* (2020) put forward the evaluation method of change propagation probability based on grey comprehensive relational analysis and the evaluation method of change propagation impact probability based on configuration change value analysis [14]. (Li and Zhao, 2014) proposed an engineering change scheduling method which combined change propagation simulation with optimization algorithm in complex product development process [15]. Ma *et al.* (2016) established an engineering change analysis model based on the design attribute network and defined the influence of change propagation on the intensity of change propagation through the quantification of change propagation influence factors [16]. Maldini *et al.* (2019) proposed methods to assess the impact of such approaches and applied them to the specific case of "product personalisation" [17]. (Zhang and Yang, 2019) constructed a complex product design structure-task network evolution model under the influence of engineering changes, and analyzed the impact of changes on design tasks [18]. Maurya *et al.* (2017) targeted such dependencies and non-creative hindrances at concept generation stage through a mixed reality implementation. They established requirements for creating a suitable design-tool and presents a proof-of-concept use-case [19]. Palumbo *et al.* (2018) presented a method of achieving accurate Life cycle assessment results, which helps with decision-making and provides support in the selection of building products and materials. [20]. Li *et al.* (2020) established an engineering change risk propagation model based on load capacity [21].

Some of the existing studies have studied the change risk of change evaluation, and the change propagation. Then based on the multi-stage complex network model, this paper analyzes the multifaceted change propagation impact from the aspect of change propagation path. In addition, there are many parts in complex products and their relationship is complex. The relationship of each stage and parts is dynamic under the influence of engineering changes. Engineering change involves a series of activities such as product design or process, related documents, components or assembly, self-made or purchased parts, production process and even suppliers. The acquisition of engineering change data for complex products is more difficult and the data is poor, with greater ambiguity. Therefore, this paper adopts the three-parameter grey relational model based on BWM and Gini coefficient method to evaluate and analyze the impact of engineering change propagation.

Many scholars have studied three-parameter interval grey number decision model [22-27]. There are also some researches on the index weight of grey relational model. (Yin and Ren, 2018) and Liu *et al.* (2020) respectively introduced entropy weight method into grey relation analysis to study the risk evaluation of tunnel, the representative volume evaluation of concrete

and the comprehensive analysis of the influencing factors of gas outburst [28, 29]. Based on entropy TOPSIS grey relational method, Gu *et al.* (2020) studied the path selection of the evaluation of the opening level of coastal cities in China and the evaluation of the implementation effect of TCM standards [30]. (Li and Zhu, 2019) studied the grey relational decision model based on AHP and DEA [31]. Based on the sensitivity and grey relational degree, Zhou *et al.* (2017) proposed a model based on combining weights and gray correlation analysis [32]. So the index weights of different schemes should be different. Therefore, this article combines the advantages of subjective and objective to comprehensively empower it and apply it to the evaluation of complex product engineering changes.

Complex products have the characteristics of many parts, a wide range of technical fields, complex component interfaces, one-off or even small batch production, and many supporting suppliers. It is different from general mass-manufactured parts and technical fields. The engineering change process of complex products need huge human, material and financial resources. If a predictive analysis of the possible impact scope can be made, manufacturing enterprise can avoid the waste of cost, and further accelerate the product development and production cycle. In this paper, the multi-stage complex network topology is firstly established for complex product engineering change, then the engineering change impact evaluation system is established. Finally, the proved three-parameter interval grey relational model is used to evaluate the impact of engineering change. The framework is shown in the Fig. 1.

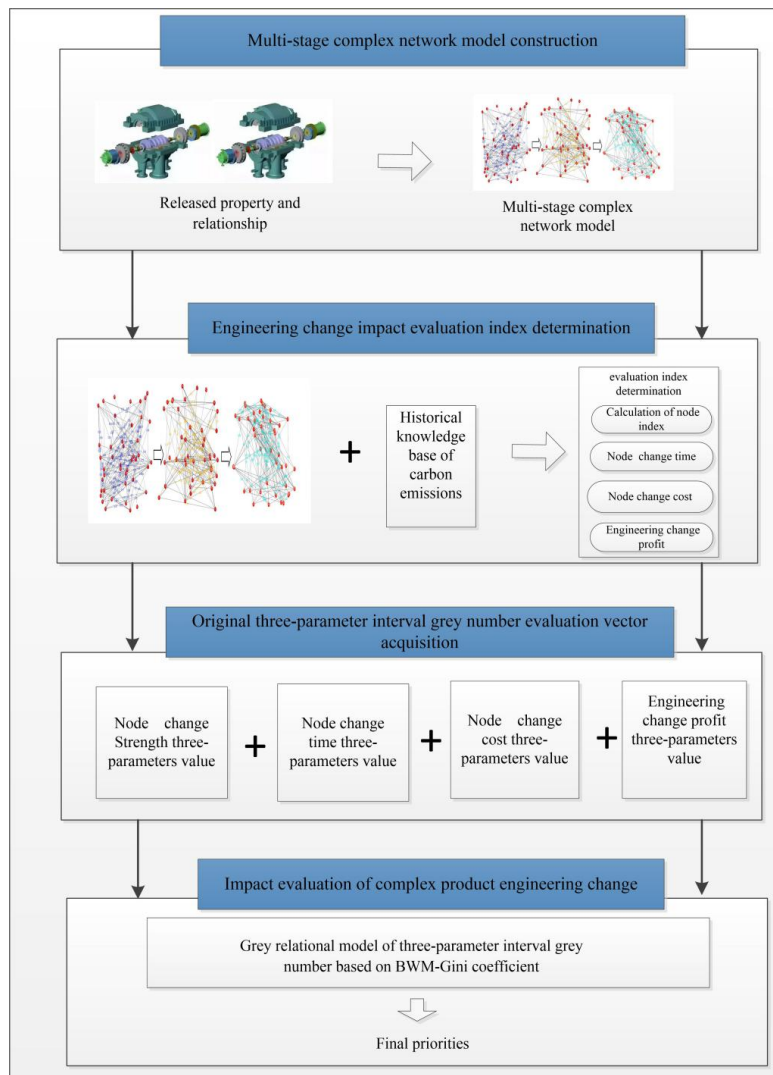


Fig. 1 Framework of the proposed complex product engineering change impact evaluation method

2. Multi-stage complex network

Engineering changes occur in product design, process, manufacturing and other stages. When these changes occur, it is necessary to respond at any time to achieve real-time change design response, rather than follow a fixed process of production. All processes will be affected when the change occurs. It is very vital about how to effectively collect, organize and manage scattered product engineering change knowledge, and use existing domain knowledge to ensure the integrity of product assembly structure. As an important part of the re-generation of product design schemes after product changes, it is critical to timely feed back the engineering change information to the design department. This article builds a multi-stage complex network based on design libraries, knowledge bases, and case libraries.

The propagation characteristic of design change will make the simple parameter change of any part may cause the chain change, and even lead to the avalanche effect of change propagation, which will bring various negative effects to the enterprise. A reasonable and effective communication path of design change can provide decision support for designers to implement design change, help improve product quality, shorten R & D time and reduce design cost. In addition, there are many professional categories of complex products, difficult processing technology, long manufacturing process and complex supporting relationship of parts. Complex products involve multiple processes in the process of engineering change. While continuously shortening the development cycle and improving the product development quality, it tends to the close coordination of design, process and manufacturing process. We integrate the complex network relationship of design, process and manufacturing process in the production process of complex products, so as to comprehensively consider the changes in each stage. The network of each stage is constructed according to its process knowledge and knowledge base. The construction process is shown in Fig. 2.

The single stage network is represented as: $G_k = (V, E_k, W_k) V = (V_i, i = 1, 2, \dots, N)$. If there are connecting edges between parts knowledge, the $e_{k,j}^k = 1$, else, $e_{k,j}^k = 0$. When the multi-stage network is calculated, the connected edges and edge weights of its indexes are added and processed. For the same connected edge, the weight value is $w_{i,j} = \sum_{\alpha}^3 w_{i,j}^{\alpha}$. The schematic diagram of the multi-stage network is shown in Fig. 3. The high speed permanent magnet synchronous variable frequency centrifugal high power chiller of G enterprise is taken as an example.

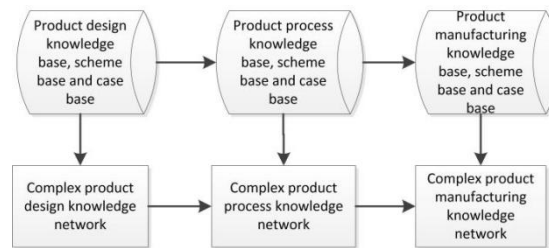


Fig. 2 Multi-stage complex network of complex product

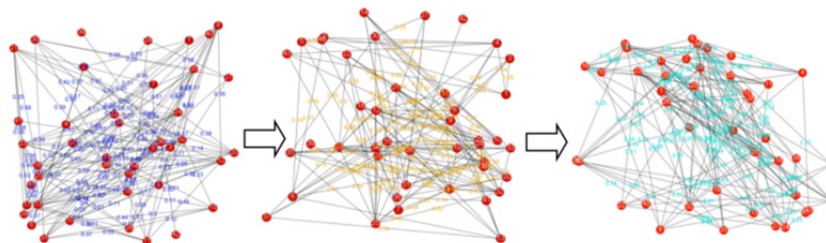


Fig. 3 Multi-stage complex knowledge network

3. Construction of engineering change evaluation index

3.1 Engineering change propagation intensity evaluation

The propagation intensity of engineering change defined in this paper includes node proximity, edge betweenness and propagation probability.

Node proximity: Node proximity is the reciprocal of total distance from the node to all other nodes: $C_i = \frac{1}{\sum_{j=1}^n \beta_{ij}}$. Where β_{ij} is the number of edges in the shortest path from the start node i to the end node j , and n is the total number of nodes. Node proximity describes the degree a node is to the center of a network. The larger the value, the more important the node is.

Edge betweenness: Edge betweenness is defined as the ratio of the number of paths passing through the edge to the total number of shortest paths in the network. Edge betweenness test is an important index to measure the role of connected edges in the whole network. The edge betweenness is expressed as:

$$G_{i,j} = \sum_h \sum_m \frac{N}{m} \frac{L_{h,m}(e_{i,j}^h)}{g_{h,m}} / m = 1, 2, \dots, N, h \neq m (h, m) \neq (i, j) \quad (1)$$

Propagation probability of connected edges: $p_{i,j}$ is the probability of propagation from node i to node j . If node j doesn't belong to the next connected edge, the propagation probability is 0. It is easier to pass through this connecting edge when the propagation probability of the edge is greater. It can be expressed as:

$$P_{ij} = p(v_j|v_i) = \frac{p(v_i \cap v_j)}{p(v_i)} = \frac{p(v_j|v_i)p(v_i)}{p(v_i)} = \frac{p_{ji}p(v_j)}{p(v_i)} \quad (2)$$

Then, the change propagation intensity can be expressed as:

$$I_{ij} = \begin{cases} \omega_1(1 - p_{ij}) + \omega_2 C_i + \omega_3 G_i, & p_{ij} \neq 0 \\ 0, & p_{ij} = 0 \end{cases} \quad (3)$$

3.2 Engineering change cost

Engineering changes of different parts will require different change costs. Changes in components can be mapped to changes in nodes in the network model (node addition and deletion). Therefore, we can evaluate the impact of customer demand change on complex product change by calculating the change cost of node change (node addition and deletion) in the network, the cost of node change in a network can be expressed as: $C_A = \sum_{i=1}^{N_A} c_{(v_i)}$, where c_{v_i} is the change cost of node change, N_A is the total number of change nodes.

The cost details involved in the product production process include: (1) Material cost: It refers to the cost of product standard consumption, supporting raw materials, product accessories and various materials used for production or providing services. It mainly includes the purchase price, related taxes, freight, loading and unloading fees, insurance premiums and other costs that can be directly attributable to the acquisition of materials. (2) Labor cost: It refers to the remuneration and other expenses paid to employees which in order to obtain the services provided by employees. It mainly includes the salary, bonus, allowance, welfare, education fund and so on. (3) Manufacturing cost: It refers to energy consumption, manufacturing accessories, labor insurance, office and fixed expenses. (4) Others: Some consumption including fuel cost, power cost, office cost and depreciation consumed by each production unit.

3.3 Engineering change time

In the process of engineering, change of different parts needs different change time. The node change time in a network can be expressed as:

$$T_A = \sum_{i=1}^{N_A} t_{(v_i)} + t_{(e_{i,j})} \quad (4)$$

Where t_{v_i} is the change time of node change. N_A is the total number of change nodes.

3.4 Engineering change profit

It refers to the positive impact obtained in the change process, such as customer satisfaction, product performance improvement and so on. The engineering change profit can be expressed as: $I_A = \sum_{i=1}^{N_A} i_{(v_i)}$. Where t_{v_i} is the engineering change profit of node change. N_A is the total number of change nodes.

The impact evaluation indexes are as shown in Table 1.

Table 1 Evaluation indexes of engineering change impact

Primary index	Secondary index	Tertiary indicators	
Engineering change impact evaluation	Change propagation intensity	Node betweenness	
		Node degree	
		Node proximity	
		Edge betweenness	
		Propagation probability of connected edges	
	Engineering change cost	Material cost	
		Labor cost	
		Manufacturing cost	
	Engineering change time	Manufacturing cost	
		Node change time	
	Engineering change profit	Edge propagation time	
		improvement of customer satisfaction	
			improvement of product quality

4. Grey relational evaluation model based on three-parameter interval grey number

4.1 Three-parameter interval grey number

From the definition of three-parameter interval grey number, it can be known that it refers to the interval grey number where the center of gravity point with the greatest possible value is known. It can be marked as $A(\otimes) = [\underline{a}, \tilde{a}, \bar{a}]$, where $\underline{a} \leq \tilde{a} \leq \bar{a}$, \underline{a} , \bar{a} are the upper and lower limits of the interval respectively. \tilde{a} is called the "center of gravity" point (Li and Zhang, 2020) [37].

When two of the three parameters \underline{a} , \tilde{a} , \bar{a} are the same, the three-parameter interval grey number degenerates to the interval grey number. When $\underline{a} = \tilde{a} = \bar{a}$, the three parameter interval grey number degenerates to the real number. In fact, the interval grey number and the real number are special cases of the three-parameter interval grey number.

Its algorithm is similar to interval grey number. Let three-parameter interval grey number $A(\otimes) = [\underline{a}, \tilde{a}, \bar{a}]$, $B(\otimes) = [\underline{b}, \tilde{b}, \bar{b}]$, then

$$A(\otimes) + B(\otimes) = [\underline{a} + \underline{b}, \tilde{a} + \tilde{b}, \bar{a} + \bar{b}] \tag{5}$$

$$\frac{A(\otimes)}{B(\otimes)} \in \left[\min \left\{ \frac{\underline{a}}{\underline{b}}, \frac{\underline{a}}{\tilde{b}}, \frac{\underline{a}}{\bar{b}}, \frac{\tilde{a}}{\underline{b}}, \frac{\tilde{a}}{\tilde{b}}, \frac{\tilde{a}}{\bar{b}}, \frac{\bar{a}}{\underline{b}}, \frac{\bar{a}}{\tilde{b}}, \frac{\bar{a}}{\bar{b}} \right\}, \max \left\{ \frac{\underline{a}}{\underline{b}}, \frac{\underline{a}}{\tilde{b}}, \frac{\underline{a}}{\bar{b}}, \frac{\tilde{a}}{\underline{b}}, \frac{\tilde{a}}{\tilde{b}}, \frac{\tilde{a}}{\bar{b}}, \frac{\bar{a}}{\underline{b}}, \frac{\bar{a}}{\tilde{b}}, \frac{\bar{a}}{\bar{b}} \right\} \right] \tag{6}$$

$$\lambda A(\otimes) = [\lambda \underline{a}, \lambda \tilde{a}, \lambda \bar{a}] \tag{7}$$

4.2 Three-parameter interval grey number grey relational model

Suppose that there are n alternative engineering change schemes. They constituted by evaluation schemes set $A = \{a_1, a_2, \dots, a_n\}$. The index set $S = \{s_1, s_2, \dots, s_m\}$ is composed of m attributes. The index value of scheme a_i under the evaluation index s_j can be expressed as $u_{ij}(\otimes) = [\underline{u}_{ij}, \tilde{u}_{ij}, \bar{u}_{ij}] (\underline{u}_{ij} \leq \tilde{u}_{ij} \leq \bar{u}_{ij}, i = 1, 2, \dots, n; j = 1, 2, \dots, m)$. The effect evaluation vector of each scheme is $u_i(\otimes) = (u_{i1}(\otimes), u_{i2}(\otimes), \dots, u_{im}(\otimes)), i = 1, 2, \dots, n$. The weight of index under each scheme is $w_{i1}, w_{i2}, \dots, w_{im}$, and $\sum_{j=1}^m w_{ij} = 1 (i = 1, 2, \dots, n)$. There are different attribute indexes with different dimensions and measurement standards. In order to increase the comparability of

alternatives, it is necessary to normalize the effect evaluation vector of decision alternatives. In this paper, we use the range transformation method to normalize the decision matrix.

For profitable attribute values:

$$x_{ij} = \frac{u_{ij}-u_j^\nabla}{u_j^*-u_j^\nabla}, \tilde{x}_{ij} = \frac{\tilde{u}_{ij}-u_j^\nabla}{u_j^*-u_j^\nabla}, \bar{x}_{ij} = \frac{\bar{u}_{ij}-u_j^\nabla}{u_j^*-u_j^\nabla} \tag{8}$$

For cost attribute values:

$$x_{ij} = \frac{\bar{u}_j^*-u_{ij}}{\bar{u}_j^*-u_j^\nabla}, \tilde{x}_{ij} = \frac{\bar{u}_j^*-\tilde{u}_{ij}}{\bar{u}_j^*-u_j^\nabla}, \bar{x}_{ij} = \frac{\bar{u}_j^*-\bar{u}_{ij}}{\bar{u}_j^*-u_j^\nabla} \tag{9}$$

Where $\bar{u}_j^* = \max_{1 \leq i \leq n} \{\bar{\mu}_{ij}\}$, $u_j^\nabla = \min_{1 \leq i \leq n} \{u_{ij}\}$, $j = 1, 2, \dots, m$

Let the normalized effect evaluation vector be:

$$x_i(\otimes) = (x_{i1}(\otimes), x_{i2}(\otimes), \dots, x_{im}(\otimes)), i = 1, 2, \dots, n \tag{10}$$

Where $x_{ij}(\otimes) \in [x_{ij}, \tilde{x}_{ij}, \bar{x}_{ij}]$ is a three-parameter interval grey number in $[0,1]$.

Recorded that $x_j^+ = \max_{1 \leq i \leq n} \{x_{ij}\}$, $\tilde{x}_j^+ = \max_{1 \leq i \leq n} \{\tilde{x}_{ij}\}$, $\bar{x}_j^+ = \max_{1 \leq i \leq n} \{\bar{x}_{ij}\}$, $x_j^- = \min_{1 \leq i \leq n} \{x_{ij}\}$, $\tilde{x}_j^- = \min_{1 \leq i \leq n} \{\tilde{x}_{ij}\}$, $\bar{x}_j^- = \min_{1 \leq i \leq n} \{\bar{x}_{ij}\}$ ($j = 1, 2, \dots, m$). Then the m -dimensional three-parameter non negative interval grey number vectors

$$x^+(\otimes) = \{x_1^+(\otimes), x_2^+(\otimes), \dots, x_m^+(\otimes)\}, x^-(\otimes) = \{x_1^-(\otimes), x_2^-(\otimes), \dots, x_m^-(\otimes)\} \tag{11}$$

are called ideal optimal scheme effect evaluation vectors and critical scheme effect evaluation vectors respectively.

We assume that the grey interval relational degree of the normalized effect evaluation vector $x_i(\otimes)$ of scheme A_i with respect to the ideal optimal scheme effect evaluation vector $x^+(\otimes)$ is $G(x^+(\otimes), x_i(\otimes))$. And the grey interval relational degree of critical scheme effect evaluation vector $x^-(\otimes)$ is $G(x^-(\otimes), x_i(\otimes))$. Assume that the weights of two grey relational degrees are α_1, α_2 ($\alpha_1 + \alpha_2 = 1$). Then,

$$G(x_i(\otimes)) = \alpha_1 G(x^+(\otimes), x_i(\otimes)) + \alpha_2 [1 - G(x^-(\otimes), x_i(\otimes))], i = 1, 2, \dots, n \tag{12}$$

is the three-parameter grey interval linear relational degree of the effect evaluation vector $x_i(\otimes)$.

$$G(x_i(\otimes)) = [G(x^+(\otimes), x_i(\otimes))]^{\alpha_1} + [1 - G(x^-(\otimes), x_i(\otimes))]^{\alpha_2}, i = 1, 2, \dots, n \tag{13}$$

is the three-parameter grey interval product relational degree of the effect evaluation vector $x_i(\otimes)$.

The distribution probability of barycenter point with the highest probability of taking the value of three-parameter interval grey number $x_{ij}(\otimes) \in [x_{ij}, \tilde{x}_{ij}, \bar{x}_{ij}]$ is $f(\tilde{x}_{ij}) \geq \sigma$. Normally, $\sigma \geq 60\%$. If $\sigma \leq 60\%$ it indicates that the decision is wrong, and the most likely value needs to be determined again. Based on the center of gravity, we can build a three-parameter interval grey number relational degree evaluation model.

Definition 1: For three-parameter interval grey number $x_{ij}(\otimes) \in [x_{ij}, \tilde{x}_{ij}, \bar{x}_{ij}]$, then

$$\gamma_{ij}^+ = \frac{3}{5} \times \frac{\bar{m}^+ + \eta \bar{M}^+}{\bar{\Delta}_{ij}^+ + \eta \bar{M}^+} + \frac{2}{5} \left[(1 - \beta) \frac{m^+ + \eta M^+}{\underline{\Delta}_{ij}^+ + \eta \underline{M}^+} \beta \frac{\bar{m}^+ + \eta \bar{M}^+}{\bar{\Delta}_{ij}^+ + \eta \bar{M}^+} \right] \tag{14}$$

is called the three-parameter grey interval relational coefficient of sub factor. x_{ij} with respect to ideal factor x_j^+ . $\eta \in (0,1)$ is the resolution coefficient. $\beta \in (0,1)$ is the decision preference coefficient. Where,

$$\underline{\Delta}_{ij}^+ = |x_j^+ - x_{ij}|, \bar{\Delta}_{ij}^+ = |\tilde{x}_j^+ - \tilde{x}_{ij}|, \bar{\Delta}_{ij}^+ = |\bar{x}_j^+ - \bar{x}_{ij}|, i = 1, 2, \dots, n; j = 1, 2, \dots, m$$

$$\begin{aligned} \underline{m}^+ &= \min_{1 \leq i \leq n} \min_{1 \leq j \leq m} \Delta_{ij}^+, \tilde{m}^+ = \min_{1 \leq i \leq n} \min_{1 \leq j \leq m} \tilde{\Delta}_{ij}^+, \bar{m}^+ = \min_{1 \leq i \leq n} \min_{1 \leq j \leq m} \bar{\Delta}_{ij}^+ \\ \underline{M}^+ &= \max_{1 \leq i \leq n} \max_{1 \leq j \leq m} \Delta_{ij}^+, \tilde{M}^+ = \max_{1 \leq i \leq n} \max_{1 \leq j \leq m} \tilde{\Delta}_{ij}^+, \bar{M}^+ = \max_{1 \leq i \leq n} \max_{1 \leq j \leq m} \bar{\Delta}_{ij}^+ \\ G(x^+(\otimes), x_i(\otimes)) &= \sum_{j=1}^m w_{ij} \gamma_{ij}^+, i = 1, 2, \dots, n \end{aligned} \tag{15}$$

is called the three-parameter grey interval relational degree of the effect evaluation vector $x_i(\otimes)$ about the ideal optimal scheme effect evaluation vector $x^+(\otimes)$.

Definition 2: For three-parameter interval grey number $x_{ij}(\otimes) \in [x_{ij}, \tilde{x}_{ij}, \bar{x}_{ij}]$,

$$\gamma_{ij}^- = \frac{3}{5} \times \frac{\tilde{m}^- + \varepsilon \bar{M}^-}{\bar{\Delta}_{ij}^- + \varepsilon \bar{M}^-} + \frac{2}{5} \times \left[(1 - \delta) \frac{\underline{m}^- + \varepsilon \underline{M}^-}{\underline{\Delta}_{ij}^- + \varepsilon \underline{M}^-} + \delta \frac{\tilde{m}^- + \varepsilon \bar{M}^-}{\bar{\Delta}_{ij}^- + \varepsilon \bar{M}^-} \right] \tag{16}$$

is called the three-parameter grey interval relational coefficient of sub factor. x_{ij} with respect to ideal factor x_j^- . $\eta \in (0, 1)$ is the resolution coefficient. $\delta \in (0, 1)$ is the decision preference coefficient. Where,

$$\begin{aligned} \underline{\Delta}_{ij}^- &= |x_{ij} - x_j^-|, \tilde{\Delta}_{ij}^- = |\tilde{x}_{ij} - \tilde{x}_j^-|, \bar{\Delta}_{ij}^- = |\bar{x}_{ij} - \bar{x}_j^-|, i = 1, 2, \dots, n; j = 1, 2, \dots, m \\ \underline{m}^- &= \min_{1 \leq i \leq n} \min_{1 \leq j \leq m} \Delta_{ij}^-, \tilde{m}^- = \min_{1 \leq i \leq n} \min_{1 \leq j \leq m} \tilde{\Delta}_{ij}^-, \bar{m}^- = \min_{1 \leq i \leq n} \min_{1 \leq j \leq m} \bar{\Delta}_{ij}^- \\ \underline{M}^- &= \max_{1 \leq i \leq n} \max_{1 \leq j \leq m} \Delta_{ij}^-, \tilde{M}^- = \max_{1 \leq i \leq n} \max_{1 \leq j \leq m} \tilde{\Delta}_{ij}^-, \bar{M}^- = \max_{1 \leq i \leq n} \max_{1 \leq j \leq m} \bar{\Delta}_{ij}^- \\ G(x^-(\otimes), x_i(\otimes)) &= \sum_{j=1}^m w_{ij} \gamma_{ij}^-, i = 1, 2, \dots, n \end{aligned} \tag{17}$$

is called the three-parameter grey interval relational degree of the effect evaluation vector $x_i(\otimes)$ about the critical scheme effect evaluation vector $x^-(\otimes)$.

4.3 Determination of weight

At present, scholars attach great importance to the development and application of subjective and objective empowerment methods in the research of evaluation. The subjective weight reflects the subjective willingness of the evaluation subject, and highlights the degree of distinction between the evaluation objects through index data information. The combination of them will make the result more objective. In this paper, the simplified BWM subjective weighting method and the Gini coefficient weighting method which can better reflect the data difference information are selected for combination weighting.

4.3.1 Determination of weight based on BWM

BWM (best-worst method) is a new method to determine the subjective weight of index proposed by Rezaei in 2014. The most frequently used method in the multiple index evaluation is AHP method. In AHP method, any two indexes are usually compared with each other to get the evaluation matrix of indexes, which needs $n(n - 1)/2$ times of comparison. The calculation process of it is complicated and will cause certain errors. However, BWM only needs $2n - 3$ calculations by selecting the best and the worst indexes and comparing them with other indexes. It simplifies the complicated process of AHP, greatly reduces the amount of data, reduces the mistakes caused by too much data, makes it easier to pass the consistency test, and improves the reliability. The calculation steps are as follows (Behzad *et al.* (2020))[33]:

- The best index X_B and the worst index X_W are selected according to experts' opinions in index set $X = \{x_1, x_2, \dots, x_n\}$.
- Experts use 1-9 point scale to score and determine the importance of other indexes relative to the optimal indexes. We construct the comparison vector $C_B = (C_{B1}, C_{B2}, \dots, C_{Bj})$. C_{Bj} rep-

resents the importance of the optimal index compared with index j . 1 means C_B and C_{B_j} are equally important. 9 means C_B is extremely important than C_{B_j} .

- We need to determine the unimportance of other indexes relative to the worst indexes and construct a comparison vector $C_w = (C_{1w}, C_{B_{2w}}, \dots, C_{jw})^T$. Where C_{jw} represents the least importance of the worst index compared with index j . 1 means C_{jw} and C_w are equally unimportant. 9 means C_{jw} and C_w are extremely unimportant.
- From the goal programming model, a mathematical programming formula is established and solved to obtain the optimal index weight $\omega_j^* = (\omega_1^*, \omega_2^*, \dots, \omega_n^*)$.

$$\begin{aligned} & \min \max_j \left\{ \left| \frac{\omega_j}{\omega_w} - a_{Bj} \right| \right\} \\ \text{s. t. } & \begin{cases} \sum_{j=1}^n \omega_j = 1 \\ \omega_j \geq 0, j = 1, 2, \dots, n \end{cases} \end{aligned} \tag{18}$$

Where ω_B is the weight of C_B , C_j is the criterion vector. ω_j is the weight of C_j . ω_B is the weight of C_w . a_{Bj} represents the importance of C_B to C_j ; a_{jw} represents the importance of C_j to C_w . It can be transformed to \min^k

$$\text{s. t. } \begin{cases} \left| \frac{\omega_B}{\omega_j} - a_{Bj} \right| \leq k \\ \left| \frac{\omega_j}{\omega_w} - a_{jw} \right| \leq k, j = 1, 2, \dots, n \\ \sum_{j=1}^n \omega_j = 1 \\ \omega_j \geq 0 \end{cases} \tag{19}$$

- Calculate the consistency ratio. The obtained K can be represented by K^* , and the consistency ratio C_R (C_1 is the given value) can be obtained from $C_R = \frac{k^*}{C_1}$.

The closer of the value is to 0, the better the consistency. When it is 0, it is consistent. If there are P experts participate in the judgment, the final weight will be calculated by weighted average, and the final weight is $\bar{\omega}_j^* = \frac{\sum_{a=1}^p \omega_j^a}{p}$.

4.3.2 Weight determination method based on Gini coefficient

Principle of Gini coefficient weighting method

Gini coefficient weighting method is an objective weighting method by calculating Gini coefficient of evaluation index and normalizing Gini coefficient of each index. First of all, the different data of evaluation objects of a specific evaluation index can be regarded as the income of different levels people. Then the Gini coefficient of a certain index can be calculated. The value of Gini coefficient can reflect the data difference between different evaluation objects. Then, In order to ensure that weight of all indexes are in the range of 0 to 1 and the sum is 1, the Gini coefficient value of each index will be normalized to get the Gini coefficient weight of the evaluation index. Zahng *et al.* (2020) [34].

Gini coefficient weight' calculation of evaluation index

We assume that G_k is the Gini coefficient of the k th index, Y_{ki} is the i th data of the k th index, and μ_k is the expected value of all data of the k th index. Then the Gini coefficient G_k of the k -th index is shown as follows:

$$G_k = \sum_{i=1}^n \sum_{j=1}^n |Y_{ki} - Y_{kj}| / 2n^2 \mu_k \tag{20}$$

$$G_k = \sum_{i=1}^n \sum_{j=1}^n |Y_{ki} - Y_{kj}| / (n^2 - n) \tag{21}$$

Especially, when the mean value of index data is not 0, the Gini coefficient is calculated by the improved formula (13). When the mean value of the index data is 0, the Gini coefficient of the index is calculated by the original formula (14). Gini coefficient of the index truly reflects the data changes of different evaluation objects of the index.

Gini coefficient weight g_k of the k -th index can be obtained by normalizing the Gini coefficient value of each index:

$$g_k = G_k / (\sum_{i=1}^m G_i) \quad (22)$$

Where g_k is Gini coefficient weight of the k th index, G_k is Gini coefficient value of the k -th index, and m is the number of indexes.

The advantages of Gini coefficient weighting method are as follows: first, the weight calculation is not affected by the unit dimension of the index, the definition of Gini coefficient itself eliminates the dimensional influence. Second, Gini coefficient value of the evaluation index reflects the difference between any two evaluation objects. Gini coefficient weight reflects the difference between the data of different evaluation objects of an index. And the weight reflects the data information of the index, which meets the requirements of the objective weighting method.

4.3.3 Combination weighting method based on BWM-Gini coefficient

The BWM method determines the index weight according to the subjective preference of the evaluator, and the method of Gini coefficient determines the objective index weight. In order to fully combine the advantages of the two methods, from the subjective and objective point of view, this paper combines BWM method and Gini coefficient method to determine the comprehensive weight of the evaluation index by linear weighting:

$$W_i^* = \xi W + (1 - \xi) W_i = [w_1^*, w_2^*, \dots, w_n^*]^T \quad (23)$$

Where W_i^* is the comprehensive weight of the decision unit i , ξ is the subjective preference coefficient, $1 - \xi$ is the objective preference coefficient ($\xi \in [0,1]$), and the specific value of ξ is given by the decision maker according to personal preference.

5. Case study

The high-speed permanent magnet synchronous centrifugal unit of G enterprise is a high-tech, high value-added and complex mechanical product involving multi-disciplinary and multi domain knowledge. It has high requirements for continuous innovation ability. Centrifugal compressor is an important part of it, which determines many functions. The product organization diagram and component composition are shown in Fig. 4 and Table 2. The continuous innovation knowledge of full capacity DC high-speed permanent magnet synchronous frequency conversion centrifugal unit involves many aspects within the enterprise, within the industry and across fields. It has the characteristics of multi domain, high frequency, massive, heterogeneous and complex. Combined with the historical case of common engineering change innovation mode of large capacity full DC high-speed permanent magnet synchronous variable frequency centrifugal unit and its design process manufacturing process knowledge base, its multi process network is analyzed to determine the evaluation index value of change impact.

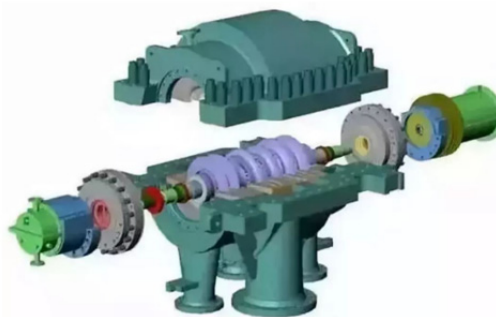


Fig. 4 Large permanent magnet synchronous centrifugal unit and permanent magnet synchronous centrifugal compressor

Table 2 Main parts and node name of permanent magnet synchronous centrifugal compressor

Node	Parts	Node	Parts
V1	mainshaft	V13	bend casing
V2	impeller rim 1	V14	curved separator
V3	roulette 1	V15	refluxer separator
V4	blade 1	V16	refluxer flow channels
V5	shrink-ring	V17	volute
V6	fixed collar	V18	impeller rim 2
V7	balance disc	V19	roulette 2
V8	reinforcement on the back of impeller	V20	blade 2
V9	thrust disc	V21	stator winding
V10	axle sleeve	V22	stator core
V11	suction chamber	V23	foundation
V12	diffuser	V24	p-m rotor

It is known that part 4 needs to be improved due to increased customer demand. There are 4 changed routes, and the impact evaluation of the changed routes is carried out. The four routes are as follows: Engineering change node route 1:4-3-2-6-5-7-9; Engineering change node route 2:4-3-2-5-8-1; Engineering change node route 3:4-3-15-16-17-24; Engineering change node route 4:1-2-3-4-14-22.

The physical schematic diagram of the change routes are shown in Fig. 5.



Fig. 5 Physical schematic diagram of the change routes

First of all, we analyze the relationship between process, design and manufacturing network of the direct drive variable frequency centrifugal compressor. The multi-stage complex network diagram can be referred to Fig. 3.

Through the calculation of index system, we can get the three parameter interval grey number of the evaluation index as follows:

$$X(\otimes) = \begin{bmatrix} [3.38,3.41,3.46][11.21,11.32,11.35][5421,5423,5425][5.98,6.05,6.11] \\ [2.97,3.21,3.04][10.71,11.24,11.46][5275,5279,5283][5.76,6.14,6.17] \\ [3.23,3.34,4.47][11.05,11.10,11.16][5865,5868,5871][6.03,6.17,6.21] \\ [3.18,3.41,3.57][11.28,11.31,11.36][5903,5932,5952][6.11,6.15,6.46] \end{bmatrix}$$

The normalized three-parameter interval grey number evaluation matrix is:

$$X(\otimes) = \begin{bmatrix} [0.59, 0.63, 0.65][0.61, 0.63, 0.65][0.80, 0.82, 0.83][0.60, 0.65, 0.70] \\ [0.67, 0.85, 1.00][0.67, 0.70, 1.00][0.73, 0.81, 1.00][0.00, 0.73, 0.75] \\ [0.00, 0.73, 0.74][0.72, 0.76, 0.79][0.00, 0.62, 0.63][0.64, 0.76, 0.79] \\ [0.53, 0.55, 0.59][0.00, 0.63, 0.69][0.57, 0.58, 0.60][0.70, 0.74, 1.00] \end{bmatrix}$$

According to formula (4), the effect evaluation vectors of ideal optimal scheme and critical scheme are obtained:

$$x^+(\otimes) = ([0.67, 0.85, 1.00], [0.72, 0.76, 1.00], [0.80, 0.82, 1.00], [0.70, 0.76, 1.00])$$

$$x^-(\otimes) = ([0.00, 0.55, 0.59], [0.00, 0.62, 0.65], [0.00, 0.57, 0.60], [0.00, 0.65, 0.70])$$

The weight matrix obtained by expert BWM method is as follows: $W = (w_1, w_2, w_3, w_4) = (0.37, 0.16, 0.32, 0.14)$

The weight obtained from Gini coefficient is as follows:

$$W = (w_1, w_2, w_3, w_4) = (0.33, 0.11, 0.31, 0.25)$$

Then we can calculate the comprehensive weight. this paper takes the preference coefficient 0.4. $W_i^* = 0.6W_B + 0.4W_J$ can be obtained from formula (17). Then we can get the comprehensive weight: $W = (w_1, w_2, w_3, w_4) = (0.35, 0.14, 0.31, 0.18)$

According to Eq. 8 and Eq. 10, the grey interval relational degree of each scheme with ideal optimal scheme and critical scheme is obtained as follows:

$$G(x^+(\otimes), x_1(\otimes)) = 0$$

$$G(x^-(\otimes), x_1(\otimes)) = 0.88$$

$$G(x^+(\otimes), x_2(\otimes)) = 0.72$$

$$G(x^-(\otimes), x_2(\otimes)) = 0.67$$

$$G(x^+(\otimes), x_3(\otimes)) = 0.80$$

$$G(x^-(\otimes), x_3(\otimes)) = 0.54$$

$$G(x^+(\otimes), x_4(\otimes)) = 0.74$$

$$G(x^-(\otimes), x_4(\otimes)) = 0.80$$

The three-parameter grey interval linear relational degree of each scheme is calculated by Eq. 5: $G(x_1(\otimes)) = 0.53, G(x_2(\otimes)) = 0.67, G(x_3(\otimes)) = 0.48, G(x_4(\otimes)) = 0.43$. These relational degree can be expressed as shown in the Fig. 6.

According to the linear relational degree of three-parameter interval grey number, we can find that the most relevant to the ideal optimal scheme is scheme 2. Change node route2 is 4-3-2-5-8-1:blade1-roulette1-impeller rim1-shrink-ring-reinforcement on the back of impeller-mainshaft. The physical schematic diagram of the change route 2 is shown in Fig. 7. We can find that the choice of engineering change route is in line with the reality.

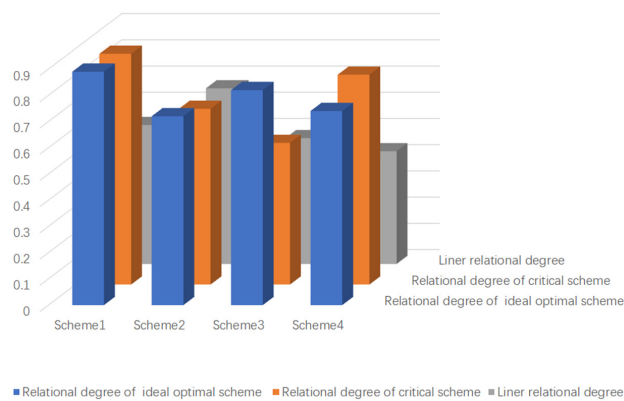


Fig. 6 Relational degree results

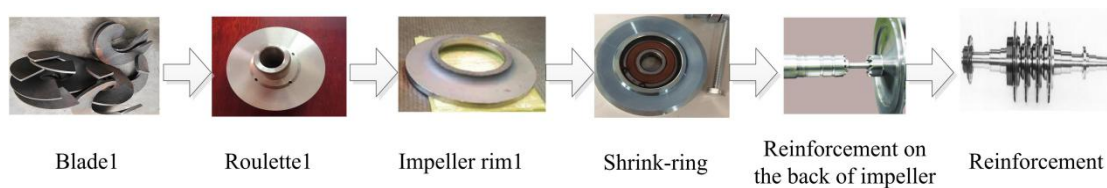


Fig. 7 Physical schematic diagram of change route 2

6. Conclusion

In this paper, an improved three parameter interval grey number is introduced into the impact assessment of complex product engineering change, and the knowledge characteristics in the change process are fully considered. Firstly, considering the influence of multi production process, a multi-stage network model considering design, process and manufacturing process is constructed based on complex network. Then the evaluation index system of engineering change impact is constructed. The evaluation method is improved based on the linear weighting method combined with BWM and Gini coefficient. In this paper, the improved three parameter interval correlation model is introduced to evaluate the impact of complex product change, which improves its utilization of uncertain knowledge. This method makes up for the deficiency of the impact evaluation method based on real numbers. In addition, this paper uses the linear weighting method to reasonably balance the subjective and objective weight proportion, so as to make the weight determination more reasonable.

In the future research, we can further study the subjective and objective comprehensive weight allocation problem, and apply this method to other research aspects of complex products. On the other hand, we can also consider the behavior, structure and function factors in the design process to improve the multi-stage complex product network. It can comprehensively solve the problem of multi-source knowledge of complex products and difficult acquisition of real numbers and improve the decision-making efficiency of complex products in all aspects.

Acknowledgement

The work was supported by National Natural Science Foundation of China(No. 72072072), Natural Science Foundation of Guangdong Province of China (No. 2019A1515010045), 2018 Guangzhou Leading Innovation Team Program (China), (No. 201909010006), Science and Technology Innovation Strategy of Guangdong Province in 2021 (pdjh2021a0054) and Jinan University Management School Funding Program (GY21012).

References

- [1] Yang, D., Sun, Y., Wu, K. (2020). Assembly reliability modelling technology using function decomposing and LSSVM, *International Journal of Simulation Modelling*, Vol. 19, No. 2, 334-345, doi: [10.2507/IJSIMM19-2-C09](https://doi.org/10.2507/IJSIMM19-2-C09).
- [2] Awaga, A.L., Xu, W., Liu, L., Zhang, Y. (2020). Evolutionary game of green manufacturing mode of enterprises under the influence of government reward and punishment, *Advances in Production Engineering & Management*, Vol. 15, No. 4, 416-430, doi: [10.14743/apem2020.4.375](https://doi.org/10.14743/apem2020.4.375).
- [3] Li, H.-Y., Xu, W., Cui, Y., Wang, Z., Xiao, M., Sun, Z.-X. (2020). Preventive maintenance decision model of urban transportation system equipment based on multi-control units, *IEEE Access*, Vol. 8, 15851-15869, doi: [10.1109/ACCESS.2019.2961433](https://doi.org/10.1109/ACCESS.2019.2961433).
- [4] Baynal, K., Sari, T., Akpınar, B. (2018). Risk management in automotive manufacturing process based on FMEA and grey relational analysis: A case study, *Advances in Production Engineering & Management*, Vol. 13, No. 1, 69-80, doi: [10.14743/apem2018.1.274](https://doi.org/10.14743/apem2018.1.274).
- [5] Sterpin Valic, G., Cukor, G., Jurkovic, Z., Brezocnik, M. (2019). Multi-criteria optimization of turning of martensitic stainless steel for sustainability, *International Journal of Simulation Modelling*, Vol. 18, No. 4, 632-642, doi: [10.2507/IJSIMM18\(4\)495](https://doi.org/10.2507/IJSIMM18(4)495).
- [6] Ocampo, L.A., Himang, C.M., Kumar, A., Brezocnik, M. (2019). A novel multiple criteria decision-making approach based on fuzzy DEMATEL, fuzzy ANP and fuzzy AHP for mapping collection and distribution centers in reverse logistics, *Advances in Production Engineering & Management*, Vol. 14, No. 3, 297-322, doi: [10.14743/apem2019.3.329](https://doi.org/10.14743/apem2019.3.329).
- [7] Cica, D., Caliskan, H., Panjan, P., Kramar, D. (2020). Multi-objective optimization of hard milling using taguchi based grey relational analysis, *Tehnički Vjesnik – Technical Gazette*, Vol. 27, No. 2, 513-519, doi: [10.17559/TV-20181013122208](https://doi.org/10.17559/TV-20181013122208).
- [8] Liu, D., Hu, B., Ding, Z., Kaisarb, E.I. (2020). Method of group decision making with interval grey numbers based on grey correlation and relative close degree, *Tehnički Vjesnik – Technical Gazette*, Vol. 27, No. 5, 1579-1584, doi: [10.17559/TV-20200601165833](https://doi.org/10.17559/TV-20200601165833).
- [9] Xiao, Y., Li, C., Song, L., Yang, J., Su, J. (2021). A multidimensional information fusion-based matching decision method for manufacturing service resource, Vol. 9, 39839-39851, doi: [10.1109/ACCESS.2021.3063277](https://doi.org/10.1109/ACCESS.2021.3063277).
- [10] Cheng, H., Chu, X. (2012). A network-based assessment approach for change impacts on complex product, *Journal of Intelligent Manufacturing*, Vol. 23 No. 4, 1419-1431, doi: [10.1007/s10845-010-0454-8](https://doi.org/10.1007/s10845-010-0454-8).
- [10] Ahmad, N., Wynn, D.C., Clarkson, P.J. (2013). Change impact on a product and its redesign process: A tool for knowledge capture and reuse, *Research in Engineering Design*, Vol. 24, No. 3, 219-244, doi: [10.1007/s00163-012-0139-8](https://doi.org/10.1007/s00163-012-0139-8).

- [11] Chen, C.-Y., Liao, G.-Y., Lin, K.-S. (2015). An attribute-based and object-oriented approach with system implementation for change impact analysis in variant product design, *Computer-Aided Design*, Vol. 62, 203-217, doi: [10.1016/j.cad.2014.11.006](https://doi.org/10.1016/j.cad.2014.11.006).
- [12] Maâzoun, J., Bouassida, N., Ben-Abdallah, H. (2016). Change impact analysis for software product lines, *Journal of King Saud University-Computer and Information Sciences*, Vol. 28, No. 4, 364-380, doi: [10.1016/j.jksuci.2016.01.005](https://doi.org/10.1016/j.jksuci.2016.01.005).
- [13] Gong, X.Q., Wu, B., Wu, F. (2021). Research on the impact of green product packaging design on ecological environment, *Fresenius Environmental Bulletin*, Vol. 30, No. 4, 3228-3232.
- [14] Zheng, Y.-J., Yang, Y., Zhang, N. (2020). A model for assessment of the impact of configuration changes in complex products, *Journal of Intelligent Manufacturing*, Vol. 31, No. 2, 501-527, doi: [10.1007/s10845-018-01461-w](https://doi.org/10.1007/s10845-018-01461-w).
- [15] Li, Y., Zhao, W. (2014). An integrated change propagation scheduling approach for product design, *Concurrent Engineering*, Vol. 22, No. 4, 347-360, doi: [10.1177/1063293X14553809](https://doi.org/10.1177/1063293X14553809).
- [16] Ma, S., Jiang, Z., Liu, W. (2016). Evaluation of a design property network-based change propagation routing approach for mechanical product development, *Advanced Engineering Informatics*, Vol. 30, No. 4, 633-642, doi: [10.1016/j.aei.2016.08.002](https://doi.org/10.1016/j.aei.2016.08.002).
- [17] Maldini, I., Stappers, P.J., Gimeno-Martinez, J.C., Daanen, H.A.M. (2019). Assessing the impact of design strategies on clothing lifetimes, usage and volumes: The case of product personalisation, *Journal of Cleaner Production*, Vol. 210, 1414-1424, doi: [10.1016/j.jclepro.2018.11.056](https://doi.org/10.1016/j.jclepro.2018.11.056).
- [18] Zhang, N., Yang, Y. (2019). Change impact analysis of complex mechanical product based on complex network theory, *Journal of Physics: Conference Series*, Vol. 1187, No. 3, Article No. 032099, doi: [10.1088/1742-6596/1187/3/032099](https://doi.org/10.1088/1742-6596/1187/3/032099).
- [19] Maurya, S., Mougnot, C., Takeda, Y. (2021). Impact of mixed reality implementation on early-stage interactive product design process, *Journal of Engineering Design*, Vol. 32, No. 1, 1-27, doi: [10.1080/09544828.2020.1851662](https://doi.org/10.1080/09544828.2020.1851662).
- [20] Palumbo, E., Soust-Verdaguer, B., Llatas, C., Traverso, M. (2020). How to obtain accurate environmental impacts at early design stages in BIM when using environmental product declaration. A method to support decision-making, *Sustainability*, Vol. 12, No. 17, Article No. 6927, doi: [10.3390/su12176927](https://doi.org/10.3390/su12176927).
- [21] Li, R., Yang, N., Zhang, Y., Liu, H. (2020). Risk propagation and mitigation of design change for complex product development (CPD) projects based on multilayer network theory, *Computers & Industrial Engineering*, Vol. 142, Article No. 106370, doi: [10.1016/j.cie.2020.106370](https://doi.org/10.1016/j.cie.2020.106370).
- [22] Gao, Y., Li, D. (2018). UAV swarm cooperative situation perception consensus evaluation method based on three-parameter interval number and heronian mean operator, *IEEE Access*, Vol. 6, 73328-73340, doi: [10.1109/ACCESS.2018.2882409](https://doi.org/10.1109/ACCESS.2018.2882409).
- [23] He, X., Li, Y., Qin, K. (2021). On a new distance measure of three-parameter interval numbers and its application to pattern recognition, *Soft Computing*, Vol. 25, 8595-8607, doi: [10.1007/s00500-021-05741-1](https://doi.org/10.1007/s00500-021-05741-1).
- [24] Li, Y., Zhu, S., Guo, S.-D. (2016). Multi-attribute grey target decision method with three-parameter interval grey number, *Grey Systems: Theory and Application*, Vol. 6, No. 2, 270-280, doi: [10.1108/GS-05-2016-0010](https://doi.org/10.1108/GS-05-2016-0010).
- [25] Nozari, H., Jafari-Eskandari, M., Kamfirozi, M.H., Mozafari, A. (2014). Using numerical taxonomy and combined bulls-eye-shapley weighting method in order to ranking websites of Iranian universities by three-parameter interval grey numbers, *Arabian Journal for Science and Engineering*, Vol. 39, 3299-3305, doi: [10.1007/s13369-013-0881-x](https://doi.org/10.1007/s13369-013-0881-x).
- [26] Xu, L.-B., Li, X.-S., Shao, J.-K., Wang, K.-J. (2018). Extension dependent degree method with mapping transformation for three-parameter interval number decision making, *Mathematical Problems in Engineering*, Vol. 2018, Article ID 1831086, doi: [10.1155/2018/1831086](https://doi.org/10.1155/2018/1831086).
- [27] Li, Y., Zhang, D.X., Liu, B. (2019). Multi-attribute decision-making method based on cosine similarity with three-parameter interval grey number, *Journal of Grey System*, Vol. 31, No. 3, 45-58.
- [28] Yin, Y., Ren, Q. (2018). Studying the representative volume of concrete using the entropy weight-grey correlation model, *Magazine of Concrete Research*, Vol. 70, No. 15, 757-769, doi: [10.1680/jmacr.17.00263](https://doi.org/10.1680/jmacr.17.00263).
- [29] Liu, H., Dong, Y., Wang, F. (2020). Gas outburst prediction model using improved entropy weight grey correlation analysis and IPSO-LSSVM, *Mathematical Problems in Engineering*, Vol. 2020, Article ID 8863425, doi: [10.1155/2020/8863425](https://doi.org/10.1155/2020/8863425).
- [30] Gu, Q., Wang, R., Ju, C. (2020). Evaluation path selection of opening-up level of chinese coastal cities based on entropy weight-topsis-grey correlation: From researches on ten coastal cities, *Journal of Coastal Research*, Vol. 115, No. 1, 636-640, doi: [10.2112/JCR-SI115-168.1](https://doi.org/10.2112/JCR-SI115-168.1).
- [31] Li, B., Zhu, X. (2019). Grey relational decision making model of three-parameter interval grey number based on AHP and DEA, *Grey Systems: Theory and Application*, Vol. 10, No. 1, 25-37, doi: [10.1108/GS-10-2018-0049](https://doi.org/10.1108/GS-10-2018-0049).
- [32] Li, Y., Zhang, D. (2020). Multi-attribute group grey target decision-making method based on three-parameter interval grey number, *Journal of Grey System*, Vol. 32, No. 3, 96-109.
- [33] Behzad, M., Zolfani, S.H., Pamucar, D., Behzad, M. (2020). A comparative assessment of solid waste management performance in the Nordic countries based on BWM-EDAS, *Journal of Cleaner Production*, Vol. 266, Article No. 122008, doi: [10.1016/j.jclepro.2020.122008](https://doi.org/10.1016/j.jclepro.2020.122008).
- [34] Zhang, D., Shen, J., Liu, P., Zhang, Q., Sun, F. (2020). Use of fuzzy analytic hierarchy process and environmental gini coefficient for allocation of regional flood drainage rights, *International Journal of Environmental Research and Public Health*, Vol. 17, No. 6, Article ID 2063, doi: [10.3390/ijerph17062063](https://doi.org/10.3390/ijerph17062063).

Bone drilling with internal gas cooling: Experimental and statistical investigation of the effect of cooling with CO₂ on reduction of temperature rise due to drill bit wear

Shakouri, E.^{a, b, *}, Haghghi Hassanalideh, H.^a, Fotuhi, S.^b

^aFaculty of Engineering, Islamic Azad University-Tehran North Branch, Tehran, Iran

^bIranian Tajhiz Sina, its. Co., Tehran, Iran

ABSTRACT

Bone drilling is a major stage in immobilization of the fracture site. During bone drilling operations, the temperature may exceed the allowable limit of 47 °C, causing irrecoverable damages of thermal necrosis and seriously threatening the fracture treatment. One of the parameters affecting the temperature rise of the drilling site is the frequency of applying the drill bit and its extent of wear. The present study attempted to mitigate the effect of drill bit wear on the bone temperature rise through the internal gas cooling method via CO₂ and to reduce the risk of incidence of thermal necrosis. To this end, drilling tests were conducted at three rotational speeds 1000, 2000, and 3000 r·min⁻¹ in two states of without cooling and with internal gas cooling by CO₂ through an internal coolant carbide drill bit, along with six drill bit states (new, used 10, 20, 30, 40, and 50 times) on a bovine femur bone. The results indicated that in the internal gas cooling state, as the number of drill bit applications increased from the new state to more than 50 times, the temperature of the hole site increased on average by $\Delta T = 2\text{-}3$ °C ($n = 1000$ r·min⁻¹), $\Delta T = 5\text{-}8$ °C ($n = 2000$ r·min⁻¹), and $\Delta T = 5\text{-}7$ °C ($n = 3000$ r·min⁻¹). Furthermore, the internal gas cooling method was able to significantly reduce the effect of the drill bit wear on the temperature rise of the drilling site and to resolve the risk of incidence of thermal necrosis regardless of the process parameters for drilling operations.

ARTICLE INFO

Keywords:

Bone;
Drilling;
Thermal necrosis;
Tool wear;
Internal gas cooling

*Corresponding author:

e_shakouri@iautn.ac.ir
(Shakouri, E.)

Article history:

Received 15 March 2021

Revised 18 May 2021

Accepted 19 May 2021



Content from this work may be used under the terms of the Creative Commons Attribution 4.0 International License (CC BY 4.0). Any further distribution of this work must maintain attribution to the author(s) and the title of the work, journal citation and DOI.

1. Introduction

Bone drilling is a major operation which is extensively utilized in orthopedic surgery. Since in complicated cases of bone fracture, the internal fixation of fracture site should be performed through screws, wires, and plates, thus creation of a hole in the bone through the drilling process is essential [1]. Drilling operation is considered a type of machining process in which a hole is created through physical contact between the cutting edges of a rotational drill bit and applying axial force. As with other machining processes, these operations lead to heat generation in the cutting zone [2]. The major sources of heat generation at the hole site during bone drilling operations are as follows:

- The energy exerted to the bone-tool interface to create a plastic deformation in the bone as well as chip formation;
- The friction between the drill bit and hole wall;
- The friction between chips and the hole wall.

The heat generated during the bone drilling is evacuated in four different ways [3]:

- Part of the heat is cleared off the hole site through the blood and interstitial fluids;
- Some heat is carried away through bone chips;
- A portion of the heat enters the tool and elevates its temperature (Fig. 1);
- Finally, some heat enters the hole site of the bone, causing its temperature elevation (Fig. 1).

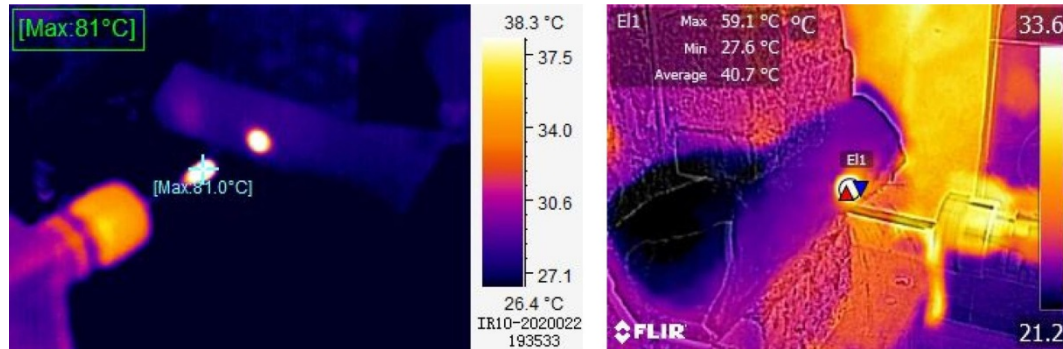


Fig. 1 Samples of thermographic images of bone drilling: heat generation in the drilling site and temperature rise of bone and drill bit

During metal drilling, around 85 % of the heat generated in the process is carried away from the system by chips [4]. However, in orthopedic surgery, as the bone has poor heat capacity and thermal conductivity, the share of the output heat by the chips is far smaller. This means that the heat generated during the bone drilling operations cannot be cleared off the system immediately, causing prolongation of the heat retention time in the bone, and eventually local temperature rise. Heat accumulation at the drilling site can cause irrecoverable damages to orthopedic surgery and patient improvement. The reason is that the local temperature rise can lead to altered nature of the alkaline phosphatase of the bone, incidence of thermal necrosis, cell death, and diminished mechanical strength at the drilling site [5]. The reduction in the mechanical strength of the bone at the hole site may dramatically reduce the success of internal fixation of the fracture site. It is because in the post-drilling stage, self-tapering screws are embedded inside these holes to perform immobilization of the fracture site. Incidence of thermal necrosis, diminished mechanical strength of the drilling site, as well as weakened interaction between the screw and bone, prevent fracture treatment in the desired direction and angle. Thermal necrosis is dependent on two factors: the extent of temperature rise of the bone and the duration of exposure to that temperature. Some researchers have determined a thermal threshold for osteonecrosis, below which no considerable damage is incurred to the bone tissue. However, beyond this temperature, the bone cells are affected; this thermal threshold for incidence of necrosis is exposure to 47 °C for 1 min. *Henriques* has presented a model for thermal damage based on *Arrhenius* relationship. The time-dependent relation of thermal damage is as follows (Eq. 1):

$$\Omega(t) = \int_0^t A \cdot \exp\left(\frac{-E_a}{R(T + 273)}\right) dt \quad (1)$$

Where, $\Omega(t)$ is the thermal damage, A represents the frequency factor ($3.1 \times 10^{98} \text{ s}^{-1}$), E_a shows the activation energy ($627 \times 10^3 \text{ J} \cdot \text{mol}^{-1}$), R denotes the universal constant of gases ($8.314 \text{ J} \cdot \text{mol}^{-1} \cdot \text{K}^{-1}$), T is the temperature (°C), and t shows the time (s). According to *Henriques* equation (Eq. 1), per every 1 °C temperature rise, the tolerable time range for the bone diminishes by half, such that beyond 53 °C, thermal necrosis occurs almost immediately [1, 4-8].

Accordingly, controlling the extent of temperature rise in bone drilling operations is a significant issue of interest to researchers in orthopedic surgery and biomedical engineering. Some researchers have tried to determine the optimum machining conditions to ensure the minimum extent of temperature rise through examining the effect of cutting parameters of drilling operations (including the drill bit diameter, drill bit geometry, rotational speed, and feed rate) [9-12]. In spite of the extensive research so far and their valuable results, it has been found that during

conventional drilling operations of the bone, despite the possibility of applying suitable process conditions to minimize the temperature rise, thermal necrosis cannot be prevented definitely. This conclusion has prompted researchers to search for alternative methods for conventional drilling in orthopedic surgical operations. Study on modern techniques including high-speed machining of bone [3, 13-15], ultrasonic assisted drilling of bone [16-21], and abrasive water jet machining of bone [22] has been able to mitigate extreme temperature rise in the cutting zone of the bone to some extent and to minimize the risk of thermal necrosis. Nevertheless, the point is that so far none of the alternative methods of traditional machining for the bone have become commonplace and been used in real surgical operations. This can be due to the following reasons:

- Most of these alternative methods are dependent on special equipment, which currently have only applications, and their usage in orthopedic surgery suffers technical, health and safety, and financial constraints (the equipment includes high speed spindle for high-speed machining; transducers and ultrasonic power supply for ultrasonic assisted machining; high-pressure pump and jet nozzle for water jet machining).
- In spite of achieving relatively desirable results by alternative machining methods, since heat generation is considered an intrinsic property of machining operations, none of the alternative processes have been able to control temperature rise precisely around the allowable range (temperature rise <10 °C) and completely eliminate the risk of thermal necrosis.

Thermodynamically, the most effective method of controlling temperature rise in machining operations is applying coolant fluids; in addition to preventing excessive temperature rise (in the tool and workpiece), these fluids help in transferring the heat from the machining system. This has prompted researchers to examine the effect of applying coolant fluids (water, normal saline) on the temperature rise of drilling site during bone drilling operations [23]. For example, in a research by Augustin *et al.* on porcine femur drilling, it was observed that application of internal water cooling (through the two-step internal coolant drill) caused the hole temperature not to exceed the critical value of 47 °C and grow to at most 40.5 °C [24]. This achievement clearly indicated the effective performance of the coolant fluid in controlling the temperature rise of the bone drilling operation.

Given the remarkable results of applying coolant fluids in controlling the temperature rise of bone drilling, the idea of employing inert gas cooling methods was developed for drilling operations of the bone. In this regard, having created a special drill machine with an internal gas cooling potential (N₂ or CO₂) through internal coolant drill bits, Shakouri *et al.* examined the effect of internal gas cooling on the temperature rise of the bone drilling process. By comparing the obtained results with the observations of conventional drilling as well as the results of drilling with external normal saline cooling, they found that internal gas cooling can constrain the extent of temperature rise at the drilling site during the bone drilling operations within the allowable range (maximum temperature rise as much as $\Delta T = 10$ °C), thereby completely eliminating the risk of thermal necrosis [25]. The internal flow of the inert gas at the site of drilling first provides adequate cooling for both the drill bit and the bone, while also supporting effective evacuation of heat and bone chips. The only notable point in this method is its dependence on the drill apparatus with the ability of gas flow passage plus the internal coolant drill bit.

Concerning bone drilling, the important point which has been observed in previous research is that with increase in the frequency of applying the bit in orthopedic surgery, it gradually wears and becomes blunt over time. This wear can be considered from different aspects:

- Bluntness of cutting edges and the flute edges of the bit;
- Changes in the point angle of the bit;
- Adhesion of a coating made of the bone mineral matrix to the cutting edges and flutes of the bit, and even clogging the flutes of the bit.

Since the extent of sharpness of the drill bit is one of the most important factors affecting the plastic deformation of the material, chip formation, and the cutting efficiency, thus blunt and

worn drill bits require exerting more force for the cutting action, causing excessive frictional heating, and eventually generation of more heat during the drilling [7]. Since the mechanical strength of the bone is far lower than that of metal workpieces, thus the forces required for bone drilling operations are not very considerable. Hence, the first two states of drill bit wear mentioned above occur at a very low rate for the drill bits used in bone drilling, and their effects do not emerge at the low frequencies of applying the drill bit. However, concerning the third state of drill bit wear, considering the temperature rise of the drilling site and evaporation of the bone tissue fluids, incidence of adhesion of a coating made of the bone mineral matrix to the cutting edges and flutes of the bit will not be inevitable even at low frequency of applying the drill bit. In a research conducted by Allan *et al.* on the effect of drill bit wear on temperature rise of conventional bone drilling operations, it was found that as the frequency of applying the drill bit increased, so did the extent of temperature rise at the drilling site [8]. In this regard, Staroveski *et al.* monitored drill wear during cortical bone drilling, and found that drill wear resulted in increased temperature and cutting forces [26]. Accordingly, in different studies, to control the course of temperature rise at the site of the drilling and to prevent incidence of thermal necrosis, the maximum allowable frequencies of applying bits has been mentioned as 40 [8, 27, 28]. In some cases, the bit wear challenge has been considered even more critical, and drilling bits have been replaced after 15 times of usage [5].

Since the desirable effect of applying internal gas cooling on significant reduction of temperature rise during the bone drilling operations has been observed [25], now this question arises whether the above method can reduce the wear rate of the drill bit and its resulting temperature rise. The aim of the present research is to investigate the effect of frequency of applying drill bit and its resulting wear on the temperature rise of the drilling site and to test the effect of internal gas cooling on the extent of temperature rise resulting from the drill bit wear (from the aspect of adhesion of a coating made of the bone mineral matrix to the cutting edges and flutes of the bit). Another goal is to determine whether internal gas cooling during the bone drilling operations can reduce the drill bit wear-induced temperature rise. Furthermore, once this internal cooling method is used, the maximum allowable times of applying the drill bit should be tested. The innovation of this research is that so far no documented report has been published regarding the effect of internal gas cooling on the drill bit wear and its resulting temperature rise.

2. Materials and methods

Due to the similarity between the mechanical properties of bovine bone and human bone, as well as its frequent usage in previous studies [1, 3, 9, 10, 12, 13, 15, 16, 22, 25], the present research has used fresh bovine femurs, which had been obtained from a local abattoir. Note that no animal was sacrificed specifically for conducting the tests in this research. Considering the necessity of creating the same conditions for all experimental states, the desirable samples with a width of 15 mm and thickness of around 8 mm have been chosen from the mid-shaft of the bovine femur diaphysis (Fig. 2). The initial temperature (T_0) of the specimens has been 27 °C before the experimental tests. Since the method proposed in this research intends to resolve the effect of drill bit wear on drilling temperature rise through internal gas cooling, thus it was necessary facilitate the gas passage through the spindle and delivering it to the internal coolant drill bit by making changes to the drill machine (Fig. 3). This tool could be made through modifying *Bosch drill GSB 16 RE* according to Fig. 4. Note that the efficiency of this drill machine in effective cooling of drilling site through gas has been demonstrated previously [9, 25]. As a tool for material removal as well as a path for concurrent transference of coolant gas to the drilling site, an internal coolant drill bit (*Mitsubishi materials MVS0320X05S060 MVS series solid Carbide drill*, internal coolant) has been used with a diameter of 3.2 mm possessing two internal channels (diameter is 0.5 mm) for gas passage (Fig. 5). According to the common protocol for temperature measurement at the drilling site in bone drilling operations, a thermocouple has been installed at the depth of 3 mm with a distance of 0.5 mm away from the hole wall [9, 13, 16, 25, 27], whereby the thermal changes have been recorded via *Thermometer Lutron TM-925*. Table 1 presents the different conditions of drilling operations employed in the present research. Based

on this table, it is observed that the drilling tests have been totally performed in 36 experimental states for drilling conditions: without cooling and with internal gas cooling, with three rotational speeds (1000, 2000, and 3000 r·min⁻¹), for six states of drill bit (new, after using 10, 20, 30, 40, and 50 times). Note that in order to ensure the accuracy and replicability of the results, every experimental state has been repeated at least three times.



Fig. 2 Bone specimens after cutting



Fig. 3 A schema of drill made with internal gas cooling

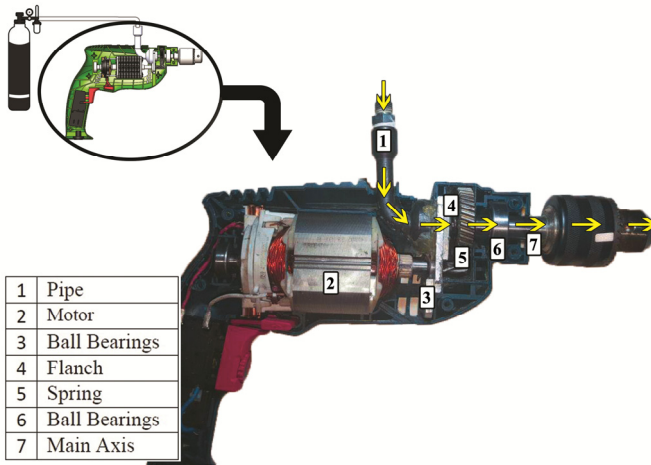


Fig. 4 A schema of drilling machine: The section shows the pathway of gas coolant



Fig. 5 Internal coolant drill bit.

Table 1 Bone drilling operational parameters

Drill bit diameter (mm)	3.2
Drill bit type	Mitsubishi materials MVS0320X05S060 MVS series solid Carbide drill, internal coolant
Rotational speed (r·min ⁻¹)	1000-2000-3000
Feed rate	Manual
Gas coolant type	CO ₂
Coolant flow rate (L·min ⁻¹)	5
Cylinder pressure (bar)	2
Gas temperature during discharge of drill tip (°C)	-11
Degree of Drill bit wear	New drill bit-& After 10-20-30-40-50 holes
Depth of drilling (mm)	8
Modes of drilling	Without cooling- With internal gas cooling
Number of iteration of tests	At least 3 times

3. Results and discussion

Figs. 6-8 present the results obtained from the bone drilling tests in two states, without drilling and along with internal gas cooling for the rotational speeds of 1000, 2000, and 3000 r·min⁻¹. Based on the above figures, it can be observed that:

- In case of not using any coolants, as the frequency of applying the drill bit increased from the new state to more than 50 times, the hole site temperature rise has grown from $\Delta T = 24\text{ }^{\circ}\text{C}$ to $34\text{ }^{\circ}\text{C}$ for rotational speed of 1000 r·min⁻¹, from $\Delta T = 29\text{ }^{\circ}\text{C}$ to $37\text{ }^{\circ}\text{C}$ for rotational speed of 2000 r·min⁻¹, and from $\Delta T = 20\text{ }^{\circ}\text{C}$ to $33\text{ }^{\circ}\text{C}$ for rotational speed of 3000 r·min⁻¹ (on average from the baseline level, $T_0 = 27\text{ }^{\circ}\text{C}$). This suggests that an increase in the frequency of applying drill bit and its resulting wear significantly influence the temperature rise of the hole site. This temperature rise occurred more quickly for the drill bit utilized more than 40 times (which has been mentioned as the last allowable limit for applying drill bits in different references [8, 27, 28]).
- The minimum temperature rise for the case of no coolant utilization was $\Delta T = 20\text{ }^{\circ}\text{C}$ belonging to the new drill bit at 1000 r·min⁻¹, which has been far beyond the allowable limit of temperature rise ($\Delta T < 10\text{ }^{\circ}\text{C}$). This means that in conventional drilling, it is not possible to control the extent of temperature rise and prevent the incidence of thermal necrosis. As the frequency of applying the drill bit increases, the conditions become further critical. Although in previous studies, the maximum allowable frequency of applying drill bits has been mentioned as 40, the above figures indicate that when no coolant is used, even new drill bits may lead to excessive temperature rise and incidence of thermal necrosis.
- In the case of drilling with internal gas cooling, as the frequency of applying the drill bit increased from new conditions to beyond 50, the hole site temperature rise (ΔT) has grown from $\Delta T = 2\text{ }^{\circ}\text{C}$ to $3\text{ }^{\circ}\text{C}$ for rotational speed of 1000 r·min⁻¹, from $\Delta T = 5\text{ }^{\circ}\text{C}$ to $8\text{ }^{\circ}\text{C}$ for rotational speed of 2000 r·min⁻¹, and from $\Delta T = 5\text{ }^{\circ}\text{C}$ to $7\text{ }^{\circ}\text{C}$ for rotational speed of 3000 r·min⁻¹ (from the baseline level, $T_0 = 27\text{ }^{\circ}\text{C}$). This highlights that when internal gas cooling is used, the increase in the frequency of applying the drill bit has had a minor impact on the temperature rise of the hole site.
- In case of the drilling with internal gas cooling, the temperature rise of the hole site (ΔT) lied within the allowable range at all rotational speeds and the drill bit wear conditions, and did not exceed the threshold of $10\text{ }^{\circ}\text{C}$. This suggests that bone drilling with internal gas cooling enjoys the ability of controlling temperature changes and preventing the incidence of thermal necrosis for both new and worn drill bits. Note that the extent of temperature rise has approached the maximum allowable limit only for the drill bit with more than 50 times of usage at 2000-3000 r·min⁻¹. Thus, it can be concluded that bone drilling with internal gas cooling guarantees controlled temperature rise at the hole site and no incidence of thermal necrosis for new and even 50-time used drill bits.
- Comparing the results obtained from Figs. 6-8, it can be seen that in both conventional drilling and drilling with internal gas cooling, across all new and worn drill bit states, as the drill bit rotational speed increased from 1000 r·min⁻¹ to 2000 r·min⁻¹, the temperature rise (ΔT) was intensified; however, with further increase in the rotational speed from 2000 r·min⁻¹ to 3000 r·min⁻¹, the extent of temperature rise of the hole site diminished. Note that, in the drilling without cooling, the minimum extent of temperature rise was obtained at 3000 r·min⁻¹, while in the bone drilling with internal gas cooling, the minimum degree of temperature rise occurred at the rotational speed of 1000 r·min⁻¹.

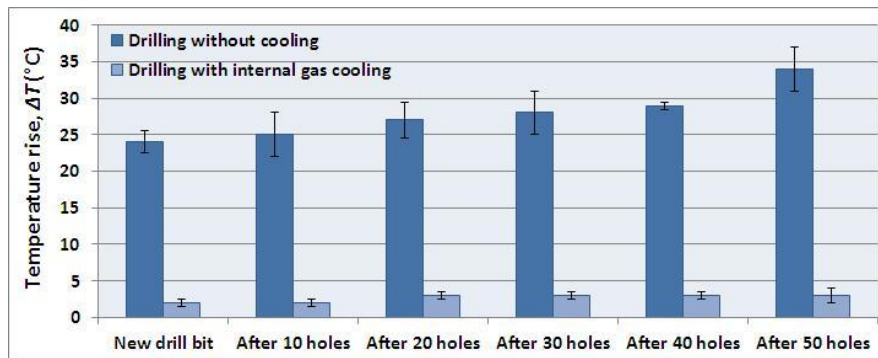


Fig. 6 Temperature change during bone drilling for different modes of drill bit wear (Comparison of drilling without cooling and drilling with internal gas cooling, $n = 1000 \text{ r}\cdot\text{min}^{-1}$)

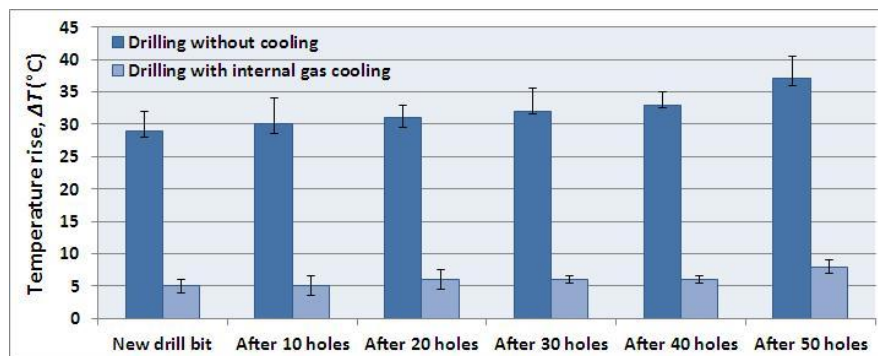


Fig. 7 Temperature change during bone drilling for different modes of drill bit wear (Comparison of drilling without cooling and drilling with internal gas cooling, $n = 2000 \text{ r}\cdot\text{min}^{-1}$)

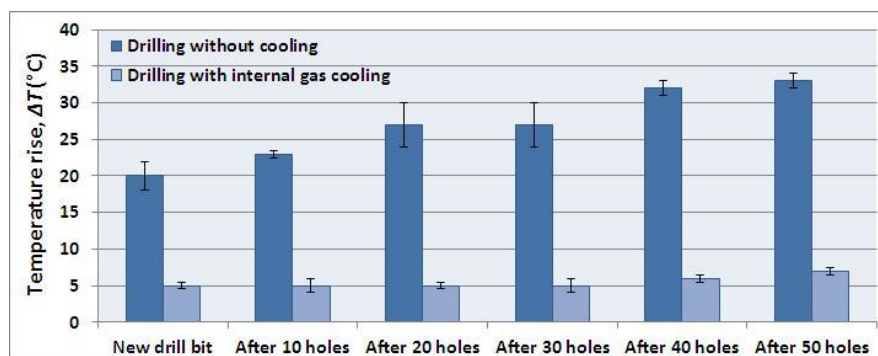


Fig. 8 Temperature change during bone drilling for different modes of drill bit wear (Comparison of drilling without cooling and drilling with internal gas cooling, $n = 3000 \text{ r}\cdot\text{min}^{-1}$)

Based on Figs. 6-8, it is observed that in the bone drilling without internal gas cooling, as the frequency of applying the drill bit increased, so did the extent of temperature rise of the hole site. This is justified considering the gradual increase in the drill bit wear and weakened cutting capability of the drill bit edges. Nevertheless, the important point in the above figures is that the maximum extent of temperature rise has occurred at $2000 \text{ r}\cdot\text{min}^{-1}$, while the minimum has been obtained at $3000 \text{ r}\cdot\text{min}^{-1}$. As a justification, the factors affecting the temperature rise during the bone drilling operations should be considered:

- Reduction of the energy required for chip formation and machine forces in response to elevated rotational speed of the drill bit;
- Increased friction and frictional heating in response to augmented rotational speed of the cutting tool;
- Increased speed of the chip evacuation in response to the elevated rotational speed of the drill bit.

As the rotational speed of the drill bit was augmented from $1000 \text{ r}\cdot\text{min}^{-1}$ to $2000 \text{ r}\cdot\text{min}^{-1}$, the machining force decreased while the chip evacuation speed increased, causing reduction of heat generation in the process to some extent. Nevertheless, since the effect of friction and frictional heating is dominant, the temperature of the hole site increased. These conditions hold for all states of the drill bit wear.

In the bone drilling with internal gas cooling, two important points are notable:

- Application of internal gas cooling has caused the temperature rise (ΔT) to become constrained within the range less than $10 \text{ }^\circ\text{C}$, and allowed 50 times of drill bit usage because of different reasons. They include increased chip evacuation speed, effective cooling of the drill bit and bone, along with diminished effects of the drill bit wear (including bluntness of the cutting edges, adhesion of the bone mineral matrix to the edges and flutes of the drill bit, and clogging of drill bit flutes).
- Since cooling with gas is far more effective than increasing the rotational speed of the drill bit for elevating the chip evacuation speed, the rise in the rotational speed from 1000 to $3000 \text{ r}\cdot\text{min}^{-1}$ did not significantly contribute to faster chip evacuation and only caused an intensified effect of friction and frictional heating. Thus, in the case of bone drilling with internal gas cooling, the minimum extent of temperature rise was obtained for both new and worn drill bits at $1000 \text{ r}\cdot\text{min}^{-1}$.

To investigate the signs of drill bit wear, some images of it have been presented in Fig. 9 after 50 times of usage for bone drilling operations without cooling and with internal gas cooling. These images have been prepared after cleaning and rinsing the drill bits, and captured under *Stereo Microscope ST1740* with maximum $50\times$ magnification. By comparing these images with the image of the new drill bit, it can be found that:

- After 50 times of applying the drill bit for bone drilling (in both without and with internal gas cooling), no notable signs of the bluntness of cutting edges and the flute edges of the bit are observed. This is due to the low mechanical strength of the bone, negligible machining forces, and high hardness of the carbide bit used in the present research. This causes minor state of wear. In case of further increasing the frequency of applying the drill bit (beyond 50 times), or using standard surgical drill bit (made of stainless steel), which has a lower hardness compared to carbide drill bit, the signs of this wear will emerge more rapidly.
- Considering adhesion of a coating made of the bone mineral matrix to the cutting edges and flutes of the bit, and concerning the substantial impacts on the bits, it is clear that the extent of this type of tool wear has been notable in the drilling without cooling, and some evident signs have remained on the tool surfaces. On the other hand, when using drilling with internal gas cooling, the signs of adhesion of a coating made of the bone mineral matrix to tool surface are very trivial and negligible. This improvement in the qualitative status of the tool and reduction of its wear result from the effect of internal gas cooling on preventing severe temperature rise as well as the effective role of the gas flow in accelerating the chip evacuation rate.

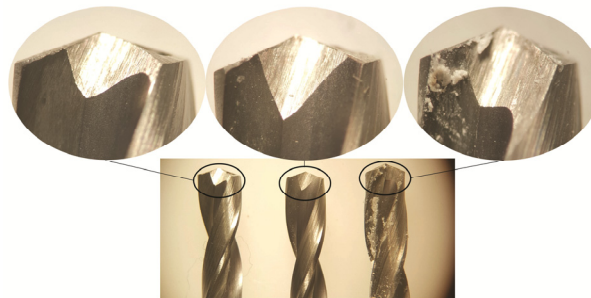


Fig. 9 Images of the abrasion of drill bits in various states (Bottom image is side view of drill bits with $10\times$ magnification; Top images are the tool tip section with $25\times$ magnification): The left image is of the new drill bit; the center image is of the drill that had drilled 50 holes (with internal gas cooling), and the right image is of the drill that had drilled 50 holes (without cooling).

Table 2 reports the set of results of the bone temperature rise in drilling operation, obtained in other studies similar to our research. To validate the results of the present research, a comparison has been made between these results and the findings of other studies. Note that in some cases, some differences existed between the drilling conditions of other studies [8, 24, 25] and the process conditions applied in the present research regarding the type of bone, rotational speed, drill bit diameter, and hole depth. Nevertheless, Table 2 indicates that, according to the results of the present research, more frequent use of the drill bit and thus the increase in its degree of wear have led to bone temperature rise [8]. Further, clearly application of internal cooling methods (with liquid or gas) has resulted in a significant reduction of the bone temperature rise. Although the liquid coolant (water or normal saline) outperformed the gas coolant (N₂ or CO₂), both cooling modes (either liquid or gas) have been sufficiently able to effectively cool the hole site and prevent exceedance of temperature rise beyond the allowable limit of $\Delta T < 10$ °C [24, 25].

Table 2 Comparison the results of the present research with other studies

Reference	Bone type	Drill bit diameter (mm)	Degree of Drill bit wear	Rotational speed (r·min ⁻¹)	Hole depth (mm)	Cooling condition	Temperature changes (°C)
Allan <i>et al.</i> [8]	Pig mandible	1.5	New	20000	5	Dry	7.5 (0.6-20.5)
			After 600 holes			Dry	13.4 (5.7-28.3)
Augustin <i>et al.</i> [24]	Porcine femur	3.4	New	1000	4-5	Dry	8
						Water	0.4
				3150	Dry	9.2	
					Water	0.6	
				1100	Dry	11.5	
					CO ₂	3.3	
Shakouri <i>et al.</i> [25]	Bovine femur	3.2	New	1920	7-8	N ₂	4.9
						Normal saline	2.9
				3200	Dry	18.1	
					CO ₂	2.5	
				3200	N ₂	5.4	
					Normal saline	1.9	
Present study	Bovine femur	3.2	New	1000	8	Dry	24 ±1.5
						CO ₂	2 ±0.5
				2000	Dry	29 ±3	
					CO ₂	5 ±1	
				3000	Dry	20 ±2	
					CO ₂	5 ±0.5	
				1000	Dry	34 ±3	
					CO ₂	3 ±1	
				2000	After 50 holes	Dry	37 ±3.5
					CO ₂	8 ±1	
3000	Dry	33 ±1					
	CO ₂	7 ±0.5					

In this section, to investigate the influence of each of the input parameters (rotational speed and the frequency of using the drill bit) on the bone temperature rise, and to determine the statistical model for predicting temperature rise, statistical analysis of the results has been performed using *Statistica* software. The relationship between the output variable (temperature rise) and input variables (rotational speed and the frequency of using the drill bit) has been examined using different regression models. Based on the maximum regression coefficient (*R*) and coefficient of determination (*R*²), the most suitable regression model has been chosen, and the

coefficients related to the regression model as well as p -value at the level of $\alpha = 0.05$ have been estimated for them. The results of statistical analysis of the bone temperature rise for the modes of bone drilling without cooling and drilling with internal gas cooling are outlined in Table 3. In the bone drilling without cooling, considering the relation obtained for predicting the bone temperature rise (growth regression), it is observed that temperature changes are only dependent on the frequency of applying the drill bit. This means that in this mode, the drill bit wear plays a significant role in the bone temperature rise, while the rotational speed of the drill bit does not have a significant impact on such rise. The independence of the bone temperature rise of the rotational speed when not using the cooling further highlights the effect of the tool wear on the bone temperature rise during drilling. However, for the drilling with internal gas cooling, considering the type of model obtained (linear regression), it can be stated that rotational speed and the drill bit wear have a direct relationship with temperature. Nevertheless, considering the coefficients obtained for these input parameters, it is evident that the tool wear has a greater impact on the temperature rise as compared to the rotational speed.

Table 3 Statistical analysis of temperature rise results.

	Drilling without cooling			Drilling with internal gas cooling		
Regression model	Growth			Linear		
Regression formula	$\Delta T = \exp(b_1 \cdot n + b_2 \cdot B + a)$			$\Delta T = (b_1 \cdot n) + (b_2 \cdot B) + a$		
Regression coefficient (R)	0.803			0.794		
Determination coefficient (R^2)	0.645			0.631		
Regression parameters	b_1	b_2	a	b_1	b_2	a
	-0.00001	0.0067	3.210	0.0014	0.0371	0.96
p -value ($\alpha = 0.05$)	0.691	0.0001	0.000	0.00047	0.027	0.241
Resultant regression equation	$\Delta T = \exp(0.0067 \cdot B + 3.210)$			$\Delta T = (0.0014 \cdot n) + (0.0371 \cdot B)$		

Possibly, one of the major concerns which may challenge the application of internal gas cooling in orthopedic surgery is the probability of incidence of hypothermia or other similar damages to the bone in response to exposure to the cool gas flow. To resolve this challenge, three points should be considered:

- To create a hole with a diameter of 3.2 mm, a major part of the bone material exposed to CO₂ gas coolant at -11 °C detaches off the bone as chips and discharges to the outside of the hole.
- Similar to the case for thermal necrosis, where temperature rise and duration of exposure to high-temperature were influential factors, for hypothermia, again time is a direct influential factor. This fact cannot be neglected that during drilling with internal coolant drill bit, the bone is exposed to the coolant gas at -11 °C. Nevertheless, since the duration of drilling operation is only some second, the bone tissue of the hole wall is at risk of exposure to the cold gas only for a very short duration, and incidence of hypothermia in the bone is very unlikely.
- The overall effect of thermal factors, including: a) temperature rise resulting from drilling, and b) temperature fall due to cool gas flow determine the final temperature of the bone tissue of the hole wall. As also indicated by the results of the present research, cooling with CO₂ at -11 °C in the best mode resulted in temperature rise of 2 °C. This is the temperature measured by a contact thermocouple at the depth of 3 mm and distance of 0.5 mm away from the hole wall. It implies no incidence of over-cooling in the bone site. This means that in the best performance state of the gas coolant, again the bone tissue temperature has not declined in relation to its initial temperature, and has experienced a minimum temperature rise of 2 °C.

The results of the current study revealed that the application of CO₂ gas cooling in the bone drilling operations caused reduced extent of temperature rise and prevented incidence of thermal necrosis. Furthermore, upon the decrease in the blunting rate of the cutting edges, reducing the extent of adhesion of the bone mineral matrix to the drill bit edges and flutes, and by preventing clogging of drill bit flutes, it slows down the drill bit wearing and reduces its impact on

the temperature rise. The very important point in the present research was independence of the desired results of internal gas cooling of the drilling process parameters (including rotational speed and feed rate). Unlike high-speed drilling and ultrasonic assisted drilling methods, which offer desired results and reduction of temperature rise only within special ranges of rotational speed and feed rate, which in case of neglecting the recommended process ranges have less satisfactory results even compared to conventional drilling [13, 15, 16], the present research indicated that the significant decrease in the temperature rise and elimination of the risk of thermal necrosis in the drilling with internal gas cooling were dependent on neither the process conditions nor even the drill bit wear, and can be easily implemented in orthopedic surgical operations.

4. Conclusion

The present research examined the effect of internal gas cooling through CO₂ on drill bit wear in bone drilling operations and its resulting temperature rise. The following results were obtained:

- In the bone drilling operations without cooling, as the frequency of applying the drill bit increased, the extent of temperature rise of the hole site was intensified considerably. The extent of elevation was more dramatic for the drill bits utilized more than 40 times. This suggested that the increase in the frequency of applying the drill bit is followed by its severe wear. Also, the tool wear significantly influences the temperature rise of the bone.
- In the bone drilling operations with internal gas cooling via CO₂, at different rotational speeds, the extent of temperature rise remained within the allowable range ($\Delta T < 10$ °C), and thermal necrosis was no longer probable to occur. Secondly, internal gas cooling could significantly reduce the effect of the drill bit wear on the bone temperature rise, and guaranteed no incidence of thermal necrosis up to 50 times of drill bit usage. Finally, the desired results of the internal gas cooling were not dependent on cutting parameters and can be adapted to orthopedic surgical operational conditions.

Declaration of conflicting interests

The author(s) declared no potential conflicts of interest with respect to the research, authorship, and/or publication of this article.

Ethical approval

All procedures and methods performed in the current study were in accordance with the Declaration of Helsinki 1964 and its later amendments. The research design and protocol were approved by the ethical standards of *Research Committee of the Islamic Azad University-Tehran North Branch*.

Informed consent

This article does not contain any studies with human participants/patient data.

Funding

This work was supported by *Iranian Tajhiz Sina, its. Co.* Grant Number 990072.

References

- [1] Hillery, M.T., Shuaib, I. (1999). Temperature effects in the drilling of human and bovine bone, *Journal of Materials Processing Technology*, Vol. 92-93, 302-308, doi: [10.1016/S0924-0136\(99\)00155-7](https://doi.org/10.1016/S0924-0136(99)00155-7).
- [2] Grzesik, W. (2010). *Podstawy skrawania materiałów konstrukcyjnych*, In Polish, WNT, Warsaw, Poland.
- [3] Shakouri, E., Ghorbani, P., Pourheidari, P., Fotuhi, S. (2021). Resection of bone by sagittal saw: Investigation of effects of blade speed, feed rate, and irrigation on temperature rise, *Proceedings of the Institution of Mechanical Engineers, Part H: Journal of Engineering in Medicine*, Vol. 235, No. 6, 625-635, doi: [10.1177/0954411921999482](https://doi.org/10.1177/0954411921999482).

- [4] Karmani, S. (2006). The thermal properties of bone and the effects of surgical intervention, *Current Orthopaedics*, Vol. 20, No. 1, 52-58, doi: [10.1016/j.cuor.2005.09.011](https://doi.org/10.1016/j.cuor.2005.09.011).
- [5] Bachus, K.N., Rondina, M.T., Hutchinson, D.T. (2000). The effects of drilling force on cortical temperatures and their duration: An in vitro study, *Medical Engineering & Physics*, Vol. 22, No. 10, 685-691, doi: [10.1016/s1350-4533\(01\)00016-9](https://doi.org/10.1016/s1350-4533(01)00016-9).
- [6] Henriques, F.C. (1947). Studies of thermal injury V. The predictability and the significance of thermally induced rate processes leading to irreversible epidermal injury, *Archives of Pathology*, Vol. 43, No. 5, 489-502.
- [7] Davidson, S.R.H., James, D.F. (2003). Drilling in bone: Modeling heat generation and temperature distribution, *Journal of Biomechanical Engineering*, Vol. 125, No. 3, 305-314, doi: [10.1115/1.1535190](https://doi.org/10.1115/1.1535190).
- [8] Allan, W., Williams, E.D., Kerawala, C.J. (2005). Effects of repeated drill use on temperature of bone during preparation for osteosynthesis self-tapping screws, *British Journal of Oral and Maxillofacial Surgery*, Vol. 43, No. 4, 314-319, doi: [10.1016/j.bjoms.2004.11.007](https://doi.org/10.1016/j.bjoms.2004.11.007).
- [9] Gholampour, S., Shakouri, E., Deh, H.H.H. (2018). Effect of drilling direction and depth on thermal necrosis during tibia drilling: An in vitro study, *Technology and Health Care*, Vol. 26, No. 4, 687-697, doi: [10.3233/THC-181246](https://doi.org/10.3233/THC-181246).
- [10] Shakouri, E., Mirfallah, P. (2019). Infrared thermography of high-speed grinding of bone in skull base neurosurgery, *Proceedings of the Institution of Mechanical Engineers, Part H: Journal of Engineering in Medicine*, Vol. 233, No. 6, 648-656, doi: [10.1177/0954411919845730](https://doi.org/10.1177/0954411919845730).
- [11] Cseke, A., Heinemann, R. (2018). The effects of cutting parameters on cutting forces and heat generation when drilling animal bone and biomechanical test materials, *Medical Engineering & Physics*, Vol. 51, 24-30, doi: [10.1016/j.medengphy.2017.10.009](https://doi.org/10.1016/j.medengphy.2017.10.009).
- [12] Shakouri, E., Ghorbani Nezhad, M. (2020). An in vitro study of bone drilling: Infrared thermography and evaluation of thermal changes of bone and drill bit, *Physical and Engineering Sciences in Medicine*, Vol. 43, 247-257, doi: [10.1007/s13246-020-00842-x](https://doi.org/10.1007/s13246-020-00842-x).
- [13] Shakouri, E., Sadeghi, M.H., Maerefat, M., Shajari, S. (2014). Experimental and analytical investigation of the thermal necrosis in high speed drilling of bone, *Proceedings of the Institution of Mechanical Engineers, Part H: Journal of Engineering in Medicine*, Vol. 228, No. 4, 330-341, doi: [10.1177/0954411914524933](https://doi.org/10.1177/0954411914524933).
- [14] Udiljak, T., Ciglar, D., Skoric, S. (2007). Investigation into bone drilling and thermal bone necrosis, *Advances in Production Engineering & Management*, Vol. 2, No. 3, 103-112.
- [15] Shakouri, E., Ghorbani Nezhad, M., Ghorbani, P., Khosravi-Nejad, F. (2020). Investigation of thermal aspects of high-speed drilling of bone by theoretical and experimental approaches, *Physical and Engineering Sciences in Medicine*, Vol. 43, 959-972, doi: [10.1007/s13246-020-00892-1](https://doi.org/10.1007/s13246-020-00892-1).
- [16] Shakouri, E., Sadeghi, M.H., Karafi, M.R., Maerefat, M., Farzin, M. (2015). An in vitro study of thermal necrosis in ultrasonic-assisted drilling of bone, *Proceedings of the Institution of Mechanical Engineers, Part H: Journal of Engineering in Medicine*, Vol. 229, No. 2, 137-149, doi: [10.1177/0954411915573064](https://doi.org/10.1177/0954411915573064).
- [17] Sun, Z., Wang, Y., Xu, K., Zhou, G., Liang, C., Qu, J. (2019). Experimental investigations of drilling temperature of high-energy ultrasonically assisted bone drilling, *Medical Engineering & Physics*, Vol. 65, 1-7, doi: [10.1016/j.medengphy.2018.12.019](https://doi.org/10.1016/j.medengphy.2018.12.019).
- [18] Bai, X., Hou, S., Li, K., Qu, Y., Zhang, T. (2019). Experimental investigation of the temperature elevation in bone drilling using conventional and vibration-assisted methods, *Medical Engineering & Physics*, Vol. 69, 1-7, doi: [10.1016/j.medengphy.2019.06.010](https://doi.org/10.1016/j.medengphy.2019.06.010).
- [19] Gupta, V., Pandey, P.M. (2018). An in-vitro study of cutting force and torque during rotary ultrasonic bone drilling, *Proceedings of the Institution of Mechanical Engineers, Part B: Journal of Engineering Manufacture*, Vol. 232, No. 9, 1549-1560, doi: [10.1177/0954405416673115](https://doi.org/10.1177/0954405416673115).
- [20] Gupta, V., Pandey, P.M. (2016). Experimental investigation and statistical modeling of temperature rise in rotary ultrasonic bone drilling, *Medical Engineering & Physics*, Vol. 38, No. 11, 1330-1338, doi: [10.1016/j.medengphy.2016.08.012](https://doi.org/10.1016/j.medengphy.2016.08.012).
- [21] Alam, K., Mitrofanov, A.V., Silberschmidt, V.V. (2011). Experimental investigations of forces and torque in conventional and ultrasonically-assisted drilling of cortical bone, *Medical Engineering & Physics*, Vol. 33, No. 2, 234-239, doi: [10.1016/j.medengphy.2010.10.003](https://doi.org/10.1016/j.medengphy.2010.10.003).
- [22] Shakouri, E., Abbasi, M. (2018). Investigation of cutting quality and surface roughness in abrasive water jet machining of bone, *Proceedings of the Institution of Mechanical Engineers, Part H: Journal of Engineering in Medicine*, Vol. 232, No. 9, 850-861, doi: [10.1177/0954411918790777](https://doi.org/10.1177/0954411918790777).
- [23] Cem Sener, B., Dergin, G., Gursoy, B., Kelesoglu, E., Slih, I. (2009). Effects of irrigation temperature on heat control in vitro at different drilling depths, *Clinical Oral Implant Research*, Vol. 20, No. 3, 294-298, doi: [10.1111/j.1600-0501.2008.01643.x](https://doi.org/10.1111/j.1600-0501.2008.01643.x).
- [24] Augustin, G., Davila, S., Udiljak, T., Staroveski, T., Brezak, D., Babic, S. (2012). Temperature changes during cortical bone drilling with a newly designed step drill and an internally cooled drill, *International Orthopaedics (SI-COT)*, Vol. 36, No. 7, 1449-1456, doi: [10.1007/s00264-012-1491-z](https://doi.org/10.1007/s00264-012-1491-z).
- [25] Shakouri, E., Haghighi Hassanalideh, H., Gholampour, S. (2018). Experimental investigation of temperature rise in bone drilling with cooling: A comparison between modes of without cooling, internal gas cooling, and external liquid cooling, *Proceedings of the Institution of Mechanical Engineers, Part H: Journal of Engineering in Medicine*, Vol. 232, No. 1, 45-53, doi: [10.1177/0954411917742944](https://doi.org/10.1177/0954411917742944).
- [26] Staroveski, T., Brezak, D., Udiljak, T. (2015). Drill wear monitoring in cortical bone drilling, *Medical Engineering & Physics*, Vol. 37, No. 6, 560-566, doi: [10.1016/j.medengphy.2015.03.014](https://doi.org/10.1016/j.medengphy.2015.03.014).

- [27] Augustin, G., Davila, S., Mihoci, K., Udiljak, T., Vedrina, D.S., Antabak, A. (2008). Thermal osteonecrosis and bone drilling parameters revisited, *Archives of Orthopaedic and Trauma Surgery*, Vol. 128, 71-77, doi: [10.1007/s00402-007-0427-3](https://doi.org/10.1007/s00402-007-0427-3).
- [28] Augustin, G., Davila, S., Udiljak, T., Vedrina, D.S., Bagatin, D. (2009). Determination of spatial distribution of increase in bone temperature during drilling by infrared thermography: Preliminary report, *Archives of Orthopaedic and Trauma Surgery*, Vol. 129, 703-709, doi: [10.1007/s00402-008-0630-x](https://doi.org/10.1007/s00402-008-0630-x).

Appendix 1

Notation

A	Arrhenius frequency factor ($3.1 \times 10^{98} \text{ s}^{-1}$)
B	Frequency of using the drill bit
E_a	Arrhenius activation energy ($627 \times 10^3 \text{ J} \cdot \text{mol}^{-1}$)
R	Universal constant of gases ($8.314 \text{ J} \cdot \text{mol}^{-1} \cdot \text{K}^{-1}$)
R	Coefficient of regression
R^2	Determination coefficient
T	Temperature (°C)
T_0	Initial temperature (baseline level) (°C)
a, b_1, b_2	Regression parameters
n	Rotational speed ($\text{r} \cdot \text{min}^{-1}$)
t	Time (s)
ΔT	Temperature rise (°C)
Ω	Arrhenius thermal damage

Joint distribution models in fast-moving consumer goods wholesale enterprise: Comparative analysis and a case study

Wang, L.^a, Chen, X.Y.^{a,*}, Zhang, H.^{a,b}

^aSchool of E-Business and Logistics, Beijing Technology and Business University, Beijing, P.R. China

^bBeijing Food Safety Research Base, Beijing, P.R. China

ABSTRACT

Joint distribution means multiple clients were provided distribution services together by only one third-party logistics company. It is a unified plan and implementation used in distribution centres and a distribution activity implemented by multiple consortia. Many problems in distribution can be solved through the joint use of distribution warehouse, vehicles and reasonable logistics business, so as to optimize the overall logistics node and route arrangement. This paper mainly discusses the model of joint distribution of fast moving consumer goods, proposes three types of the optimization model of joint distribution system with Chaopi as an example. We draw the conclusion that Chaopi Trading Co., Ltd. is a joint distribution system optimization business model. This paper puts forward several basic distribution models and analyzes them in combination with practical applications, which has strong practical significance. Although the development of public distribution in China is not very fast, it is an inevitable trend. Through the efforts and explorations of the governments of various countries, there will be more and more choices of public distribution models.

ARTICLE INFO

Keywords:

Logistics;
Joint distribution;
Wholesale enterprise;
Fast-moving consumer goods;
Distribution models;
Optimization

*Corresponding author:

845190504@qq.com
(Chen, X.Y.)

Article history:

Received 27 March 2021
Revised 23 May 201
Accepted 15 June 2021



Content from this work may be used under the terms of the Creative Commons Attribution 4.0 International Licence (CC BY 4.0). Any further distribution of this work must maintain attribution to the author(s) and the title of the work, journal citation and DOI.

1. Introduction

With the continuous improvement of China's economy and the rapid development of people's living standard, the sales volume of fast-moving consumer goods (FMCG) increase year by year, which shows the good growth and extensive market demands. Practice has proved that the key factor for the success of fast-moving consumer goods enterprises is market power, and logistics is an important factor for the formation of it. Therefore, efficient logistics system is one of the key factors to support the success of FMCG enterprises. In order to create competitive advantages, FMCG distribution enterprises need to improve their profit level and ensure their survival and development. In recent years, with the continuous expansion of FMCG sales, the integration of FMCG sales channels and the acceleration of innovation, FMCG sales outlets are expanding rapidly. In order to meet the needs of enterprise scale expansion and market competition, they strive to reduce operating costs and improve the reaction speed of stores and consumers. In order to improve the efficiency of operation and logistics and create important material conditions, FMCG distribution enterprises have improved the logistics infrastructure, storage conditions and transport capacity, and they have actively used advanced logistics technology.

Joint distribution, also known as third-party logistics (3PLs) service sharing, refers to that only one 3PLs company provides distribution service for multiple customers. It is a unified plan and implementation for the use of distribution centers and a distribution activity implemented by multiple consortia. Generally speaking, enterprises are usually decentralized and unable to integrate logistics resources. Due to the different logistics objects, many enterprises often have the problems of unbalanced utilization rate of distribution warehouse, unreasonable lines and high vacancy rate of vehicles. But it can be realized through the joint use of logistics, distribution warehouse and vehicles, so as to optimize the overall logistics node and route arrangement, so as to make an efficient and green logistics through unified commodity distribution.

From the perspective of enterprises, the first is to reduce the cost of distribution and the capital occupation, and the sharing of resources among enterprises can reduce the capital investment and cost of logistics chain.

Secondly, it is to increase the coverage of the network service. The enterprises may choose the distribution with far distance and limited transportation, if without the network service, which can be improved by joint distribution, because it can improve the service level and visibility with the help of network service.

Then, core business of the enterprise can be strengthened. As companies no longer invest too much energy in the distribution sectors, trivial problems no longer occur in the distribution process, therefore it will not take any time to resolve, so that we can concentrate on our core business, have more investment in human resource, put more financial resources on the core issues, and enhance the competitiveness of enterprises.

In addition, it can also improve the technological content. In order to optimize the joint distribution process, it is necessary to unify the identification and packaging, reduce the manual operation, improve the utilization of high-tech, and prepare for the future development.

Finally, in order to improve the degree of specialization of distribution, joint distribution is to complete the detailed planning of time, place and route according to the requirements of various enterprises through professional distribution companies, so that all enterprises can accept and implement network integration and realize the social sharing of resources. In this way, we can make the distribution process more efficient and professional.

From a social point of view, the first is the unified management of joint distribution vehicles, which can achieve a high loading rate of vehicles and avoid repeating the previous transportation routes, cross transportation, circuitous transportation and occupation of road resources. So we can easily relieve the pressure of traffic congestion.

Secondly, joint distribution can reduce the waste of vehicles, with the reduction of the pollution caused by vehicle exhaust and vehicle noise.

Finally, joint distribution means resource centralized management. Based on the conditions of joint distribution, enterprises will build more warehouses. They will not blindly build all kinds of enterprises according to their own interests. From the overall consideration, the problem of scattered and large-scale construction of small warehouses will be solved, and the abuse of land resources can be reduced.

In addition, the concept of joint distribution breaks the traditional single model of transport. It can integrate resources and optimize logistics social system.

Joint distribution is a more reasonable way to meet the needs of customers. In this way, all kinds of resources of the enterprise can be integrated. From an economic or social point of view, its advantages are obvious.

2. Literature review

Foreign scholars call the scheduling problems of distribution vehicle as Vehicle Scheduling Problem (VSP), which was first proposed in 1959 by the Dantzig and Ramser, and was soon attracted by the operations, applied mathematics, combinatorial mathematics, graph theory and network analysis, logistics science, computer applications, and other subject matter experts, transport planners, and managers of great importance, as the field of operations research and combinatorial optimization of front and hotspot issues [1]. In a retailer case study, Claudia and Laura

(2014) mentioned that the importance of 3PLs, aggregation and multi-user platforms must be recognised by transport planners in supporting the use of intermodal transport by retailers and other large shippers [2]. As for 3PLs and self-delivery logistics firms, Chun and Jim(2013) investigated which delivery technique is more efficient by comparing logistics capabilities, logistics services, and logistics performances based upon transaction cost analysis and resource-based theory [3]. The empirical results in this study could be strategic logistics management guidelines based upon the theoretical relationships among logistics capabilities, logistics service, and logistics performance for 3PL users and self-delivery logistics firms. Liu (2015) proposed a conceptual model that delineates the determinants of consumers' perceived service quality and tested the model in the Chinese logistic companies [4]. Based on the former analysis, he presented separately the activated measures of domestic 3PLs by corporate side, the supply side, and the government's policy support. Conducting two in-depth case studies of 3PLs, Cabigiosu *et al.* (2015) showed that 3PLs extensively rely on service modularity with standard procedures as their constitutive element [5]. A bi-objective model is developed to minimize the total shipping cost and time simultaneously. Lopes (2020) evaluated the relationship between the service capabilities and performance of the 3PLs providers in UK and Taiwan, China [6]. The range of service provision offered by 3PLs does not directly influence the 3PLs' financial performance. However, 3PLs providers with service capabilities that correspond to the key priorities of customers will gain superior financial performance through a better operational performance. In terms of criteria and methods, Aguezzoul (2014) presented a literature review on 3PLs selection decision and revealed that 3PLs selection is empirical in nature and is related to a region/country, industrial sector, and logistics activities outsourced [7]. Cost is the most widely adopted criterion, followed by relationship, services, and quality. From the perspective of 3PLs providers, Arthanari (2016) found that uncertainty, order frequency, and transaction size, but not asset specificity, are significantly associated with 3PLs service, which in turn is significantly associated with value-to-client and benefit-to-3PLs provider [8]. However, there are still some difficulties in the development of 3PLs.

As for the design of logistics scheme and route, many scholars have made many contributions to improve the efficiency. Moutaoukil, Neubert and Derrouiche (2015) focused on the consolidation of goods flows by using a Distribution Center to redesign the flow of goods inside the city while not increase the cost, reduce pollution and make the city more attractive [9]. Freile and Mula (2020) considered the topics of reverse logistics, waste management and vehicle routing and scheduling to introduce the area of Green Logistics [10]. Hu *et al.* (2019) provided the metrics of logistics service suppliers used for environmental performance measurement and the barriers and drivers that may hinder or facilitate the adoption of these initiatives, which contributes to the knowledge of environmental sustainability for logistics and transportation [11]. In order to evaluate the smart logistics solutions, simulation techniques is proposed by Alberto and Anna (2014) to present the current state of practice in modelling smart logistics solutions, provides a roadmap in simulation techniques for urban freight transport solutions and improves the knowledge around the patterns currently followed [12]. A global enterprise must continuously improve the efficiency of logistic operations between supply chain collaborators. Integrating logistic services, resources, and necessary information flows in the supply chain to ensure efficiency and efficacy is critically important to these companies. So Trappey *et al.* (2016) systematically designed, analyzed, and evaluated an improved framework for one-stop logistic services [13]. Collaborative two-echelon logistics joint distribution network was organized by Li *et al.*(2020) through a negotiation process via logistics service providers or participants existing in the logistics system, which can effectively reduce the crisscross transportation phenomenon and improve the efficiency of the urban freight transportation system^[14]. Awaga *et al* (2020) investigated the role of logistics service providers in the implementation of a differentiated supply chain ^[15]. In addition, De Marco *et al.* (2014) researched the factors that influence logistics service provider's efficiency in urban distribution systems [15].

In conclusion, there are many scholars in the study of logistics distribution model, and now no one can be suitable for China's joint distribution model, so this paper is to introduce a common distribution model focuses on in-depth analysis of its characteristics, and hope that joint distribution of development has played a certain role.

3. Joint distribution introduction and comparative analysis

The purpose of joint distribution is to integrate the resources reasonably and effectively and make the best use of the resources. The joint distribution of working modes can be considered globally and can be represented by the following diagram (Fig. 1).

It can be said that in order to realize the joint distribution from suppliers to consumers, there must be good coordination, such as transportation system, information technology, personnel capacity, etc. Only when all parties make concerted efforts to carry out the distribution operation can they be unified. In addition, each company has its own characteristics. Because the project cannot be fully implemented, there are many joint distribution models. Different companies need to choose their own common distribution mode in order to operate effectively. According to the utilization degree of logistics resources, distribution can be divided into three models: joint distribution system optimization model, joint distribution field connection and sharing and distribution facilities use type.

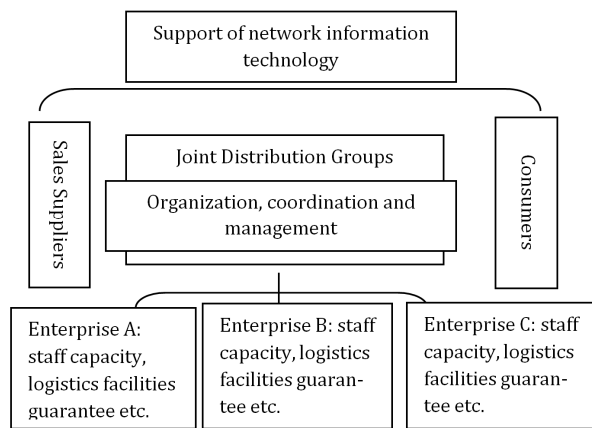


Fig. 1 Joint distribution operation model

3.1 Model 1: Joint distribution system optimization

Professional logistics companies provide the best solution through customer demand, plan and arrange for each user, and make the best processing system in terms of delivery time, quantity, frequency, route, etc., in the premise that all users can accept, comprehensive planning, and reasonable layout.

Main technical conditions: Firstly, all customers have the same conditions. We cannot deviate too much from their delivery time or quantity. The second one is the support of transportation system. Transportation is the basis of distribution system. Once the transportation system is integrated, it can provide guarantee for other aspects of the logistics system. The third is the support of information technology. With the continuous development of society, information technology, network technology and e-commerce technology will continue to innovate, and get the inevitable trend of logistics informatization. If there is no other supports, the joint distribution system will be difficult to carry on. The pattern is shown as Fig. 2.

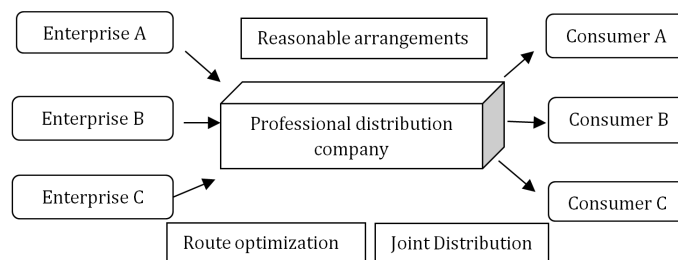


Fig. 2 Optimized joint distribution system schematic

3.2 Model 2: Joint distribution field connection and sharing

The purpose of joint distribution is to unite multiple users to share a distribution field. In general, it can be relatively concentrated in the customer's location. The traffic, roads and sites in the area are relatively crowded, and too many vehicles will cause trouble. Moreover, it is very difficult to go to each customer to prepare for their individual needs. Therefore, multiple users can set up distribution receiving points or cargo handling points together.

Main technical conditions: Firstly, it is the capacity of staff. Logistics and distribution now requires more than mere labour force, besides the IT staff needs to have knowledge of the equipment. Secondly, it is the organization, coordination and management of the various joint distribution models. We may need to organize and manage, and common distribution with warehouse sharing emphasizes this, because it brings the various organizations together in order. Finally, it is the site requirements, which may be connected to a unique requirement yard ground Shared common distribution model. Because the first site needs to be suitable for all customers pick from, and the area should be large enough, or we may have the phenomenon of congestion. In this way, it will have the same effect with direct distribution to the customer. The reason why this model is to the problems of bringing together distribution via vehicles, siting and establishing pick point.

Fig. 3 shows the diagram of location sharing type common distribution business model. After the production is completed, suppliers A, B, C need to make delivery to the customers according to their demands. In the distribution, each supplier completes the process, but the last step is that goods are concentrated on a common place - the yard to build a connection. When the goods delivered, the customers A, B, C will go to the freight yard to pick up their own goods.

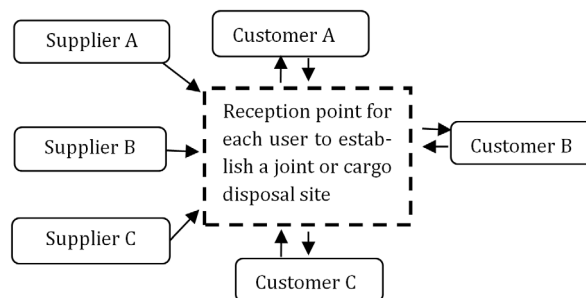


Fig. 3 Shared-off location joint distribution schematic

3.3 Model 3: Distribution facility use type

When many different distribution companies are located in the same city or region, in order to save the investment cost of distribution centres and improve the efficiency of distribution and transportation, many enterprises will establish joint venture partnership and establish joint distribution center, or some enterprises will use the existing distribution centres and distribution facilities to implement distribution jointly for different enterprise users.

Main technical conditions: Firstly, the implementation of joint distribution needs to be guaranteed by perfect logistics facilities, such as transportation equipment, storage equipment, shelves, loading and unloading machinery, office equipment, etc. Secondly, for employees, they must use the appropriate logistics facilities. Then, they need to choose the use and type of standard distribution facilities according to their own characteristics.

As can be seen from

Fig. 4, this is a common type of distribution facilities. In the left column are distribution companies A, B, C, which can also be manufacturers. Their purpose is to use together distribution centres or other facilities, such as sorting machines and warehouses. As mentioned earlier, some companies sell in two seasons, the sales season and the off-season. In the off-season, enterprises do not want to leave warehouses idle, and if they can share facilities and equipment, they will reduce costs. Vehicles can also be used together during distribution. When distribution enter-

prises A and B have customers who need to deliver goods, the vehicles can be used together if the vehicles and locations permit, so as to avoid the distribution enterprises A and B from delivering by themselves.

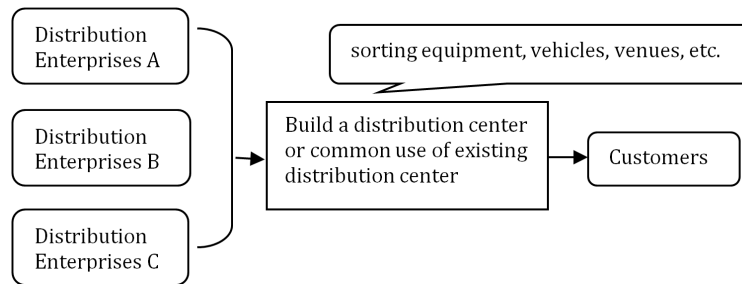


Fig. 4 Distribution facilities using type common schematic distribution model

3.4 Comparative analysis of three models

The three joint distribution of operating models introduced earlier have different characteristics and advantages, and the uses of them are different. We put the following three models here and make a comparison (Table 1).

In fact, each model has its own advantages, and no one is a panacea. Not all companies can apply to the three joint distribution model, and not all business needs a joint distribution. If the cost of a single distribution is less than the implementation of a joint distribution, we do not need to implement it. In the implementation process, the corresponding conditions require more attention paid to personnel management, vehicle scheduling, warehouse distribution, etc. It can be said that joint distribution as a whole, each part of the nodes is not disconnected. There are gains and losses.

Table 1 Comparative analysis of three models

Business model	M1: System optimized	M2: Field connection and sharing	M3: Distribution facilities use type
Contrast species			
Applications in the distribution system	Distribution throughout the application, from the manufacturer to the customer all have to use the whole distribution process	Finally, the application delivery process, only the last link use pick	Applied to a particular aspect of the distribution, use common facilities needed
Advantages	<ol style="list-style-type: none"> 1. It can control the entire distribution process, easy to manage 2. To the greatest possible to meet the needs of suppliers and customers 3. Out significantly lower risk 4. You can cross out the whole distribution process, and focus on strengthening the core competencies 	<ol style="list-style-type: none"> 1. Deliver to the destination can save time and improve distribution efficiency 2. Self-built warehouse cost savings 3. In terms of customers, facilitate their management 	<ol style="list-style-type: none"> 1. Saving the cost of purchasing the facility 2. Easy to use, and you can make a joint application distribution channel
The main technical conditions required	<ol style="list-style-type: none"> 1. Sound distribution system 2. Professional distribution logistics companies 3. Supporting transport system 4. Support information technology 	<ol style="list-style-type: none"> 1. Relatively concentrated customer location 2. There must be space to build pick point 3. Access to professional yard land management, more customers would easily lead to confusion 	<ol style="list-style-type: none"> 1. Sales of the best seasonal difference 2. To produce a similar product attributes 3. To complete logistics equipment
Suitable business	Basically applies to all businesses, hoping to outsource logistics companies	The geographical distribution of the relative concentration of customers, such as supermarkets, centralized stores, schools, etc.	There are seasonal or a distinguished enterprise logistics links and common use of similar businesses can benefit

4. Beijing Chaopi Trading Co., Ltd joint distribution pattern

4.1. Beijing Chaopi Trading Co., Ltd

Beijing Chaopi Trading Company Limited (Chaopi Company) is a subsidiary of Beijing Jingkelong Group Co., Ltd. The registered capital of this company is 384 million yuan, and the total asset is 1.3 billion yuan. This company engages in FMCG distribution, brand agency, terminal services, logistics and distribution business of commercial wholesale and comprehensive service combined with 3PLs enterprises. The company engages in food, drinks and other FMCG. Operators and agents at home and abroad are more than 300 commercial brands, operating more than 9,000 kinds of commodities, has a long-term and stable sales channels.

4.2 Chaopi Company joint distribution pattern analysis

The business model of Chaopi Company is based on the demand of end customers (Fig. 5). It makes the distribution according to the inventory and product management of the whole supply chain. "Super dispatch model" makes arrangements for delivery time, path planning and quantity. According to the working standards of commodity nature, the utilization rate of cargo hold volume is generally more than 90 % of that of freight cars, and the cost can be greatly reduced. This application model is a typical application of general distribution system optimization in actual distribution.

The joint distribution of the company makes 200-300 suppliers' goods centralized in the logistics distribution centre, and the distribution is arranged in the city according to the customers' orders. Customers can also order in small quantities and in multiple batches according to their own requirements, so as to reduce the bundling of customers' funds and improve the market share of commodity sales. Chaopi distribution centre integrates the orders of different customers into one vehicle, with an average of 10-30 suppliers and 4-5 terminal customers. The distribution and transportation costs are shared by the suppliers, end users and Chaopi Company, so as to reduce the inventory and transportation costs of upstream and downstream enterprises with a huge export and achieve a win-win situation. At the same time, it can also ensure the timeliness of distribution and commodity turnover rate. According to the characteristics that the recovery rate of fast moving consumer goods outside the city is more than 70 %, the distribution solution of "planned replenishment" is adopted, with an average of 150,000 containers per day, of which 750 sets are ordered by customers, 200 containers per day, and 4,500 kinds of products per set; 203 daily working vehicles, with an average of 4000 containers per vehicle. Because the scheme is powerful, and the powerful information platform has set up the "early warning" function, so that suppliers have enough time to allocate goods, so as to minimize the loss. Therefore, the tidal skin model is worth learning from.

If Chaopi do not implement joint distribution model, suppliers A, B and C distribute apart in the previous model. As a result, it is inevitable that there will be no delivery or high vacancy rate, and the distribution model of small batch and multi batch is not suitable for fast-moving consumer goods.

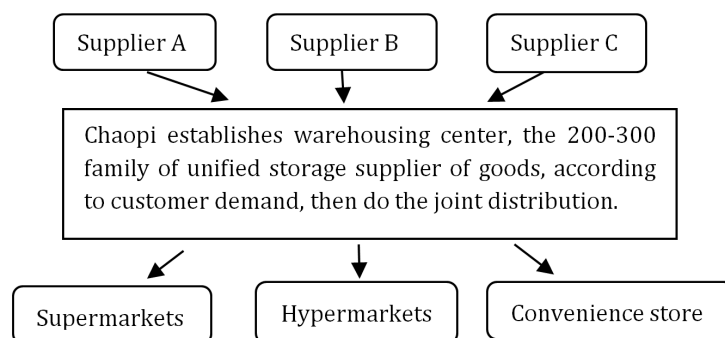


Fig. 5 Chaopi Company joint distribution

Compared to the previous model, it can be seen that Chaopi optimizes the entire middle part of logistics chain and collects all the suppliers and distributors. In this way, the distributor's order is issued to the supplier, and then the delivery plan is implemented to the final delivery. This is a complete system, which reduces duplication and distribution, vacancy rate, etc., and the out rate will be significantly improved. This is good for both suppliers and distributors.

Based on "Chaopi Model" research and investigation, we can make a conclusion that a joint distribution model has significant benefits. In terms of economic or social development, this model is desirable. The advantages are:

- Saving input costs

Select joint distribution model can solve the problems of self-distribution appears to rent the library (or self-built warehouse), vehicle distribution efficiency and management, especially in the season without having to hire more warehouse costs. Variable cost manufacturers choose joint distribution of freight costs just been brought, there will be no investment in fixed costs, which they can use to save money to further strengthen the core competitiveness for the sake of the company's development.

- Avoiding shortage cost

Manufacturers consider criteria for the distribution of cost and time from different aspects, but in tight supply, the case of a small amount of orders, there is no choice. Supply not on time will be out of stock, and will affect the sales. Since the joint distribution plan is strong, and there are warnings out, so that manufacturers have "enough" time for stocking ready information platform, so that we can effectively prevent the occurrence of shortage cost.

- Increasing turnover

If manufacturers are faced with hundreds of distribution points, sales and inventory requirements are not the same. In order to ensure timely delivery, manufacturers will choose large-tonnage truck delivery, shipping time will be very long, commodity turnover will be increased, and the liquidity of turnover will be affected. In this way, it will cause customers a great impact. Adoption of a joint distribution model, Chaopi Company will integrate each customer's order. In the city, they use the unified distribution, and transportation costs are apportioned to the three parties, greatly reducing inventory costs and transportation costs downstream, while timeliness and turnover rate can be guaranteed.

- Improving the overall efficiency of delivery

Import and distribution of trucks loaded cargo compartment, full rate is often less than 50 %, which is a tremendous waste. On the distribution lines, the phenomenon often repeats, and sometimes a small order needs a delivery. Chaopi's joint distribution model is the overall arrangements for the delivery time, times, travel routes and the quantity of goods, delivery route optimization, consolidation work carried out according to the nature of goods, specifications, usually a lorry can be done 4-5 home delivery the amount of cargo tank capacity utilization up to 90 %, an average transport truck supplier 10-30, 3-4 stores 750 containers of goods, delivery vehicles from "floating warehouses" into a "replenishment train".

Logistics and distribution system relies to a large extent complete and convenient urban transport system, starting from the current situation and development trend of Beijing city transportation, logistics and distribution system must take intensive, efficient path, otherwise it is difficult to adapt to the construction needs of the world of the city. Logistics industry with significant economies of scale characteristics, only through continuous integration of various logistics resources to achieve a high degree of intensification and scale, in order to reduce logistics costs of enterprises and society, and joint distribution is not only the realization of highly intensive and large-scale the best choice, but also the construction and development direction of metropolitan distribution system. "Chaopi model" had a very good practice, and achieved good results. It's worth further research and promotion of Chaopi's success.

5. Fast-moving consumer goods joint distribution problems and counter-measures encountered

5.1 Diversification may bring difficulty of management

Management is essential for a business. Generally good management means good development. The inevitable thing of joint distribution of Chaopi is that the ownership relations are too complicated. There exist some disadvantages: different circulation levels, inefficient distribution, and diverse requirements. Each client will have their own distribution requirements, and no one will put the common interests first, so that the management will be difficult. Organization and coordination will be very difficult.

FMCG achieves unified logistics and distribution decisions on the distribution of this platform. It's unnecessary for the companies to hire many managers, and what they should do is have clear division of labour, to prevent each manager being responsible for only one aspect of the mission. Only in this way, will we ensure few errors and more harmonization of all corporate merchandise storage, distribution and other aspects.

5.2 The distribution of benefits may cause disagreement

When doing the joint distribution, what various vendors required the number of items or attributes are not the same. For example, they are used in the same vehicle distribution, some bulky, but lightweight, and some heavy weight, but occupy less area, so items are on the same car, how to count the costs of distribution, we need to have them clearly defined. So when the joint distribution assets to strengthen the internal organizational structure put into use, the division of transparency need monitor efforts to improve the cost-sharing mechanisms and public distribution of benefits principle, need to sign joint distribution agreement for those participating in a more stable unit must, need to focus strictly on divided responsibilities, rights and benefits, members must abide by every cooperation, and need to assume their respective responsibilities and equal treatment. Only by doing so, can each company successfully implement joint distribution.

5.3 The logistics standardization is difficult

If you want to have a greater joint distribution costs of exploitation, logistics standardization is a factor which cannot be unconsidered. Due to differences between each enterprise product packaging, volume, weight, etc., the goods stacked, placed on the link will face great difficulties. Logistics will involve the issues of choice and reference, which are obstacles the joint distribution need to overcome.

Enterprises can start from the inside of the logistics system, overall, the development of technical standards for its various subsystems of facilities, equipment, special tools, etc., and operations standards. Secondly, studies between each subsystem technology standards and business standards will work. According to the requirements, the standard of the entire logistics system is uniform. After studying logistics systems and other systems related to seek unified standard system of logistics, making the logistics standardization can be easy to promote the implementation.

5.4 It's easy to reveal business secrets

Joint distribution is likely to result in the disclosure of business secrets, since the implementation of a joint distribution pattern should be unified management, unified planning and scheduling. Since each company wants unity, we need to discuss and communicate. However, in the distribution process, the expansion list may leak. In the same industry, due to the sharing of information and open, competitive strategy, business development will adversely affect, which is one of the reasons why many companies do not participate in joint distribution.

Therefore, enterprises should pay attention to this aspect, and strengthen management, so as to avoid supplier information leakage. The implementation of a common distribution is to the trust as a precondition. In addition, we need to take effective prevention, surveillance measures to strictly control systems, and make the best-marked confidential matters cooperation agreement, specifying the rights and obligations.

6. Conclusion

In this paper, we did an in-depth research in a joint distribution business model, including joint distribution of conceptual meaning, with three business models and future development, and so on. Based on this, the paper focuses on the logistics of joint distribution, with an example of Beijing Chaopi Trading Company, who uses joint distribution system optimization model to bring the maximum benefit for its producers and sellers, and what the company should pay attention to. On the other two models, joint distribution field connection and sharing and distribution facilities use models, the paper analyzes their processes, features and technical support. Then the paper tells the future direction of development of joint distribution. The purpose of the paper is to let more people know the joint distribution, more in-depth understand the joint distribution, and to choose their own model of operation of enterprises.

Possible shortcomings of this paper are: First, there may exist some cognitive bias or insufficiency of the joint distribution due to most respect and regard of Beijing Chaopi Trading Company, and lack of enough information may have an impact on research. Second, the paper will inevitably have some flaws limited by the individual's knowledge and ability, and we look forward to your corrections.

In fact, China's logistics market potential is huge, and the implementation of joint distribution management will become the development trend of modern logistics. Realization of joint distribution has a long way to go, and the process is bound to encounter a lot of frustration. However, no matter how hard the process, joint distribution will be widely used for the majority of enterprise logistics efficiency, comprehensive, and competitiveness enhancement. From the international market, Japan and other countries are in very common use of joint distribution model. I believe, in the near future, our country will see the benefits brought by joint distribution and use it in a wide range.

No matter from the economic level or social level, the joint distribution model is reasonable. However, in the actual operation, joint distribution companies have many problems to resolve, like different commodity business or attributes. From the perspective of competition, some large companies are reluctant to share with others, because it will increase the cost of other distribution enterprises and enhance the rival's competitiveness. From the perspective of interests, every enterprise does not want to disclose its business secrets, but sometimes it can be seen as "secret" from the orders of some enterprises. So many companies are making some "inconsistency", which requires the guidance of the government. It is understood that China's current policies, no matter in law, have many things to do for a normative system, while some developed countries have established relatively sound laws. The core of joint distribution is to organize distribution uniformly, save cost, save social resources and improve transportation. Therefore, many countries are actively promoting this model, coordinating the logistics distribution capacity and improving the logistics environment. For example, they are trying to solve the problem of distrust among enterprises. Because there is no sound legal system now, I don't know which party the responsibility belongs to, nor which makes some enterprises dare not try. When the government intervenes, there are clear legal provisions and the implementation of supervision can effectively solve these problems. Therefore, we expect the government to attach importance to the logistics industry, and through the joint efforts of relevant departments, the city will have a substantial joint distribution development pattern.

Foundation

- 2018 Beijing Talents foundation of organization department of Beijing Municipal Committee of the CPC (2018000026833ZS09).
- Beijing Philosophy and Social Science (17GLB013).
- Science and technology innovation service capacity provincial (19008021111) (19008021171) (19002020217).

References

- [1] Vieira, J.G.V., Fransoo, J.C. (2015). How logistics performance of freight operators is affected by urban freight distribution issues, *Transport Policy*, Vol. 44, 37-47, [doi: 10.1016/j.tranpol.2015.06.007](https://doi.org/10.1016/j.tranpol.2015.06.007).
- [2] Gómez, S.C.G., Cruz-Reyes, L., González, B.J.J., Fraire, H.H.J., Pazos, R.R.A., Martínez, P.J.J. (2014). Ant colony system with characterization-based heuristics for a bottled-products distribution logistics system, *Journal of Computational and Applied Mathematics*, Vol. 259, Part B, 965-977, [doi: 10.1016/j.cam.2013.10.035](https://doi.org/10.1016/j.cam.2013.10.035).
- [3] Wu, Y.-C.J., Huang, S.K. (2013). Making on-line logistics training sustainable through e-learning, *Computers in Human Behavior*, Vol. 29, No. 2, 323-328, [doi: 10.1016/j.chb.2012.07.027](https://doi.org/10.1016/j.chb.2012.07.027).
- [4] Liu, Y. (2015). An empirical study on customers' satisfaction of third-party logistics services (3PLS), In: *Proceedings of the 2015 International Conference on Education, Management and Computing Technology*, Atlantis Press, 1361-1365, [doi: 10.2991/icemct-15.2015.282](https://doi.org/10.2991/icemct-15.2015.282).
- [5] Cabigiosu, A., Campagnolo, D., Furlan, A., Costa, G. (2015). Modularity in KIBS: The case of third-party logistics service providers, *Industry and Innovation*, Vol. 22, No. 2, 126-146, [doi: 10.1080/13662716.2015.1023012](https://doi.org/10.1080/13662716.2015.1023012).
- [6] Lopes, H.S., Lima, R.S., Leal, F. (2020). Simulation project for logistics of Brazilian soybean exportation, *International Journal of Simulation Modelling*, Vol. 19, No. 4, 571-582, [doi: 10.2507/IJSIMM19-4-529](https://doi.org/10.2507/IJSIMM19-4-529).
- [7] Aguezzoul, A. (2014). Third-party logistics selection problem: A literature review on criteria and methods, *Omega*, Vol. 49, 69-78, [doi: 10.1016/j.omega.2014.05.009](https://doi.org/10.1016/j.omega.2014.05.009).
- [8] Shi, Y., Zhang, A., Arthanari, T., Liu, Y. (2016). Third-party purchase: An empirical study of Chinese third-party logistics users, *International Journal of Operations & Production Management*, Vol. 36, No. 3, 286-307, [doi: 10.1108/IJOPM-11-2014-0569](https://doi.org/10.1108/IJOPM-11-2014-0569).
- [9] Moutaoukil, A., Neubert, G., Derrouiche, R. (2015). Urban freight distribution: The impact of delivery time on sustainability, *IFAC-PapersOnLine*, Vol. 48, No. 3, 2368-2373, [doi: 10.1016/j.ifacol.2015.06.442](https://doi.org/10.1016/j.ifacol.2015.06.442).
- [10] Freile, A.J., Mula, J., Campuzano-Bolarin, F. (2020). Integrating inventory and transport capacity planning in a food supply chain, *International Journal of Simulation Modelling*, Vol. 19, No. 3, 434-445, [doi: 10.2507/IJSIMM19-3-523](https://doi.org/10.2507/IJSIMM19-3-523).
- [11] Hu, H., Wu, Q., Zhang, Z., Han, S. (2019). Effect of the manufacturer quality inspection policy on the supply chain decision-making and profits, *Advances in Production Engineering & Management*, Vol. 14, No. 4, 472-482, [doi: 10.14743/apem2019.4.342](https://doi.org/10.14743/apem2019.4.342).
- [12] Trappey, A.J.C., Trappey, C.V., Govindarajan, U.H., Chuang, A.C., Sun, J.J. (2017). A review of essential standards and patent landscapes for the internet of things: A key enabler for Industry 4.0, *Advanced Engineering Informatics*, Vol. 33, 208-229, [doi: 10.1016/j.aei.2016.11.007](https://doi.org/10.1016/j.aei.2016.11.007).
- [13] Li, H.-Y., Xu, W., Cui, Y., Wang, Z., Xiao, M., Sun, Z.-X. (2020). Preventive maintenance decision model of urban transportation system equipment based on multi-control units, *IEEE Access*, Vol. 8, 15851-15869, [doi: 10.1109/ACCESS.2019.2961433](https://doi.org/10.1109/ACCESS.2019.2961433).
- [14] Awaga, A.L., Xu, W., Liu, L., Zhang, Y. (2020). Evolutionary game of green manufacturing mode of enterprises under the influence of government reward and punishment, *Advances in Production Engineering & Management*, Vol. 15, No. 4, 416-430, [doi: 10.14743/apem2020.4.375](https://doi.org/10.14743/apem2020.4.375).
- [15] De Marco, A., Cagliano, A.C., Mangano, G., Perfetti, F. (2014). Factor influencing logistics service providers efficiency in urban distribution systems, *Transportation Research Procedia*, Vol. 3, 499-507, [doi: 10.1016/j.trpro.2014.10.031](https://doi.org/10.1016/j.trpro.2014.10.031).

Designing a warehouse internal layout using a parabolic aisles based method

Zhang, Z.Y.^{a,*}, Liang, Y.^b, Hou, Y.P.^a, Wang, Q.^c

^aSchool of Logistics, Beijing Wuzi University, Beijing, P.R. China

^bBeijing Chaoyang District Committee of the Revolutionary Committee of the Chinese Kuomintang, Beijing, P.R. China

^cManufacturing Engineering and Order Delivery Center, Beiqi Foton Motor Co., Ltd, Beijing, P.R. China

ABSTRACT

Refined layout is a basis of warehousing efficiency. Straight aisle is a typical feature of current warehouse internal layouts. The purpose of this paper is to explore the possibility of using curve aisles for warehouse layout. By Choosing typical non-traditional layouts and transforming their inclined cross-aisle trajectory into parabola, two parabolic aisle layouts, parabolic Flying-V and parabolic Fishbone, are constructed. For unit-load warehouses, based on the morphological characteristic analysis and the parabolic types selection, the picking distance model and the cross-aisle length formula are presented. Interval Numerical Simulation Method (INSM) and Genetic Algorithms (GA) are adopted to solve the model respectively in order to verify the results. This research breaks through the realistic situation of straight aisle leading warehouse layout, and enriches the relevant layout theory. The calculation results of 100 warehouses with different sizes show that the picking distance of parabolic Flying-V could be reduced by 0.22-0.62 % compared with the straight layout, and the theoretical possible improvement space has been compressed by 2.42-12.26 %. Its length of cross-aisle is shortened by -0.03-3.10 %. The picking distance of parabolic Fishbone could be only reduced by 0.02-0.04 %. The theoretical possible improvement space has been compressed by 1.27-1.83 %. But its length of cross-aisle will increase by 4.63-19.50 % significantly. We believe that the layout of non-rectangular complex special-shaped warehouses based on curve trajectory aisles would become an important research topic. In addition, after some necessary modifications to the objectives and constraints, the proposed method in this paper may also be used for the arrangement of machines and devices in a workshop in principle.

ARTICLE INFO

Keywords:

Layout design;
Warehouse internal layout;
Parabolic aisle layout;
Layout efficiency;
Simulation;
Optimization;
Interval numerical simulation method (INSM);
Genetic algorithms (GA)

*Corresponding author:

zyfzzy@263.net
(Zhang, Z.Y.)

Article history:

Received 8 April 2021

Revised 26 April 2021

Accepted 5 May 2021



Content from this work may be used under the terms of the Creative Commons Attribution 4.0 International Licence (CC BY 4.0). Any further distribution of this work must maintain attribution to the author(s) and the title of the work, journal citation and DOI.

1. Introduction

Warehouse is an important social logistics infrastructure. The level of warehouse system planning and design directly affects the overall logistics efficiency of a country. We know that the travel distance of a picking tour is an imperative factor in improving warehouse operation efficiency [1]. The efficiency of warehouse processes could be improved by reducing travel time and cost in replenishment and order picking [2]. The layout of internal aisle in warehouses is the basis of storage space planning and warehouse operation scheduling management, which directly affects the area utilization rate, the access efficiency, the difficulty of layout adjustment, the overall operation energy consumption and the total cost of warehousing. With the rapid development of warehouse operation and management technology, warehouse enlargement and au-

tomation are the future development trends. The benefit of lean warehouse layout research will be more fully reflected in the construction of more and more intelligent super-large warehouses.

Traditional warehouse layouts lack detailed quantitative research on the efficiency mechanism of aisle layout itself. In practice, it is usually based on the qualitative analysis to choose a basic layout mode, and then to match the specification parameters such as aisle width, function area size and shelf size according to relevant design specifications. For the common rectangular warehouses, most of them are based on experience and intuition, using the layout of parallel shelves and orthogonal straight track aisles (as shown in Fig. 1) [3].

In 2009, Gue and Meller break away from the traditional conventions, and innovatively put forward two new warehouse internal layouts with inclined cross-aisles: Flying-V and Fishbone (as shown in Fig. 2) [4]. Numerical simulation results show that, for the unit-load warehouse, these two new non-traditional layouts based on the cross-aisle angle modelling and optimization can reduce the average total picking distance by about 10 % and 20 % respectively compared with the traditional layouts based on empiricism.

Literature review shows that both the traditional layouts based on parallel orthogonal aisle mode selection and the non-traditional layouts based on aisle angle modelling and optimization have a problem or shortcoming. The aisle trajectory is basically a straight line or piecewise straight line by default. The layout design revolves around the direction and distribution of the cross and picking aisles of the straight-line trajectory. There is no research on warehouse aisle layout based on curved line trajectory has been found in the literature. Choosing straight aisle has become a default research paradigm of warehouse internal layout design.

Aiming at the problem or shortcoming, this research widens the view of aisle trajectory selection and proposes the conception of exploring the curve path layout method. Focusing on the curve aisle layout problem, we selected two typical non-traditional layouts, Flying-V and Fishbone, to carry out the curve transformation of the parabolic cross-aisle trajectory. The straight trajectory of the inclined cross-aisles in the original layout is changed into a parabola, but the straight characteristics of the horizontal or vertical cross-aisle remain unchanged (as shown in Fig. 3).

The parabolic aisle layout expands the trajectory shape of the cross-aisle, and could obtain a layout scheme with higher picking efficiency (Because it has enlarged the feasible region of the optimization model.) without significantly affecting the utilization ratio of warehouse area (Because it does not change the number of the cross-aisles.). In order to balance the contradiction between picking efficiency and utilization ratio of warehouse area better, we introduce the cross-aisle length index in our model.

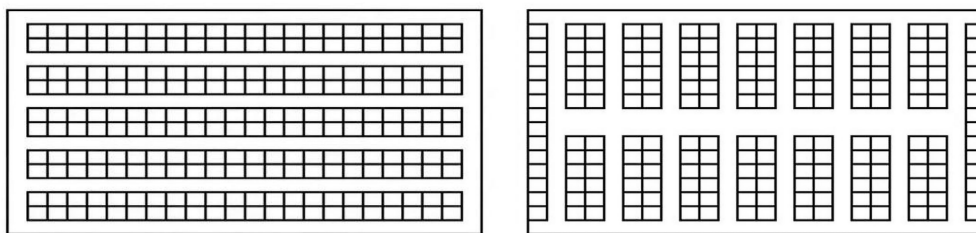


Fig. 1 Two typical kinds of traditional warehouse internal layouts

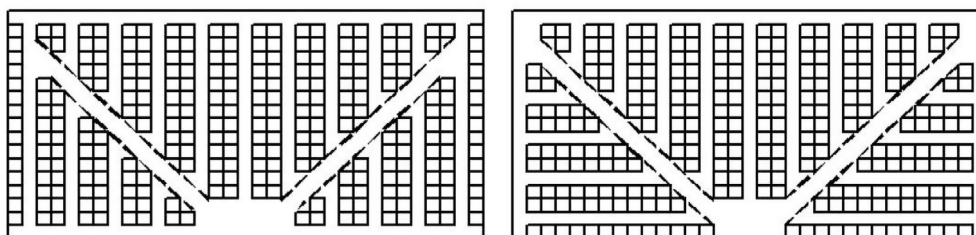


Fig. 2 Flying-V and Fishbone internal layouts of warehouse

This paper continues with the following content. The next section is a literature review. The third section describes the modelling process of the parabolic layout. The fourth section provides the model of the corresponding straight layout. The fifth section gives out the methodology of the model solving. The sixth section presents our numerical results with discussions. The last section concludes this paper.

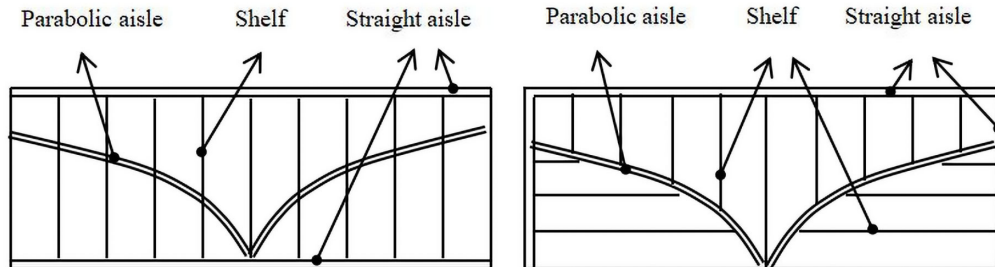


Fig. 3 Parabolic Flying-V and parabolic Fishbone internal layouts of warehouse

2. Literature review

The new non-traditional layout of Gue and Meller attracted wide attention from academia, and became a research hotspot soon. Pohl *et al.* studied the optimization of Fishbone layout under the dual-command [5]. The results show that the background of dual-command significantly reduces the advantage of Fishbone layout compared with traditional layout. Pohl *et al.* investigated the impact of different warehousing strategies on Flying-V and Fishbone layout under single and dual-command [6]. The results show that the optimal warehouse design parameters under stochastic strategy also perform well under turnover rate strategy. Gue *et al.* presented the aisle layout optimization problem in multiple P&D (Pickup and Deposit) points and unit-load warehouses [7]. Flying-V and Inverted-V warehouse models are established respectively. The numerical results show that the advantage of Flying-V aisle design is not as significant as that of the single P&D point. Cardona *et al.* made an in-depth analysis of the cross-aisle angle in Fishbone layout [8]. According to the fixed and uncertain length and width of warehouse, the determination of optimal aisle angle and its robust stability are discussed, which provides a theoretical basis for the flexible decision-making of actual warehouse layout design. Ö.Öztürkoğlu *et al.* based on the idea of increasing the number of cross-aisles in traditional warehouse layout and optimizing the angles of its cross and picking aisles, presented three non-traditional warehouse layouts, Chevron, Leaf and Butterfly [9]. Angular modelling and optimization analysis show that these three non-traditional warehouse layouts can reduce the total picking distance by 19.53 %, 21.72 % and 22.52 % respectively compared with traditional warehouse layout. Some practical applications of non-traditional warehouse layout are also discussed. Clark and Meller introduced the vertical travel parameter to modify the picking time model, and investigated the impact of vertical movement on Flying-V and Fishbone layout on multi-storey shelves [10]. The results show that the vertical operation of shelves has a great impact on Flying-V layout, but not on Fishbone layout. Jiang *et al.* improved Fishbone layout by considering the characteristics of drive-in racking, and obtained a Leaf-like layout [11]. Liu *et al.* based on Fishbone layout, according to the general storage principle, studied the optimization of storage location allocation by using of the genetic Algorithms and MATLAB tool [12]. Ö.Öztürkoğlu *et al.* considered the relationship between the location of a single pallet and the aisle, constructed a constructive multiple P&D points unit-load warehouse aisle design network-based model [13]. Particle swarm optimization is used to optimize the aisle design scheme. Cardona *et al.* proposed a very practical three-dimensional detailed design method of Fishbone layout [14]. This method considers the influence of aisle width, forklift speed, rental fee and maintenance cost, etc. Marco Bortolini *et al.* proposed a layout of inserting one or more straight non-orthogonal cross-aisles into rectangular warehouses [15]. The picking distance and warehouse area loss of this kind of layout under unit-load are also analysed. The average picking time and warehouse parameters under random warehousing strategy and individual operation instructions are obtained. The proposed layout is

essentially a straight aisle Flying-V and its expansion. When the optimal layout is adopted, the picking distance can be reduced by 7-17 %. Liu *et al.* studied the problem of solving the optimal Fishbone layout by means of the genetic Algorithms [16]. Akhilesh Mesa discussed the non-traditional layout method of multiple P&D points and unit-load warehouses with multiple cross aisles [17]. Unlike other designs in the past, the aisles are arranged in diamonds. In essence, the layout proposed in this paper can still be regarded as a combination of two Fishbone layouts. Mowrey *et al.* applied the idea of non-orthogonal inclined aisle to the internal layout of retail stores [18]. In order to make full use of the limited space in the store and show more goods to customers, this research expands the practical application scope of non-traditional layout. Zhang *et al.* proposed the Twin Leaf method of warehouse aisle layout in view of the deficiencies of Leaf layout [19]. Three basic characteristics of the Twin Leaf layout are analysed. Compared with Leaf layout, Twin Leaf layout can reduce the picking distance by 1.02 % on average, and the theoretical possible improvement space can be compressed by 45.45 %.

To sum up, in the past ten years, non-traditional warehouse layout methods have been deeply studied by scholars all over the world and applied by some American enterprises. These researches can be roughly classified into two major categories: the first one is the innovation of basic layout methods. Five non-traditional layout methods, Flying-V, Fishbone, Chevron, Leaf and Butterfly are presented. The second one is the efficiency analysis of basic layouts in specific warehousing operating environment. For example, the impact of different practical operating environments, such as single-command, dual-command, multiple P&D points warehouses, specific warehousing strategy requirements, location assignment optimization, etc.

In fact, the budding idea of non-orthogonal design of warehouse aisles could be traced back to the 1960s. Moder and Thornton analysed the influence of pallet placement angle and aisle width on the utilization ratio of warehouse area through mathematical modelling [20]. Francis studied the optimal layout of rectangular warehouses based on the assumption of straight path and the consideration of picking and construction cost [21, 22]. Berry put forward a proposal to arrange pallets around a diagonal aisle into different roadways according to the characteristics of inventory units [23]. White studied the Euclidean efficiency estimation of radial aisles in non-rectangular warehouses [24]. Under the assumption of continuous space, Euclidean efficiency of four and six radial aisles is estimated. Bassan *et al.* based on Francis's research, considered the aisle structure parameters, and analysed the impact of the internal layout of warehouse on the overall operating cost of warehouse [25]. The total cost function is constructed to optimize the warehouse layout. In the early stage, these scattered discussions on the design ideas and methods of non-orthogonal warehouses layout were relatively shallow. Their basic limitation is that they are only preliminary theoretical discussions, no practical design specifications, lack of practical application case testing, and thus they failed to arouse attention. Since then, relevant research has entered a relatively quiet period of about 30 years.

3. Research models

Based on the analysis of morphological characteristics, the selection of parabolic type and the efficiency modelling of layout, the research is carried out in turn. For the convenience of analysis and comparison, the idea of continuous space modelling is adopted to build the efficiency model of the parabolic layout in unit-load warehouses [9]. The cross-aisle length is introduced as a supplementary evaluation index to the optimization of the layout efficiency.

3.1. Assumptions and symbols

There are many factors affecting the layout of warehouse aisles. For the convenience of discussion, the following premise assumptions and parameter symbols are specially made.

Assumptions:

- 1) The warehouse is rectangular.
- 2) Neglect the influence of warehouse height on the layout of warehouse aisle.
- 3) Only one storage or picking operation is carried out for goods at a certain location in the warehouse, and one-way moving distance is used.

- 4) One-time completion the operation of goods in the whole warehouse.
- 5) Consider the situation of a single P&D point, and every warehousing operation passes through the P&D point.
- 6) The widths of the cross and picking aisles in warehouse are neglected in our optimization models. For the convenience of comparison, we adopted the same assumption described in Ö.Öztürkoğlu *et al.* [9]. Although this continuous model with zero width aisles is not completely consistent with the reality, it is close enough for our research purposes, especially for super-large warehouses.
- 7) The volume of goods and the size of pallets or shelves in the warehouse are all neglected when modelling and analysing.

Symbols:

- P&D: Pickup and Deposit point, the entrance of goods;
 O, x, y : O is the origin of the coordinate system. The origin is located at the P&D point. The length direction of the warehouse is set to x axis and the width direction is set to y axis.
 w : Half of the length of warehouse horizontal direction;
 h : Total vertical width of warehouse;
 $N(x, y)$: The location coordinates of any storage point in the warehouse: $-w \leq x \leq w, 0 \leq y \leq h$;
 α : The cross-aisle angle of the right half of the warehouse under the straight Flying-V layout;
 β : The cross-aisle angle of the right half of the warehouse under the straight Fishbone layout;
 α^* : The optimal angle of the cross-aisle when the picking distance of the straight Flying-V layout is the smallest;
 β^* : The optimal angle of the cross-aisle when the picking distance of the straight Fishbone layout is the smallest.

3.2. Morphological characteristics of the parabolic layout

These two parabolic layouts are both bilateral symmetrical, so we only need to take the discussion on the right half of the warehouse. According to the different possible intersection positions of the parabolic cross-aisle and the warehouse edge, they are divided into two different sub-morphologies (as shown in Fig. 4 and Fig. 5).

In the sub-form 1 of parabolic Flying-V as shown in Fig. 4(a), the right half warehouse is divided into two picking sub-areas, A and B, by the parabolic cross-aisle. In the sub-form 2 of parabolic Flying-V as shown in Fig. 4(b), the right half warehouse is divided into three picking sub-areas, A, B and C, by the parabolic cross-aisle and the line segment. Similarly, in the two sub-forms of parabolic Fishbone shown in Fig. 5(a) and Fig. 5(b), their right half warehouses are both divided into two picking sub-areas, A and B, by the parabolic cross-aisle respectively.

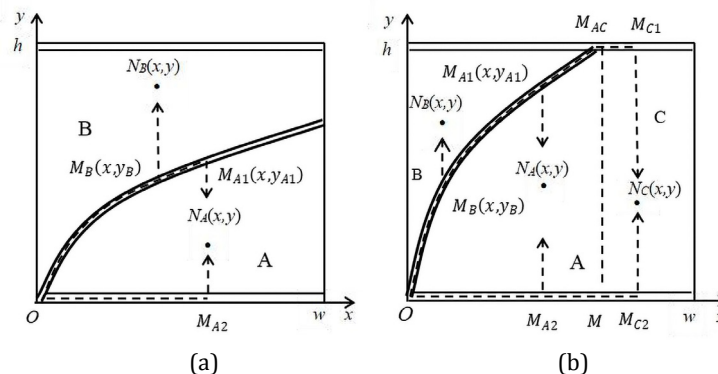


Fig. 4 Two sub-forms of parabolic Flying-V layout

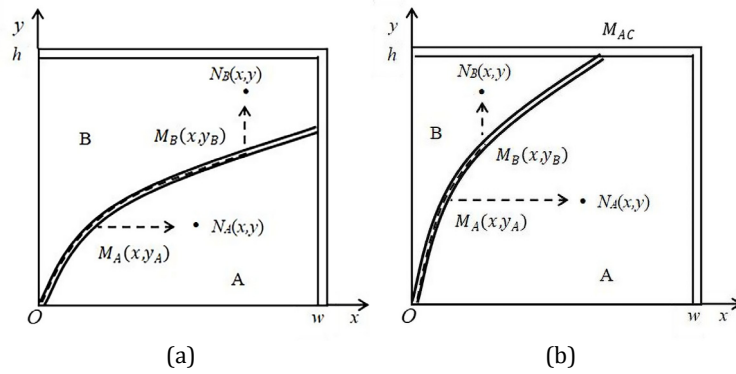


Fig. 5 Two sub-forms of parabolic Fishbone layout

3.3. Efficiency model for the parabolic layout

The parabolic layout efficiency model consists of two parts. The first part is the total picking distance model. The second is the length formula of the cross-aisle. Picking distance is the core index reflecting the efficiency of picking operation. The cross-aisle length is the main factor affecting the utilization rate of warehouse area, which can be used as a supplementary index for layout efficiency evaluation. The parabolic type of the parabolic cross-aisle should be determined first, and the basic picking distance formula of each picking sub-region is derived. Then the average total picking distance model and the length formula of the cross-aisle are obtained by integration.

Determination of the parabolic type

Because our discussions are all taken in the right half of the warehouse, the parabolic cross-aisle must pass through the P&D point (the coordinate origin O) of the warehouse, so the selected parabola should pass through the first quadrant and the origin. There are two basic types of parabola passing through the origin, they take x axis and y axis as the axis of symmetry respectively. That are $x = ay^2 + by$ and $y = ax^2 + bx$. The opening direction of the parabola is determined by the positive and negative of parameter a . Obviously, the parabola corresponding to $a < 0$ does not meet this basic requirement and should be discarded. Therefore, the only optional parabola is: $x = ay^2 + by, a > 0$ and $y = ax^2 + bx, a > 0$. On this basis, combined with the characteristics of two kinds of parabolic layout (especially, the dual equivalence of thin-high warehouse and flat warehouse under Fishbone layout), through the trial calculation of typical thin-high, square and flat warehouse, the parabola of type $x = ay^2 + by, a > 0, b > 0$ is synthetically determined as the basis of modeling. In addition, because the study only involves the first quadrant, there are, $x > 0, y > 0$, see Eq. 1.

$$x(y) = ay^2 + by \quad (a > 0, b > 0, x > 0, y > 0) \tag{1}$$

Based on the selected basic parabola type, according to the different integral variables, two expressions of the corresponding parabolic arc length (S) formula are given incidentally, as shown in Eq. 2, Eq. 3 and Eq. 4.

$$S = S(x) = S(y) \tag{2}$$

$$S(x) = \frac{1}{4a} [\sqrt{4ax + b^2 + 1} \times \sqrt{4ax + b^2} + \ln|\sqrt{4ax + b^2 + 1} + \sqrt{4ax + b^2}| - \sqrt{b^2 + 1} \times b - \ln|\sqrt{b^2 + 1} + b|] \tag{3}$$

$$S(y) = \frac{1}{4a} [\sqrt{(2ay + b)^2 + 1} \times (2ay + b) + \ln|\sqrt{(2ay + b)^2 + 1} + (2ay + b)| - \sqrt{b^2 + 1} \times b - \ln|\sqrt{b^2 + 1} + b|] \tag{4}$$

Picking distance model of the parabolic layout

For convenience of comparison, the optimization model of average total picking distances of the parabolic layouts under unit-load are constructed by using the idea of continuous space modelling [9].

- 1) Picking distance of parabolic Flying-V. Based on the results of morphological analysis in Fig. 4. and the selected parabolic equation type (1), we can obtain that:

$$y_{A1} = \frac{\sqrt{4ax+b^2}-b}{2a} \quad (5)$$

- Picking distance $D_{PFV}^{A1}(x, y)$ in A region of sub-form 1.

$$D_{PFV}^{A1}(x, y) = \min \{D_{PFV}^{A1_1}(x, y), D_{PFV}^{A1_2}(x, y)\} \quad (6)$$

$$D_{PFV}^{A1_1}(x, y) = d_{OM_{A1}} + d_{M_{A1}N_A} \quad (7)$$

$$d_{OM_{A1}} = S(x) \quad (8)$$

$$d_{M_{A1}N_A} = y_{A1} - y \quad (9)$$

$$D_{PFV}^{A1_2}(x, y) = x + y \quad (10)$$

- The basic picking distance $D_{PFV}^{B1}(x, y)$ in B region of sub-form 1.

$$D_{PFV}^{B1}(x, y) = d_{OM_B} + d_{M_B N_B} \quad (11)$$

$$d_{OM_B} = S(x) \quad (12)$$

$$d_{M_B N_B} = y - y_{A1} \quad (13)$$

- Picking distance of region A in sub-form 2 $D_{PFV}^{A2}(x, y)$.

$$D_{PFV}^{A2}(x, y) = \min \{D_{PFV}^{A2_1}(x, y), D_{PFV}^{A2_2}(x, y)\} \quad (14)$$

$$D_{PFV}^{A2_1}(x, y) = D_{PFV}^{A1_1}(x, y) (0 < x < ah^2 + bh) \quad (15)$$

$$D_{PFV}^{A2_2}(x, y) = x + y \quad (16)$$

- Picking distance of region B in sub-form 2 $D_{PFV}^{B2}(x, y)$.

$$D_{PFV}^{B2}(x, y) = D_{PFV}^{B1}(x, y) (0 < x < ah^2 + bh) \quad (17)$$

- Picking distance of area C in sub-form 2 $D_{PFV}^{C2}(x, y)$.

$$D_{PFV}^{C2}(x, y) = \min \{D_{PFV}^{C2_1}(x, y), D_{PFV}^{C2_2}(x, y)\} \quad (18)$$

$$D_{PFV}^{C2_1}(x, y) = d_{OM_{AC}} + d_{M_{AC}M_{C2}} + d_{M_{C2}N_C} \quad (19)$$

$$d_{OM_{AC}} = S(y) (y = h) = \frac{1}{4a} \left[\left(\sqrt{(2ah+b)^2 + 1} \times (2ah+b) + \ln \left| \sqrt{(2ah+b)^2 + 1} + (2ah+b) \right| \right) - \sqrt{b^2 + 1} \times b - \ln \left| \sqrt{b^2 + 1} + b \right| \right] \quad (20)$$

$$d_{M_{AC}M_{C2}} = x - (ah^2 + bh) \quad (21)$$

$$d_{M_{C2}N_C} = h - y \quad (22)$$

$$D_{PFV}^{C2_2}(x, y) = x + y \quad (23)$$

- Based on the above continuous space modelling assumption, the optimal average total picking distance of parabolic Flying-V is E_{PFV}^* as shown in Eq. 24.

$$E_{PFV}^* = \min \{ \min(E_{PFV}^{A1}), \min(E_{PFV}^{B1}) \} \quad (24)$$

$$E_{PFV}^{A1} = \frac{1}{wh} \left(\int_0^w \int_0^{y_{A1}(x)} D_{PFV}^{A1_1}(x, y) dy dx + \int_0^w \int_{y_{A1}(x)}^h D_{PFV}^{A1_2}(x, y) dy dx \right) \quad (25)$$

$$E_{PFV}^{B1} = \frac{1}{wh} \left(\int_0^{ah^2+bh} \int_0^{y_{A1}(x)} D_{PFV}^{A1_1}(x, y) dy dx + \int_0^{ah^2+bh} \int_{y_{A1}(x)}^h D_{PFV}^{A1_2}(x, y) dy dx + \int_{ah^2+bh}^w \int_0^h D_{PFV}^{C2_2}(x, y) dy dx \right) \quad (26)$$

2) Picking distance of parabolic Fishbone. From the analysis of morphological features shown in Fig. 5, it is found that the basic picking distance formulas for the two sub-forms of parabolic Fishbone layout are the same. They are recorded as $D_{PFB}^A(x, y)$ and $D_{PFB}^B(x, y)$.

$$D_{PFB}^A(x, y) = d_{OM_A} + d_{M_A N_A} \tag{27}$$

$$d_{OM_A} = S(y) \tag{28}$$

$$d_{M_A N_A} = x - (ay^2 + by) \tag{29}$$

$$D_{PFB}^B(x, y) = D_{PFB}^A(x, y) \tag{30}$$

Based on the assumption of continuous modelling, the optimal average total picking distance of parabolic Flying-V layout is E_{PFB}^* see Eq. 31.

$$E_{PFB}^* = \min\{\min(E_{PFB}^1), \min(E_{PFB}^2)\} \tag{31}$$

$$E_{PFB}^1 = \frac{1}{wh} \left(\int_0^w \int_0^{y_{A1}(x)} D_{PFB}^A(x, y) dy dx + \int_0^w \int_{y_{A1}(x)}^h D_{PFB}^B(x, y) dy dx \right) \tag{32}$$

$$E_{PFB}^2 = \frac{1}{wh} \left(\int_0^h \int_{ay^2+by}^w D_{PFB}^A(x, y) dx dy + \int_0^h \int_0^{ay^2+by} D_{PFB}^B(x, y) dx dy \right) \tag{33}$$

Main aisle length formula for parabolic layout

From Figs. 4 and 5, the optimal parabolic cross-aisle lengths T_{PFV} and T_{PFB} of Flying-V and Fishbone are respectively:

$$T_{PFV} = \begin{cases} S^*(y)(y = h), & a^*h^2 + b^*h < w \\ S^*(x)(x = w), & a^*h^2 + b^*h \geq w \end{cases} \tag{34}$$

$$T_{PFB} = \begin{cases} S^*(y)(y = h), & a^*h^2 + b^*h < w \\ S^*(x)(x = w), & a^*h^2 + b^*h \geq w \end{cases} \tag{35}$$

4. Reference models

To analyse the efficiency of parabolic layout, the corresponding straight layout should be taken as a reference. However, in the historical literature, the layout efficiency analysis of straight Flying-V and straight Fishbone does not consider the cross-aisle length, and is discrete modelling. To unify the comparison benchmark, it is necessary to reconstruct the picking distance model of straight Flying-V and straight Fishbone and the length formula of their cross-aisle.

4.1 Picking distance model of straight layout

Similarly, according to the different intersection positions between the cross-aisle and the edge of the warehouse, the straight Flying-V layout also has two different sub-form, as shown in Fig. 6. In sub-form 1, the right half warehouse is divided into two regions, A and B, by the cross-aisle; in sub-form 2, the right warehouse is divided into three sub-regions A, B and C, by the cross-aisle and line segment MM_{AC} . Similarly, the straight Fishbone layout also has two different sub-forms, as shown in Fig. 7. The right half warehouse is divided into two picking sub-areas, A and B, by the cross-aisle.

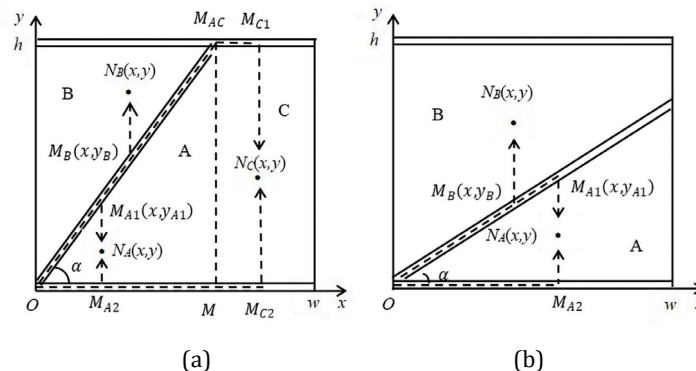


Fig. 6 Two sub-forms of straight Flying-V layout

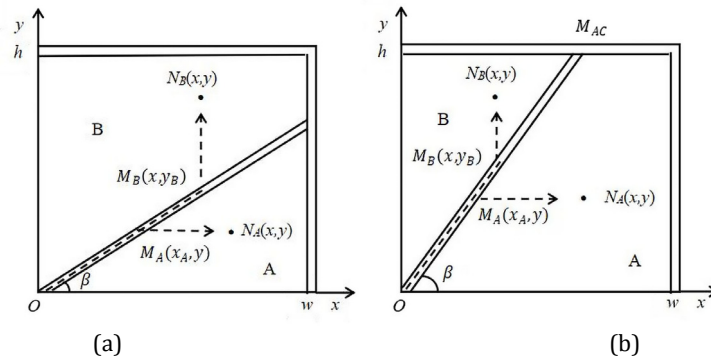


Fig. 7 Two sub-forms of straight Fishbone layout

Picking distance for straight Flying-V

In the following passage, $D_{SFV}^{A1}(x, y)$ and $D_{SFV}^{B1}(x, y)$ respectively represent the basic picking distances of A and B sub-regions in sub-form 1; $D_{SFV}^{A2}(x, y)$, $D_{SFV}^{B2}(x, y)$ and $D_{SFV}^{C2}(x, y)$ represent the basic picking distances of A, B and C sub-regions in sub-form 2, respectively.

$$D_{SFV}^{A1}(x, y) = \min \{ D_{SFV}^{A1_1}(x, y), D_{SFV}^{A1_2}(x, y) \} \quad (36)$$

$$D_{SFV}^{A1_1}(x, y) = \frac{x}{\cos \alpha} + x \tan \alpha - y \quad (37)$$

$$D_{SFV}^{A1_2}(x, y) = x + y \quad (38)$$

$$D_{SFV}^{B1}(x, y) = \frac{x}{\cos \alpha} + y - x \tan \alpha \quad (39)$$

$$D_{SFV}^{A2}(x, y) = \min \{ D_{SFV}^{A2_1}(x, y), D_{SFV}^{A2_2}(x, y) \} \quad (40)$$

$$D_{SFV}^{A2_1}(x, y) = \frac{x}{\cos \alpha} + x \tan \alpha - y \quad (41)$$

$$D_{SFV}^{A2_2}(x, y) = x + y \quad (42)$$

$$D_{SFV}^{B2}(x, y) = \frac{x}{\cos \alpha} + y - x \tan \alpha \quad (43)$$

$$D_{SFV}^{C2}(x, y) = \min \{ D_{SFV}^{C2_1}(x, y), D_{SFV}^{C2_2}(x, y) \} \quad (44)$$

$$D_{SFV}^{C2_1}(x, y) = \sqrt{\left(\frac{h}{\tan \alpha}\right)^2 + h^2} + \left(x - \frac{h}{\tan \alpha}\right) + (h - y) \quad (45)$$

$$D_{SFV}^{C2_2}(x, y) = x + y \quad (46)$$

Based on the assumption of continuous modelling, the optimal average total picking distance of straight Flying-V is E_{SFV}^* shown in Eq. 47.

$$E_{SFV}^* = \min \{ \min(E_{SFV}^1), \min(E_{SFV}^2) \} \quad (47)$$

$$E_{SFV}^1 = \frac{1}{wh} \left(\int_0^w \int_0^{x \tan \alpha} D_{SFV}^{A1}(x, y) dy dx + \int_0^w \int_{x \tan \alpha}^h D_{SFV}^{B1}(x, y) dy dx \right) \quad (48)$$

$$E_{SFV}^2 = \frac{1}{wh} \left(\int_0^{\frac{h}{\tan \alpha}} \int_0^{x \tan \alpha} D_{SFV}^{A2}(x, y) dy dx + \int_0^{\frac{h}{\tan \alpha}} \int_{x \tan \alpha}^h D_{SFV}^{B2}(x, y) dy dx + \int_{\frac{h}{\tan \alpha}}^w \int_0^h D_{SFV}^{C2}(x, y) dy dx \right) \quad (49)$$

Picking distance for straight fishbone

From Figure 7, we know that the basic picking distance formula of A and B sub-regions in the two sub-forms of straight-line Fishbone layout are the same respectively. So, we can use $D_{SFV}^A(x, y)$ and $D_{SFV}^B(x, y)$ to express the basic picking distance formulas of A and B picking area respectively.

$$D_{SFV}^A(x, y) = \frac{y}{\sin \beta} + x - y \cot \beta \quad (50)$$

$$D_{SFVB}^B(x, y) = \frac{x}{\cos \beta} + y - x \tan \beta \tag{51}$$

Based on the continuous modelling assumption mentioned above, the optimal average total picking distance of straight-line Fishbone layout E_{SFVB}^* can be obtained by the double integral of the above basic picking distance formulas.

$$E_{SFVB}^* = \min\{\min(E_{SFVB}^1), \min(E_{SFVB}^2)\} \tag{52}$$

$$E_{SFVB}^1 = \frac{1}{wh} \left(\int_0^w \int_0^{x \tan \beta} D_{SFVB}^A(x, y) dy dx + \int_0^w \int_{x \tan \beta}^h D_{SFVB}^B(x, y) dy dx \right) \tag{53}$$

$$E_{SFVB}^2 = \frac{1}{wh} \left(\int_0^h \int_{\frac{y}{\tan \beta}}^w D_{SFVB}^A(x, y) dy dx + \int_0^h \int_0^{\frac{y}{\tan \beta}} D_{SFVB}^B(x, y) dy dx \right) \tag{54}$$

4.2 Main aisle length for straight layout

From Fig. 6 and Fig. 7, the optimal inclined cross-aisle lengths T_{SFVB} and T_{SFVB} of straight Flying-V and Fishbone are Eq. 55 and Eq. 56 respectively.

$$T_{SFVB} = \begin{cases} \frac{h}{\sin \alpha^*}, & \alpha^* > \arctan(h/w) \\ \frac{w}{\cos \alpha^*}, & \alpha^* \leq \arctan(h/w) \end{cases} \tag{55}$$

$$T_{SFVB} = \begin{cases} \frac{h}{\sin \beta^*}, & \beta^* > \arctan(h/w) \\ \frac{w}{\cos \beta^*}, & \beta^* \leq \arctan(h/w) \end{cases} \tag{56}$$

5. Model solving

Since the double integral of the average total picking distance models established in this paper are all extremely difficult to obtain the analytical expressions, the analytical optimization analysis process which has been successfully used in aisle angle optimization by Öztürkoğlu *et al.* couldn't be carried out [9]. In order to solve this problem and to ensure the reliability of the results, we decided to adopt the Interval Numerical Simulation Method (INSM) and the Genetic Algorithms (GA) respectively to solve this model. INSM which has been successfully applied by Zhang Zhiyong *et al.* [19]. GA is widely used to solve this type of model. Both methods require differential discretization of the model first.

5.1 Differential discrete processing

According to the general principle of differential discretization, w and h of the right half warehouse are discretized by m and n meshes respectively. (x_i, y_j) is used to represent the coordinates of the central points of each grid block.

$$\left. \begin{aligned} x_i &= \frac{w}{m} \times (i - 0.5) \quad i = 1, 2, \dots, m \\ y_j &= \frac{h}{n} \times (j - 0.5) \quad j = 1, 2, \dots, n \end{aligned} \right\} \tag{57}$$

In order to calculate and interpret the results directly and conveniently, the pallet can be understood as a square with a side length of 1, and the length and width of the warehouse can be set as an integral multiple of the side length of the square pallet. See Eq. 58. It is worth pointing out that this setting will not affect the conclusions of relevant analysis.

$$\frac{w}{m} = \frac{h}{n} = 1 \tag{58}$$

5.2 Interval numerical simulation method

Based on the above discretization results, INSM could be carried out. It should be noted that the parameters a and b of parabolic trajectory equation have a non-closed theoretical range, and they also have a certain compensation effect on the layout efficiency of warehouse aisles with each other. The so-called mutual compensation effect of parabolic aisle trajectory parameters means that when one parameter value is fixed and unchanged, the layout efficiency will change

regularly with the change of another parameter value. Therefore, reasonable determination of bounded numerical simulation interval fixing method for a and b needs to be specially dealt with in conjunction with specific problems. After a lot of trial calculations and analysis, the simulation-based optimization intervals selected for the 100 warehouses in this paper are: $a \in [0, 2], b \in [0.1, 100]$.

5.3 Genetic algorithms

The specific parameters of applying Genetic Algorithms (GA) to solve the model in this paper are as follows:

The individual coded with natural numbers. The individual consisted of a and b . The value ranges are: $a \in [0, 2], b \in [0.1, 100]$, same as the optimization interval selected in INSM above. The size of the population is 200. The fitness function by taking the inverse of the objective function (Eq. 59).

$$F1 = \frac{1}{E_{PFV}^*}; F2 = \frac{1}{E_{SFV}^*}; F3 = \frac{1}{E_{PFB}^*}; F4 = \frac{1}{E_{SFB}^*} \tag{59}$$

According to the adaptive priority determined by the weighted roulette method, individuals with higher fitness values have a higher probability of contributing to the next generation for one or more offspring [26]. Once individuals were selected, they were subjected to a two-point crossover operation. After a lot of trial calculations and analysis, the crossover probability is 0.8 in this paper. The single point mutation method has been adopted. After a lot of trial calculations and analysis, the mutation probability is 0.1. The maximum number of generations is 200 in this paper.

6. Results and analysis

6.1 Efficiency analysis indicators

As a reference, we also calculated the minimum total picking distance of the 100 sample warehouses using the traditional orthogonal straight aisle layout and the ideal direct flight operation: EC^* and EZ^* . They are regarded as the upper and lower bounds of the total picking distance of various non-traditional layout, respectively, as shown in Eq. 60 and Eq. 61.

$$EC^* = \sum_{i=1}^m \sum_{j=1}^n (x_i + y_j) \tag{60}$$

$$EZ^* = \sum_{i=1}^m \sum_{j=1}^n \sqrt{(x_i^2 + y_j^2)} \tag{61}$$

Other efficiency analysis indicators are:

$$\left. \begin{aligned} EB_{PFV} &= \frac{E_{PFV}^*}{EC^*} \times 100 \\ EB_{SFV} &= \frac{E_{SFV}^*}{EC^*} \times 100 \\ EZB &= \frac{EZ^*}{EC^*} \times 100 \end{aligned} \right\} \tag{62}$$

$$\left. \begin{aligned} TS_{PFV} &= EB_{PFV} - EZB \\ TS_{SFV} &= EB_{SFV} - EZB \end{aligned} \right\} \text{(The theoretical possible improvement space of} \tag{63}$$

parabolic Flying-V and straight Flying-V)

$$TGB_{FV} = \frac{(T_{SFV} - T_{PFV})}{T_{SFV}} \times 100 \tag{64}$$

$$\left. \begin{aligned} EB_{PFB} &= \frac{E_{PFB}^*}{EC^*} \times 100 \\ EB_{SFB} &= \frac{E_{SFB}^*}{EC^*} \times 100 \end{aligned} \right\} \tag{65}$$

$$\left. \begin{aligned} TS_{PFB} &= EB_{PFB} - EZB \\ TS_{SFB} &= EB_{SFB} - EZB \end{aligned} \right\} \text{(The theoretical possible improvement space of} \tag{66}$$

parabolic Fishbone and straight Fishbone)

$$TGB_{FB} = \frac{(T_{SFB} - T_{PFB})}{T_{SFB}} \times 100 \quad (67)$$

6.2 Numerical results

With the help of MATLAB tools, the minimum total picking distance and the length of cross-aisle of 100 warehouses with lengths and widths ranging from 10 to 100 (interval 10) were analysed and solved. The data range covers the size of conventional warehouses, and the results are representative. If we ignore the calculated error, the results of INSM and GA are basically consistent with each other. Among them, the percentage values of picking distance of two kinds of straight-line layout and direct-flying operation of square warehouse are about 85.29, 80.47 and 76.52 respectively, which are basically consistent with the results of the relevant references [4, 7]. This shows that the accuracy of the calculation results in this paper is satisfactory. We draw Figs. 8 to 13 with the data.

6.3 Characteristics of parabolic Flying-V

Parabolic Flying-V layout has three characteristics compared with straight Flying-V layout in rectangular warehouses with unit-load.

- Semi-square warehouses ($w/h = 1$). The total picking distance can be reduced by about 0.35-0.37 %, and the theoretical possible improvement space has been compressed by about 3.38-3.57 %. The picking efficiency is improved slightly. The length of the cross-aisle could be shortened by 2.01-2.62 %. The area utilization rate is slightly improved.
- Semi-flat warehouses ($w/h > 1$). The total picking distance can be reduced by about 0.38-0.62 %, the theoretical possible improvement space has been compressed by 3.66-12.26 %. The picking efficiency is improved obviously, and the change rule is roughly gradually greater, the flatter the warehouse, the bigger the value. The length of the cross-aisle could be shortened by 1.92-0.03 %, and the change rule is roughly gradually smaller, the flatter the warehouse, the smaller the value. That is to say, the more significant the picking efficiency improved, the less the warehouse area utilization rate increased.
- Semi-thin and tall warehouses ($w/h < 1$). Only when ($2/3 \leq w/h < 1$), the total picking distance could be reduced by about 0.22-0.31 %, the theoretical possible improvement space has been compressed by 2.42-3.12 %, and the picking efficiency is improved slightly. The length of cross-aisle could be shortened by 2.38-3.10 %, and the area utilization rate is also improved slightly. For other warehouses with $w/h < 2/3$ (ignoring 7/10 outliers), straight Flying-V layouts are better.

6.4 Characteristics of parabolic fishbone

Parabolic Fishbone layout also has three characteristics compared with straight-line Fishbone layout in rectangular warehouses with unit-load.

- Semi-square warehouses ($w/h = 1$). The optimal parabola Fishbone degenerates to the optimal straight Fishbone. That is to say, the straight Fishbone layout is better. It is not difficult to understand that this feature is determined by the symmetrical distribution of the aisles in Fishbone layout.
- Semi-flat warehouses ($w/h > 1$). Only when $w/h \geq 3$ (ignoring calculation error), the total picking distance could be reduced by about 0.02-0.04 %, the theoretical possible improvement space has been compressed by about 1.27-1.83 %, and the picking efficiency is improved slightly. However, its length of the cross-aisle will increase by 4.63-19.50 %, which means the reduction of the utilization rate of warehouse area. For other warehouses with $1 < w/h < 3$ (ignoring calculation error), straight Fishbone layouts are better.

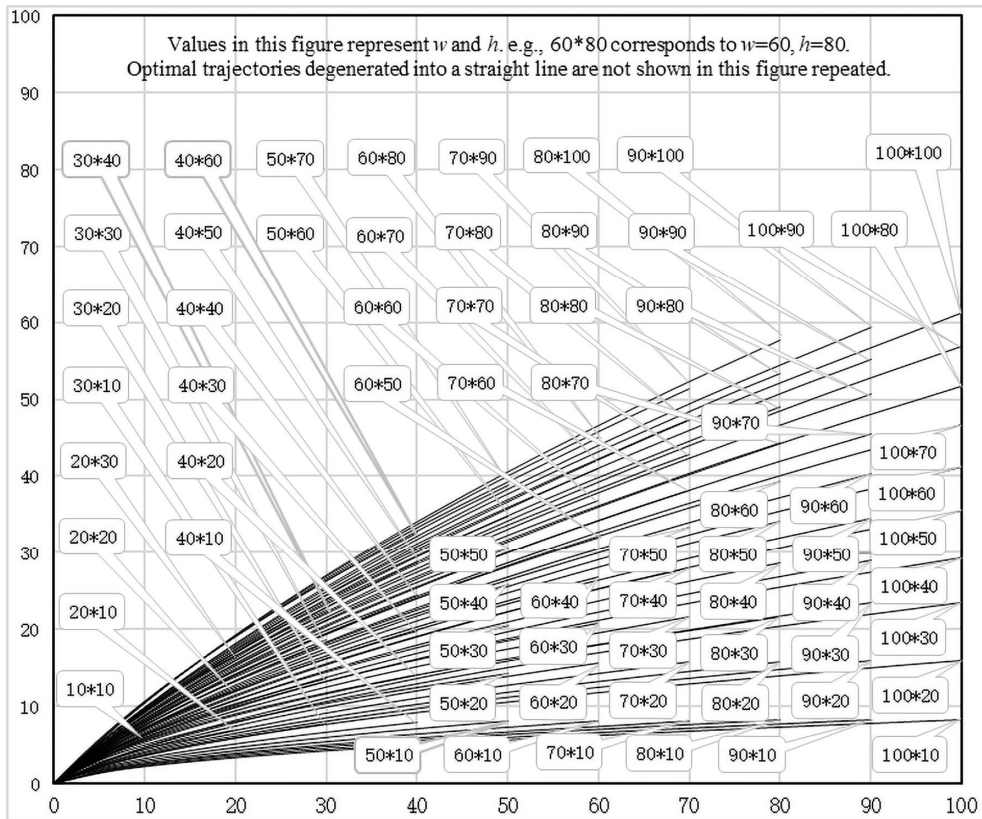


Fig. 8 Optimal main aisle trajectory map of parabolic Flying-V of 100 warehouses

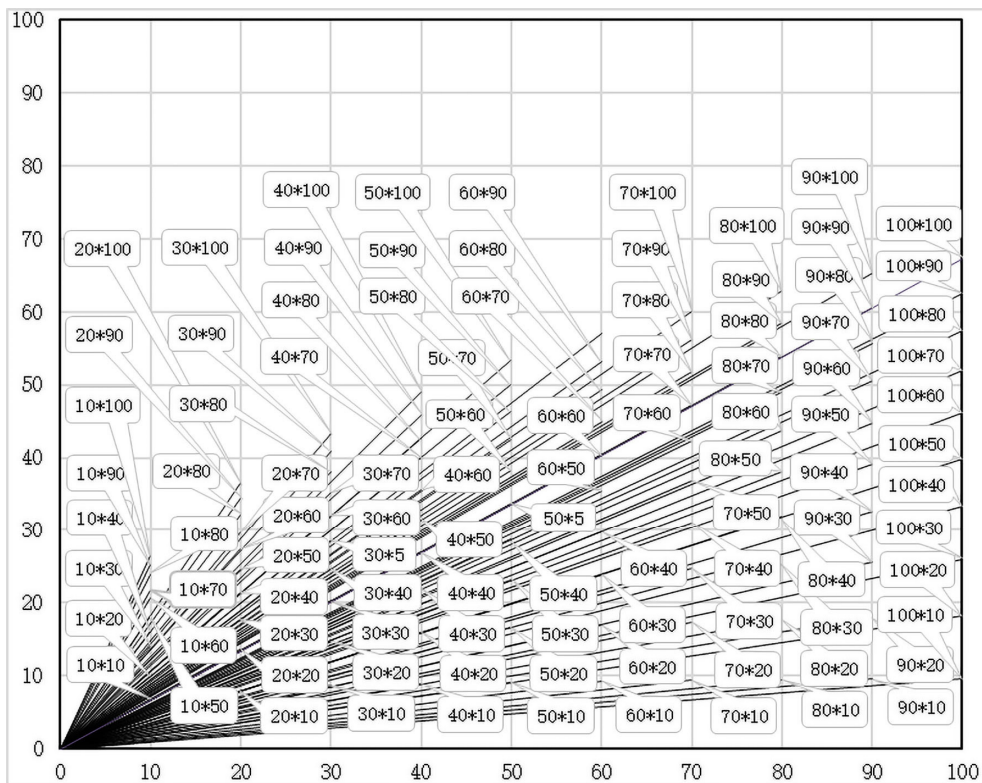


Fig. 9 Optimal main aisle trajectory map of straight Flying-V of 100 warehouses

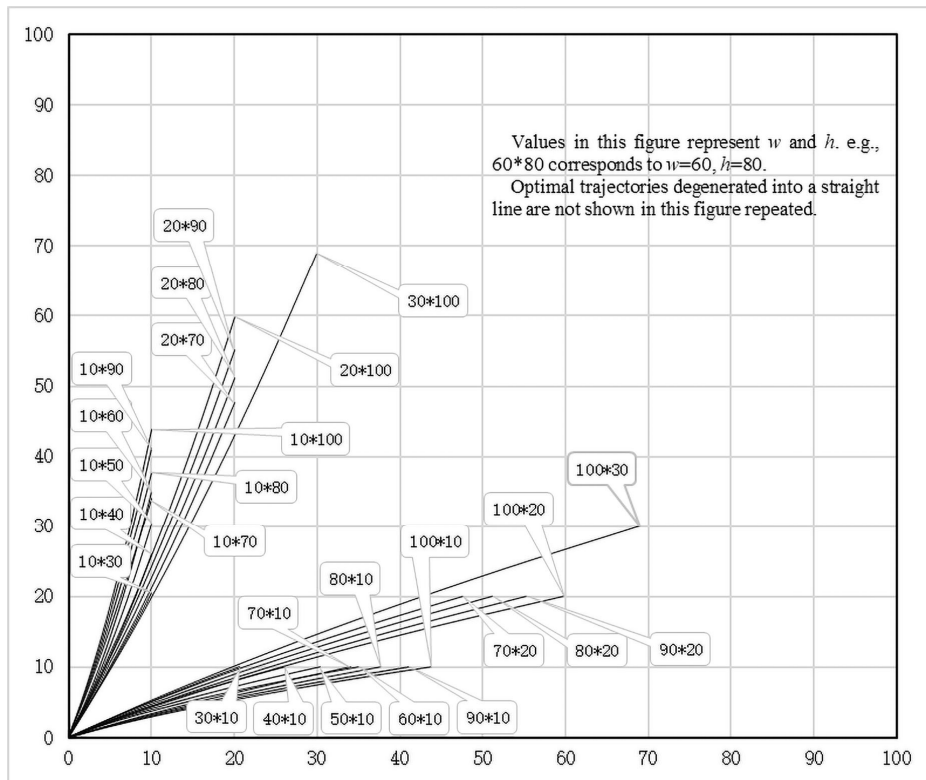


Fig. 10 Optimal main aisle trajectory map of parabolic Fishbone of 100 warehouses

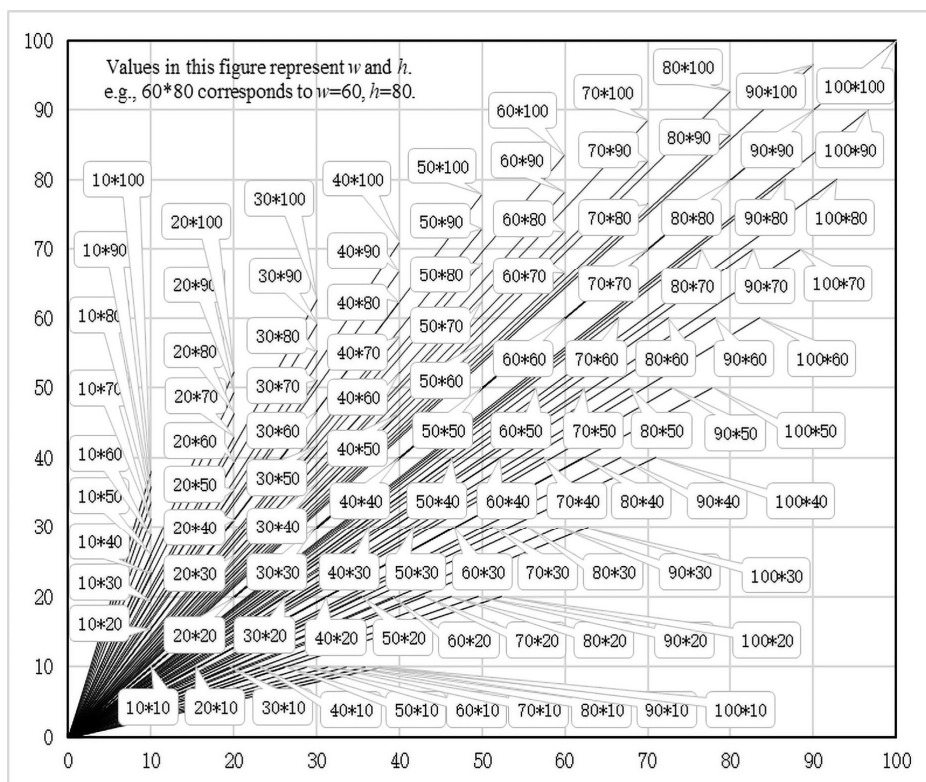


Fig. 11 Optimal main aisle trajectory map of straight Fishbone of 100 warehouses

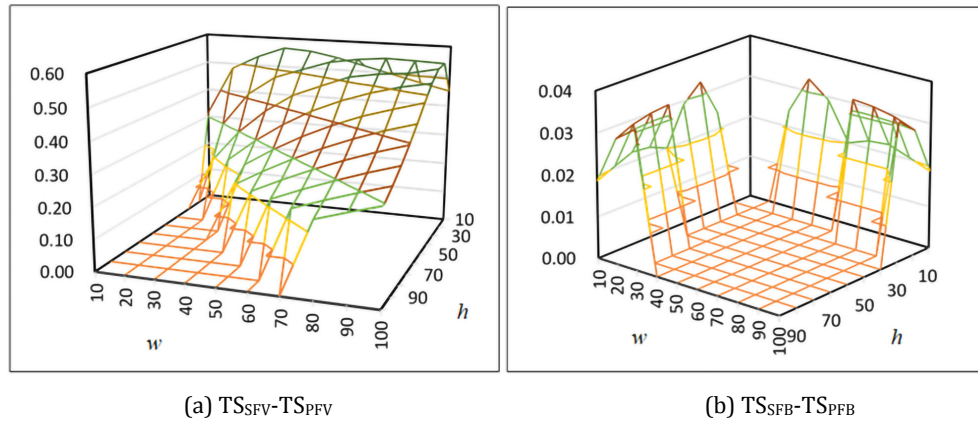


Fig. 12 Distribution diagrams of $TS_{SFV}-TS_{PFV}$ and $TS_{SFB}-TS_{PFB}$ and $TSSFB-TSPFB$ of 100 warehouses

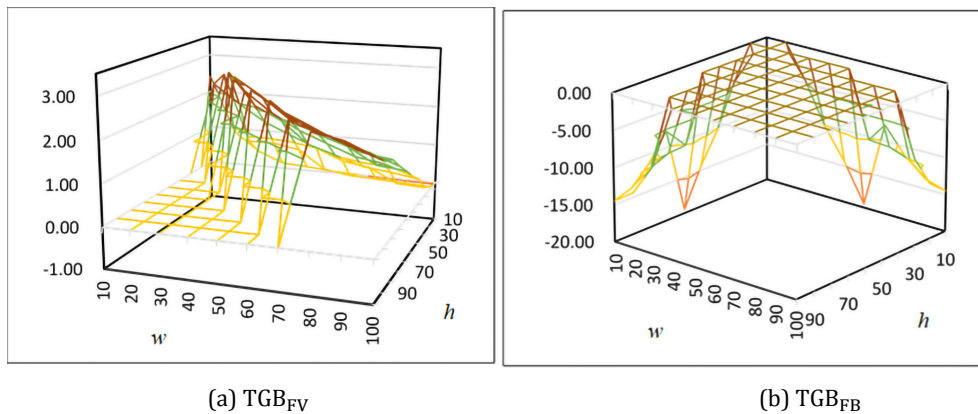


Fig. 13 Distribution diagrams of TGB_{FV} and TGB_{FB} of 100 warehouses

- Semi-thin and tall warehouses ($w/h < 1$). They have the same characteristics as the semi-flat warehouse. For Fishbone layout, thin and tall warehouses and flat warehouses with inverted aspect ratio are dual layouts. Let the optimal layout of the flat warehouse rotated 90 degrees counter clockwise with the P&D point as the centre first, and then turn 180 degrees around the longitudinal axis, the optimal layout of thin and tall warehouse with inverted width-height ratio can be obtained. The optimal parabolic trajectory equation of another warehouse can be obtained by interchanging x and y in the optimal parabolic trajectory equation of one warehouse.

7. Conclusion

Parabolic layout has its own characteristics and advantages. Although the non-closed theoretical range of parabolic trajectory equation parameters a and b and the mutual compensation effect in layout efficiency bring some technical difficulties to the related analysis, the parabolic transformation effect of two typical straight non-traditional layouts preliminarily verifies the scientificity and feasibility of the idea. This research enriches the relevant theory of warehouse aisle layout, and provides certain theoretical and technical basis for further tapping the efficiency potential of warehouse layout, breaking through the realistic situation of straight aisle leading warehouse layout.

Through the analysis of layout characteristics, the selection of parabolic type and the introduction of cross-aisle length index, the efficiency optimization models of two parabolic layouts under unit-load are constructed. The calculation results of 100 warehouses with different sizes show that the picking distance of parabolic Flying-V could be reduced by 0.22%-0.62% compared with the straight layout, and the theoretical possible improvement space has been compressed by 2.42-12.26 %. Its length of cross-aisle is shortened by -0.03 - 3.10 %. The picking

distance of parabolic Fishbone could be only reduced by 0.02-0.04 %. The theoretical possible improvement space has been compressed by 1.27-1.83 %. But its length of cross-aisle will increase by 4.63-19.50 % significantly.

The results contribute to the solution of manufacturing logistics problems, and the formation of green production mode. The objective of logistics solutions is to influence and manage material flows in the right way which is very important for manufacturing systems. The solution of manufacturing logistics problems in specific market area requires the utilization of the means of algorithmization, heuristics, mathematical statistics, modelling and computer simulation [27]. Green production mode is an advanced manufacturing mode. From the perspective of enterprises, reducing the operating cost of green manufacturing mode through scientific and technological innovation is a very good decision-making scheme for enterprises [28].

Future research directions include: based on the parabolic layout, combined with the actual needs of warehousing operation and management, putting forward more scientific and reasonable target of multi-attribute comprehensive measurement of efficiency; investigating the effects of task interleaving (dual-command), multiple P&D points, and different warehousing strategies; and further studying the warehouse design guidelines to enrich and perfect the layout principle of curve trajectory aisle [29]. Based on the analysis of efficiency mechanism, the practical design rules of the corresponding layout will be studied, which can provide reference for the formulation of non-linear warehouse layout design specifications. Also, many practical warehousing problems, such as the order assignment, the order batching and the picker routing of large wave picking warehouses which have been modelled by Ardjmand *et al.* [30], can be integrated with the non-linear warehouse layout. With the continuous development of social economic technology, intelligent control units have become the trend of manufacturing enterprises [31], we believe that the layout of non-rectangular complex special-shaped warehouses based on curve trajectory aisle could become an important research topic.

In addition, the proposed method in this paper may also be used in principle for the arrangement of machines and devices in a workshop. However, compared with the internal layout of a warehouse, the layout in a workshop is much more complex. For example, there are many big differences in sizes, shapes, site occupations, handling tools and process relations of different machines and devices. The specific processing technology relationship between machines and devices and materials and personnel must also be considered. Therefore, although the optimization methods can be used to finely study the workshop layout problem, the objectives and constraints of the corresponding mathematical model will be much more complex. However, we do believe that with the popularization of modern large-scale intelligent factories, the fine workshop layout using mathematical models and simulation optimization technology will become an important research direction.

Acknowledgement

The research is partly supported by the Key Project of National Social Science Foundation of China (grant no. 20AJY016). The authors gratefully acknowledge Professor Mincong Tang, the anonymous reviewers and some editorial board members for their valuable opinions and suggestions.

References

- [1] Thomas, L.M., Meller, R.D. (2015). Developing design guidelines for a case-picking warehouse, *International Journal of Production Economics*, Vol. 170, Part C, 741-762, [doi: 10.1016/j.ijpe.2015.02.011](https://doi.org/10.1016/j.ijpe.2015.02.011).
- [2] Ardjmand, E., Shakeri, H., Singh, M., Sanei Bajgiran, O. (2018). Minimizing order picking makespan with multiple pickers in a wave picking warehouse, *International Journal of Production Economics*, Vol. 206, 169-183, [doi: 10.1016/j.ijpe.2018.10.001](https://doi.org/10.1016/j.ijpe.2018.10.001).
- [3] Yuan, T. (2016). *Warehouse management*, Third edition, Machinery Industry Press, Beijing, China, [doi: cnpedu.com/books/book/2049485.htm](http://cnpedu.com/books/book/2049485.htm).
- [4] Gue, K.R., Meller, R.D. (2009). Aisle configurations for unit-load warehouses, *IIE Transactions*, Vol. 41, No. 3, 171-182, [doi: 10.1080/07408170802112726](https://doi.org/10.1080/07408170802112726).
- [5] Pohl, L.M., Meller, R.D., Gue, K.R. (2010). Optimizing fishbone aisles for dual-command operations in a warehouse, *Naval Research Logistics*, Vol. 56, No. 5, 389-403, [doi: 10.1002/nav.20355](https://doi.org/10.1002/nav.20355).

- [6] Pohl, L.M., Meller, R.D., Gue, K.R. (2011). Turnover-based storage in non-traditional unit-load warehouse designs, *IIE Transactions*, Vol. 43, No. 10, 703-720, doi: [10.1080/0740817X.2010.549098](https://doi.org/10.1080/0740817X.2010.549098).
- [7] Gue, K.R., Ivanović, G., Meller, R.D. (2012). A unit-load warehouse with multiple pickup and deposit points and non-traditional aisles, *Transportation Research, Part E: Logistics and Transportation Review*, Vol. 48, No. 4, 795-806, doi: [10.1016/j.tre.2012.01.002](https://doi.org/10.1016/j.tre.2012.01.002).
- [8] Cardona, L.F., Rivera, L., Martínez, H.J. (2012). Analytical study of the fishbone warehouse layout, *International Journal of Logistics Research and Applications*, Vol. 15, No. 6, 365-388, doi: [10.1080/13675567.2012.743981](https://doi.org/10.1080/13675567.2012.743981).
- [9] Öztürkoğlu, Ö., Gue, K.R., Meller, R.D. (2012). Optimal unit-load warehouse designs for single-command operations, *IIE Transactions*, Vol. 44, No. 6, 459-475, doi: [10.1080/0740817X.2011.636793](https://doi.org/10.1080/0740817X.2011.636793).
- [10] Clark, K.A., Meller, R.D. (2013). Incorporating vertical travel into non-traditional cross aisles for unit-load warehouse designs, *IIE Transactions*, Vol. 45, No. 12, 1322-1331, doi: [10.1080/0740817X.2012.724188](https://doi.org/10.1080/0740817X.2012.724188).
- [11] Jiang, M.X., Feng, D.Z., Zhao, Y.L., Yu, M.F. (2013). Optimization of logistics warehouse layout based on the improved Fishbone layout, *Systems Engineering – Theory & Practice*, Vol. 33, No. 11, 2920-2929, doi: [sys-engi.com/CN/Y2013/V33/I11/2920](https://doi.org/10.1016/j.se.2013.11.023).
- [12] Liu, Y.Q., Zhang, Y.H., Jiao, N. (2014). Slotting optimization allocation of storage based on fishbone, *Logistics Sci-Tech*, Vol. 37, No. 12, 66-70.
- [13] Öztürkoğlu, Ö., Gue, K.R., Meller, R.D. (2014). A constructive aisle design model for unit-load warehouses with multiple pickup and deposit points, *European Journal of Operational Research*, Vol. 236, No. 1, 382-394, doi: [10.1016/j.ejor.2013.12.023](https://doi.org/10.1016/j.ejor.2013.12.023).
- [14] Cardona, L.F., Soto, D.F., Rivera, L., Martínez, H.J. (2015). Detailed design of fishbone warehouse layouts with vertical travel, *International Journal of Production Economics*, Vol. 170, Part C, 825-837, doi: [10.1016/j.ijpe.2015.03.006](https://doi.org/10.1016/j.ijpe.2015.03.006).
- [15] Bortolini, M., Faccio, M., Gamberi, M., Manzini, R. (2015). Diagonal cross-aisles in unit load warehouses to increase handling performance, *International Journal of Production Economics*, Vol. 170, Part C, 838-849, doi: [10.1016/j.ijpe.2015.07.009](https://doi.org/10.1016/j.ijpe.2015.07.009).
- [16] Liu, Q., Yang, P.H., Liu, R.Q., Yang, Y.Y. (2016). Optimization model of warehouse layout and determination of optimal angle based on genetic algorithms, *Journal of Hebei North University (Natural Science Edition)*, Vol. 32, No. 3, 21-27, doi: [j.issn.1673-1492.2016.03.006](https://doi.org/10.1016/j.jhebu.2016.03.006).
- [17] Mesa, A. (2016). *A methodology to incorporate multiple cross aisles in a non-traditional warehouse layout*, Master's thesis, Ohio University, from http://rave.ohiolink.edu/etdc/view?acc_num=ohiou1480669754531612, accessed June 1, 2021.
- [18] Mowrey, C.H., Parikh, P.J., Gue, K.R. (2018). A model to optimize rack layout in a retail store, *European Journal of Operational Research*, Vol. 271, No. 3, 1100-1112, doi: [10.1016/j.ejor.2018.05.062](https://doi.org/10.1016/j.ejor.2018.05.062).
- [19] Zhang, Z.Y., Wang, Q., Liang, Y. (2019). Twin leaf method for warehouse internal layout and its aisles angle optimization, *Systems Engineering*, Vol. 37, No. 2, 70-80, from <http://www.cnki.com.cn/Article/CJFDTotal-GCXT201902007.htm>, accessed June 1, 2021.
- [20] Moder, J.J., Thornton, H.M. (1965). Quantitative analysis of the factors affecting floor space utilization of palletized storage, *Journal of Industrial Engineering*, Vol. 16, No. 1, 8-18.
- [21] Francis, R.L. (1967). On some problems of rectangular warehouse design and layout, *Journal of Industrial Engineering*, Vol. 18, No. 10, 595-604.
- [22] Francis, R.L. (1967). Sufficient conditions for some optimum-property facility designs, *Operations Research*, Vol. 15, No. 3, 448-466, doi: [10.1287/opre.15.3.448](https://doi.org/10.1287/opre.15.3.448).
- [23] Berry, J.R. (1968). Elements of warehouse layout, *International Journal of Production Research*, Vol. 7, No. 2, 105-121, doi: [10.1080/00207546808929801](https://doi.org/10.1080/00207546808929801).
- [24] White, J.A. (1972). Optimum design of warehouses having radial aisles, *AIIE Transactions*, Vol. 4, No. 4, 333-336, doi: [10.1080/05695557208974871](https://doi.org/10.1080/05695557208974871).
- [25] Bassan, Y., Roll, Y., Rosenblatt, M.J. (1980). Internal layout design of a warehouse, *AIIE Transactions*, Vol. 12, No. 4, 317-322, doi: [10.1080/05695558008974523](https://doi.org/10.1080/05695558008974523).
- [26] Goldberg, D.E., Holland, J.H. (1988). Genetic algorithms and machine learning, *Machine Learning*, Vol. 3, 95-99, doi: [10.1023/A:1022602019183](https://doi.org/10.1023/A:1022602019183).
- [27] Straka, M., Khouri, S., Lenort, R., Besta, P. (2020). Improvement of logistics in manufacturing system by the use of simulation modelling: A real industrial case study, *Advances in Production Engineering & Management*, Vol. 15, No. 1, 18-30, doi: [10.14743/apem2020.1.346](https://doi.org/10.14743/apem2020.1.346).
- [28] Awaga, A.L., Xu, W., Liu, L., Zhang, Y. (2020). Evolutionary game of green manufacturing mode of enterprises under the influence of government reward and punishment, *Advances in Production Engineering & Management*, Vol. 15, No. 4, 416-430, doi: [10.14743/apem2020.4.375](https://doi.org/10.14743/apem2020.4.375).
- [29] Sebo, J., Busa Jr., J. (2020). Comparison of advanced methods for picking path optimization: Case study of dual-zone warehouse, *International Journal of Simulation Modelling*, Vol. 19, No. 3, 410-421, doi: [10.2507/IJSIMM19-3-521](https://doi.org/10.2507/IJSIMM19-3-521).
- [30] Burinskiene, A., Lorenc, A., Lerher, T. (2018). A simulation study for the sustainability and reduction of waste in warehouse logistics, *International Journal of Simulation Modelling*, Vol. 17, No. 3, 485-497, doi: [10.2507/IJSIMM17\(3\)446](https://doi.org/10.2507/IJSIMM17(3)446).
- [31] Li, H.-Y., Xu, W., Cui, Y., Wang, Z., Xiao, M., Sun, Z.-X. (2020). Preventive maintenance decision model of urban transportation system equipment based on multi-control units, *IEEE Access*, Vol. 8, 15851-15869, doi: [10.1109/ACCESS.2019.2961433](https://doi.org/10.1109/ACCESS.2019.2961433).

Optimization of disassembly line balancing using an improved multi-objective Genetic Algorithm

Wang, Y.J.^{a,*}, Wang, N.D.^a, Cheng, S.M.^a, Zhang, X.C.^a, Liu, H.Y.^a, Shi, J.L.^a, Ma, Q.Y.^a, Zhou, M.J.^a

^aSchool of Mechanical Engineering and Automation, Dalian Polytechnic University, P.R. China

ABSTRACT

Disassembly activities take place in various recovery operations including remanufacturing, recycling, and disposal. Product disassembly is an effective way to recycle waste products, and it is a necessary condition to make the product life cycle complete. According to the characteristics of the product disassembly line, based on minimizing the number of workstations and balancing the idle time in the station, the harmful index, the demand index, and the number of direction changes are proposed as new optimization objectives. So based on the analysis of the traditional genetic algorithm into the precocious phenomenon, this paper constructed the multi-objective relationship of the disassembly line balance problem. The disassembly line balance problem belongs to the NP-hard problem, and the intelligent optimization algorithm shows excellent performance in solving this problem. Considering the characteristics of the traditional method solving the multi-objective disassembly line balance problem that the solution result was single and could not meet many objectives of balance, a multi-objective improved genetic algorithm was proposed to solve the model. The algorithm speeds up the convergence speed of the algorithm. Based on the example of the basic disassembly task, by comparing with the existing single objective heuristic algorithm, the multi-objective improved genetic algorithm was verified to be effective and feasible, and it was applied to the actual disassembly example to obtain the balance optimization scheme. Two case studies are given: a disassembly process of the automobile engine and a disassembly of the computer components.

ARTICLE INFO

Keywords:
Assembly;
Disassembly;
Line balancing;
Multi-objective optimization;
Remanufacturing;
Product recovery;
Product life cycle;
NP-hard problem;
Improved genetic algorithm

***Corresponding author:**
wangyj@dlpu.edu.cn
(Wang, Y.J.)

Article history:
Received 13 May 2021
Revised 23 May 2021
Accepted 4 June 2021



Content from this work may be used under the terms of the Creative Commons Attribution 4.0 International License (CC BY 4.0). Any further distribution of this work must maintain attribution to the author(s) and the title of the work, journal citation and DOI.

1. Introduction

With the continuous development of science and technology, the demand for new products is increasing, and the number of waste products and components is increasing, which will inevitably cause pollution to the environment. In order to solve the shortage of resources and realize sustainable development, the enterprise must pay attention to the recycling and reuse of waste products. Disassembly is the basic action of product recycling, extracting useful parts and recycling harmful parts to achieve a circular economy and green manufacturing.

In recent years, more and more researchers have devoted themselves to the disassembly line balancing problem (DLBP). Gungor and Gupta [1] analyzed and described the DLBP problem and put forward the influencing factors. Avikal *et al.* [2] used heuristic algorithm to solve DLBP problem, but there are some limitations. Altekin and Akkan [3] used a linear programming method to optimize DLBP to achieve the purpose of a balanced disassembly line. The Genetic Algorithm was used to solve the disassembly line balancing problem and the optimal solution was obtained

in an effective time. Kailayci *et al.* adopted a simulated annealing algorithm, which had strong processing capacity and better local search capability than other algorithms. However, it took a long time and had a weak ability to obtain a globally optimal solution [4, 5]. Nikola *et al.* solved the DLBP problem under multi-objective conditions in actual production [6-10]. Ding *et al.* [11] proposed an ant colony algorithm based on Pareto to optimize the four objectives. Cao *et al.* solved disassembly line balancing problems with different algorithms [12-22].

By analyzing the above works of literature and methods, it is easy to see intelligent optimization algorithms such as Genetic Algorithm, which have excellent performance in solving multi-objective optimization problems.

Given the shortcomings of the above researches, an improved genetic algorithm for solving the disassembly line balancing problem was proposed, and its advantages for solving this kind of problem were analyzed and verified through specific problems and examples.

The paper is organized as follows. The mathematical model is summarized in Section 2. Optimization and analysis with multiple objectives are also described in this section. Section 3 is the presentation of the solution. The case analysis and discussion are reported in Section 4. Finally, the conclusions are reported in Section 5.

2. Mathematical models

2.1 Basic assumptions

There are many uncertainties in the actual disassembly process, and these uncertainties are bound to affect the production beat of the disassembly online operation. Considering the application scope of the model in practice, this paper ignores extreme phenomena in the process of building the U-shaped DLBP model, so the following assumptions are made.

- 1) The production beat is unchanged.
- 2) The disassembly resources are the same or similar in structure.
- 3) The resource is completely disassembled, and the operation stops after the disassembly to the last part.
- 4) All disassembly tasks are performed on the disassembly line with no missing parts during the operation.
- 5) Operator proficiency and experience are the same, that is, the disassembly time of each part does not vary from operator to operator
- 6) During the disassembly, the required parts are guaranteed to be intact, that is, the disassembly process can bring economic benefits.
- 7) The disassembly time of the parts is not affected by external factors such as product quality, and there is no dependence between the parts.
- 8) The disassembly process is carried out according to the disassembly task and cannot be disassembled.
- 9) Operating time is normally distributed $T_{ij} \sim N(\mu, \sigma^2)$.
- 10) The constraints are as follows.
 - a) The total operation time of each workstation shall not exceed the production beat.
 - b) The same disassembly operation shall not be carried out in two or more workstations.

2.2 Basic parameters

Assuming that each unassembled part is a disassembly task, the number of parts is n (also known as the number of disassembly tasks). T is the set of all the tasks, $T = \{1, 2, 3, \dots, n\}$. N is the number of workstations. CT is the production beat. The parameter t_k represents the sum of activity time of all disassembly tasks allocated on the workstation k .

2.3 Decision variables

The variable x_{ik} represents the relationship between task i and workstation k , $x_{ik} = 1$, otherwise $x_{ik} = 0$.

$$x_{ik} = \begin{cases} 1, & \text{task } i \text{ is assigned to workstation } k \\ 0, & \text{else} \end{cases}$$

The balanced optimization of the disassembly line should not only consider the balanced distribution of work tasks but also include the environment and resources. The products to be dismantled may contain harmful substances, such as heavy metals and chemical poisons, which should be given priority in the disassembly operation. The main purpose of disassembly is to recycle and use the spare parts with surplus value, and the valuable parts should be dismantled as soon as possible. To minimize the disassembly time of the product to be disassembled, the number of changes of disassembly orientation is also included in the optimization space to shorten the disassembly time.

In this paper, five objectives of disassembly line balancing are considered and optimized.

- 1) Minimum number of workstations.
- 2) Balance the free time of each workstation.
- 3) Disassemble high-demand components as soon as possible.
- 4) Disassemble hazardous parts as soon as possible.
- 5) The least change of direction for disassembling.

$$\min F_1 = k \tag{1}$$

$$\min F_2 = \sum_{k=1}^N (CT - t_k) \tag{2}$$

$$F = \sum_{i=1}^N (CT - t_k)^2 \tag{3}$$

$$\min F_3 = \sum_{k=1}^N (CT - t_k)^2 \tag{4}$$

$$\min F_5 = \sum_{i=1}^N in_{PS_i} \tag{5}$$

$$\min F_4 = \sum_{i=1}^N id_{PS_i} \tag{6}$$

where $n_{PS_i} = \begin{cases} 1 & \text{needed} \\ 0 & \text{else} \end{cases}$, $d_{PS_i} = \begin{cases} 1 & \text{harmful} \\ 0 & \text{else} \end{cases}$.

The direction indicators are introduced to evaluate the solution sequence. The smaller the value, the less the change of direction in the disassembly process, the better the solution will be. The following relation is used to represent each direction of the disassembly process relative to the parts and workstations.

$$f_{PS_i} = \begin{cases} -3 & - Z \text{ direction} \\ -2 & - Y \text{ direction} \\ -1 & - X \text{ direction} \\ 1 & + X \text{ direction} \\ 2 & + Y \text{ direction} \\ 3 & + Z \text{ direction} \end{cases} \tag{7}$$

The direction indicators are expressed in the form of decision variables.

$$\min F_5 = \sum_{i=1}^{N-1} F_i, F_i = \begin{cases} 1, & f_{PS_i} \neq f_{PS_{i+1}} \\ 0, & f_{PS_i} = f_{PS_{i+1}} \end{cases} \tag{8}$$

The multi-objective disassembly line balance is represented as the following model by the above balance objectives.

$$\min F = (F_3, F_4, F_5, F_6) \quad (9)$$

s.t.

$$\sum_{j=1}^n t_j / CT \leq N \leq n \quad (10)$$

$$\sum_{j=1}^n (x_{jk} \cdot t_j) \leq CT, \forall j \in (1, 2, \dots, N) \quad (11)$$

$$\sum_{j=1}^n (j \cdot x_{ja}) \leq \sum_{j=1}^n (j \cdot x_{jk_j}), \forall (a, k_j) = 1 \quad (12)$$

The objective function (Eq. 1) represents the minimum number of workstations. The objective function (Eq. 2) means to balance the free time of each workstation. The objective function (Eq. 5) represents the index value of disassembling parts with high demand first. The objective function (Eq. 6) represents the index value of priority disassembly of hazardous parts. The objective function (Eq. 8) represents the least change of direction for disassembling.

The constraint function (Eq. 10) means that the number of workstations should be no less than the number of theoretical workstations and no more than the number of disassembly tasks. The constraint function (Eq. 11) represents that the disassembly time in each workstation shall not exceed the production beat. The constraint function (Eq. 12) means the disassembly sequence must meet the disassembly priority relationship.

3. Presentation of solution and used genetic operations

Genetic Algorithm (GA) was proposed in 1967 by a scientific research team led by John Holland of the University of Michigan [23]. It is a natural evolution-based algorithm for intelligent optimization search based on the concept of biological evolution and the laws of biogenetics and natural selection. GA relies on the information exchange of the individuals in the community and population search, to encode the parameters of the solution as genes, and several genes constitute a chromosome, as an individual, many chromosomes experience generation genetic by crossover, selection and mutation operation, the search results gradually converge to the region where the optimal solution is located until the optimal solution is found. The advantage of GA in solving the problem of activity order optimization is that the optimal solution can be found without going through the space of all solutions, and the solution effect for the multi-objective optimization problem is significant.

3.1 Coding

Encoding methods include binary encoding, float-point encoding, real number encoding, and so on. Given the disassembly line activity tasks, by using a chromosome encoding rules based on activity order successively, n disassembly elements are arranged in a row, corresponding to a gene site, and according to the priority diagram of activity order, these disassembly elements are assigned to each workstation and are coded according to the sequence of processes in the workstation. The weighted time value of the process shall not be higher than the scheduled production rhythm in the workstation. Zero insertion [24] is used to represent the start (or end) position of the activity element of the current workstation. There are n activities and $k + 1$ zeros. The activity element between two adjacent zeros is the same workstation.

3.2 Initial population generation

The quality of the initial population has an obvious impact on the evolution process and the efficiency of the algorithm. In order to ensure the diversity of individuals and solutions in the initial population, the topological sorting random search is used to generate the initial population. The process is as follows.

- According to the diagram of activity priority order, the task i without pre-task is found in the complete set of tasks (population) and put into the new set T_1 , and the task i and its related sequences are deleted in the operation sequence diagram.
- Repeat the above operations until the task set the empty set, and finish the task assignment. The selected task is put into the corresponding gene position in each step, and the obtained sequence is the initial feasible disassembly sequence.

3.3 Decoding

The coding adopts a one-dimension group solution sequence based on the task, which cannot determine the individual's merits and demerits. The solution sequence needs to be allocated to each workstation [25, 26]. The operation is as follows.

- Start the first workstation $j = 1$.
- Initialize the current workstation time and remaining time.
- Find task i in the solution sequence. When the task time allocated exceeds the current remaining time, the assignment fails. Open a new workstation randomly and initialize the current workstation time and remaining time. Else assign task i to the current workstation, update the workstation time and remaining time, and cycle until permutation sequence.

By decoding each individual and inserting zeros between workstations, each workstation and task assignment in the population can be determined, and the visualization of the algorithm can be improved.

3.4 Fitness

Fitness function plays an important role in the evaluation of individuals in GA search evolution. Only the objective function can be used to optimize the system in the solution space. In the Genetic Algorithm space, the objective function is transformed into individual fitness according to certain rules, and the fitness value is evaluated to realize the judgment of the feasible solution in the solution space.

3.5 Genetic operators

Selection

Roulette is the most commonly used selection method. The sampling idea is that the probability of the selected individual inheriting the next generation is directly proportional to the fitness value. The higher the evaluation of the fitness function of the individual, the greater the probability of inheriting to the next generation. This is the probability p_{is} of an individual selected in function (13).

$$p_{is} = F_i / \sum_{j=1}^M F_j, i = 1 \sim M \quad (13)$$

Crossover

Crossover is an important way to form new individuals. Two chromosomes are selected from the selected population, and some genes are exchanged with specific rules to form new individuals after recombination [27].

Because the random crossover method in traditional methods often leads to a large number of repetitions and conflicts, results in infeasible solutions and affects the operational efficiency of the algorithm, this process uses two-point mapping crossover method, randomly determines two crossover points on the parent chromosome, sorts some genes between the two chromatids of the father generation and adopts partial mapping to save the genes on both sides of the crossover point and put them into a new individual, thus producing two new offspring individuals. Assuming that the third and fifth gene locus are randomly selected as the crossover points, the sequence {6, 3, 7}, {2, 4, 9} before the two crossover points in the parent generation can be preserved, and the sequence {8, 5, 1} between the two crossover points in the parent 2 is {1, 5, 8}. The specific process is shown in Fig. 1.

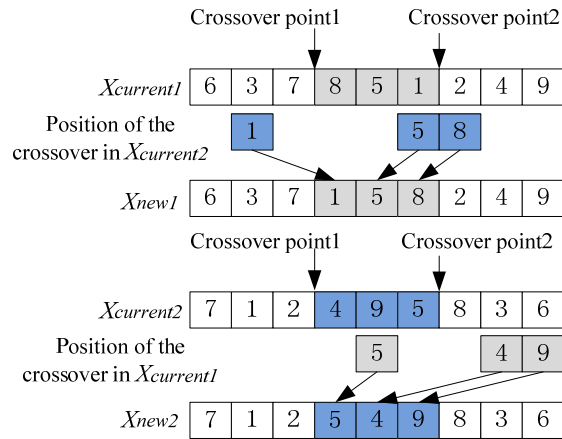


Fig. 1 The diagram of crossover

Mutation

Similar to the crossover operation, the mutation will produce infeasible solutions due to the constraints of the activity priority relationship. In this process, single-point variation is used. A mutation point (position 4 in Fig. 2) is randomly generated on the chromosome of the parent generation. According to the activity priority diagram, the pre-process and post-process of the mutation point are found out, so that the pre-process and its previous gene position, post-process and its subsequent gene position can be retained. Position 4 is randomly inserted into the nearest gene position between the pre-process and the post-process in the chromosome, and then the above genes are integrated to generate new progeny chromosomes. If the selected mutation position does not have an optional insertion position, the mutation point can be re-selected.

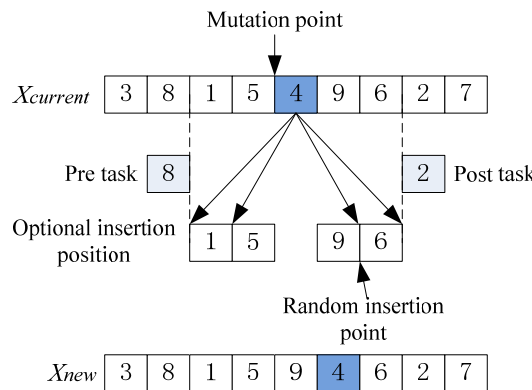


Fig. 2 The diagram of mutation

3.6 Termination conditions

As a search tool of repeated iterations, GA approximates the optimal value infinitely through multiple evolutionary cycles, instead of just calculating the optimal solution. Therefore, it is necessary to determine the termination condition and the generations of genetic iteration. At the beginning of the algorithm, the number of iterations should be set as small as possible, and then increases iterations as appropriate. When the number of iterations exceeds the required maximum number of generations the algorithm stops.

3.7 Implementation process

Although the individuals of the initial population are feasible, it is impossible to determine whether the optimal individuals appear in the early stage of the algorithm. Therefore, the probability of crossover and mutation can be increased to enhance the optimization ability of the algorithm. In the later stage of iteration, when the algorithm converges gradually, the individual fitness value becomes higher. In order not to destroy the excellence of genes in individuals, the probability of crossover and mutation is often reduced to improve the operation efficiency of the algorithm. In this paper, the adaptive crossover and mutation probability are used. The symbols used to run the algorithm are as follows: M is the maximum number of iterations, m is the number of iterations, P_c is the crossover probability. P_m is the mutation probability. P_{cmin} is the minimum crossover probability, P_{cmax} is the maximum probability. P_{mmin} is the minimum mutation probability. P_{mmax} is the maximum mutation probability.

$$P_c = P_{cmax} + \frac{P_{cmin} - P_{cmax}}{M} m \quad (14)$$

$$P_m = P_{mmax} + \frac{P_{mmin} - P_{mmax}}{M} m \quad (15)$$

Step1: Determination of parameters. Select the value of NP , P_c , P_m .

Step2: Initialization population. Order $t = 0$, the initial population $P(0)$ with NP individuals are generated under the condition of the beat constraint and the priority of tasks.

Step3: Fitness assessment. The fitness value of each individual in the T generation population is calculated.

Step4: Selection. $N(P)$ individuals are selected from the T generation population and cloned into the $T + 1$ generation.

Step5: Crossover.

Step6: Mutation.

Step7: Optimal preservation strategy.

Step8: Repeat. Order $t \leftarrow t + 1$, when the termination condition is met, it ends. Else, turn to Step3.

4. Case studies: The practical application and analysis

4.1 Disassembly of the computer components

The disassembly information of a computer component with 8 parts is shown in Table 1. The disassembly of the parts is shown in Fig. 3. The improved Genetic Algorithm is used to solve the problem.

Matlab R2012b software is used to realize the algorithm program on the windows10 system platform, and the above examples are solved [28]. The minimum number of workstations is 4, the hazard index H is 7, the demand is $D = 211$, the direction index is $R = 7$. The optimal solution is given in Table 2. Table 3 shows the optimal disassembly series solution and the workstation after balancing. Among them, disassembly tasks 1 and 5 are assigned to workstation 1, and workstation 2 is mainly responsible for disassembly tasks 3, 6, 2, and so on. In addition, the optimal solution removes high demand parts 3, 6, 2, and hazardous parts 7 earlier, allowing seven directions to change, and the calculation time of the algorithm is less than 1s. The equilibrium and hazard objectives of the solution obtained are the same as those in reference [29], while the demand index is better than that in reference [29], and there is one more direction index than reference [29]. Therefore, the overall performance of the solution obtained is better than that in reference [29].

The optimal solutions obtained by these two single objective algorithms are shown in Table 2, and the parameter design in reference [29] is combined with the DLBP problem. After repeated tests on the quality of the solution and the efficiency of the algorithm, the parameters in this paper are set as follows: $NP = 1$, $M = 100$, $P_{cmin} = 0.5$, $P_{cmax} = 0.95$, $P_{mmin} = 0.005$, $P_{mmax} = 0.01$. After calculation, the optimal value is obtained and the operation time is analyzed.

The optimal disassembly series solutions are shown in Table 3. Comparing the improved Genetic Algorithm with the traditional Genetic Algorithm, it can be seen that the test results are more prominent than the traditional algorithm in dealing with this problem, and the running time is shorter.

Table 1 The disassembly information for eight components

Disassembly tasks	Disassembly operation	Time	Demands	Harmful	Direction
1	Disassembly PC top cover (TC)	14	360	N	-x
2	Disassembly floppy disk driver (FD)	10	500	N	+x
3	Disassembly hard disk driver (HD)	12	620	N	-x
4	Disassembly bottom plate (BP)	18	480	N	-x
5	Disassembly PCI card	23	540	N	+y
6	Disassembly RAM modular	16	750	N	+z
7	Disassembly power supply (PU)	20	295	Y	-x
8	Disassembly mother board (MB)	14	360	N	-x

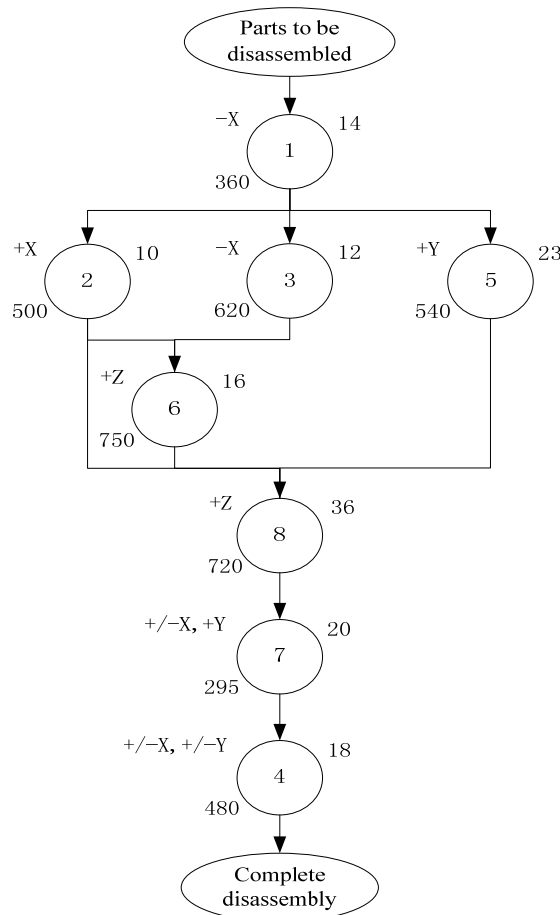


Fig. 3 The activity priority relationship of components

Table 2 The comparison of optimization results

Algorithm	Number of workstations S	Balance index	Demand quantity	Harmful index	Direction index
		F	D	H	R
Reference [29] GA	4	211	19275	7	-
Improved GA	4	211	19025	7	7

Table 3 The optimal disassembly series solution of DLBP

		Workstation <i>i</i>				
		S1	S2	S3	S4	
Disassembly series	1	14				Free time 0 s
	5	23				
	3		12			
	6		16			
	2		10			
	8			36		
	7				20	
	4				18	
Total time		37	38	36	38	
Idle time		3	2	4	2	

4.2 Disassembly of the automobile engine

Taking the automobile engine disassembly example in reference [30] as the research object, the engine is completely disassembled, and Fig. 4 shows the engine disassembly diagram. The original enterprise did not consider the damage and demand of disassembly, and the variability is poor, so it cannot adapt to the change of disassembly task in time. Now the improved Genetic Algorithm is used to improve the engine cylinder block disassembly line. The relevant data are shown in Table 4.

The bearing, toothed belt, belt, connection key, connection pin, and other parts in the assembly are simply removed and replaced with a group of assembly and fasteners to reduce the number of disassembly parts. In addition, the disassembly operation was investigated to obtain detailed disassembly data such as operation time, disassembly priority relationship, constraints, disassembly demands, hazards, and direction changes of each part. Standard operating time (SST) on line disassembly was measured. Standard operating time is the time taken by a skilled worker to complete a process at a normal speed under normal operation. The disassembly operation time is measured by the stopwatch method in industrial engineering, and the optimization goal is taken into account the damage of parts, demand, and the change of operation direction.

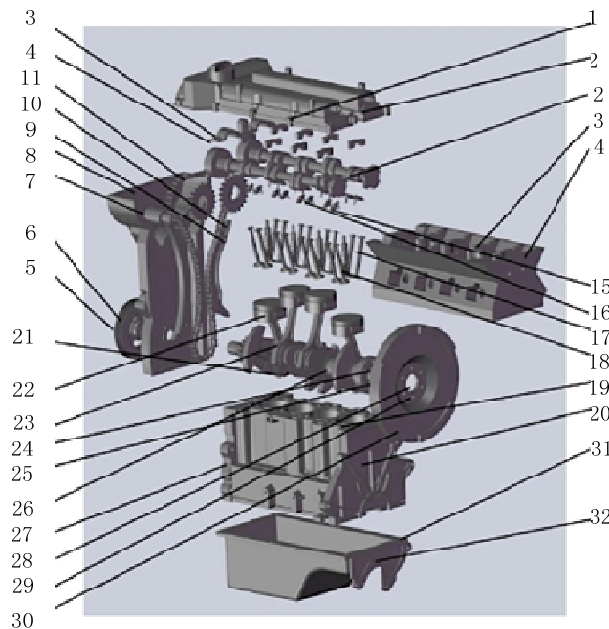


Fig. 4 The engine disassembly diagram

Table 4 The engine part elements

No.	Name	Time	Demand	Harmful	Direction
1	Camshaft coverscrew	5×12	5	N	+z
2	Camshaft cover	3	65	N	+z
3	Camshaft cover plate screw	4×20	15	N	+z
4	Camshaft cover plate	2×8	15	N	+z
5	Starting claw	6.5	35	N	+x
6	Pulley	20	40	N	+x
7	Side cylinder head screw	6.5	45	N	+x
8	Side cylinder head	5.5	65	N	+x
9	Chain restraint screw	4.5×4	8	N	+x
10	Chain restraint mechanism	3	8	N	+x
11	Chain	10	15	N	+z
12	Camshaft	3.2	60	N	+z
13	Cylinder head cover screw	4×8	70	N	+z
14	Top cylinder head cover	21	30	N	+z
15	Rocker fastening screw	8×16	45	N	+z
16	Rocker	3×16	95	N	+z
17	Valve	4×16	50	N	+z
18	spark plug	28×4	40	Y	+z
19	Cylinder block screw	5.5	40	N	+z
20	Cylinder Block	20	95	N	+z
21	Connecting rod cover	10×4	65	N	+z
22	Connecting rod	5×4	40	N	+z
23	Connecting rod screw	7×4	40	N	+z
24	Crankshaft bearing cover screw	5×10	25	N	+z
25	Crankshaft bearing cover	3×5	15	N	+z
26	Crankshaft	20	95	N	+z
27	Cylinder Black	23	30	N	+z
28	Flywheel nut	15	30	N	-x
29	Flywheel screw	5.5×6	45	N	-x
30	Flywheel	30	50	N	-x
31	Seat screw	5×12	65	N	+z
32	Seat	6	30	N	+z

Input the operation sequence matrix of the automobile engine of the disassembly line and program it on Matlab2012b. The given beat CT is 120s. The parameters of the algorithm are as follows: $NP = 50$, $MaxGen = 150$, $GAP = 0.9$. By optimizing multiple objective functions, the algorithm in this paper achieves the prediction results, jumps out of the local optimal solution to obtain a better solution, and the searchability is significantly improved. The optimization results are shown in Fig. 5.

The zeroing operation in encoding and decoding can isolate each workstation. After the operation, the balancing result of linear layout and U-shaped layout is shown in Fig. 6. The number of workstations in linear layout optimization is 15, while the number of U-shaped layouts is 9. Therefore, the U-shaped layout can minimize the number of workstations and has a certain economy.

The station allocation and operating time range volatility are shown in Table 5 and Table 6. The range volatility is the ratio of idle time to total operating time. All the data fluctuate within the 10 % range. It can be concluded that the assignment and optimization of work elements of both linear and U-shaped workstations in DLBP problem are reasonable, which proves the scientific and effectiveness of the model. The utilization rate of each workstation in the disassembly line under the U-shaped layout is higher than that of the traditional straight line, and the idle waiting time in the workstation is smaller, which shows a significant difference between the two types of disassembly lines. It is proved that the U-shaped layout is better and can achieve the balance effect.

The algorithms can find out a better solution, the number of workstations, balance index, resource index got better optimization, such as the direction indicators have improved, can achieve better solving the performance. The feasibility of the proposed improved genetic algorithm in solving the balance problem of a multi-objective U-shaped disassembly line is verified. The optimization results of straight layout and U-shaped layout are compared, and it is proved that U-shaped layout is more suitable for disassembly line layout.

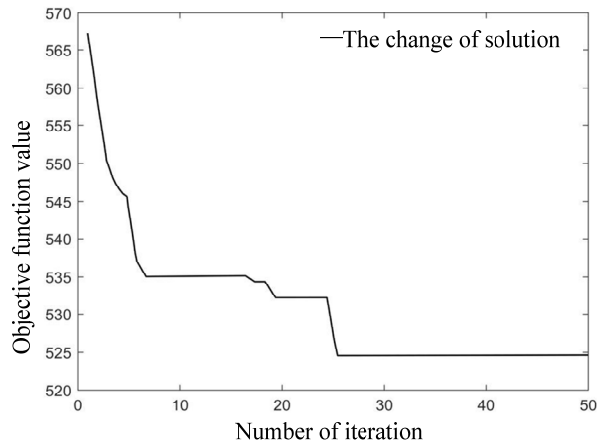
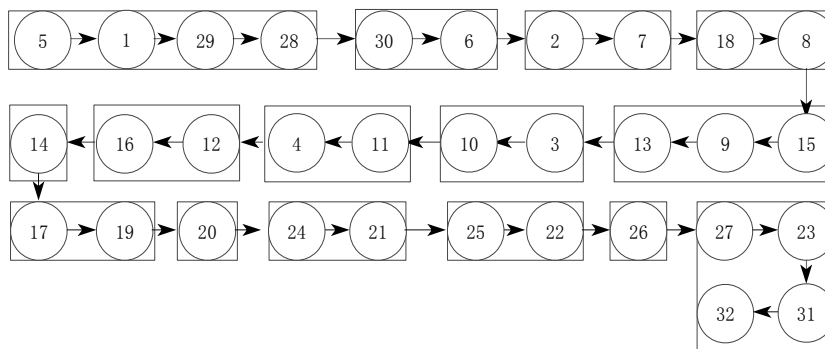
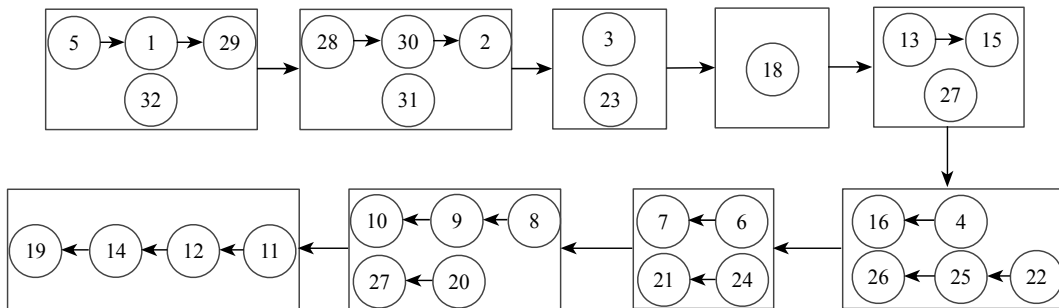


Fig. 5 The optimal results



(a) The balancing result of linear disassembly line layout



(b) The balancing result of U-shaped disassembly line layout

Fig. 6 The balancing results

Table 5 The workstation allocation of liner disassembly line layout

Workstation number	Station time (s)	Idle time (s)	Range fluctuation Range volatility (%)
1	114.5	5.5	0.56
2	59.5	60.5	6.13
3	117.5	2.5	0.25
4	72.5	47.5	4.85
5	109	11	1.11
6	114	6	0.61
7	119	1	0.10
8	110	10	1.01
9	55	65	6.58
10	117	3	0.3

Table 6 The workstation allocation of U-shaped disassembly line layout

Workstation number	Station time (s)	Idle time (s)	Range fluctuation (%)
1	105.5	14.5	1.47
2	108	12	1.21
3	108	12	1.21
4	112	8	0.81
5	119	1	0.10
6	119	1	0.10
7	116.5	3.5	0.35
8	11.35	6.5	0.66
9	89.2	30.8	3.12

5. Conclusion

In this study, an improved Genetic Algorithm is used to solve the disassembly line balancing problem. On the premise of ensuring balance, considering the influence of other targets on balance, such as hazard, demand, and disassembly direction index, adopting real coding strategy and topological ordering, the optimal solution of the problem is obtained by improving the crossover and mutation operation. The examples show that DLBP-GA is feasible to solve practical problems, has good adaptability to multi-objective optimization problems, and can better balance operating time and improve the utilization rate of the equipment. Compared with the traditional linear layout, the U-shaped disassembly line layout has more compact space, which can reduce the material handling and walking distance of personnel, and the operators can make faster adaptation to the changes of external demand, which is in line with the concept of flexible production. The U-shaped disassembly line is a line balance form that is more in line with the lean production theory, and the specific engine disassembly problem is solved.

In this paper, there are some directions for further research on the disassembly line, including the following contents. In the optimization goal, new optimization can be combined with cost, profit, scrap parts, and other issues. Other representative intelligent optimization algorithms can be selected for fusion, and the clustering optimization method based on Pareto can also be used for multi-objective optimization problems to increase the feasibility of the algorithm to search for the optimal solution. This paper mainly studies the balance of disassembly lines of a single variety, and the subsequent research can be extended to the study of mixed-flow disassembly lines of multiple varieties, and establish a disassembly line model based on complex random operation time. The optimization objective of this paper is to optimize the total number of workstations when the production beat is known. Subsequent researchers can consider optimizing the production beat and establishing a new disassembly line balance model under the premise of a certain number of workstations.

Acknowledgments

The research was funded by the National Natural Science Foundation of China (No.71603035), Natural Science Foundation of Liaoning province (LJKZ0532), and Natural Science Foundation of Liaoning province (No. J2020108).

References

- [1] Güngör, A., Gupta, S.M. (2002). Disassembly line in product recovery, *International Journal Production Research*, Vol. 40, No. 11, 2569-2589, doi: [10.1080/00207540210135622](https://doi.org/10.1080/00207540210135622).
- [2] Avikal, S., Mishra, P.K., Jain, R. (2014). A fuzzy AHP and PROMETHEE method-based heuristic for disassembly line balancing problems, *International Journal of Production Research*, Vol. 52, No. 5, 1306-1317, doi: [10.1080/00207543.2013.831999](https://doi.org/10.1080/00207543.2013.831999).
- [3] Altekin, F.T., Akkan, C. (2012). Task-failure-driven rebalancing of disassembly lines, *International Journal of Production Research*, Vol. 50, No. 18, 4955-4976, doi: [10.1080/00207543.2011.616915](https://doi.org/10.1080/00207543.2011.616915).
- [4] Kalayci, C.B., Gupta, S.M. (2011). A hybrid genetic algorithm approach for disassembly line balancing, In: *Proceedings of the 42nd Annual Meeting of Decision Science Institute*, Boston, Massachusetts, USA, 2142-2148.

- [5] Kalayci, C.B., Gupta, S.M., Nakashima, K. (2011). A simulated annealing algorithm for balancing a disassembly line, In: Matsumoto, M., Umeda, Y., Masui, K., Fukushige, S. (eds), *Design for innovative value towards a sustainable society*, Springer-Verlag, Berlin, Germany, 714-719, doi: [10.1007/978-94-007-3010-6_143](https://doi.org/10.1007/978-94-007-3010-6_143).
- [6] Wu, W., Liu, W., Zhang, F., Dixit, V. (2021). A new flexible parking reservation scheme for the morning commute under limited parking supplies, *Networks and Spatial Economics*, In press, 2021, doi: [10.1007/s11067-021-09538-5](https://doi.org/10.1007/s11067-021-09538-5).
- [7] Palakodati, S.S.S., Chirra, V.R., Dasari, Y., Bulla, S. (2020). Fresh and rotten fruits classification using CNN and transfer learning, *Revue d'Intelligence Artificielle*, Vol. 34, 617-622, doi: [10.18280/ria.340512](https://doi.org/10.18280/ria.340512).
- [8] Xiao, Y., Li, C., Song, L., Yang, J., Su, J. (2021). A multidimensional information fusion-based matching decision method for manufacturing service resource, *IEEE Access*, Vol. 9, 39839-39851, doi: [10.1109/ACCESS.2021.3063277](https://doi.org/10.1109/ACCESS.2021.3063277).
- [9] Pilati, F., Ferrari, E., Gamberi, M., Margelli, S. (2021). Multi-manned assembly line balancing: workforce synchronization for big data sets through simulated annealing, *Applied Science*, Vol. 11, No. 6, Article No. 2523, doi: [10.3390/app11062523](https://doi.org/10.3390/app11062523).
- [10] Chutima, P., Suchanun, T. (2019). Productivity improvement with parallel adjacent U-shaped assembly lines, *Advances in Production Engineering & Management*, Vol. 14, No. 1, 51-64, doi: [10.14743/apem2019.1.311](https://doi.org/10.14743/apem2019.1.311).
- [11] Ding, L., Tan, J., Feng, Y., Gao, Y. (2009). Multi-objective optimization for disassembly line balancing based on Pareto ant colony algorithm, *Computer Integrated Manufacturing System*, Vol. 15, 1406-1413, doi: [10.13196/j.cims.2009.07.160.dinglp.005](https://doi.org/10.13196/j.cims.2009.07.160.dinglp.005).
- [12] Cao, J., Xia, X., Wang, L., Zhang, Z., Liu, X. (2019). A novel multi-efficiency optimization method for disassembly line balancing problem, *Sustainability*, Vol. 11, No. 24, Article No. 6969, doi: [10.3390/su11246969](https://doi.org/10.3390/su11246969).
- [13] Özceylan, E., Kalayci, C.B., Güngör, A., Gupta, S.M. (2019). Disassembly line balancing problem: A review of the state of the art and future directions, *International Journal of Production Research*, Vol. 57, No. 15-16, 4805-4827, doi: [10.1080/00207543.2018.1428775](https://doi.org/10.1080/00207543.2018.1428775).
- [14] Deniz, D., Ozcelik, F. (2019). An extended review on disassembly line balancing with bibliometric & social network and future study realization analysis, *Journal of Cleaner Production*, Vol. 225, 697-715, doi: [10.1016/j.jclepro.2019.03.188](https://doi.org/10.1016/j.jclepro.2019.03.188).
- [15] Gupta, S.M., Erbis, E., McGovern, S.M. (2019). Disassembly sequencing problem: A case study of a cell phone. In: *Proceedings of Conference on Environmentally Conscious Manufacturing IV*, Philadelphia, Pennsylvania, USA, doi: [10.1117/12.577196](https://doi.org/10.1117/12.577196).
- [16] Xia, X., Liu, W., Zhang, Z., Wang, L., Cao, J., Liu, X. (2019). A balancing method of mixed-model disassembly line in a random working environment, *Sustainability*, Vol. 11, No. 8, Article No. 2304, doi: [10.3390/su11082304](https://doi.org/10.3390/su11082304).
- [17] Song, S., Zhang, W., Zhang, L. (2016). Product disassembly sequence planning based on improved artificial bee colony algorithm, *China Mechanical Engineering*, Vol. 27, No. 17, 2384-2390, doi: [10.3969/j.issn.1004-132X.2016.17.019](https://doi.org/10.3969/j.issn.1004-132X.2016.17.019).
- [18] Yu, B., Wu, E., Chen, C., Yang, Y., Yao, B.Z., Lin, Q. (2017). A general approach to optimize disassembly sequence planning based on disassembly network: A case study from automotive industry, *Advances in Production Engineering & Management*, Vol. 12, No. 4, 305-320, doi: [10.14743/apem2017.4.260](https://doi.org/10.14743/apem2017.4.260).
- [19] Lv, Y., Zhang, J., Qin, W. (2017). A genetic regulatory network-based sequencing method for mixed-model assembly lines, *Advances in Production Engineering & Management*, Vol. 12, No. 1, 62-74, doi: [10.14743/apem2017.1.240](https://doi.org/10.14743/apem2017.1.240).
- [20] Yang, M.S., Ba, L., Liu, Y., Zheng, H.Y., Yan, J.T., Gao, X.Q., Xiao, J.M. (2019). An improved genetic simulated annealing algorithm for stochastic two-sided assembly line balancing problem, *International Journal of Simulation Modelling*, Vol. 18, No. 1, 175-186, doi: [10.2507/IJSIMM18\(1\)CO4](https://doi.org/10.2507/IJSIMM18(1)CO4).
- [21] Wang, Y., Yang, O. (2017). Research on industrial assembly line balancing optimization based on genetic algorithm and witness simulation, *International Journal of Simulation Modelling*, Vol. 16, No. 2, 334-342, doi: [10.2507/IJSIMM16\(2\)CO8](https://doi.org/10.2507/IJSIMM16(2)CO8).
- [22] Suszyński, M., Żurek, J., Legutko, S. (2014). Modeling of assembly sequences using hypergraph and directed graph, *Tehnički Vjesnik – Technical Gazette*, Vol. 21, No. 6, 1229-1233.
- [23] Holland, J.H. (1975). *Adaptation in natural and artificial systems*, The University of Michigan Press, MIT Press, Michigan, USA, 28-35.
- [24] Su, Y., Zhang, Z., Hu, Y. (2016). A variable neighborhood search algorithm for disassembly line balancing problem, *Modern Manufacturing Engineering*, Vol. 10, 19-23, doi: [10.16731/j.cnki.1671-3133.2016.10.005](https://doi.org/10.16731/j.cnki.1671-3133.2016.10.005).
- [25] Zhang, J., Fang, J.B., Gao, L. (2015). Disassembly sequence planning based on quantum genetic algorithm, *Modern Manufacturing Engineering*, Vol. 4, 110-115, doi: [10.16731/j.cnki.1671-3133.2015.04.013](https://doi.org/10.16731/j.cnki.1671-3133.2015.04.013).
- [26] Seidi, M., Saghari, S. (2016). The balancing of disassembly line of automobile engine using genetic algorithm in fuzzy environment, *Industrial Engineering and Management Systems*, Vol. 15, No. 4, 364-373, doi: [10.7232/iems.2016.15.4.364](https://doi.org/10.7232/iems.2016.15.4.364).
- [27] Zhang, X.F., Wei, G., Guo, Y.R., Hu, Z.Y. (2014). Study on change response performance of disassembly model for design for disassembly, *Mechanical Design and Manufacturing*, Vol. 1, 251-253, doi: [10.19356/j.cnki.1001-3997.2014.01.077](https://doi.org/10.19356/j.cnki.1001-3997.2014.01.077).
- [28] Guo, H., Liang, J., Zhang, S. (2015). Optimization and examples in Matlab GA toolbox GADS, *Electronic Design Engineering*, Vol. 23, No. 10, 27-32, doi: [10.14022/j.cnki.dzsjgc.2015.10.009](https://doi.org/10.14022/j.cnki.dzsjgc.2015.10.009).
- [29] McGovern, S.M., Gupta, S.M. (2007). A balancing method and genetic algorithm for disassembly line balancing, *European Journal of Operational Research*, Vol. 179, No. 3, 692-708, doi: [10.1016/j.ejor.2005.03.055](https://doi.org/10.1016/j.ejor.2005.03.055).
- [30] Li, Y. (2015). *Automobile engine structure and disassembly*, Beijing Institute of Technology press, Beijing, China.

Modelling and optimization of sulfur addition during 70MnVS4 steelmaking: An industrial case study

Kovačič, M.^{a,b,c,*}, Lešer, B.^a, Brezocnik, M.^d

^aŠtore Steel, d.o.o., Štore, Slovenia

^bUniversity of Ljubljana, Faculty of Mechanical Engineering, Ljubljana, Slovenia

^cCollege of Industrial Engineering Celje, Celje, Slovenia

^dUniversity of Maribor, Faculty of Mechanical Engineering, Maribor, Slovenia

ABSTRACT

Štore Steel Ltd. is one of the major flat spring steel producers in Europe. Among several hundred steel grades, 70MnVS4 steel is also produced. In the paper optimization of steelmaking of 70MnVS4 steel is presented. 70MnVS4 is a high-strength microalloyed steel which is used for forging of connecting rods in the automotive industry. During 70MnVS4 ladle treatment, the sulfur addition in the melt should be conducted only once. For several reasons the sulfur is repeatedly added and therefore threatening clogging during continuous casting and as such influencing surface defects occurrence and steel cleanliness. Accordingly, the additional sulfur addition was predicted using linear regression and genetic programming. Following parameters were collected within the period from January 2018 to December 2018 (78 consequently cast batches): sulfur and carbon cored wire addition after chemical analysis after tapping, carbon, manganese and sulfur content after tapping, time between chemical analysis after tapping and starting of the casting, ferromanganese and ferrosilicon addition and additional sulfur cored wire addition. Based on modelling results it was found out that the ferromanganese is the most influential parameter. Accordingly, 12 consequently cast batches (from February 2019 to October 2019) were produced with as lower as possible addition of ferromanganese. The additional sulfur addition in all 12 cases was not needed. Also, the melt processing time, surface quality of rolled material and sulfur cored wire consumption did not change statistically significantly after reduction of ferromanganese addition. The steel cleanliness was statistically significantly better.

ARTICLE INFO

Keywords:

Metallurgy;
Steelmaking;
High-strength steel 70MnVS4;
Microalloyed steel;
Modelling;
Optimization;
Evolutionary algorithms;
Genetic programming;
Multiple linear regression

*Corresponding author:

miha.kovacic@store-steel.si
(Kovačič, M.)

Article history:

Received 3 April 2021
Revised 5 June 2021
Accepted 12 June 2021



Content from this work may be used under the terms of the Creative Commons Attribution 4.0 International Licence (CC BY 4.0). Any further distribution of this work must maintain attribution to the author(s) and the title of the work, journal citation and DOI.

1. Introduction

Producing melted steel is commonly called primary steelmaking (i.e., primary metallurgy). The melted steel (made from ore or scrap) can be additionally treated – typically in ladles. These essential processes in modern steelmaking are called ladle treatment or secondary steelmaking (i.e., secondary metallurgy). They are slag formation, deoxidation, alloying, inclusions modification, desulfurization, dephosphorization, analyses of chemical composition of steel and slag, heating (i.e., temperature adjustment), stirring, refining (i.e., melt purification), homogenization and degassing [1-3].

The addition of alloys is preferably conducted during secondary steelmaking. They can be added also during casting, into the tundish, using bulk material or as wired products. The dissolution of alloys in liquid steel is influenced by their physical and chemical properties, melt su-

perheat, location of addition and stirring. Most important are melting point and density which determine either the additive will float (and entrained in melt or slag) or sink during assimilation. Consequently, for efficient alloying following areas have been developing: scrap (input material) design [4-6], alloys design [7-10], and interactions with the liquid bath [11, 12].

The price of produced steel is mostly influenced by – beside the electric energy consumption – the added alloys which are at high temperatures and presence of oxygen prone to burning-off [13, 14]. Accordingly, the alloys consumption could be increased together with the need of adding the alloys several times threatening the production pace, melt homogenization, purification and further melt solidification (e.g. timing, temperature, clogging). The burn-off of alloys prediction is aggravated due to the diversity of steelmaking technologies and equipment.

In this study sulfur addition (i.e., sulfur burn-off) during 70MnVS4 steelmaking in Štore Steel Ltd. was modeled. During ladle treatment, instead of only one sulfur addition, the sulfur was repeatedly added several times threatening clogging during continuous casting and as such influencing surface defects occurrence and steel cleanliness. Accordingly, the additional sulfur addition was predicted using multiple linear regression and the genetic programming. The genetic programming has been used several times in Štore Steel Ltd. for modelling and optimization (e.g., [15-19]).

In the beginning of the paper the problem regarding repeatedly added sulfur is presented together with the steelmaking technology. Afterwards, the sulfur addition prediction using multiple linear regression and genetic programming is presented including the implementation of findings in the actual steelmaking process. At the end of the paper, the conclusions are drawn and future work is emphasized.

2. Materials, methods and execution of experiment

70MnVS4 is a high-strength microalloyed steel which is used for forging of connecting rods in the automotive industry. In Štore Steel Ltd., which is one of Europe's major flat spring steel producers, 70MnVS4 steel is produced from scrap that is melted using an electric arc furnace. After melting the first chemical composition analysis is conducted.

After reaching tapping temperature, the melt is discharged into the ladle. The ladle is transported to the ladle furnace. The average batch weighs 50 t. The slag is formed using dolomite, quartz and fluorite. The melting bath is deoxidized using ferromanganese and ferrosilicon. Also alloying using ferrovanadium and homogenization (i.e., argon stirring) are carried out. Then the second chemical composition analysis is conducted. Based on this analysis the sulfur is added for the first time using sulfur cored wire. The melt is homogenized again and also the third chemical composition is conducted. Based on the chemical composition slight adjustments of alloying elements can be made using ferrosilicon, ferromanganese and ferrovanadium. Also for several reasons, the sulfur cored wire should be added again. It is well known that the sulfur forms inclusions which cause clogging of tundish submerged entry nozzles during continuous casting and as such influencing surface defects occurrence and steel cleanliness. After chemical composition adjustments the fourth chemical composition analysis is performed.

The ladle is transported to the continuous caster. The melt pours into the tundish after the ladle sliding gate is opened, with continuous casting being established throughout a casting system with impact pod, stoppers, submerged entry nozzles and water-cooled copper molds. During casting also the final chemical composition is determined which is also stated on the inspection certificate. For casting of the 180 mm square billets, a two strand continuous caster with 9 m radius is used. The solidification is conducted throughout primary cooling in the mold and secondary cooling using water sprays. The billets are cooled down on turnover cooling bed.

The billets are reheated up to rolling temperature and rolled into round bars with a diameter of up to 50 mm. The same rolled bar surface is also examined using the automatic control line. The surface control is based on the flux leakage method, meaning that the surface of the material is locally magnetized and that deviations of magnetic flux (i.e., flux leakage) at the opened surface defects are detected. During surface control the data on number of examined bars, bars with defects and defects length are stored in the informational system.

Table 1 Parameters collected within the period from January 2018 to December 2018 for 78 consequently cast batches of 70MnVS6 steel

Batch	Carbon content after the second chemical composition analysis after tapping (C2), (%)	Manganese content after the second chemical composition analysis after tapping (MN2), (%)	Silicon content after the second chemical composition analysis after tapping (Si2), (%)	Sulfur content after the second chemical composition analysis after tapping (S2), (%)	Carbon cored wire addition after the second chemical composition analysis after tapping (CW2), (tn)	Sulphur cored wire addition after the second chemical composition analysis after tapping (SW2), (tn)	Time between the second chemical analysis after tapping and final chemical composition analysis at starting of the casting (T2F), (min)	Ferro-manganese (FEMN), (kg)	Ferrosilicon (FESi), (kg)	Additional sulfur cored wire addition (SWA), (tn)
76124	0.56	0.80	0.20	0.022	30	237	106	25	54	11
76487	0.54	0.74	0.15	0.019	80	223	103	75	44	80
76488	0.54	0.79	0.16	0.020	180	223	82	23	107	27
76516	0.61	0.76	0.14	0.023	50	250	82	54	79	0
76517	0.61	0.72	0.18	0.030	120	200	90	76	53	25
76518	0.59	0.74	0.20	0.028	80	180	95	64	117	25
76519	0.59	0.73	0.20	0.030	40	170	97	75	122	10
76520	0.61	0.78	0.23	0.023	40	200	83	32	90	0
76561	0.55	0.71	0.18	0.021	40	230	81	95	75	0
76668	0.58	0.79	0.18	0.026	50	215	84	27	34	0
76669	0.55	0.77	0.19	0.022	70	193	79	47	128	15
76670	0.57	0.80	0.18	0.024	0	193	80	23	133	0
76671	0.62	0.78	0.20	0.022	0	228	87	28	44	0
76672	0.60	0.79	0.22	0.024	120	187	73	29	79	30
76673	0.62	0.82	0.24	0.030	0	173	93	0	73	15
76674	0.63	0.79	0.24	0.024	20	220	101	21	0	14
76675	0.61	0.75	0.19	0.023	0	192	81	51	77	0
76676	0.60	0.77	0.20	0.018	30	200	89	41	73	10
76767	0.57	0.74	0.19	0.024	90	200	90	55	124	45
76768	0.56	0.76	0.20	0.021	0	210	24	59	97	60
77048	0.53	0.81	0.16	0.027	270	193	85	18	98	0
77049	0.57	0.84	0.19	0.021	0	197	83	0	88	27
77076	0.52	0.79	0.18	0.023	200	240	104	25	64	50
77077	0.56	0.76	0.19	0.018	80	220	82	56	130	0
77078	0.57	0.76	0.19	0.022	60	200	91	56	54	45
77082	0.54	0.77	0.20	0.018	40	243	87	45	44	0
77083	0.61	0.81	0.20	0.023	70	200	81	22	118	13
77085	0.60	0.77	0.20	0.019	90	237	97	42	33	0
77086	0.63	0.74	0.20	0.024	100	190	82	72	110	190
77161	0.58	0.79	0.17	0.020	0	227	107	25	46	0
77162	0.60	0.78	0.19	0.025	60	190	87	36	119	0
77409	0.61	0.73	0.19	0.012	80	190	98	84	51	28
77410	0.55	0.78	0.17	0.017	160	220	77	35	97	0
77411	0.56	0.76	0.17	0.023	70	207	87	44	91	38
77412	0.61	0.78	0.19	0.024	50	193	85	32	94	0
77413	0.54	0.81	0.19	0.018	200	237	92	16	45	0
77414	0.59	0.81	0.22	0.017	40	227	68	16	89	0
77415	0.54	0.80	0.20	0.023	0	218	76	16	81	0
77416	0.60	0.84	0.19	0.018	120	213	87	0	102	22
77501	0.58	0.76	0.20	0.030	0	197	90	58	54	12
77766	0.58	0.75	0.18	0.021	210	237	88	65	65	0
77767	0.60	0.78	0.17	0.025	200	190	87	32	117	0
77768	0.60	0.77	0.16	0.022	40	190	95	44	128	0
77769	0.63	0.78	0.18	0.027	40	185	84	34	104	0
77770	0.63	0.74	0.17	0.013	120	217	86	70	50	22
77771	0.60	0.77	0.17	0.022	160	200	87	44	119	27
77772	0.60	0.79	0.18	0.026	340	183	102	23	109	0
77773	0.61	0.78	0.18	0.018	80	215	113	35	107	0
77783	0.61	0.76	0.17	0.019	200	233	90	54	64	9
77784	0.61	0.73	0.17	0.025	80	190	91	88	129	0
77792	0.60	0.79	0.18	0.018	150	237	83	38	44	0
77978	0.69	0.78	0.17	0.019	0	227	88	36	62	32
77979	0.59	0.70	0.16	0.024	110	207	74	115	135	37
77980	0.56	0.74	0.18	0.027	130	175	106	77	116	27
77981	0.56	0.76	0.16	0.026	0	190	97	67	116	19
77982	0.54	0.71	0.15	0.029	30	190	93	104	63	30
77983	0.56	0.75	0.16	0.025	120	197	86	74	116	0
77984	0.55	0.71	0.16	0.030	180	180	83	106	117	8
78224	0.58	0.78	0.19	0.022	60	213	101	40	52	50
78225	0.66	0.81	0.19	0.013	0	227	90	22	123	63
78376	0.55	0.74	0.22	0.029	100	200	86	75	122	80
78420	0.53	0.73	0.15	0.014	100	227	95	95	64	12
78421	0.57	0.75	0.16	0.024	100	200	79	57	126	32
78681	0.63	0.74	0.17	0.020	50	237	89	73	65	17
78682	0.61	0.73	0.16	0.025	0	197	83	84	132	0
78683	0.67	0.79	0.18	0.029	0	182	92	33	107	7
78903	0.53	0.70	0.18	0.017	80	250	83	105	56	8
78904	0.59	0.77	0.21	0.022	40	224	91	52	113	30
78905	0.54	0.72	0.21	0.027	40	200	95	94	110	30
78906	0.57	0.73	0.21	0.026	120	210	90	83	114	24
78907	0.56	0.75	0.17	0.015	160	248	75	62	78	20
78908	0.56	0.75	0.18	0.018	90	237	94	63	120	20
78909	0.61	0.78	0.18	0.022	0	207	127	45	118	0
78910	0.66	0.80	0.18	0.025	80	200	92	19	103	20
79233	0.62	0.77	0.19	0.210	80	213	93	41	46	0
79234	0.62	0.70	0.15	0.035	0	150	90	113	132	0
79604	0.57	0.81	0.16	0.001	40	247	100	11	57	30
79605	0.59	0.76	0.17	0.022	40	232	105	52	107	32

The following parameters were collected within the period from January 2018 to December 2018 for 78 consequently cast batches of 70MnVS6 (Table 1):

- Carbon (C2), manganese (MN2), silicon (SI2) and sulfur (S2) content after the second chemical composition analysis after tapping in weight percentage (%). Carbon, manganese and sulfur are required according to technical delivery conditions. Manganese and silicon also help deoxidization. Manganese and sulfur form the manganese sulfide inclusions in the steel which improve machinability and enable cracking during connection rod production.
- Sulphur (SW2) and carbon (CW2) cored wire addition after the second chemical composition analysis after tapping in meters (m). Their addition depends on their actual content in the melt and also final chemical composition required by technical delivery conditions.
- Time between the second chemical analysis after tapping and final chemical composition analysis at starting of the casting (T2F) in minutes (min). This time is related with ladle treatment time – from tapping until continuous casting where based on slag formation, alloying, refining and homogenization the chemical reactions took place including sulfur burn-off.
- Ferromanganese (FEMN) and ferrosilicon (FESI) addition in kilograms (kg). Ferromanganese and ferrosilicon are used as deoxidizers and also alloys.
- Additional sulfur cored wire addition (SWA) in meters (m). Due to possibility of undesirable clogging of tundish submerged entry nozzles during continuous casting this additional sulfur cored wire addition should be minimized.

For the purpose of this research, we used two methodological approaches: a multiple linear regression method and the genetic programming method.

In multiple linear regression, the linear relationship between a scalar response (i.e., dependent output variable) and one or more explanatory variables is established (i.e., input variables) [19]. Conventional linear regression method is based on a deterministic approach. A multiple linear regression method is widely used technique in different engineering fields [20].

In contrast to linear regression, however, the genetic programming is a non-deterministic evolutionary optimization approach that mimics a biological evolution [21]. The genetic programming is similar to a very well-known method of genetic algorithm. Both methods are evolutionary computation techniques frequently used for complex optimization tasks in various fields (see for example [19, 21-25]).

The genetic programming usually involves very complex structures (i.e., organisms and/or potential solutions of the problem) that are manipulated during simulated evolution [19]. The shapes of the organisms depend on the problem to be solved. Organisms in the genetic programming are composed of functional and terminal genes. Functional genes are most often basic mathematical operations (e.g., addition, subtraction, multiplication, division, power function, exponential function). Terminal genes are usually explanatory variables of the system under study. A set of constants can be added to a set of terminal genes. The goal of the genetic programming is to find an individual organism (a mathematical model) that best solves the problem we deal with [19].

3. Modelling of additional sulfur cored wire addition

On the basis of the collected data in Table 1, the prediction of additional sulfur cored wire addition was conducted using linear regression and genetic programming. For the fitness function, the average absolute deviation between predicted and experimental data was selected. It is defined as:

$$\Delta = \frac{\sum_{i=1}^n |Q_i - Q'_i|}{n} \quad (1)$$

where n is the size of the monitored data and Q'_i and Q_i are the actual and the predicted additional sulfur cored wire addition in meters, respectively.

3.1 Modelling of additional sulfur cored wire addition using multiple linear regression

On the basis of the multiple linear regression results, it is possible to conclude that the model does not significantly predict the additional sulfur cored wire addition ($p > 0.05$, ANOVA) and that only 7.21 % of total variances can be explained by independent variables variances (R -squared). Accordingly, there are also no significantly influential parameters ($p > 0.05$).

$$SWA = 45.73 \cdot C2 + 265.49 \cdot SI2 - 143.37 \cdot MN2 - 114.30 \cdot S2 + 0.024 \cdot CW2 + 0.042 \cdot SW2 - 0.112 \cdot T2F + 0.389 \cdot FEMN + 0.049 \cdot FESI - 188.14 \quad (2)$$

The average absolute deviation from experimental data is 17.25 meters (m).

Regardless ANOVA results, the influences of individual parameters on the additional sulfur cored wire addition while separately changing individual parameter within the individual parameter range were calculated (Fig. 1). It is possible to conclude that according to multiple linear regression results the most influential is ferromanganese addition (FEMN).

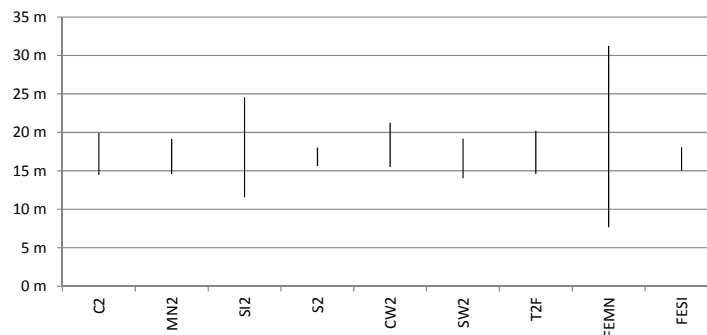


Fig. 1 Calculated influences of individual parameters on additional sulfur cored wire addition using the multiple linear regression model

3.2 Modelling of additional sulfur cored wire addition using genetic programming

For the purpose of this research, we used the basic arithmetical operations of addition, subtraction, multiplication and division (i.e., function genes), as well as independent variables (i.e., terminal genes) of the process to construct a potential successful solution. Each organism in each generation is evaluated for all fitness cases (i.e., for all combinations of input variables) and compared with the corresponding experimental values of dependent output variable according to the Eq. 1. The processes of genetic altering and evaluating of organisms is repeated until the successful solution is obtained [19].

We used in-house genetic programming system developed in AutoLISP programming language with the following evolutionary parameters: population size 2000, maximum number of generations 500, reproduction probability 0.3, crossover probability 0.7, maximum permissible depth of organisms in the creation of the population 6, maximum permissible depth after the operation of crossover of two organisms 30. Genetic operations of reproduction and crossover were used. We implemented tournament selection method with the tournament size of 7. Modelling experiment involved 200 runs.

The best mathematical model for prediction of additional sulfur cored wire addition obtained from 200 runs of genetic programming system is given in Eq. 3. Its average absolute deviation from experimental data is 10.80 m.

Similarly, as in case of multiple linear regression, we calculated the influence of individual parameter on the additional sulfur cored wire addition while separately changing individual parameter value within its range (Fig. 2). It is possible to conclude that according to the genetic programming results the most influential input variable is ferromanganese (FEMN) and ferrosilicon (FESI) additions.

$$\begin{aligned}
 \text{SWA} = & \frac{0.541 \left(2 \cdot \text{FEMN} + \frac{0.541 \cdot \text{FESI}}{\text{FEMN} \cdot \text{FESI} \left(\frac{0.541}{\text{C2}(1-\text{SI2}) + \text{FESI} \cdot \text{SI2}} \right)} \right)}{\text{C2} - \text{FEMN} - \frac{0.541 \cdot \text{FESI}}{\text{C2} - \text{SI2}} - \frac{\text{FESI}}{\text{C2} - \text{FEMN} \cdot \text{SI2}^2}} + \\
 & \text{SI2} \left(\text{FEMN} - \text{SI2} + \frac{0.541 \cdot \text{FESI}}{\text{C2} - \text{FEMN} \cdot \text{SI2}} + \right. \\
 & \left. \text{SI2} \left(\frac{\text{FESI}}{\text{C2} - \text{FEMN} + \frac{0.541 \cdot \text{FESI}}{\text{C2}(1-\text{SI2}) + \text{FESI} \cdot \text{SI2}}} + \frac{\text{FESI}}{\text{C2} - \text{FEMN} \cdot \text{SI2}^2} + \frac{0.541(\text{C2} - \text{FEMN} \cdot \text{SI2}) \left(2 \cdot \text{FEMN} + \frac{0.541 \cdot \text{FESI}}{\text{C2} + \frac{0.541 \cdot \text{FESI}}{\text{C2} - \text{FEMN} \cdot \text{SI2}}} \right)}{\text{C2}^2 - 1.293 \cdot \text{FESI} + \text{C2} \cdot \text{FEMN}(-2.082 - \text{SI2}) + 2.082 \cdot \text{FEMN}^2 \cdot \text{SI2}} \right) + \right. \\
 & \left. \frac{2 \cdot \text{FEMN} + \frac{0.541 \cdot \text{FESI}}{\text{C2} + \frac{0.541 \cdot \text{FESI}}{\text{C2} - \text{FEMN} \cdot \text{SI2}}}}{\text{C2} - \text{C2} \cdot \text{SI2} + \frac{\text{FESI}(-1 + \text{SI2}) + \text{SI2}(\text{C2} - \text{FEMN} \cdot \text{SI2})(\text{FEMN}(-1 + \text{SI2}) + \text{SI2}^2)}{\text{C2} - \text{FEMN} \cdot \text{SI2}}} \right) \quad (3)
 \end{aligned}$$

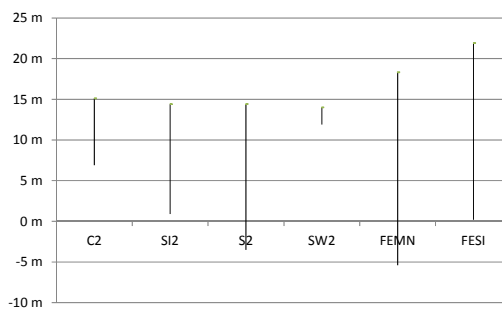


Fig. 2 Calculated influences of individual parameters on additional sulfur cored wire addition using the genetic programming model

4. Results and discussion

Regardless ANOVA results obtained using linear regression, the steelmaking process was changed. In the period from February 24, 2019 to October 17, 2019, a total of 12 batches of 70MnVS6 were produced with minimal ferromanganese additions (FEMN). Please bear in mind that during steelmaking, both ferromanganese and ferrosilicon were used for deoxidization. The results are gathered in the Table 2. It is possible to conclude that the additional sulfur cored wire addition was not necessary.

The average absolute deviation from experimental data gathered within period of changed steelmaking process is 19.54 m and 3.99 m at linear regression model and genetically obtained model, respectively. The genetic programming model outperformed the linear regression model for 4.90-times.

Also the role of other parameters which were not changed should be clarified. Carbon, manganese and silicon content after the second chemical composition analysis after tapping varies due to different scrap chemical composition (i.e., input material chemical composition) and additions and alloys which are added during tapping. They are also affected by later carbon, manganese and silicon addition. The same is with time between the second chemical analysis after tapping and final chemical composition analysis at starting of the casting which is influenced by technological and maintenance delays and also peak electricity period [17, 26]. The only possible changes could be attributed to ferromanganese and ferrosilicon additions.

After implementation of changes into production the addition of ferromanganese significantly decreased for 233.03 %, i.e., from 50.29 kg to 21.58 kg (t-test, $p < 0.05$). It must be emphasized that micro cleanliness before and after changes in production was also analyzed. According to technical delivery conditions, the K3 and K4 values without taking into account sulfur type of inclusions, determined according to DIN 50 602 were required. Micro cleanliness has been improved statistically significantly after changing of steelmaking process (t-test, $p < 0.05$). K3 and K4 values decreased from 6.49 to 4.58 and from 3.49 to 1.58, respectively.

Table 2 Parameters collected within the period from February 2019 to October 2019 for 12 consequently cast batches of 70MnVS6 using minimal ferromanganese additions

Batch	Carbon content after the second chemical composition analysis after tapping (C2), (%)	Manganese content after the second chemical composition analysis after tapping (MN2), (%)	Silicon content after the second chemical composition analysis after tapping (SI2), (%)	Sulfur content after the second chemical composition analysis after tapping (S2), (%)	Carbon cored wire addition after the second chemical composition analysis after tapping (CW2), (t)	Sulphur cored wire addition after the second chemical composition analysis after tapping (SW2), (t)	Time between the second chemical analysis after tapping and final chemical composition analysis at starting of the casting (TZF), (min)	Ferro-manganese (FEMN), (kg)	Ferrosilicon (FESI), (kg)	Additional sulfur cored wire addition (SWA), (t)
80210	0.018	0.57	0.82	0.19	100	240	88.00	46	53	0
80211	0.032	0.55	0.76	0.24	30	180	74.00	47	107	0
80212	0.032	0.56	0.81	0.25	0	160	119.00	11	93	0
80214	0.033	0.62	0.79	0.19	0	163	87.00	32	119	0
80215	0.029	0.65	0.80	0.19	40	180	81.00	23	124	0
80595	0.027	0.57	0.79	0.21	0	180	97.00	29	99	0
81393	0.033	0.53	0.80	0.20	160	213	85.00	21	98	0
81394	0.028	0.58	0.82	0.18	120	239	94.00	0	52	0
81692	0.026	0.63	0.80	0.21	200	178	93.00	21	96	0
81881	0.007	0.58	0.81	0.21	60	259	79.00	12	38	0
81882	0.016	0.64	0.83	0.25	140	220	78.00	0	82	0
82076	0.028	0.60	0.80	0.19	60	170	75.00	17	106	0

Time between the second chemical analysis after tapping and final chemical composition analysis at starting of the casting, scrap rate of rolled material after automatic control line inspection, and casting, based on evaluation score, have not been changed statistically significantly after changing of steelmaking process (t-test, $p < 0.05$). Please mind that casting evaluation score is obtained using in-house software which evaluate casting based on casting parameters (e.g., stopper rod movements, vibrators, melt level in the mold).

5. Conclusion

In this paper the prediction of additional sulfur addition (i.e., sulfur burn-off) during 70MnVS4 steelmaking in Štore Steel Ltd. was presented. During ladle treatment, instead of only one sulfur addition, the sulfur was repeatedly added several times threatening clogging during continuous casting and as such influencing surface defects occurrence and steel cleanliness.

Accordingly, following parameters were collected within the period from January 2018 to December 2018 for 78 consequently cast batches of 70MnVS6:

- carbon, manganese, silicon and sulfur content after the second chemical composition analysis after tapping,
- sulphur and carbon cored wire addition after the second chemical composition analysis after tapping,
- time between the second chemical analysis after tapping and final chemical composition analysis at starting of the casting,
- ferromanganese and ferrosilicon addition,
- additional sulfur cored wire addition.

Based on these data additional sulfur addition was predicted using linear regression and genetic programming. On the basis of the linear regression results, it is possible to conclude that the model does not significantly predict the additional sulfur cored wire addition ($p > 0.05$, ANOVA) and that only 7.21 % of total variances can be explained by independent variables variances (R -squared).

Similarly, additional sulfur addition was predicted using genetic programming system. Also the influences of individual parameters on the additional sulfur cored wire addition while separately changing individual parameter within the individual parameter range were calculated. It is possible to conclude that the most influential are ferromanganese and ferrosilicon addition.

Based on modelling results the steelmaking process was changed. In the period from February 2019 to October 2019 a total of 12 batches of 70MnVS6 were produced with minimal ferromanganese additions. The additional sulfur cored wire addition was not necessary.

After implementation of changes into production, the addition of ferromanganese significantly decreased, micro cleanliness has been improved statistically significantly after changing of steelmaking process. Some other parameters discussed earlier have not been changed statistically significantly after changing of steelmaking process (t-test, $p < 0.05$).

In the future burn-off of other alloys and cost reduction analysis for most important steel grades produced in Štore Steel Ltd. will be conducted.

References

- [1] Szekely, J., Carlsson, G., Helle, L. (1989). *Ladle metallurgy*, Springer-Verlag, New York, USA, doi: [10.1007/978-1-4612-3538-5](https://doi.org/10.1007/978-1-4612-3538-5).
- [2] Seetharaman, S. (2014). *Treatise on process metallurgy, Volume 3: Industrial Processes*, Elsevier, Oxford, United Kingdom, doi: [10.1016/C2010-0-67121-5](https://doi.org/10.1016/C2010-0-67121-5).
- [3] Holappa, L. (2014). Chapter 1.6 – Secondary steelmaking, In: Seetharaman, S. (ed.), *Treatise on Process Metallurgy*, Elsevier, Amsterdam, Netherlands, 301-345, doi: [10.1016/B978-0-08-096988-6.00012-2](https://doi.org/10.1016/B978-0-08-096988-6.00012-2).
- [4] Çamdali, Ü., Yetişken, Y., Ekmekçi, İ. (2012). Determination of the optimum cost function for an electric arc furnace and ladle furnace system by using energy balance, *Energy Sources, Part B: Economics, Planning, and Policy*, Vol. 7, No. 2, 200-212, doi: [10.1080/15567240903030521](https://doi.org/10.1080/15567240903030521).
- [5] Ekmekçi, İ., Yetişken, Y., Çamdali, Ü. (2007). Mass balance modeling for electric arc furnace and ladle furnace system in steelmaking facility in Turkey, *Journal of Iron and Steel Research International*, Vol. 14, No. 5, 1-6, doi: [10.1016/S1006-706X\(07\)60064-8](https://doi.org/10.1016/S1006-706X(07)60064-8).
- [6] Singh, V., Reddy, K.V.K., Tripathy, S.K., Kumari, P., Dubey, A.K., Mohanty, R., Satpathy, R.R., Mukherjee, S. (2021). A sustainable reduction roasting technology to upgrade the ferruginous manganese ores, *Journal of Cleaner Production*, Vol. 284, Article No. 124784, doi: [10.1016/j.jclepro.2020.124784](https://doi.org/10.1016/j.jclepro.2020.124784).
- [7] Schade, J., Argyropoulos, S.A., McLean, A. (1990). Assimilation and recovery characteristics of innovative cored wire additions for steelmaking, In: Bergman, R.A. (ed.), *Proceedings of Metallurgical Society of Canadian Institute of Mining and Metallurgy, Ferrous and Non-Ferrous Alloy Processes*, Pergamon Press, Ontario, Canada, 117-142, doi: [10.1016/B978-0-08-040411-0.50014-6](https://doi.org/10.1016/B978-0-08-040411-0.50014-6).
- [8] Savinov, R., Wang, Y., Shi, J. (2020). Microstructure and properties of CeO₂-doped CoCrFeMnNi high entropy alloy fabricated by laser metal deposition, *Journal of Manufacturing Processes*, Vol. 56, Part B, 1245-1251, doi: [10.1016/j.jmapro.2020.04.018](https://doi.org/10.1016/j.jmapro.2020.04.018).
- [9] Babu, S.S. (2022). Tools for alloy design, In: Caballero, F.G. (ed.), *Encyclopedia of Materials: Metals and Alloys*, Elsevier, Amsterdam, Netherlands, 245-262, doi: [10.1016/B978-0-12-819726-4.00142-3](https://doi.org/10.1016/B978-0-12-819726-4.00142-3).
- [10] Zhou, Y., Zhu, R., Wei, G. (2021). Application of submerged gas-powder injection technology to steelmaking and ladle refining processes, *Powder Technology*, Vol. 389, 21-31, doi: [10.1016/j.powtec.2021.05.003](https://doi.org/10.1016/j.powtec.2021.05.003).
- [11] Liu, Z., Zhang, L., Wang, M., Zhao, Z., Gao, L., Chu, M. (2021). New understanding on reduction mechanism and alloying process of rich manganese slag: Phase formation and morphological evolution, *Powder Technology*, Vol. 380, 229-245, doi: [10.1016/j.powtec.2020.11.071](https://doi.org/10.1016/j.powtec.2020.11.071).
- [12] Řeháčková, L., Novák, V., Váňová, P., Matýšek, D., Konečná, K., Smetana, B., Dobrovská, J. (2021). High – temperature interaction of molten Fe–C–O–Cr alloys with corundum, *Journal of Alloys and Compounds*, Vol. 854, Article No. 157128, doi: [10.1016/j.jallcom.2020.157128](https://doi.org/10.1016/j.jallcom.2020.157128).
- [13] Chen, D., Lu, B., Chen, G., Yu, W. (2017). Influence of the production fluctuation on the process energy intensity in iron and steel industry, *Advances in Production Engineering & Management*, Vol. 12, No. 1, 75-87, doi: [10.14743/apem2017.1.241](https://doi.org/10.14743/apem2017.1.241).
- [14] Natschläger, S., Stohl, K. (2007). Metallurgical simulation of the eaf-process, *IFAC Proceedings Volumes*, Vol. 40, No. 11, 207-211, doi: [10.3182/20070821-3-CA-2919.00030](https://doi.org/10.3182/20070821-3-CA-2919.00030).
- [15] Kovacic, M., Brezocnik, M. (2018). Reduction of surface defects and optimization of continuous casting of 70MnVS4 steel, *International Journal of Simulation Modelling*, Vol. 17, No. 4, 667-676, doi: [10.2507/IJSIMM17\(4\)457](https://doi.org/10.2507/IJSIMM17(4)457).
- [16] Kovačič, M., Senčič, S. (2012). Modeling of pm10 emission with genetic programming, *Materiali in tehnologije/Materials and technology*, Vol. 46, No. 5, 453-457, from <http://mit.imt.si/Revija/izvodi/mit125/kovacic.pdf>, accessed April 13, 2021.
- [17] Kovačič, M., Stopar, K., Vertnik, R., Šarler, B. (2019). Comprehensive electric arc furnace electric energy consumption modeling: A pilot study, *Energies*, Vol. 12, No. 11, Article No. 2142, doi: [10.3390/en12112142](https://doi.org/10.3390/en12112142).
- [18] Kovačič, M., Salihu, S., Gantar, G., Župerl, U. (2021). Modeling and optimization of steel machinability with genetic programming: Industrial study, *Metals*, Vol. 11, No. 3, Article No. 426, doi: [10.3390/met11030426](https://doi.org/10.3390/met11030426).
- [19] Brezocnik, M., Župerl, U. (2021). Optimization of the continuous casting process of hypoeutectoid steel grades using multiple linear regression and genetic programming — An industrial study, *Metals*, Vol. 11, No. 6, Article No. 972, doi: [10.3390/met11060972](https://doi.org/10.3390/met11060972).
- [20] Montgomery, D.C., Runger, G.C. (2003). *Applied statistics and probability for engineers*, Third edition, John Wiley & Sons, Hoboken, New Jersey, USA.
- [21] Koza, J.R. (1992). *Genetic programming: On the programming of computers by means of natural selection*, MIT Press, Cambridge, USA.
- [22] Gračnar, A., Kovačič, M., Brezocnik, M. (2020). Decreasing of guides changing with pass design optimization on

- continuous rolling mill using a genetic algorithm, *Materials and Manufacturing Processes*, Vol. 35, No. 6, 663-667, [doi: 10.1080/10426914.2019.1645337](https://doi.org/10.1080/10426914.2019.1645337).
- [23] Amjad, M.K., Butt, S.I., Anjum, N., Chaudhry, I.A., Faping, Z., Khan, M. (2020). A layered genetic algorithm with iterative diversification for optimization of flexible job shop scheduling problems, *Advances in Production Engineering & Management*, Vol. 15, No. 4, 377-389, [doi: 10.14743/apem2020.4.372](https://doi.org/10.14743/apem2020.4.372).
- [24] Jurkovic, Z., Cukor, G., Brezocnik, M., Brajkovic, T. (2018). A comparison of machine learning methods for cutting parameters prediction in high speed turning process, *Journal of Intelligent Manufacturing*, Vol. 29, No. 8, 1683-1693, [doi: 10.1007/s10845-016-1206-1](https://doi.org/10.1007/s10845-016-1206-1).
- [25] Kovačič, M., Župerl, U. (2020). Genetic programming in the steelmaking industry, *Genetic Programming and Evolvable Machines*, Vol. 21, 99-128, [doi: 10.1007/s10710-020-09382-5](https://doi.org/10.1007/s10710-020-09382-5).
- [26] Stopar, K., Kovačič, M., Kitak, P., Pihler, J. (2017). Electric arc modeling of the EAF using differential evolution algorithm, *Materials and Manufacturing Processes*, Vol. 32, No. 10, 1189-1200, [doi: 10.1080/10426914.2016.1257859](https://doi.org/10.1080/10426914.2016.1257859).

Calendar of events

- 6th International Conference on 3D Printing Technology and Innovations, May 24-25, 2021, Berlin, Germany.
- 38th Global Summit on Nanoscience and Technology, June 21-22, 2021, Osaka, Japan.
- International Conference on Manufacturing Models and Cloud Manufacturing, July 15-16, 2021, Stockholm, Sweden.
- International Conference on Industrial Production Methods and Flow Production, August 5-6, 2021, Montreal, Canada.
- 15th International Conference on Micromachining Technology, October 18-19, 2021, Dubai, United Arab Emirates.
- 35th Annual European Simulation and Modelling Conference, October 27-29, 2021, Rome, Italy.
- 32nd DAAAM International Symposium, October 28-29, 2021, Virtual conference.
- International Mechanical Engineering Congress and Exposition, November 1-4, 2021, Virtual conference.
- 15th International Conference on Robotics and Smart Manufacturing, November 15-16, 2021, Copenhagen, Denmark.

Notes for contributors

General

Articles submitted to the *APEM journal* should be original and unpublished contributions and should not be under consideration for any other publication at the same time. Manuscript should be written in English. Responsibility for the contents of the paper rests upon the authors and not upon the editors or the publisher. The content from published paper in the *APEM journal* may be used under the terms of the Creative Commons Attribution 4.0 International Licence (CC BY 4.0). For most up-to-date information please see the APEM journal homepage apem-journal.org.

Submission of papers

A submission must include the corresponding author's complete name, affiliation, address, phone and fax numbers, and e-mail address. All papers for consideration by *Advances in Production Engineering & Management* should be submitted by e-mail to the journal Editor-in-Chief:

Miran Brezocnik, Editor-in-Chief
UNIVERSITY OF MARIBOR
Faculty of Mechanical Engineering
Chair of Production Engineering
Smetanova ulica 17, SI – 2000 Maribor
Slovenia, European Union
E-mail: editor@apem-journal.org

Manuscript preparation

Manuscript should be prepared in *Microsoft Word 2010* (or higher version) word processor. *Word .docx* format is required. Papers on A4 format, single-spaced, typed in one column, using body text font size of 11 pt, should not exceed 12 pages, including abstract, keywords, body text, figures, tables, acknowledgements (if any), references, and appendices (if any). The title of the paper, authors' names, affiliations and headings of the body text should be in *Calibri* font. Body text, figures and tables captions have to be written in *Cambria* font. Mathematical equations and expressions must be set in *Microsoft Word Equation Editor* and written in *Cambria Math* font. For detail instructions on manuscript preparation please see instruction for authors in the *APEM journal* homepage apem-journal.org.

The review process

Every manuscript submitted for possible publication in the *APEM journal* is first briefly reviewed by the editor for general suitability for the journal. Notification of successful submission is sent. After initial screening, and checking by a special plagiarism detection tool, the manuscript is passed on to at least two referees. A double-blind peer review process ensures the content's validity and relevance. Optionally, authors are invited to suggest up to three well-respected experts in the field discussed in the article who might act as reviewers. The review process can take up to eight weeks on average. Based on the comments of the referees, the editor will take a decision about the paper. The following decisions can be made: accepting the paper, reconsidering the paper after changes, or rejecting the paper. Accepted papers may not be offered elsewhere for publication. The editor may, in some circumstances, vary this process at his discretion.

Proofs

Proofs will be sent to the corresponding author and should be returned within 3 days of receipt. Corrections should be restricted to typesetting errors and minor changes.

Offprints

An e-offprint, i.e., a PDF version of the published article, will be sent by e-mail to the corresponding author. Additionally, one complete copy of the journal will be sent free of charge to the corresponding author of the published article.

APEM

journal

Advances in Production Engineering & Management

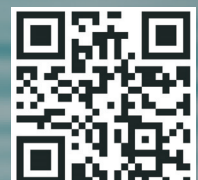
Chair of Production Engineering (CPE)
University of Maribor
APEM homepage: apem-journal.org

Volume 16 | Number 2 | June 2021 | pp 141-264

Contents

Scope and topics	144
Hybrid ANFIS-Rao algorithm for surface roughness modelling and optimization in electrical discharge machining Agarwal, N.; Shrivastava, N.; Pradhan, M.K.	145
A multi-objective optimal decision model for a green closed-loop supply chain under uncertainty: A real industrial case study Fang, I.W.; Lin, W.-T.	161
Improved Genetic Algorithm (VNS-GA) using polar coordinate classification for workload balanced multiple Traveling Salesman Problem (mTSP) Wang, Y.D.; Lu, X.C.; Shen, J.R.	173
Change impact analysis of complex product using an improved three-parameter interval grey relation model Yang, W.M.; Li, C.D.; Chen, Y.H.; Yu, Y.Y.	185
Bone drilling with internal gas cooling: Experimental and statistical investigation of the effect of cooling with CO₂ on reduction of temperature rise due to drill bit wear Shakouri, E.; Haghighi Hassanalideh, H.; Fotuhi, S.	199
Joint distribution models in fast-moving consumer goods wholesale enterprise: Comparative analysis and a case study Wang, L.; Chen, X.Y.; Zhang, H.	212
Designing a warehouse internal layout using a parabolic aisles based method Zhang, Z.Y.; Liang, Y.; Hou, Y.P.; Wang, Q.	223
Optimization of disassembly line balancing using an improved multi-objective Genetic Algorithm Wang, Y.J.; Wang, N.D.; Cheng, S.M.; Zhang, X.C.; Liu, H.Y.; Shi, J.L.; Ma, Q.Y.; Zhou, M.J.	240
Modelling and optimization of sulfur addition during 70MnVS4 steelmaking: An industrial case study Kovačič, M.; Lešer, B.; Brezocnik, M.	253
Calendar of events	262
Notes for contributors	263

Published by CPE, University of Maribor



apem-journal.org